ANTHROPOGENIC DEVELOPMENT OVER THE LAST ~200 YEARS LEAVES PHYSICAL AND GEOCHEMICAL IMPRINTS IN LAKE SEDIMENT RECORDS

Alexandre Baud

Department of Biology

McGill University, Montreal

December 2022

A thesis submitted to McGill University in partial fulfillment of requirements of the degree of

Doctor of Philosophy

TABLE OF CONTENTS

ACKNOWLEDGMENTS

I would like to thank my supervisor, Rene Gregory-Eaves for having given me so many opportunities throughout my PhD program. I was very lucky to have had such an involved supervisor like you are. I also want to thank all of the past and current members of the Gregory-Eaves lab for their insights, comments, our discussions and hangouts. It was great working with all of you. A special thank you to Michelle Gros for having assisted on the logistics of so many aspects of my projects. Thank you to every research assistant that have helped with laboratory work: Sandrine Beaumont-Courteau, Joey El-Achkar, Michelle Cheng, Ben Ralston Daniel.

I also want to thank my co-director, Pierre Francus and his technician Arnaud De Coninck for having enabled great research in the best of conditions. Another special thank you goes to Jean-Philippe Jenny, it was great to assist you in subsampling these sediment cores at LacCore. Your passion for science definitely inspired me to pursue further in research and in paleolimnology. You have been a great help in my early career and allowed me to travel to amazing learning institute so thank you very much.

Thank you to the McGill Biology department, for fostering a great learning environment. A special thank you to Frank Scopelleti for always having your door open and crafting some ingenious tools for our research and field trips.

Thank you to the members of my supervisory committee: Brian Leung and Bernhard Lehner for your comments and providing insightful ideas even though some of my research might have been a bit outside your expertise.

Thank you to all my co-authors, especially Dermot Antoniades, for always having made your lab available for us and always being willing to lend equipment and thank you to your students, especially Yohanna Klanten. Thank you, Adam Jeziorski, it was great working with you. Thank you, John Smol, for all the time you have spent editing our manuscripts and sharing your stories about paleo.

A huge thank you to all of the LakePulse team, especially Yannick Huot who led this formidable idea and effort that was the LakePulse field campaign. Thank you, Maxime Fradette, it was great sampling the lakes with you and thank you for always being willing to help on various GIS-related projects. Thank you to the ELA staff, and the researchers there, this week at ELA was unforgettable.

Thank you, Marie-Pier Hebert, and Egor Katkov for all our discussions together, I really enjoyed TAing the limnology class with you.

Thank you to the GRIL and its members, you have truly given a broader sense and relevance to my research. You have also given me the opportunity to meet some wonderful people.

Thank you, Bernadette Connell for having opened your door at the Cooperate Institute for Research in the Atmosphere and enabling me to discover the new learning opportunities.

Thank you to the R, ArcGIS and Stackoverflow communities, and to every author I have cited, without these resources there are many aspects of this thesis that couldn't have been done.

Thank you to every single one of my teachers and professors for your drive to teach and empower others to learn.

Thank you to all of my friends with whom I was able to share my reflections and have great discussions. A special thank you to Pierre Rogy; thank you for having introduced me to R, thank you for challenging my ideas and offering me another take on things. Thank you to my partner Sarah Dimmock, for always being here for me, listening to my science non-sense days after days.

Thank you to my brother for always being the role-model I look up to.

Thank you to my parents for having given me the freedom to experience things in life, through this freedom you have given me a sense of responsibilities and given me the confidence to undertake a project of this size.

Et enfin, un immense merci à mes grands-parents. J'ai eu énormément de chance de pouvoir vivre si proche de vous pendant si longtemps, même si maintenant nous habitons loin l'un de l'autre. Je garderai pour toujours ces souvenirs de nous marchant autours du réservoir du Cheylas, ou de nos sorties pour cueillir des champignons à Theys. Vous m'avez donné l'amour et le respect de la nature que j'espère pouvoir partager avec autrui.

ABSTRACT

Lakes, and the environment in general, have been subjected to important modifications when considering the last 200 years. While local case studies are informative about the specific modification brought to their environment, generalizing changes over large geographic areas is insightful to more clearly define the magnitude, scale and frequency of environmental change. My PhD thesis aims to: (1) identify the spatial and temporal patterns of lake sedimentation rates over the past ~200 years; and (2) quantify the magnitude and direction of geochemical change recorded in lake sediments and identify predictors associated with their distribution and dynamics across the landscape. In my first chapter, I focused on the global variation in lake sedimentation rates using published records and considered both the spatial and temporal distribution of lake sedimentation rates. In this chapter, I was able to shed light on the acceleration of lake sedimentation rates around the world and to demonstrate a significant association between increasing sedimentation rates and anthropogenic land use metrics such as cropland and urban cover. In my second chapter, I narrowed in on Eastern Canada, a region which spans thousands of square kilometers and comprises a wide range of land use and climate using a network of 37 sediment cores. In this chapter, after having developed a reproducible framework for producing ^{210}Pb-based chronologies, I found that predictors of lake sedimentation rate at a global scale were also significant when considering this smaller geographical extent. These findings reinforced the idea that anthropogenic contributions were highly influential in determining lake sedimentation rate patterns. In my third chapter, using the same network of sediment cores, I investigated the spatio-temporal distribution of their

geochemical constituents. In this chapter, I characterized the specific sediment geochemical constituents responsible for observed differences across Eastern Canada, which was primarily a gradient of organic to inorganic content. Organic content in sediment was most abundant for lakes of the Boreal Shield, Atlantic Maritime and Highlands while lakes set in the Mixedwood Plains were more abundant in inorganic sedimentary constituents that are rich in elements such as titanium, strontium and calcium. Another finding of this chapter was the detection of a gradient in sedimentary metals such as lead and zinc, which were found in all study lakes, but differed in magnitude across lakes and through time. Watershed land-use, measured as human population and cropland cover were key predictors of sedimentary composition, with metals co-varying most with human population, while watershed geology accounted for a lot of variation in both the organic and inorganic content of the sediment. Finally, in my fourth chapter, I considered the effect of lake acidification and eutrophication, key environmental stressors, on the concentration and accumulation of lead (Pb) in lake sediments. I collected sediment cores for this chapter from the Experimental Lakes Area (IISD-ELA), where whole-lake manipulations had been carried out during the late 1960s to present. I hypothesized that Pb accumulation rates would be muted in acidified lakes relative to reference lakes, whereas eutrophied lakes would show accelerated Pb accumulation rates, due changes in Pb solubility and retention. My results aligned with my hypothesis, and I found dissolved organic carbon (DOC) was the strongest predictor of Pb accumulation in lake sediments across the intervention period, likely because DOC contributed favorably the deposition and retention of metals in the sediment. Overall, my PhD thesis demonstrated the profound impact of human activities on the cycling of numerous sedimentary properties, including sedimentation rates and the distribution of geochemical constituents across multiple scales. The time series and model results developed not only inform site specific landscape management, but also contribute key data for more global modelling efforts.

RÉSUMÉ

Les lacs et l'environnement en général ont été sujets à de nombreuses modifications pendant les 200 dernières années. Bien que les études locales soient pertinentes pour documenter les modifications apportées à un environnement spécifique, il serait judicieux d'avoir une vue plus globale de ces changements pour améliorer notre compréhension de la magnitude, de l'échelle ainsi que de la fréquence du changement environnemental. La recherche développée au sein de ma thèse de doctorat vise à (1) identifier les tendances spatiales et temporelles liées aux taux d'accumulation des sédiments lacustres et (2) à quantifier la magnitude ainsi que la direction du changement géochimique enregistré par les sédiments lacustres ainsi que les facteurs en lien avec leur distribution et abondance à travers le territoire. Dans mon premier chapitre, je me suis concentré sur la variation mondiale des taux de sédimentation lacustres en utilisant la distribution spatiale et temporelle de registres publiés dans la littérature scientifique. Dans ce chapitre, j'ai été en mesure de mieux cerner le phénomène d'accélération des taux de sédimentation à travers le monde. J'ai aussi été capable de démontrer l'importante association entre la couverture du territoire liée à l'activité humaine, comme celle des terres cultivées ou de l'urbanisation, sur l'augmentation des taux de sédimentation lacustres. Dans mon second chapitre, je me suis concentré sur une région spécifique, celle de l'Est canadien, couvrant plusieurs milliers de kilomètres carrés et arborant une grande variété d'utilisation du sol et de climat, en utilisant un réseau de 37 carottes sédimentaires. Dans ce chapitre, après avoir développé une méthode de production de chronologies au ^{210}Pb applicable à l'ensemble des lacs, j'ai été en mesure de discerner que les variables qui participent au contrôle des taux

de sédimentation à l’échelle mondiale étaient tout aussi importantes lorsque l’on considérait une zone géographique plus réduite. Cette découverte renforce donc l’idée que l’impact anthropique influence grandement les tendances des taux de sédimentation. Dans mon troisième chapitre, en utilisant le même réseau de carottes sédimentaires que celui considéré dans mon second chapitre, j’ai étudié la distribution spatiale et temporelle des composants géochimiques sédimentaires. Pour ce chapitre, j’ai été en mesure de déterminer qu’un gradient du taux de matière organique et inorganique dans les sédiments était responsable des variations géochimiques des sédiments des lacs de l’Est canadien. Ainsi, les sédiments des lacs du bouclier canadien, des maritimes atlantiques et hautes terres atlantiques possèdent une plus grande fraction de matière organique alors que ceux situés dans les plaines à forêts mixtes contiennent plus de matière inorganique, riche en titane, strontium ou calcium. Une autre découverte intéressante faite dans ce chapitre porte sur la présence de métaux comme le plomb ou le zinc, qui ont été détectés dans tous les lacs étudiés, mais dont l’ampleur variait selon les lacs et selon la période. L’occupation des sols qui composent les bassins versants des lacs, notamment à travers la présence de population humaine ou de terres cultivées, fut trouvée comme ayant un rôle très important sur la composition géochimique sédimentaire. Les métaux étaient souvent associés avec la présence de population humaine, alors que la géologie du bassin versant expliquait en majeure partie les variations liées aux taux de matière organique et inorganique du sédiment. Finalement, pour mon quatrième chapitre, j’ai voulu considérer l’effet potentiel de facteurs de stress communs sur les écosystèmes lacustres, comme l’acidification ou l’eutrophisation, sur la concentration en plomb dans leurs sédiments. Pour ce faire, j’ai collecté des carottes sédimentaires provenant de la zone des Lacs

Expérimentaux (IISD-ELA), là où des manipulations à l'échelle de lacs entiers ont été menées durant la fin des années 1960 jusqu'à aujourd'hui. J'ai émis l'hypothèse que l'accumulation du Pb dans les lacs acidifies seraient relativement réduit par rapport aux lacs références, alors que pour les lacs eutrophisés, je m'attendais à ce que ces lacs montrent une accélération de l'accumulation du Pb en lien avec des changements de solubilité et de rétention du plomb. En accord avec mes hypothèses, mes résultats ont mis en évidence le contrôle important que possède la matière organique dissoute (DOC) sur l'accumulation du plomb dans le sédiment à travers les périodes de manipulation, notamment car le DOC favorise la déposition et la rétention de métaux dans le sédiment. En règle générale, ma thèse de doctorat aura démontré l'impact profond qu'ont les activités humaines sur la dynamique de nombreuses propriétés sédimentaires, notamment sur les taux de sédimentations ainsi que sur la composition géochimique du sédiment, et ce, à travers des échelles locales, régionales et mondiale. Les séries chronologiques et les modèles développés auront non seulement servis à informer sur l'entretien et à la gestion du paysage de sites spécifiques, mais fournissent également des données clés pour le développement de modèles environnementaux à l'échelle mondiale.

PREFACE

Thesis format and style

This thesis is presented as a manuscript-based format. It includes a general introduction, followed by four manuscripts numbered Chapter I, Chapter II, Chapter III and Chapter IV, with connecting statements and a general conclusion. The manuscripts presented in this thesis have either been published (Chapter I, II and IV), or reviewed by a scientific journal (Chapter III) in the disciplines related to paleolimnological and global environmental change. Supplementary materials are available as appendices for each of the four chapters (Supplementary A, Supplementary B, Supplementary C and Supplementary D) with two appendices labelled Supplementary CA and CB available for Chapter III. Data have been deposited in Zenodo archives, open to the public once publications have been accepted in peer-reviewed journals.

The body of this thesis is composed of the following contributions:

<u>Chapter I</u>:

Baud, A., Jenny, JP., Francus, P., Gregory-Eaves, I. (2021) Global acceleration of lake sediment accumulation rates associated with recent human population growth and land-use changes. J Paleolimnol 66, 453–46. Available from: https://doi.org/10.1007/s10933-021-00217-6

Data made available at: https://zenodo.org/record/5360710

Chapter II :

Baud, A., Aulard, C., Ghanbari, H. Fradette, M., Antoniades, D., del Giorgio, P., Huot, Y., Francus, P., Smol, JP., Greogory-Eaves, I. (2022) A framework for ^{210}Pb model selection and its application to 37 cores from Eastern Canada to identify the dynamics and drivers of lake sedimentation rates. Earth Surf. Proc. and Landf., 1– 13. https://doi.org/10.1002/esp.5391

Data and R-script made available at: https://zenodo.org/record/7372968

Chapter III:

Baud, A., Francus, P., Smol, JP., Antoniades, D., Greogory-Eaves, I. (minor revision). Geochemical changes in Eastern Canadian lake sediment cores spanning the last ~150 years highlight a relative shift towards increased metals and erosive materials. CATENA

Data made available at: https://zenodo.org/deposit/7429470

Chapter IV:

Baud, A., Smol, J.P., Meyer-Jacob, C., Paterson, M., Francus, P., Gregory-Eaves, I. (2022). The impacts of whole-lake acidification and eutrophication on the accumulation of lead in sediments from manipulated lakes in the Experimental Lakes Area (IISD-ELA). Environ. Pollut., 120829. https://doi.org/10.1016/j.envpol.2022.120829

Data made available at: https://zenodo.org/record/7429531

To make the formatting style consistent throughout this thesis, I modified the numbering of the tables, figures and supplementary information from original publications, and have followed the format from the journal CATENA, which is the journal my 3rd chapter has been submitted to. The use of first-person plural refers to all co-authors included throughout the four chapters. In all other section of the thesis, the first singular person is used. The tables, figures and supplementary information associated with each chapter can be found at the end of each specific chapter.

Contribution of Authors

All the aforementioned chapters have been written and developed with the close collaboration of both my supervisors: Irene Gregory-Eaves and Pierre Francus, along with feedback from members of the Gregory-Eaves lab. For each chapter, co-authors were also responsible for providing ideas, editorial feedback, grant acquisition and laboratory expenses. Below will be detailed account for the contribution of each co-author.

Chapter I

Original project idea was developed by Irene Gregory-Eaves (IGE) and Jean-Philippe Jenny (JPJ). I was responsible for the digitization of all source articles, data analysis and original creation of the manuscript. I also acknowledge the help of Sandrine Beaumont-Courteau for her help with some aspects of data digitization. IGE, JPJ and Pierre Francus (PF) contributed feedback and editorial comments on the writing of the manuscript.

Chapter II

Field sampling was designed and performed in collaboration with the NSERC network LakePulse. The methodological framework developed in this chapter was elaborated by myself and IGE. IGE, PF, Dermot Antoniades, Paul del Giorgio, John Smol and Yannick Huot were responsible for funding acquisition. Maxime Fradette, Candice Aulard and Hamid Ghanbari helped with data investigation. All participating authors were also involved in reviewing and editing the manuscript.

Chapter III

For chapter 3, density measures were operated by Louis-Frederic Daigle (INRS) and ITRAX scans by Arnaud de Coninck (INRS). I was responsible for the development of the methods and statistical analysis along with the writing of the manuscript. All participating authors were also involved in reviewing and editing the manuscript. Irene Gregory-Eaves, Pierre Francus, Dermot Antoniades and John Smol were also responsible for funding acquisition.

Chapter IV

For chapter 4, Maxime Fradette and I conducted the lake sediment core sampling and Michael Paterson provided guidance on the selection of reference lakes. Carsten Meyer-Jacob and Irene Gregory-Eaves provided early comments on the idea developed in the manuscript. All participating authors contributed to reviewing and editing the manuscript. Irene Gregory-Eaves, Pierre Francus and John Smol were responsible for funding acquisition.

Statement of Originality

The research projects presented herein investigate the overarching themes of environmental and geomorphological change experienced across the last 150 - 200 years. They integrate the physical and geochemical basis of lake sediments to generate insights into the magnitude and direction of environmental change. This thesis aims to do so by focusing on multiple geographical regions. The relative importance of different variables on the scale of physical and geochemical responses archived in lake sediments are judiciously examined, reflecting broader environmental change. Across these chapters, the novelty can be found from the scale of the investigation, the methodological framework put forward and/or by application of novel instruments geared towards the study of lake sediment archives.

<u>Chapter I</u>

Lake sedimentation rates are a key metric of global environmental change, as these measurements are critical for calculating burial rates of many elements. This study led to the creation of the largest, worldwide inventory of lake sedimentation rates over the last ~150 years. Comprised of nearly 500 lake sediment cores, distributed on every continent of the Earth, I delineated lake watersheds and tested the association between lake sedimentation rates and land use metrics. While numerous paleolimnological investigations had been performed over the last 50 – 70 years, there was no synthesis evaluating the contribution of land use on the trends and patterns observed in sedimentation rates. To this end, we compiled all publications from 1989 – 2016 CE made in the *Journal of Paleolimnology* and selected records with available chronologies spanning the last 150 years. Among the key findings gathered via this investigation is the net global acceleration in lake sedimentation rates – depicted as both sediment accumulation rate (mm yr^{-1}) and mass accumulation rate (g cm^{-2} yr^{-1}) – with an onset around 1950 CE. Another interesting finding that holds implications for the study of global environmental flux, is the fact that lake sedimentation rates were observed to have increased by 3 – 4 folds since pre-industrial conditions. We found these increases in lake sedimentation rate to be most often associated with the presence of urban or cropland cover in the watershed of these lakes, demonstrating the influence of humankind on its environment.

Chapter II

The establishment of lake sediment chronologies is arguably one of the most critical aspects of any paleolimnological investigation. A reliable chronology is essential to contextualize any of the trends quantified from sediment archives. Despite this paramount importance, a study led by Barsanti and colleagues (2020) demonstrated the clear lack of reproducibility and agreement within the scientific communities when establishing lake sediment chronologies. These considerations become of growing concerns when investigating multiple lakes across the landscape, where a reproducible and objective framework for establishing chronologies is required. Using radioisotopic activities measured from 37 sediment cores collected across Eastern Canada, we set ourselves to develop a methodological framework aimed to evaluate the applicability and ease the selection of the three main dating models. This investigation also served to build-upon the findings of my previous chapter, where we tested the influence of anthropogenic land use on sediment accumulation rates. Focusing this time on a regional network of 37 sites, our findings reinforced the idea that human population and agricultural land in lake watersheds contributed to greater sedimentation rates.

Chapter III

For this study, we took advantage of the application of novel, non-destructive high-resolution instruments geared towards the study of lake sediment archives. These instruments provide millimetric resolution data on the physical and geochemical composition of lake sediment, which allow for the investigation of variation in geochemical elements relative abundances across the Eastern Canadian landscape, and the identification of the variables associated with their distribution. While current investigations of lake sediment geochemical change typically focus on a single element and/or a specific site location, our study evaluated the distribution and variation of a suite of geochemical elements across 37 lake records. For this chapter, a considerable methodological effort was put together to investigate the applicability of XRF-scanners intensities and their comparison with elemental concentrations considering emerging normalization procedures. The measurement of elemental concentrations also served as a basis to compare against current Canadian environmental sediment guidelines. To synthesize our findings, we adapted a statistical methodology enabling the creation of new insights into the magnitude and direction of geochemical change and the visualization of lake sediment geochemical trajectories. In this study, we found variables related to in-lake productivity, erosive material and metals to be responsible for the heterogenous composition of lake sediments across Eastern Canada. We also report on the influence of watershed geological build-up and current watershed land-use conditions on the distribution of these geochemical elements.

Chapter IV

While regional sampling programs like the ones conducted in my 3rd chapter have the potential to yield insights into the distribution of geochemical elements across the landscape, the mechanisms impacting the burial of different sediment constituents remained difficult to pinpoint. The geochemical data generated from sediment records will generally correspond to the complex interactions among emission, transport and burial processes. Based on earlier work, we know that common stressors of lake health, such as eutrophication and acidification, have the potential to influence the accumulation of sedimentary constituents, especially metals. However, to clearly resolve the mechanisms associated with these stressors, it would be favorable to isolate specific drivers in an experimental setting. To study this effectively, we collected 7 sediment cores from the IISD-ELA where whole-lake manipulations have been carried out since in the late 1960s. The sediment cores sampled in 2018 captured two main treatments: Eutrophication and Acidification. Sediment cores from reference lakes (untreated) were also sampled. These archives were used to model the variation in elemental Pb accumulation in responses to the experimental manipulation. Complementary temporally resolved water chemistry monitoring data, collected and archived by the IISD-ELA, were also considered to determine the most influential parameters associated with the expected contrasting accumulation of Pb in lake sediment records in relation to experimental manipulations. Our findings supported our predictions and yielded contrasting Pb accumulation patterns between acidified and eutrophied systems: little to no enrichment in elemental Pb was recorded in acidified lakes while a significantly greater accumulation of elemental Pb was recorded in eutrophied system. We were also able to identify the significance of epilimnetic dissolved organic carbon in mediating the burial of elemental Pb in lake sediments.

LIST OF ABBREVIATIONS

Abbreviation	***Meaning***
A.H.	Atlantic Highlands ecoregion
A.M.	Atlantic Maritime ecoregion
A_{tx}	^{210}Pb Inventory at time t_x (Bq m^{-2})
B.S.	Boreal Shield ecoregion
Bq	Becquerel
CE	Current Epoch
C.F.C.S.	Constant Flux Constant Sedimentation
Chl-*a*	Chlorophyll *a*
C.I.C.	Constant Initial Concentration
cps	Counts per second
C.R.S.	Constant Rate of Supply
C_{tx}	Unsupported ^{210}Pb activity at time t_x (Bq kg^{-1})
DOC	Dissolved Organic Content
e.d.f.	Estimated Degree of Freedom
ICP-AES	Inductively coupled plasma atomic emission spectroscopy
ICP-MS	Inductively coupled plasma mass spectrometry
IISD-ELA	International Institute for Sustainable Development - Experimental Lakes Area
Inc.Coh	Molybdenum Incoherence to Coherence ratios
ISQG	Interim Freshwater Sediment Quality Guidelines
LOI	Loss on Ignition
M.W.P.	Mixedwood Plains ecoregion
MAR	Mass Accumulation Rate (g cm^{-2} $year^{-1}$)
PEL	Probable Effect Levels
SAR	Sediment Accumulation Rate (mm $year^{-1}$)
SOM	Soil Organic Matter
XRF	X-Ray Fluorescence
λ	^{210}Pb disintegration constant ($\lambda = 0.03114$ $year^{-1}$)

LIST OF TABLES

LIST OF FIGURES

LIST OF APPENDICES

GENERAL INTRODUCTION

Lakes as Earth's geographical features

Lakes can be defined as small cavities or depressions across the Earth landscape, filled continuously or perennially with fresh- or salt-water (Tundisi and Tundisi, 2012). It is estimated there are millions, to hundreds of millions of lakes distributed globally (Verpoorter et al., 2014; Messager et al., 2016). Lakes are most often associated with glaciated landscapes found in Canada, Scandinavia, and Russia. This is because most of the lakes present nowadays are the results of scouring from the last glaciation that began ~100 000 years ago (Wetzel, 1983). Lakes are inter-connected to the environment via multiple pathways and are often part of the land-to-ocean aquatic continuum (Syvitski et al., 2005; Foster et al., 2011). From high mountains headwater lakes to low elevation floodplain seepage lakes, water carries erosive material that is transported by rivers and fed into lakes before entering the ocean. Due to the topographic underpinning of lakes, lakes are profoundly influenced by their watershed, defined as the land area draining into the lake. The watershed's vegetation, land use and topology have the potential to alter the amount and the chemistry of the material transported across the landscape within riverine systems or determine the constituents leached out (Fraterrigo and Downing, 2008; Taranu and Gregory-Eaves, 2008; Richard Albert et al., 2010; Ady and Patoine, 2016; Keller et al., 2019). The material transported by rivers is often referred to as the allochthonous input. Allochthonous input generally describes any material or constituent entering the lake through overland-flow, groundwater, or wet and dry atmospheric deposition (Telmer et al., 2006; Cremer et al., 2010; Crann et al., 2015). In contrast, autochthonous inputs refer to materials or organisms that are produced within the lake itself (Meybeck, 1995; Anderson et al., 2020). Because of their key location on the landscape, lakes serve as important connectivity links for the transfer of matter from the terrestrial to the aquatic and marine ecosystems (Wolfe et al., 2006; Rodriguez et al., 2020). As such, lakes are hubs for numerous biogeochemical cycles (Porcal et al., 2009; Helms et al., 2013) and will generally provide habitat for a wide range of biological communities.

Lake Sediments as environmental archives

Lake sediments, present at the bottom of lakes, are characterized by a variety of constituents, ranging in their typology and mineralogy from inorganic forms of sand, silt, clay and organic matter (Bloemsma et al., 2012). Encapsulating matter derived from the hydrosphere, lithosphere and atmosphere, lakes through their sedimentological archives can record the state of the changing environment (Last and Smol, 2002a; Landers et al., 2008; Wiklund et al., 2018). As such, throughout the years and across the landscapes, lakes are continuously recording environmental change. This capacity combined with the abundance of lakes on the landscape has earned these ecosystems the recognition of being “ecological sentinels”. Furthermore, the information about past environmental change recorded in lake sediment may arise from local and/or distant sources. For some lakes, most notably lakes in the High Arctic, where in-lake production and watershed contribution are low, sources of atmospheric deposition can contribute in an important fraction of the material deposited (Engstrom et al., 2014; Anderson et al., 2020).

Artic lakes, in turn, are often used as indicators of global environmental change. Lake sediment archives, collected as sediment cores, can provide a continuous record of the past dynamics, reflective of a lake's surrounding environmental conditions. Using a wide range of biotic and abiotic parameters preserved in lake cores, sediments can provide proxies that are helpful for reconstructing shifts in lake ecosystem properties and of the surrounding conditions. These proxies include, but are not limited to, species remains such as Cladocera or diatoms that have left fossilized silica-based cell walls or body parts that remain preserved within lake sediments (Wigdahl-Perry et al., 2016; Griffiths et al., 2021; Cheng et al., 2022; Kahlert et al., 2022). The study of these biological assemblages and past environmental conditions have provided insightful information on past trajectories and have allowed for quantitative inferences of historical environmental conditions to be drawn (Ruggiu et al., 1998; Last and Smol, 2002b; Bennion and Simpson, 2011). One example is the use of diatom assemblages' relative abundance data and the associated "realized" pH niche of each taxon, which is then used to reconstruct a lake's pH history and how it varied with acid deposition on the landscape (Jeziorski et al., 2008).

Lake sediment chronologies and contextualization of sediment archives

Central to the study of lake sediment archives is the determination of sediment chronologies required to adequately contextualize the timing of environmental change inferred from lake sediment cores. The establishment of lake sediment chronologies often relies on the use of radioisotopes and their decaying properties (Appleby, 1998; Appleby, 2002). Two of the main radioisotopes include carbon-14 (^{14}C) and lead-210 (^{210}Pb). The former is used principally to date ancient sediments on the timescale of 1000s to 10,000 of years (Nelson et al., 1977; Blaauw and Christen, 2011). ^{14}C is well suited to investigate past long-term climate questions (Russell et al., 1993; Wolter et al., 2017), provide insights into Earth's condition and landscapes during the Holocene (Huang et al., 2004; Jambrina-Enríquez et al., 2016; Jenny et al., 2019) and the Pleistocene (Talbot and Lærdal, 2000). On the other hand, ^{210} Pb is mainly used to date more recent sediments on the timescale of 75-150 years (Appleby, 1998). Stemming from this temporal restriction, ^{210}Pb chronologies mainly serve to answer questions about environmental change that have occurred since the Industrial Revolution. Despite its capital importance and repeated use in the community, the establishment of ^{210}Pb-based age-depth profiles remains a challenging endeavor and arguably lacks standardization across laboratories and analysts (Barsanti et al., 2020). These challenges are in part due to the existence of multiple dating models, each relying on slightly different assumptions (Sanchez-Cabeza and Ruiz-Fernández, 2012). As a result, different models may be best suited to cater to different sedimentological regimes. To date, the main models used for ^{210}Pb establishment of sediment chronologies are the Constant flux constant sedimentation (C.F.C.S), which relies on a linear and constant rate of accumulation of sediment (Crozaz et al., 1964); the constant initial concentration (C.I.C.), which assumes a constant concentration of ^{210}Pb (C_0) at the formation of each sediment interval and finally (Appleby and Oldfieldz, 1983), the Constant Rate of Supply (C.R.S.), which assumes a constant rate of supply of ^{210}Pb to the sediment from the atmosphere and surrounding catchment (Appleby and Oldfield, 1978) (Figure E1).

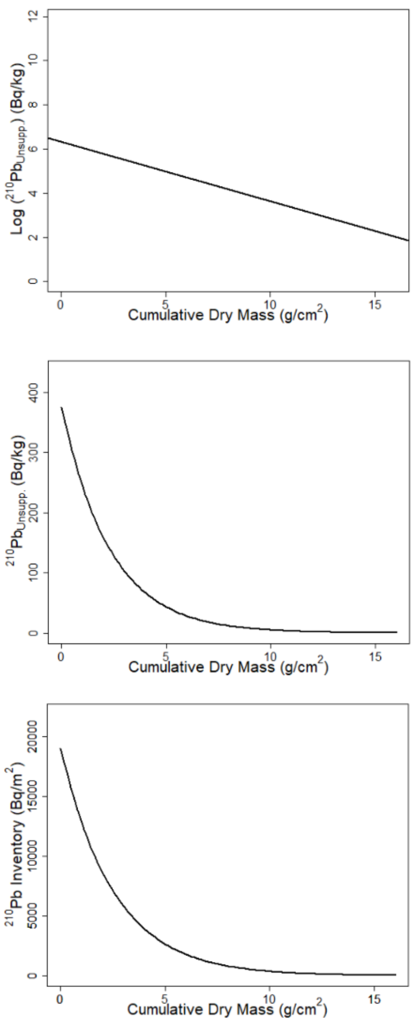

Model	Assumption	Equation
Constant Flux Constant Sedimentation model (CFCS)	· Assumes a constant sedimentation rate along the entire core · Activity of unsupported ^{210}Pb is expected to decay as a function of the cumulative dry mass of the sediment in the core	$\text{Log}(C_{t_x}) = \text{Log}(C_0)\ e^{-\lambda \frac{m}{MAR}}$
Constant Initial Concentration model (CIC)	· Assumes a constant activity of unsupported ^{210}Pb in each sediment layer as it is formed · Increases in the flux of sedimentary particles from the water column will proportionally increase amounts of unsupported ^{210}Pb deposited to the sediment floor	$C_{t_x} = C_0 e^{-\lambda t_x}$
Constant Rate of Supply model (CRS)	· Assumes a constant fallout of ^{210}Pb from the atmosphere, yielding a constant rate of supply of unsupported ^{210}Pb to the sediment surface · Unsupported ^{210}Pb of the initial activity (at time zero) will be inversely proportional to the mass accumulation rate, such that increases in burial driven by sediment erosion or autochthonous production results in dilution of unsupported ^{210}Pb	$A_{t_x} = A_0 e^{-\lambda t_x}$

Symbols used in tables: $\boldsymbol{\lambda}$, ^{210}Pb disintegration constant (λ = 0.03114 year^{-1}); $\boldsymbol{m}$, Cumulative dry mass of sediment (g); $\boldsymbol{MAR}$, Sediment mass accumulation rate (g cm^{-2} year^{-1}); $\boldsymbol{C_{t_x}}$, Unsupported ^{210}Pb activity at time t_x (Bq kg^{-1}); $\boldsymbol{t_x}$, Time x (in years); $\boldsymbol{\Delta t}$, Elapsed time between the deposition of two intervals ($\Delta t = t_i - t_j$, years); $\boldsymbol{A_{t_x}}$, $^{210}Pb_{unsupp.}$ accumulated below interval corresponding to time t_x (Bq m^{-2});

Figure E1. Graphical representation of the three chronological models with associated assumptions and equations regarding age-establishment. (Top) Constant Flux Constant Sedimentation (C.F.C.S.); (Center) Constant Initial Concentration (C.I.C.); (Bottom) Constant

Rate of Supply (C.R.S.). For each model, the black line represents the model's graphical assumption. Modified from Baud et al., (2022).

Further confidence in a chronology can be improved through independent validation, for example by using annually laminated sediment (i.e., varves) or other independent markers to ensure an accurate age assignment to sediment intervals. To this end, other radioisotopes, such as Cesium-137 (^{137}Cs) have been used to validate chronologies. Peak abundance of ^{137}Cs is expected to occur around 1963 CE, as a result of atmospheric nuclear testing (Wright et al., 1999). Another peak of ^{137}Cs is also expected around 1986 CE, mainly over north Europe, associated with the Chernobyl explosion. However, some concerns exist regarding the mobility of this isotope in the sedimentary columns, particularly in organic rich sediment matrices (Davis et al., 1984; Klaminder et al., 2012). Other independent markers, such as the emergence of pollen species, such as *Ambrosia* (ragweed), have also been used (Blais et al., 1995). This marker is associated with the onset of European colonization and development of European-style farming across the Americas. While the establishment of sediment chronologies is important to contextualize environmental change adequately, these chronologies also serve to determine lake sedimentation rates. In turn, lake sedimentation rates can provide insight into various aspects of lake health such as oxygenation conditions of the water column, nutrient budgets (Räsänen et al., 1992) and water clarity (Schiefer et al., 2013).

The environmental significance of lake sedimentation rates

Lake sedimentation rates hold a very important control on lake processes and have high significance for global geochemical budgets (Foster et al., 2011; Anderson et al., 2020). For example, sedimentation rates have the potential to greatly influence the amount of carbon that is stored within lake sediments, an important “sink” in global carbon budget (Heathcote et al., 2015). In reservoirs, lake sedimentation rate is also very important as it can contribute to the reduction of hydroelectric potential of a system over time (United States. Soil Conservation, 1983; Wang and Chunhong, 2009), thus requiring intensive management implications. Since sedimentation rates encapsulate the gross burial of matter, collected by lakes across their catchment and from the production within their water column, lake sediments can yield many insights into the functioning of an ecosystem. To date there has been limited number of published synthetic studies on lake sedimentation rates; one example Brothers et al.’s (2008) global synthesis which reported that large-scale geographical variables such as latitude explained significant variation in lake sedimentation rates. Examples of regional-scale investigations of lake sedimentation rates include the North American Paleoecological Investigations of Recent Lake Acidification (PIRLA) project where sediment cores from 32 lakes distributed across four regions (Adirondack Mountains, Northern New England, Northern Florida and Northern Great Lakes) were collected. This work demonstrated that increasing lake sedimentation rates were associated with recent catchment disturbances (as expected) and potentially further influenced by increases in atmospheric nitrogen deposition (Binford et al., 1993). The European synthesis of lake sedimentation rates led by Rose et al. (2011) also demonstrated temporal increases in lake sediment accumulation rates in over 70% of the 207 lakes sampled and reported on the important heterogeneity in the sediment accumulation rates compiled across lake types. Mountainous lakes had, on average, sediment accumulation rates 10-times below the rates measured from lowland high alkalinity lakes (Rose et al., 2011).

This important heterogeneity in lake sedimentation rates can be further influenced by conditions of lake watersheds, especially considering topography and dominating land-use (Blais and Kalff, 1995; Crann et al., 2015; Bonk et al., 2016). Recently, Jenny et al. (2019) have reported on an increase in the rate of lake sedimentation rates at the end of the Holocene. Their paired analyses of pollen records provided convincing data that sedimentation rates increased when forested watersheds were converted into croplands. Overall, the literature suggests that changes in land-use and geographical features can explain variation in sedimentation rates within a sediment core and among lake cores.

Anthropogenic development and its impact on the environment and the significance of lake sediment archives

While imprints of anthropogenic pollution can be traced back to pre-industrial times (Abbott and Wolfe, 2003; Cooke and Bindler, 2015), as early as the Roman period (Hong et al., 1994), it is since the inception of the Industrial Revolution that the production, deposition and cycling of numerous elements have been most dramatically modified (Boden et al., 2017; Hoesly et al., 2018). Many elements have been subjected to important increases in their production and deposition on the landscape. For example, using 47 ^{210}Pb-dated sediment cores collected across North-Eastern America, an area of important anthropogenic development, Dunnington et al. (2020) demonstrated that the majority of lakes records showed a relative increase in anthropogenic lead concentrations starting between 1880 – 1920 CE. Similar patterns in concentration and accumulation rates have also been reported for other heavy metals (Cd, Cr, Hg, Zn), which have been the focus of ore mining across many locations on the globe since the early 1800s (Muir et al., 2009; Kelly et al., 2010; Engstrom et al., 2014). These elements can make their way to the environment through wet and dry deposition, having been volatilized in the atmosphere from the smelting of ores containing a fraction of these metals (Nriagu and Coker, 1983; Jasiak et al., 2021). As was recognized early on by Goldschmidt, these elements often appear as a mix of sulphur-compounds, owing their classification of Chalcophile elements (Goldschmidt, 1954). This co-occurrence of metals and sulfur leads to further consequences when smelted because smelting of these ores will release sulfur-based products such as sulphate (SO_4^{2-}) (Nriagu and Coker, 1983; Keller et al., 2001). SO_4^{2-} is known to contribute to the acidification of the landscape (Schindler et al., 1980; Ginn et al., 2007). An infamous example comes from the region of Sudbury, Ontario, where metallurgical development led elevated rates of acid-deposition in the 1950s and 1970s (Dixit et al., 1987; Palmer et al., 1989; Keller et al., 2019), mediated from the smelting of these elements. Together with the increased production and release of these heavy metals, other compounds such as carbon dioxide (CO_2) were also released and contributed to a warming atmosphere.

As stated in the most recent report from the International Panel Climate Change (IPCC), human-mediated release of greenhouse gases has warmed the climate at a rate unprecedented over the last 2000 years (Pörtner et al., 2022). This warming has had and continues to have tremendous repercussions in many areas of the world, especially at extreme latitudes where the effects of global warming has been elevated (Kerr, 2007; Deutsch et al., 2008). The release and warming potential of these greenhouse gases have participated in the modification of numerous sediment-mediated biogeochemical cycles (Monteith et al., 2007; Gu and Adler, 2013; Huisman et al., 2018). Along with modifications of these biogeochemical cycles, anthropogenic development has also precipitated important modifications on Earth's hydrological cycles (Syvitski et al., 2005; Grill et al., 2015; Grill et al., 2019). As described in Syvitski et al. (2005), with the creation of numerous reservoirs for hydro-electrical power generation or increased flow control, the extent of sediment reaching the ocean coastline from the mainland has dramatically been reduced.

Emerging technologies for the study of environmental change in lake sediment

To investigate the relative environmental change experienced by a region as captured by lake sediment, it is important to have access to high-resolution time series data. This is especially relevant when considering the modifications that have occurred across the last ~200 years. Sedimentation rates are expected, for many lakes, to be low, with lakes generally accumulating between 0.1 – 1 mm of sediment per year (Brothers et al., 2008). Thus, having to rely on discrete sediment intervals, subsampled at 1 cm or 0.5 cm have the potential to incorporate between 5 years to ~100 years of sediment accumulation per interval. In the last decade, new technologies have emerged enabling the study of lake sediment physical and geochemical properties at a millimetric to sub-millimetric resolution (Rothwell and Rack, 2006). These technologies include scanners, such as the micro-X-ray fluorescence (XRF) (Croudace et al., 2006a) or the computed tomography (CT) scanners (Ashi, 1997; Fouinat et al., 2017). The former has been developed to generate elemental relative abundance data from lake sediment archives. XRF scanners rely on measuring emission energy of the core upon excitation at specific energies (Croudace et al., 2006b), expressing elemental counts as a measure of fluorescence intensity (count per second – cps). In the literature, this tool is often reported as being semi-quantitative (Naeher et al., 2013; Avşar et al., 2014). That is, XRF scanners are only thought to be able to provide insights into the relative change when considering a single core. While there are many applications targeting a single core or multiple cores from the same lake (e.g., Miller et al., 2015; Gregory et al., 2019b; Davidson et al., 2021), applications comparing cores from multiple lakes remain limited. XRF scanners have been used across both the marine and inland water ecosystems, and numerous studies have reported on the importance of various elemental proxies (Croudace and Rothwell, 2015). Recent applications of XRF-scanners have been used to track environmental metal pollution, by estimating the relative abundance of heavy metals in the sediment (McComb et al., 2014; Fielding et al., 2020). These scanners are also useful to estimate the erosive fraction of lake sediment that is usually rich in titanium, strontium, aluminum and rubidium (Boës et al., 2011; Barreiro-Lostres et al., 2015). Other biogenic or chemical properties at the water-sediment interface have also been reported in the literature (Kalugin et al., 2007; Stepanova et al., 2015; Chawchai et al., 2016).

Several authors have suggested that with additional processing of XRF-data, one can harness the full quantitative nature of XRF-data, but little consensus exists over the processing of XRF data. To this end, multiple authors have attempted to compare XRF data with elemental concentrations derived from classical analytical chemistry via Inductively Coupled Plasma Mass Spectrometry (ICP-MS) or Inductively Coupled Plasma Atomic Emission Spectroscopy (ICP-AES) (Gregory et al., 2019a). One publication that attempted this comparison relied on the normalization of XRF-wet sediment abundance to dry sediment (i.e., dividing by water content or density) (Gregory et al., 2019b). Another publication which assessed the comparison of XRF-generated abundance data with elemental concentrations standardized XRF elemental intensities using statistical techniques aimed at reducing the residual covariance associated with compositional data (Weltje et al., 2015). However, no one has yet tested multiple calibration methods using a suite of sediment cores collected from numerous lakes.

Objectives of the thesis

From this literature review, we identified multiple knowledge gaps pertaining to our understanding of global environmental change and its influence on the physical and geochemical properties of lake sediments. One of the current limitations that this thesis aims to bridge is to integrate local studies and regional syntheses to consider dynamics and drivers at more global scale, considering lake sedimentation rates since the onset of the Industrial Revolution. Our knowledge of the predictors associated with variation in lake sedimentation rates over this period is also limited, but land use has emerged in several previous studies. The first chapter of this thesis aims to fill these gaps by creating a global database of lake sedimentation rates using published records. Using this database, the goal is to evaluate spatial and temporal distribution in lake sedimentation rates over the last ~200 years. To consider the contribution of land-use within a lake watershed, this feature was delineated using digital elevation models, and then applied to extract the land-use associated with each lake. Building on observations from this first chapter, my second chapter addresses the temporal and spatial variation in lake sedimentation rate over regions of Eastern Canada. Focusing on a smaller geographical extent serves as a test to evaluate whether similar inferences as the ones observed from global variation in lake sedimentation rates can be drawn. Adapting to this spatial extent, chapter II quantifies the contribution of land-use and climate on variation in lake sedimentation rates using data gathered from Canadian historical census surveys and Canadian historical meteorological stations. For this second chapter, I collected a network of 37 sediment cores from Eastern Canada and established lake sediment chronologies using ^{210}Pb. Despite its ubiquitous use, the establishment of lake sediment ^{210}Pb chronologies has often demonstrated a lack of repeatability and uniformity across research laboratories. Hence, in addition to providing a sense of the variation in sedimentation rates experienced within this region, this second chapter will also serve as an opportunity to generate a framework aimed to improve on the reproducibility of ^{210}Pb chronological establishment.

While chapter I and chapter II address the influence of global environmental change on the physical properties of lake sediments, chapter III and chapter IV consider the geochemical variation archived in lake sediments over the last ~200 years. To improve on our current knowledge of the magnitude, scale and frequency of impacts induced by anthropogenic development over this period, chapter III relies on the use of emerging instruments, such as XRF-scanners, tailored towards the quantification of geochemical abundances in lacustrine sediment archives. These high-resolution data will serve to investigate the spatio-temporal distribution of multiple lake sediment geochemical constituents to characterize the specific sediment geochemical constituents potentially responsible for observed differences across Eastern Canada. This third chapter also aims to shed light on the standardization requirements to improve the applicability of XRF-scanners intensities with their comparison with elemental concentrations generated from more classical wet chemistry extraction and analytical methods (i.e., ICP-AES and ICP-MS). Lastly, my fourth chapter aims to improve our current understanding of the mechanisms involved in the burial of various sediment constituents, focusing specifically on elemental lead. While common stressors of lake health, such as eutrophication and acidification are expected to have the potential to influence the accumulation of sedimentary constituents, these processes are often masked when performing regional sampling programs like the ones conducted in my 3rd chapter because within lake and watershed processes happen simultaneously. To clearly resolve the burial processes associated with the impact of these stressors directly on lakes, it would be favorable to isolate specific drivers in experimental settings. To this end, I retrieved for this chapter sediment cores from lakes located in the Experimental Lakes Area (IISD-ELA), where experimental lake acidification and eutrophication have been carried out since the late 1960s. As such, the study of these sediment archives has the potential to enable the isolation of specific drivers associated with experimental settings, whereby some of the complex interactions among emission, transport and burial processes would be reduced, allowing for the identification of the mechanisms and potential thresholds influential in the accumulation of elemental lead in lake sediments.

References

Abbott, M.B., Wolfe, A.P., 2003. Intensive pre-Incan metallurgy recorded by lake sediments from the Bolivian Andes. Science, 301, 1893-1895

Ady, F.D., Patoine, A., 2016. Impacts of land use and climate variability on algal communities since~ 1850 CE in an oligotrophic estuary in northeastern New Brunswick, Canada. J. Paleolimnol., 55, 151-165

Anderson, N.J., Engstrom, D.R., Leavitt, P.R., Flood, S.M., Heathcote, A.J., 2020. Changes in coupled carbon–nitrogen dynamics in a tundra ecosystem predate post-1950 regional warming. Communications Earth & Environment, 1, 1-6

Appleby, P., 1998. Dating recent sediments by 210 Pb: Problems and solutions.

Appleby, P., 2002. Chronostratigraphic techniques in recent sediments, Tracking environmental change using lake sediments. Springer, pp. 171-203.

Appleby, P., Oldfieldz, F., 1983. The assessment of 210Pb data from sites with varying sediment accumulation rates. Hydrobiologia, 103, 29-35

Appleby, P.G., Oldfield, F., 1978. The calculation of lead-210 dates assuming a constant rate of supply of unsupported 210Pb to the sediment. Catena, 5, 1-8

Ashi, J., 1997. 11. COMPUTED TOMOGRAPHY SCAN IMAGE ANALYSIS OF SEDIMENTS1.

Avşar, U., Hubert-Ferrari, A., Jónsson, S., De Batist, M., Fagel, N., Geirsdóttir, Á., Miller, G.H., 2014. A semi-quantitative method to estimate organic matter content of lake sediments using ITRAX micro-XRF core scanner data, EGU General Assembly Conference Abstracts, pp. 10704

Barreiro-Lostres, F., Brown, E., Moreno, A., Morellón, M., Abbott, M., Hillman, A., Giralt, S., Valero-Garcés, B., 2015. Sediment delivery and lake dynamics in a Mediterranean mountain watershed: Human-climate interactions during the last millennium (El Tobar Lake record, Iberian Range, Spain). Sci. Total Environ., 533, 506-519. https://doi.org/10.1016/j.scitotenv.2015.06.123

Barsanti, M., Garcia-Tenorio, R., Schirone, A., Rozmaric, M., Ruiz-Fernández, A.C., Sanchez-Cabeza, J.-A., Delbono, I., Conte, F., Godoy, J.D.O., Heijnis, H., 2020. Challenges and limitations of the 210Pb sediment dating method: Results from an IAEA modelling interlaboratory comparison exercise. Quaternary Geochronology, 59, 101093

Bennion, H., Simpson, G.L., 2011. The use of diatom records to establish reference conditions for UK lakes subject to eutrophication. J. Paleolimnol., 45, 469-488

Binford, M.W., Kahl, J.S., Norton, S.A., 1993. Interpretation of 210Pb profiles and verification of the CRS dating model in PIRLA project lake sediment cores. J. Paleolimnol., 9, 275-296

Blaauw, M., Christen, J.A., 2011. Flexible paleoclimate age-depth models using an autoregressive gamma process. Bayesian analysis, 6, 457-474

Blais, J.M., Kalff, J., 1995. The influence of lake morphometry on sediment focusing. Limnol. Oceanogr., 40, 582-588

Blais, J.M., Kalff, J., Cornett, R.J., Evans, R.D., 1995. Evaluation of210Pb dating in lake sediments using stable Pb, Ambrosia pollen, and137Cs. J. Paleolimnol., 13, 169-178

Bloemsma, M., Zabel, M., Stuut, J., Tjallingii, R., Collins, J.A., Weltje, G.J., 2012. Modelling the joint variability of grain size and chemical composition in sediments. Sedimentary Geology, 280, 135-148

Boden, T., Andres, R., Marland, G., 2017. Global, regional, and national fossil-fuel co2 emissions (1751-2014)(v. 2017), Environmental System Science Data Infrastructure for a Virtual Ecosystem (ESS-DIVE) (United States); Carbon Dioxide Information Analysis Center (CDIAC), Oak Ridge National Laboratory (ORNL), Oak Ridge, TN (United States).

Boës, X., Rydberg, J., Martinez-Cortizas, A., Bindler, R., Renberg, I., 2011. Evaluation of conservative lithogenic elements (Ti, Zr, Al, and Rb) to study anthropogenic element enrichments in lake sediments. J. Paleolimnol., 46, 75-87. https://doi.org/10.1007/s10933-011-9515-z

Bonk, A., Kinder, M., Enters, D., Grosjean, M., Meyer-Jacob, C., Tylmann, W., 2016. Sedimentological and geochemical responses of Lake Żabińskie (north-eastern Poland) to erosion changes during the last millennium. J. Paleolimnol., 56, 239-252

Brothers, S., Vermaire, J.C., Gregory-Eaves, I., 2008. Empirical models for describing recent sedimentation rates in lakes distributed across broad spatial scales. J. Paleolimnol., 40, 1003-1019

Chawchai, S., Kylander, M.E., Chabangborn, A., Löwemark, L., Wohlfarth, B., 2016. Testing commonly used X-ray fluorescence core scanning-based proxies for organic-rich lake sediments and peat. Boreas, 45, 180-189

Cheng, Y., Baud, A., Gregory-Eaves, I., Simmatis, B., Smol, J.P., Griffiths, K., 2022. Climate change and nutrient enrichment altering sedimentary diatom assemblages since pre-industrial time: evidence from Canada’s most populated ecozone.

Cooke, C.A., Bindler, R., 2015. Lake sediment records of preindustrial metal pollution, Environmental contaminants. Springer, pp. 101-119.

Crann, C.A., Patterson, R.T., Macumber, A.L., Galloway, J.M., Roe, H.M., Blaauw, M., Swindles, G.T., Falck, H., 2015. Sediment accumulation rates in subarctic lakes: Insights into age-depth modeling from 22 dated lake records from the Northwest Territories, Canada. Quaternary Geochronology, 27, 131-144

Cremer, H., Bunnik, F., Donders, T., Hoek, W., Koolen-Eekhout, M., Koolmees, H., Lavooi, E., 2010. River flooding and landscape changes impact ecological conditions of a scour hole lake in the Rhine-Meuse delta, The Netherlands. J. Paleolimnol., 44, 789-801

Croudace, I., Rindby, A., Rothwell, R., 2006a. New techniques in sediment core analysis. Geological Society Special Publication

Croudace, I.W., Rindby, A., Rothwell, R.G., 2006b. ITRAX: description and evaluation of a new multi-function X-ray core scanner. Geological Society, London, Special Publications, 267, 51-63

Croudace, I.W., Rothwell, R.G., 2015. Micro-XRF Studies of Sediment Cores: Applications of a non-destructive tool for the environmental sciences. Springer. 9401798494

Crozaz, G., Picciotto, E., De Breuck, W., 1964. Antarctic snow chronology with Pb210. Journal of Geophysical Research, 69, 2597-2604

Davidson, K.B., Holmes, B.E., Spooner, I.S., Dunnington, D.W., Walker, T.R., Lake, C.B., Su, C.-C., 2021. Application of the paleolimnological method to assess metal contaminant distribution (As, Cu, Pb, Zn) in pulp mill stabilization basin sediments, Nova Scotia, Canada. Environ. Sci. Pollut. Res., 28, 51342-51355. https://doi.org/10.1007/s11356-021-14212-x

Davis, R.B., Hess, C.T., Norton, S.A., Hanson, D.W., Hoagland, K.D., Anderson, D.S., 1984. 137Cs and 210Pb dating of sediments from soft-water lakes in New England (USA) and Scandinavia, a failure of 137Cs dating. Chem. Geol., 44, 151-185

Deutsch, C.A., Tewksbury, J.J., Huey, R.B., Sheldon, K.S., Ghalambor, C.K., Haak, D.C., Martin, P.R., 2008. Impacts of climate warming on terrestrial ectotherms across latitude. PNAS, 105, 6668-6672

Dixit, S.S., Dixit, A.S., Evans, R.D., 1987. Paleolimnological evidence of recent acidification in two Sudbury (Canada) lakes. Sci. Total Environ., 67, 53-67

Dunnington, D.W., Roberts, S., Norton, S.A., Spooner, I.S., Kurek, J., Kirk, J.L., Muir, D.C., White, C.E., Gagnon, G.A., 2020. The distribution and transport of lead over two centuries as recorded by lake sediments from northeastern North America. Sci. Total Environ., 737, 140212. https://doi.org/10.1016/j.scitotenv.2020.140212

Engstrom, D.R., Fitzgerald, W.F., Cooke, C.A., Lamborg, C.H., Drevnick, P.E., Swain, E.B., Balogh, S.J., Balcom, P.H., 2014. Atmospheric Hg emissions from preindustrial gold and silver extraction in the Americas: A reevaluation from lake-sediment archives. Environ. Sci. Technol., 48, 6533-6543

Fielding, J.J., Croudace, I.W., Kemp, A.E., Pearce, R.B., Cotterill, C.J., Langdon, P., Avery, R., 2020. Tracing lake pollution, eutrophication and partial recovery from the sediments of Windermere, UK, using geochemistry and sediment microfabrics. Sci. Total Environ., 722, 137745. https://doi.org/10.1016/j.scitotenv.2020.137745

Foster, I.D., Collins, A., Naden, P., Sear, D., Jones, J., Zhang, Y., 2011. The potential for paleolimnology to determine historic sediment delivery to rivers. J. Paleolimnol., 45, 287-306

Fouinat, L., Sabatier, P., Poulenard, J., Reyss, J.-L., Montet, X., Arnaud, F., 2017. A new CT scan methodology to characterize a small aggregation gravel clast contained in a soft sediment matrix. Earth Surface Dynamics, 5, 199-209

Fraterrigo, J.M., Downing, J.A., 2008. The influence of land use on lake nutrients varies with watershed transport capacity. Ecosystems, 11, 1021-1034

Ginn, B.K., Cumming, B.F., Smol, J.P., 2007. Long-term lake acidification trends in high-and low-sulphate deposition regions from Nova Scotia, Canada. Hydrobiologia, 586, 261-275

Goldschmidt, V.M., 1954. Geochemistry. LWW. 0038-075X

Gregory, B.R., Patterson, R.T., Reinhardt, E.G., Galloway, J.M., 2019a. The iBox-FC: A new containment vessel for Itrax X-ray fluorescence core-scanning of freeze cores. Quat. Int., 514, 76-84

Gregory, B.R., Patterson, R.T., Reinhardt, E.G., Galloway, J.M., Roe, H.M., 2019b. An evaluation of methodologies for calibrating Itrax X-ray fluorescence counts with ICP-MS concentration data for discrete sediment samples. Chem. Geol., 521, 12-27. https://doi.org/10.1016/j.chemgeo.2019.05.008

Griffiths, K., Jeziorski, A., Paquette, C., Taranu, Z.E., Baud, A., Antoniades, D., Beisner, B., Hamilton, P.B., Smol, J.P., Gregory-Eaves, I., 2021. Multi-trophic level responses to environmental stressors over the past~ 150 years: Insights from a lake-rich region of the world. Ecol. Indicators, 127, 107700

Grill, G., Lehner, B., Lumsdon, A.E., MacDonald, G.K., Zarfl, C., Liermann, C.R., 2015. An index-based framework for assessing patterns and trends in river fragmentation and flow regulation by global dams at multiple scales. Environ. Res. Lett., 10, 015001. http://dx.doi.org/10.1088/1748-9326/10/1/015001

Grill, G., Lehner, B., Thieme, M., Geenen, B., Tickner, D., Antonelli, F., Babu, S., Borrelli, P., Cheng, L., Crochetiere, H., 2019. Mapping the world's free-flowing rivers. Nature, 569, 215-221

Gu, G., Adler, R.F., 2013. Interdecadal variability/long-term changes in global precipitation patterns during the past three decades: global warming and/or pacific decadal variability? ClDy, 40, 3009-3022

Heathcote, A.J., Anderson, N.J., Prairie, Y.T., Engstrom, D.R., Del Giorgio, P.A., 2015. Large increases in carbon burial in northern lakes during the Anthropocene. Nature Communications, 6, 1-6

Helms, J.R., Mao, J., Schmidt-Rohr, K., Abdulla, H., Mopper, K., 2013. Photochemical flocculation of terrestrial dissolved organic matter and iron. Geochimica et Cosmochimica Acta, 121, 398-413

Hoesly, R.M., Smith, S.J., Feng, L., Klimont, Z., Janssens-Maenhout, G., Pitkanen, T., Seibert, J.J., Vu, L., Andres, R.J., Bolt, R.M., 2018. Historical (1750–2014) anthropogenic emissions of reactive gases and aerosols from the Community Emissions Data System (CEDS). Geosci. Model Dev., 11, 369-408

Hong, S., Candelone, J.-P., Patterson, C.C., Boutron, C.F., 1994. Greenland ice evidence of hemispheric lead pollution two millennia ago by Greek and Roman civilizations. Science, 265, 1841-1843

Huang, C.C., MacDonald, G., Cwynar, L., 2004. Holocene landscape development and climatic change in the low arctic, Northwest Territories, Canada. Palaeogeogr., Palaeoclimatol., Palaeoecol., 205, 221-234

Huisman, J., Codd, G.A., Paerl, H.W., Ibelings, B.W., Verspagen, J.M., Visser, P.M., 2018. Cyanobacterial blooms. Nature Reviews Microbiology, 16, 471-483

Jambrina-Enríquez, M., Sachse, D., Valero-Garcés, B.L., 2016. A deglaciation and Holocene biomarker-based reconstruction of climate and environmental variability in NW Iberian Peninsula: the Sanabria Lake sequence. J. Paleolimnol., 56, 49-66

Jasiak, I., Wiklund, J., Leclerc, E., Telford, J., Couture, R., Venkiteswaran, J., Hall, R., Wolfe, B., 2021. Evaluating spatiotemporal patterns of arsenic, antimony, and lead deposition from legacy gold mine emissions using lake sediment records. Appl. Geochem., 134, 105053. https://doi.org/10.1016/j.apgeochem.2021.105053

Jenny, J.P. et al., 2019. Human and climate global-scale imprint on sediment transfer during the Holocene. Proc Natl Acad Sci U S A, 116, 22972-22976. 10.1073/pnas.1908179116

Jeziorski, A., Yan, N.D., Paterson, A.M., DeSellas, A.M., Turner, M.A., Jeffries, D.S., Keller, B., Weeber, R.C., McNicol, D.K., Palmer, M.E., 2008. The widespread threat of calcium decline in fresh waters. Science, 322, 1374-1377

Kahlert, M., Rühland, K.M., Lavoie, I., Keck, F., Saulnier-Talbot, E., Bogan, D., Brua, R.B., Campeau, S., Christoffersen, K.S., Culp, J.M., 2022. Biodiversity patterns of Arctic diatom assemblages in lakes and streams: Current reference conditions and historical context for biomonitoring. Freshwat. Biol., 67, 116-140

Kalugin, I., Daryin, A., Smolyaninova, L., Andreev, A., Diekmann, B., Khlystov, O., 2007. 800-yr-long records of annual air temperature and precipitation over southern Siberia inferred from Teletskoye Lake sediments. Quaternary Research, 67, 400-410. https://doi.org/10.1016/j.yqres.2007.01.007

Keller, W., Heneberry, J., Edwards, B.A., 2019. Recovery of acidified Sudbury, Ontario, Canada, lakes: a multi-decade synthesis and update. Environ. Rev., 27, 1-16

Keller, W.B., Dillon, P., Heneberry, J., Malette, M., Gunn, J., 2001. Sulphate in Sudbury, Ontario, Canada, lakes: recent trends and status. Water, Air, Soil Pollut., 130, 793-798

Kelly, E.N., Schindler, D.W., Hodson, P.V., Short, J.W., Radmanovich, R., Nielsen, C.C., 2010. Oil sands development contributes elements toxic at low concentrations to the Athabasca River and its tributaries. PNAS, 107, 16178-16183

Kerr, R.A., 2007. Global warming is changing the world. Science, 316, 188-190

Klaminder, J., Appleby, P., Crook, P., Renberg, I., 2012. Post-deposition diffusion of 137Cs in lake sediment: Implications for radiocaesium dating. Sedim, 59, 2259-2267

Landers, D.H., Simonich, S., Jaffe, D., Geiser, L., Campbell, D.H., Schwindt, A., Schreck, C., Kent, M., Hafner, W., Taylor, H.E., 2008. The fate, transport, and ecological impacts of airborne contaminants in western national parks (USA). Western Airborne Contaminants Assessment Project Final Report. Corvallis

Last, W.M., Smol, J.P., 2002a. Tracking Environmental Change Using Lake Sediments: Volume 1: Basin Analysis, Coring, and Chronological Techniques. Springer Science & Business Media. 0792364821

Last, W.M., Smol, J.P., 2002b. Tracking environmental change using lake sediments: volume 2: physical and geochemical methods. Springer Science & Business Media. 1402006284

McComb, J.Q., Rogers, C., Han, F.X., Tchounwou, P.B., 2014. Rapid screening of heavy metals and trace elements in environmental samples using portable X-ray fluorescence spectrometer, A comparative study. Water, Air, Soil Pollut., 225, 1-10

Messager, M.L., Lehner, B., Grill, G., Nedeva, I., Schmitt, O., 2016. Estimating the volume and age of water stored in global lakes using a geo-statistical approach. Nature communications, 7, 1-11

Meybeck, M., 1995. Global distribution of lakes, Physics and chemistry of lakes. Springer, pp. 1-35.

Miller, H., Croudace, I.W., Bull, J.M., Cotterill, C.J., Dix, J.K., Taylor, R.N., 2015. Modern pollution signals in sediments from Windermere, NW England, determined by micro-XRF and lead isotope analysis, Micro-XRF Studies of Sediment Cores. Springer, pp. 423-442.

Monteith, D.T., Stoddard, J.L., Evans, C.D., De Wit, H.A., Forsius, M., Høgåsen, T., Wilander, A., Skjelkvåle, B.L., Jeffries, D.S., Vuorenmaa, J., 2007. Dissolved organic carbon trends resulting from changes in atmospheric deposition chemistry. Nature, 450, 537-540

Muir, D., Wang, X., Yang, F., Nguyen, N., Jackson, T., Evans, M., Douglas, M., Kock, G., Lamoureux, S., Pienitz, R., 2009. Spatial trends and historical deposition of mercury in eastern and northern Canada inferred from lake sediment cores. Environ. Sci. Technol., 43, 4802-4809

Naeher, S., Gilli, A., North, R.P., Hamann, Y., Schubert, C.J., 2013. Tracing bottom water oxygenation with sedimentary Mn/Fe ratios in Lake Zurich, Switzerland. Chem. Geol., 352, 125-133. https://doi.org/10.1016/j.chemgeo.2013.06.006

Nelson, D.E., Korteling, R.G., Stott, W.R., 1977. Carbon-14: direct detection at natural concentrations. Science, 198, 507-508

Nriagu, J.O., Coker, R.D., 1983. Sulphur in sediments chronicles past changes in lake acidification. Nature, 303, 692-694

Palmer, G., Dixit, S., Macarthur, J., Smol, J., 1989. Elemental analysis of lake sediment from Sudbury, Canada, using particle-induced X-ray emission. Sci. Total Environ., 87, 141-156

Porcal, P., Koprivnjak, J.-F., Molot, L.A., Dillon, P.J., 2009. Humic substances—part 7: the biogeochemistry of dissolved organic carbon and its interactions with climate change. Environ. Sci. Pollut. Res., 16, 714-726

Pörtner, H.O., Roberts, D.C., Adams, H., Adler, C., Aldunce, P., Ali, E., Begum, R.A., Betts, R., Kerr, R.B., Biesbroek, R., 2022. Climate change 2022: impacts, adaptation and vulnerability.

Räsänen, M., Salonen, V.-P., Salo, J., Walls, M., Sarvala, J., 1992. Recent history of sedimentation and biotic communities in Lake Pyhäjärvi, SW Finland. J. Paleolimnol., 7, 107-126

Richard Albert, M., Chen, G., MacDonald, G.K., Vermaire, J.C., Bennett, E.M., Gregory-Eaves, I., 2010. Phosphorus and land-use changes are significant drivers of cladoceran community composition and diversity: an analysis over spatial and temporal scales. Can. J. Fish. Aquat. Sci., 67, 1262-1273

Rodriguez, A., McKee, B., Miller, C., Bost, M., Atencio, A., 2020. Coastal sedimentation across North America doubled in the 20th century despite river dams. Nature communications, 11, 1-9

Rose, N.L., Morley, D., Appleby, P.G., Battarbee, R.W., Alliksaar, T., Guilizzoni, P., Jeppesen, E., Korhola, A., Punning, J.-M., 2011. Sediment accumulation rates in European lakes since AD 1850: trends, reference conditions and exceedence. J. Paleolimnol., 45, 447-468

Rothwell, R.G., Rack, F.R., 2006. New techniques in sediment core analysis: an introduction. Geological Society, London, Special Publications, 267, 1-29. https://doi.org/10.1144/GSL.SP.2006.267.01.01

Ruggiu, D., Luglié, A., Cattaneo, A., Panzani, P., 1998. Paleoecological evidence for diatom response to metal pollution in Lake Orta (N. Italy). J. Paleolimnol., 20, 333-345

Russell, E.W., Davis, R.B., Anderson, R.S., Rhodes, T.E., Anderson, D.S., 1993. Recent centuries of vegetational change in the glaciated north-eastern United States. J. Ecol., 647-664

Sanchez-Cabeza, J., Ruiz-Fernández, A., 2012. 210Pb sediment radiochronology: an integrated formulation and classification of dating models. Geochimica et Cosmochimica Acta, 82, 183-200

Schiefer, E., Petticrew, E.L., Immell, R., Hassan, M.A., Sonderegger, D.L., 2013. Land use and climate change impacts on lake sedimentation rates in western Canada. Anthropocene, 3, 61-71

Schindler, D., Hesslein, R., Wagemann, R., Broecker, W., 1980. Effects of acidification on mobilization of heavy metals and radionuclides from the sediments of a freshwater lake. Can. J. Fish. Aquat. Sci., 37, 373-377

Stepanova, O., Trunova, V., Sidorina, A., Zvereva, V., Melgunov, M., Petrovskii, S., Krapivina, S., Fedotov, A., Rakshun, Y.V., 2015. Investigating bottom sediments from proglacial Lake Ehoy (Eastern Sayan Ridge) by means of SR-XRF. Bulletin of the Russian Academy of Sciences: Physics, 79, 118-121

Syvitski, J.P., Vorosmarty, C.J., Kettner, A.J., Green, P., 2005. Impact of humans on the flux of terrestrial sediment to the global coastal ocean. Science, 308, 376-80. 10.1126/science.1109454

Talbot, M.R., Lærdal, T., 2000. The Late Pleistocene-Holocene palaeolimnology of Lake Victoria, East Africa, based upon elemental and isotopic analyses of sedimentary organic matter. J. Paleolimnol., 23, 141-164

Taranu, Z.E., Gregory-Eaves, I., 2008. Quantifying relationships among phosphorus, agriculture, and lake depth at an inter-regional scale. Ecosystems, 11, 715-725

Telmer, K.H., Daneshfar, B., Sanborn, M.S., Kliza-Petelle, D., Rancourt, D.G., 2006. The role of smelter emissions and element remobilization in the sediment chemistry of 99 lakes around the Horne smelter, Quebec. Geochem.: Explor. Environ., Anal., 6, 187-202. https://doi.org/10.1144/1467-7873/05-099

Tundisi, J.G., Tundisi, T.M., 2012. Limnology. CRC Press/Balkema, Leiden, The Netherlands. 10.1201/b11386

United States. Soil Conservation, S., 1983. National engineering handbook. Section 3, Sedimentation. U.S. Dept. of Agriculture, Soil Conservation Service, Washington, D.C.

Verpoorter, C., Kutser, T., Seekell, D.A., Tranvik, L.J., 2014. A global inventory of lakes based on high-resolution satellite imagery. Geophysical Research Letters, 41, 6396-6402

Wang, Z.-y., Chunhong, H., 2009. Strategies for managing reservoir sedimentation. International Journal of Sediment Research, 24, 369-384

Weltje, G.J., Bloemsma, M., Tjallingii, R., Heslop, D., Röhl, U., Croudace, I.W., 2015. Prediction of geochemical composition from XRF core scanner data: a new multivariate approach including automatic selection of calibration samples and quantification of uncertainties, Micro-XRF studies of sediment cores. Springer, pp. 507-534.

Wetzel, R.G., 1983. Limnology. 2nd ed. ed. Saunders, Philadelphia. 0030579139 9780030579134

Wigdahl-Perry, C.R., Saros, J.E., Schmitz, J., Calcote, R., Rusak, J., Anderson, D., Hotchkiss, S., 2016. Response of temperate lakes to drought: a paleolimnological perspective on the landscape position concept using diatom-based reconstructions. J. Paleolimnol., 55, 339-356

Wiklund, J.A., Kirk, J.L., Muir, D.C., Carrier, J., Gleason, A., Yang, F., Evans, M., Keating, J., 2018. Widespread atmospheric tellurium contamination in industrial and remote regions of Canada. Environ. Sci. Technol., 52, 6137-6145

Wolfe, B.B., Hall, R.I., Last, W.M., Edwards, T.W., English, M.C., Karst-Riddoch, T.L., Paterson, A., Palmini, R., 2006. Reconstruction of multi-century flood histories from oxbow lake sediments, Peace-Athabasca Delta, Canada. Hydrological Processes: An International Journal, 20, 4131-4153

Wolter, J., Lantuit, H., Herzschuh, U., Stettner, S., Fritz, M., 2017. Tundra vegetation stability versus lake-basin variability on the Yukon Coastal Plain (NW Canada) during the past three centuries. The Holocene, 27, 1846-1858

Wright, S., Howard, B., Strand, P., Nylén, T., Sickel, M., 1999. Prediction of 137Cs deposition from atmospheric nuclear weapons tests within the Arctic. Environ. Pollut., 104, 131-143

CHAPTER I - Global acceleration of lake sediment accumulation rates associated with recent human population growth and land-use changes

Alexandre Baud[1], Jean-Philippe Jenny[2], Pierre Francus[3,4] and Irene Gregory-Eaves[1]

[1]Biology Department, McGill University, Montréal, Québec, H3A 1B1, Canada

[2]Université Savoie Mont Blanc, INRAE, CARRTEL, 74200 Thonon-les-Bains, France

[3]Centre Eau Terre Environnement, Institut National de la Recherche Scientifique (INRS), Québec City, Québec, G1K 9A9, Canada

[4]GEOTOP - Research Centre on the Dynamics of the Earth System, Montréal, Québec, H2X 3Y7, Canada

Manuscript published in *Journal of Paleolimnology* in December 2021

Abstract

Sediment Accumulation Rate (SAR; measured as mm yr^{-1}) and Mass Accumulation Rate (MAR; measured as g cm^{-2} yr^{-1}) data were collected from published lake core records that spanned the past ~ 150 years, from approximately 500 sites worldwide. For each lake, key watershed characteristics including watershed size, slope, land use and climate were extracted, with the goal of quantifying the relative importance of these variables as drivers of SAR and MAR. General additive models provided evidence of accelerated global lake sediment infilling rates after AD 1950. Whereas the onset of sedimentation acceleration varied across ecoregions, global lake MAR values were found to have increased ~3-fold on average, since baseline conditions pre-1900 (i.e. $\mu_{baseline} = 0.040 \pm 0.044$ g cm^{-2} yr^{-1} and $\mu_{modern} = 0.13 \pm 0.22$ g cm^{-2} yr^{-1}). The significant drivers, identified through Linear Mixed Effect modeling of MAR time series, were watershed population density (log-transformed) and watershed cropland density (log-transformed). Our results highlight important spatial heterogeneity in SAR and MAR among lakes, precluding the use of simple modeling approaches. SAR and MAR were found to be moderately correlated to one another, despite the potential for post-depositional disparities between segments of the sediment cores. We identified organic matter content (loss-on-ignition, LOI) as a significant co-variate that could be used to correct inflated very recent SAR rates. Our empirical analyses suggest that, despite a wide range of natural variability among lakes, both SAR and MAR increased globally and the increases appear to be mainly the result of enhanced watershed activities associated with agriculture and urbanization.

Introduction

Growing human populations and changes in land use strongly alter mass fluxes and geochemical cycles on Earth (Syvitski et al. 2005; Ellis 2011; IPCC 2014; Jenny et al. 2019), with consequences for inland waters and lakes (Issaka and Ashraf 2017). More specifically, soil erosion and sediment transfer to lakes can be affected by direct and indirect human activities, such as mining (Couillard et al. 2004), emission and transport of heavy metals (Engstrom et al. 2014) or dust (Neff et al. 2008), reduction in forest cover (Schiefer et al. 2013), and expansion of cultivated (Taranu and Gregory-Eaves, 2008) and urban areas (Kim et al. 2014). With millions of lakes distributed globally (Downing et al. 2006; Verpoorter et al. 2014; Messager et al. 2016), inland water bodies are ubiquitous geographic features on Earth. Lakes have been recognized as ecological “sentinels” (Williamson et al. 2008), capable of preserving a record of changes in the hydrosphere, lithosphere and atmosphere within their sediment archives. Indeed, sediment cores provide a continuous record of past environmental conditions by accumulating material transported by riverine networks, overland flow, and atmospheric deposition, as well as matter produced within the lake. With the advent in the 1970s of sediment dating techniques that use fallout ^{210}Pb (Appleby and Oldfield 1978), and growing public concern for environmental issues (Dunlap 1991), analysis of physical, biological and chemical variables in centennial-scale lake sediment records emerged as a powerful means to investigate recent environmental change (Last and Smol 2006). Over the last five decades, considerable efforts and coring programs were initiated globally, providing a rich collection of published data on recent lake sediment accumulation rates (Rose et al. 2011). Dated sediment records from around the world provided valuable insights into changes in lake sediment deposition rates and helped identify “hotspots” of sediment accumulation. Yet, synthesis of spatial-temporal variability in lake sediment accumulation rates for the last 150 years, at the global scale, is missing. Our objective in this study was to analyze the spatial and temporal distribution of recent lake sediment accumulation rates across the globe.

We used published age-depth models for lake sediment cores to create a large database of both Sediment Accumulation Rate (SAR), expressed as mm yr^{-1}, and Mass Accumulation Rate (MAR), expressed as g cm^{-2} yr^{-1}. SAR is a metric of sedimentation rates that is widely reported in the literature, enabling the creation of a large global dataset. SAR is helpful in that it can inform investigators about how long a core they must retrieve, for example, to reach pre-industrial-period sediments. Interpreting SAR records can, however, be somewhat misleading because topmost sediments in the core have not yet been subjected to biogeochemical diagenesis and compaction to the same extent as deeper sediments. The SAR metric is also prone to artifacts that result from the coring technique used, e.g. freeze coring vs. gravity coring. On the other hand, dry sediment Mass Accumulation Rate (MAR), which tends to be less widely reported relative to SAR, is not affected by compaction and dewatering because it quantifies the mass of the sediment accumulated over time (g cm^{-2} yr^{-1}). MAR also has additional strengths for global model applications. Indeed, MAR can be used in combination with measurements of concentrations of sediment variables (e.g. carbon, diatoms, pollen) to calculate burial rates in lakes and watershed-scale sediment flux (Hobbs et al. 2013; Engstrom and Rose 2013).

Because land-use modification is a key driver of changes in lake trophic state and sediment properties (Keatley et al. 2011; Jenny et al. 2016), this study tested the hypothesis that intensification of human activities within lake watersheds, expressed here as population and cropland density, has had a significant positive impact on lake sediment accumulation rates globally. At the outset, we acknowledge that climate variables temperature and precipitation may also influence lake sediment accumulation rates, and these effects should be more easily discernible in remote regions where human population densities are low and agricultural activities are minimal to non-existent. This work builds upon an earlier study by Brothers et al. (2008), who focused on mean lake sedimentation rates for the last 150 years. Here, however, we focused on both spatial and temporal variations in lake sediment accumulation rates and included watershed metrics of land use. This kind of analysis is possible when paleolimnological data are used in conjunction with geographic information system (GIS), the latter enabling drainage basin delineation and simulation of the effects of watershed land use changes (Wang et al. 2008; Bhaduri et al. 2000). A considerable amount of information is readily available with regard to past climate and historical land use (Klein 2016), which when coupled to GIS and paleolimnology, enables insights into past and current responses of lakes to natural and anthropogenic drivers.

Materials and methods

Collection and analysis of lake sedimentation rate data

Sedimentation rate data from lakes around the world, measured as SAR or MAR, were collected from 304 articles published in the *Journal of Paleolimnology* between 1988 and 2016. Estimated age and associated sediment depth were retrieved using the software Digitizeit (Rakap et al. 2016). SAR (mm yr^{-1}) for these cores was calculated by dividing the depth difference (mm) between two contiguous samples by the age difference (yr) between them. MAR (g cm^{-2} yr^{-1})

were compiled for a subset of sites (~30%) for which data were available, using a similar digitizing approach. In addition, data for Loss on Ignition (LOI), a proxy for organic matter content in sediments, were retrieved from source articles, when reported. Although not all articles reported the LOI method used, most LOI measurements followed the protocols of Dean (1974), Heiri et al. (2001) or John (2004), which consist of burning a subsample of dry, weighed sediment at 550ºC for a period of ~4 hours, re-weighing and reporting the weight lost on combustion as percent organic matter. LOI measurements were used to evaluate the potential contribution of sediment diagenesis (organic matter mineralization) after deposition, when interpreting recent elevated SAR values (mm yr^{-1}). We recorded the core retrieval method used in each study and used the information to see if we could detect differences in sediment accumulation rate that might arise from different coring techniques.

When data from more than one sediment core were available for a lake, the core from the deepest-water site was selected for this synthetic analysis. This method is consistent with the Rose et al. (2011) synthesis of European lake sedimentation rates, in which the authors found that SAR data from sediment cores taken in deep-water areas are likely to be more representative of lake-wide sediment accumulation in the basin. In cases of duplicate sediment cores, the most complete and reliably dated core was selected. Finally, when more than one dating approach was used in a lake, we selected the ^{210}Pb -dated core for which the constant rate of supply (C.R.S.) model had been applied, as most chronologies (>75%) were generated using this model (Figure I.1).

Geomorphological, human and climate drivers

Geographic coordinates, lake surface area, maximum depth and altitude measurements were collected for each lake. Where this information was not available, additional publications on the study lake were consulted. If the desired information could still not be retrieved from supplemental sources, Google Earth Pro was used to obtain the geographic coordinates and altitude of the study site. In such cases, we referred to maps in the original source paper to ensure the coordinates corresponded to the appropriate lake. Google Earth Pro was also used to calculate the surface area for small lakes, if such data were missing. A preliminary test was conducted using a set of 10 lakes with known surface areas, to verify that measurements made with Google Earth Pro were accurate. For lakes with a surface area ≥ 10 ha, each lake's polygon and hydrological drainage basin coordinates were retrieved from HydroLAKES (Messager et al. 2016); this provided information for 55% of the lakes in our database. The remaining 45% of sites were either lakes < 10 ha or lakes for which the polygon corresponded to a collection of basins that conflicted with the definition of lake presented in source articles. Not to discard 45% of the full dataset, each lake polygon was drawn manually, and its watershed was delineated using a 3-sec Flow Direction Raster layer acquired from the SHuttle Elevation Derivatives at multiple Scales (HydroSHEDS) datasets (Lehner and Grill, 2013). The flow direction layers, available from 56° South to 60° North, were derived from the Shuttle Radar Topography Mission (SRTM) digital elevation model (DEM) (https://eros.usgs.gov/) and were determined on a pixel basis from the direction of the steepest descent of a pixel to its neighboring one (Lehner et al. 2006). Digital Elevation Models (DEMs) were used to support the validity of the drawn watershed, and the measured values for catchment area, which includes lake surface area, were compared to source article values when such information was available.

The delineated watersheds were then used to extract the associated Cropland (km^2/9 km^2 grid cell) and Population Count (inhabitants/9 km^2 grid cell) over time from 1800 to 2015, using the Anthropogenic land-use estimates for the Holocene (Hyde 3.2 dataset). In cases for which the watershed was not delineated because it was outside of the 56° South to 60° North range (scope of HydroSHEDS dataset), or when smaller than the pixel from the Hyde 3.2 Land-Use registry (~9 km^2), the associated land-use value was extracted to match the point coordinate representing the centroid of the lake polygon. Using a similar approach, historical mean annual temperature and mean annual precipitation data were collected for each lake from NOAA's National Climatic Data Center (NCDC), for which the time series spans from 1900 to 2014. Terrestrial ecoregions acquired from The Nature Conservancy (http://maps.tnc.org/gis_data.html) were used to discriminate among major habitat types and biomes, which grouped together regions that experience similar climate regimes, have similar biodiversity patterns and thresholds, and have experienced comparable human development (Olson and Dinerstein 2002).

Numerical analyses

All statistical analyses were carried out using the R open-source software and map production was done using ArcMap. Average recent SAR values were mapped for all our study lakes (Figure I.2); these measurements correspond to average SAR values over a subset of our original dataset, featuring every digitized rate estimate for the time interval between AD 1963 (± 10 yrs) and the coring dates. Focusing on these more recent estimates was done to reduce errors associated with ^{210}Pb dating, which tend to be relatively small for younger dates. Often, ^{137}Cs profiles can be used as an independent marker of sediment chronology, as AD 1963 corresponds to the year of maximum global ^{137}Cs fallout from atmospheric nuclear bomb testing. Whereas ^{137}Cs activity can sometimes present problems associated with post-depositional mobility, it can be a reliable chronological marker in recent lake sediments in certain lake types (Davis et al. 1984; Klaminder et al. 2012). Hence, we consistently used the post-1963 period to define the “modern period”. Environmental and sedimentological variables responsible for significant variation in average SAR and MAR over time were identified by fitting stepwise multiple linear regression models. Log-transformation and log(x+1) transformation were used to approach normality of the residuals (Zuur et al. 2009). To reduce the potential influence of rapidly deposited event layers from, e.g., flooding, earthquakes, dam breaches, each sediment profile (SAR or MAR) was screened for outliers. This was done by independent linear interpolation of each sedimentation rate metric (SAR or MAR) across each lake for five different timesteps, which were selected by considering the time covered by the dating intervals and the numbers of dated intervals. For each of these timesteps, the absolute difference in sedimentation rate (expressed as SAR_{diff} or MAR_{diff}) between the mean value for each lake and the individual estimate (SAR or MAR) was computed. A SAR_{diff} or MAR_{diff} estimate was considered an outlier if it was more than two standard deviations away from the previous and next SAR_{diff} or MAR_{diff} estimate (Barnett and Lewis 1994). If in three or more of the five timesteps were identified any outliers within a profile, the sediment record (SAR or MAR) for that lake was removed. This criterion was justified on the basis that it independently identified all “flash sedimentary events” originally reported in source articles. This step identified 28 of 286 (10%) SAR profiles and 18 of 112 (16%) MAR profiles as containing rapidly deposited layers.

To quantify and predict temporal variations in sediment accumulation rate (SAR and MAR) globally, general additive models (GAMs) (Wallace and Green 2002) were fitted using the *mgcv* package in R (Wood 2011). This method is well suited for such analyses as the dataset is composed of repeated sedimentation rate measurements within a single core and across many lakes. Only sediment cores with five or more dated intervals were evaluated for temporal variation in SAR and MAR. We only retained records for cores retrieved by gravity, push, and Limnos corers, by divers, or by a piston or Livingstone corer, for which the core top could be visually inspected, i.e., in cases when a clear core barrel was used. As mentioned, limiting corer types reduces potential variability in deformational forces associated with coring, which could result in spurious variations in sediment accumulation rate. Finally, to reduce large errors associated with older ^{210}Pb dates (> 100 years old), the dataset was further refined to include only intervals after AD 1850. A graphical summary of the steps in our analyses are presented in Appendices Chapter I (Figure A.1). Breakpoint analyses were performed on the fitted GAM models to identify the timing of changes in the slope of response variables using R-package *davies.test::segmented* (Muggeo 2003). Although we evaluated the variation in SAR, most of our statistical analyses were designed to identify the drivers responsible for the spatio-temporal changes in MAR globally. Despite having fewer sites, our emphasis on the MAR dataset was motivated by providing more conservative estimates of modern fluxes of sediments to the lakes. We used the Mann-Kendall trend test (Mann, 1945) to evaluate the proportion of increasing and decreasing MAR trends and a *post hoc* Tukey-test (Miller, 1981;

Yandell, 1997) to assess the grouping of significant differences in MAR baseline across ecoregions. Stepwise multiple Linear Mixed Effect (LME) models were computed using the R-package (*nlme*) (Pinheiro et al. 2017) to determine the global drivers that account for the temporal variations observed in sedimentation rates. For both GAM and LME models, the R-package *ACF::itsadug* was used to investigate the structure of the residuals and to detect potential presence of temporal autocorrelation (van Rij et al. 2016). When necessary, autocorrelation classes (corAR1, corARMA) were supplied to the model and their inclusion in the equation assessed through the Akaike information criterion (AIC).

Sediment core chronologies

A total of 304 published articles were retained for digitizing purposes, providing us with 486 individual sediment age-depth profiles from unique locations. Of these 486 profiles, 422 were from lakes, 54 were from reservoirs, and the remaining 10 sites included wetlands, lagoons, or embayments (Figure I.1). Of the 486 cores digitized, 463 records were dated using ^{210}Pb, 271 measured ^{137}Cs activity and 38 used varve counting. For 367 records, core chronology was established using the constant rate of supply (C.R.S.) model, whereas the constant initial concentration (C.I.C.) model was used to develop chronologies for 42 records, and the constant flux-constant sedimentation (C.F.C.S.) model was used for 11. A few studies either did not report the model used or estimated ages using cross-correlation between empirical ^{210}Pb inventories or known stratigraphic events. From these digitized records, we were able to gather 448 Sediment Accumulation Rate (SAR) and 143 Mass Accumulation Rate (MAR) profiles. Both SAR and MAR were available for 104 cores.

Results

Predicting modern mean sediment accumulation rate (SAR)

Spatial variations in lake SAR depend on the latitudinal position of the coring site. Mean sediment accumulation rates between AD 1963 and the date of coring decreased as a function of latitude, from a mean SAR value of 3.97 ± 3.54 mm yr^{-1} at mid-latitudes (20°N - 50°N) to 1.12 ± 0.57 mm yr^{-1} in the Arctic region (65°N - 90°N). At lower and mid-latitudes (Eastern North America, Western Europe and Eastern Asia), lakes have greater sediment accumulation rates, with values in more industrialized regions higher than for counterparts in non-industrialized regions at the same latitude (Figure I.2). We also detected a significant difference in the mean SAR between lakes and reservoirs (μ_{lake}= 3.36 ± 3.33 mm yr^{-1}, $\mu_{reservoir}$= 6.49 ± 5.58 mm yr^{-1}, t-value = -2.71, p = 0.012), but given the relatively low number of SAR profiles from reservoirs (n=54), we did not conduct further statistical tests comparing lakes to reservoirs.

Stepwise multiple linear regression models indicated that of all the variables evaluated (Table A.2), log-transformed average cropland density (total km^2 cropland area per 9 km^2 grid cell, averaged between 1963 and present) was found to be the strongest predictor, accounting for 33% (p = 5.90e-7) of the variation in log-transformed mean SAR between 1963 and the date of the core retrieval. Additional significant variables that explain variation in mean modern SAR included annually averaged mean monthly temp, averaged across 1963 and present (explaining 4% of the variation, p = 7.26e-6), square-root transformed altitude (2%, p = 0.0032) and annual sum of mean monthly precipitation averaged between 1963 and present (1%, p =0.053). Together, these variables accounted for ~40% of the total variance in log-transformed mean SAR (1963 to present) and yielded the following predictive equation:

$\text{Log(Mean SAR}_{\text{1963-Present}}\text{) (mm yr}^{-1}\text{)} = 0.53 + 0.17 \times \log(\text{Mean Cropland}_{\text{1963-Present}} + 1)\ (\text{km}^2) + 0.012 \times \text{Mean Temperature}_{\text{1963-Present}}\ (°\text{C}) - 2.7\text{e-}3 \times \text{Altitude}^{½}\ (\text{m. asl}) - 7.7\text{e-}4 \times \text{Mean Precipitation}_{\text{1963-Present}}\ (\text{mm})$

A similar model, evaluating the drivers responsible for variation in mean SAR (averaged between AD 1850 and present) was also developed to enable investigators to predict, using the equation, the core length that would be required to extend back in time to pre-industrial conditions. The model equation is presented in Appendices Chapter I.

Temporal and spatial variations in lake SAR and MAR

Globally, lake sedimentation rates, expressed as SAR, increased substantially during the 20th century, as shown in our GAM analysis of z-transformed time series (Figure I.3A). From baseline conditions ca. 1850 to current times, global lake mean SAR have nearly quadrupled ($\mu_{baseline}$= 1.18 ± 1.07 mm yr^{-1} vs. μ_{modern}= 4.11 ± 5.01 mm yr^{-1}). Breakpoint analysis indicated that SAR acceleration occurred around 1966 (Figure I.3A, p = 5.61e-12). Similar to what was observed for SAR trends, our general additive model also detected a non-linear increase in MAR between 1850 and 2014, based on the lake-specific, z-transformed data (Figure I.3B). With our MAR estimates, we detected a breakpoint around 1945 (p = 0.034), although there was a smoother increase in MAR than observed in SAR. Global lake MARs were found to have tripled since the end of the nineteenth century ($\mu_{baseline}$= 0.040 ± 0.044 g cm^{-2} yr^{-1} vs. μ_{modern}= 0.13 ± 0.22 g cm^{-2} yr^{-1}).

We then considered how trends in MAR values differed among ecoregions, given that these regional delineations have been shown to be effective for other environmental metrics

(Anderson-Teixeira et al. 2012). Baseline MAR values showed modest differences among selected ecoregions (Figure A.3) with MAR estimates across ecoregions constrained within the reported average MAR value, plus or minus one standard deviation ($\mu_{baseline}$= 0.040 ± 0.044 g cm^{-2} yr^{-1}). Based on a *post hoc* Tukey test, however, we found that lakes set in tundra and temperate conifer forest regions had similar baseline MAR estimates, but were significantly different from those measured in temperate broadleaf mixed forests. Furthermore, greater MAR value distributions were detected in the temperate broadleaf mixed forests. Lakes set in the boreal forest, temperate grasslands or xeric/desert ecoregions had intermediate baseline MAR values and did not differ significantly from lakes in the tundra/temperate conifer forest or temperate broadleaf mixed forests. GAM analyses of the z-transformed MAR time series by lake showed that all ecoregions recorded relatively stable MAR during most of the 20th century, but thereafter experienced an increase at most sites (Figure A.4 & A.5). However, differences in the timing of MAR increases were recorded among ecoregions. The two ecoregions showing the earliest breakpoint, around 1930, are temperate broadleaf mixed forests and temperate grasslands (savannas and shrublands); both regions span the eastern coast of North America, most of Europe and Eastern Asia. Lakes in other ecoregions were found to have MAR that increased later, after 1950 (Table I.1). Boreal forest/taiga was the only ecoregion where the timing of the breakpoint was not significant and the GAM displayed two periods of increased sedimentation rates, with the first occurring from ~1850 – 1915 and the second showing a steep beginning around 1966 to present (Figure A.4).

Spatio-temporal drivers of lake MAR

Watershed population density (p <.0001; log(x+1)-transformed) and watershed cropland density (p = 0.041; log(x+1)-transformed) were both significant predictors of spatio-temporal mass accumulation rates (log-transformed) when we applied a linear mixed effect model that accounts for *LakeID*, nested within *Ecoregion* as a random factor (n=62 lakes). Neither mean annual temperature nor mean annual precipitation accounted for a significant amount of the variation in MAR. Overall, the multivariate model accounted for ~42% of the variation in the fixed effect for mass sediment accumulation rate and up to 92%, when considering the random effect associated with lake and ecoregion (Table A.6).

Relationships between MAR and SAR

MAR and SAR were only moderately correlated, using linear regression approaches (marginal r^2 = 0.37; F-statistic = 297.3; p = < 2.2e-16) (Figure I.4A). When using both SAR and LOI (Loss-on-Ignition) to predict MAR, the prediction improved substantially (marginal r^2 = 0.60; F-statistic = 376.6; p = < 2.2e-16; Figure I.4B), when applied to the 56 sites that had both accumulation rate measures. Analysis of the variance table that compares models with and without LOI, further highlights the significance of including LOI in the regression model (F-statistic = 288.18, p = < 2.2e-16).

Discussion

Global increases in lake SAR and MAR

Our large-scale empirical analysis of lake sedimentation rates sheds new light on the growing evidence that the modification of Earth's natural landscape is significantly altering surrounding water bodies (Rodriguez et al. 2020). Lakes are accumulating sediments ~3-4x more rapidly than they did ~150 years ago. The strongest drivers of the recent spatial and temporal increases in sedimentation rates (post-1963) in lakes across the globe are indices of human presence in watersheds (human population density and cropland cover). We also detected spatial heterogeneity in SAR and MAR among ecoregions.

Our estimated global baseline (before AD 1900) lake sediment accumulation rate was 1.18 mm yr^{-1} (± 1.07 mm yr^{-1}). This baseline sediment accumulation rate value agrees well with a previous synthesis value, in which the authors reported a global lake SAR of 0.75 mm yr^{-1} by the late Holocene, which was already elevated by forest clearance that started in the mid-Holocene (Jenny et al. 2019). Over the last 150 years, sediment accumulation rates increased globally by nearly a factor of four, and even with the more conservative mass accumulation rates, we observed a three-fold increase over baseline conditions. When we examined the global distribution of average modern SAR, we found greater values in warmer and more anthropogenically modified watersheds (tropical and subtropical moist broadleaf forests, Mediterranean forests, woodlands and scrub and temperate broadleaf and mixed forests). The distribution of SAR across the globe also exhibited a negative relationship with latitude, as was reported previously (Brothers et al. 2008). Sedimentation estimates in lakes at middle to higher latitudes (20°N - 50°N), regions where important anthropogenic development has occurred

(Ellis 2011), display greater variability. This variability is thought to arise from the presence of natural, protected landscapes (Watson et al. 2016) yielding moderate lake sedimentation rates, whereas anthropogenically influenced areas have greater SAR values.

With respect to both metrics of lake sedimentation, MAR and SAR, statistical breakpoint analysis performed on records spanning the last 100-150 years indicated an acceleration from the baseline, pre-1900 sedimentation, during the interval 1930-1980. During those decades, agriculture intensified and there was growth of densely populated areas (Ellis 2011). This time frame is also recognized as a period of increased global production and application of fertilizer (Waters et al. 2016). The post-1950 period known as the "Great Acceleration" was defined by examining many ecological and socio-economic time series that reflect intensification of human activities that affected many processes across the planet (Steffen et al. 2015), including land-cover transformation, increased rates of ore extraction and modifications to the global hydrosphere (Syvitski et al. 2005, 2020; Ellis 2011). The discrepancy across ecoregions in terms of the timing of the onset of MAR acceleration provides further evidence that anthropogenic landscape transformations influence lake sedimentation rates. Some of the most populated ecoregions, e.g. temperate mixed forests and temperate grasslands, were the first to experience a rapid increase in MAR during the early 1930s. Other less densely populated, more remote ecoregions, experienced similar increases, but later, in the 1960s or 1980s.

We found that the most important predictor of modern sediment accumulation rate (SAR) in lakes of our global dataset was the abundance of cropland density in a lake's watershed. Numerous studies (Keatley et al. 2011; Anderson et al. 2020) have reported on the association between lake eutrophication and cropland density and the agricultural practices tied to it, especially the application fertilizer and consequent lake nutrient loading. Other variables that helped constrain our global model in predicting spatial variation in SAR worldwide included annual mean monthly temperature, altitude, and mean annual precipitation. Our model has strong predictive power for *a priori* estimation of lake SAR, which is a useful metric for a variety of paleolimnological studies, such as "top-bottom" comparisons (Smol 2009). In those studies, investigators compare characteristics of modern sediment to those in baseline, pre-disturbance deposits. For such studies, it is important to be able to estimate the sediment depth at which baseline conditions prevailed. This metric of sedimentation (SAR), however, is prone to "inflation" in the most recent sediments that have not yet been subject to the process of compaction (Maier et al. 2013). The higher water content in shallow sediments near the top of cores (Håkanson 1983) and the relative lack of sediment diagenesis in very recent deposits, results in an apparent increase in SAR relative to deeper in the core (Gälman et al. 2008). This accounts for the only moderate fit between MAR_{obs} and MAR_{pred} when using SAR as an explanatory variable, and is also evident when comparing SAR and MAR temporal variations (Figure I.3 A, B). Through creation of a parallel dataset, we identified organic matter content (LOI) as an important co-variate in predicting MAR from SAR. LOI is an estimate of the amount of organic matter (OM) combusted at 550ºC, and OM is a sediment variable that captures some of the diagenetic transformation of sediment in the core through time. We reckon that estimates of MAR at sites worldwide can be improved by combining measures of SAR, LOI and water content as independent variables in regression equations. We encourage authors to publish LOI and water content data or submit them to open-data portals, so that models of MAR can be improved.

Human land use as a driver of global lake sedimentation in post-industrial times

When we considered the subset of lakes for which MAR measurements and ancillary data were available (62 lakes in predominantly temperate ecoregions), we found that the temporal variation in MAR was best explained by human-induced landscape modifications, and that the variation attributed to land use was much greater than that associated with climate. The linear mixed effect model results indicated that higher population densities at the watershed level explained the greatest amount of variation in MAR, but cropland density was also significant. Increasing MAR in cropland or urbanized areas is expected to first arise from land denudation associated with the transformation of a natural landscape into agriculture or urbanized areas (Guy et al. 1963; Hinderer and Einsele 2001; Jenny et al. 2019). More rapid sedimentation, however, is not limited to increased erosional inputs from the watershed. Associated eutrophication of lakes leads to modification of aquatic communities and supports higher standing biomass and productivity of algae and cyanobacteria (Taranu et al. 2015), which can lead to greater autochthonous sedimentation. Nutrient enrichment from watershed agriculture has led to hypolimnetic hypoxia in numerous lakes worldwide (Jenny et al. 2016), which enhances organic matter preservation during and after deposition. Thus, there are multiple pathways by which greater human population densities and agricultural activities affect lake sedimentation rates, measured as SAR or MAR (Figure I.5).

Although we were able to explain some of the spatio-temporal variation in MAR, we suspect that the analyses could be improved by amassing a larger database. One hypothesis that might explain why MAR increases in some circumstances, despite an absence of cropland or urban development, is that modest eutrophication could occur as a consequence of long-distance atmospheric transport and deposition of dust and reactive nitrogen (Neff et al. 2008; Heathcote et al. 2015). Another possible explanation for recorded changes in lake sedimentation is hydrological modifications of inland waters. Rates of reservoir construction and management of lake volume have increased greatly since the industrial revolution (Syvitski et al. 2005; Rodriguez et al. 2020) and are widespread (Grill et al. 2015). We identified at least 28 lakes in our dataset that had one or more reservoirs upstream. There could be more such lakes, but databases for small dams are incomplete. Hydrologic changes via alteration of tributary discharges or other pathways (Gagnon-Poiré et al. 2021; Simmatis et al. 2020) can alter sedimentation dynamics and modify sediment focusing (Lehman 1975), thereby affecting measurements of sediment accumulation. Furthermore, there could be synergistic influences on sedimentation between land use and climate, or among land use, climate and limnological conditions (hypoxia), which might be detected with a larger dataset.

Implication for predictive models of lake sedimentation and carbon storage

Our dataset provides a strong foundation for improving emerging models of global carbon sequestration. Robust measures of MAR, along with measurements of sediment organic carbon concentration, are variables required to determine a lake's carbon burial rate (USGS 2010). Whereas numerous authors have reported temporal increases in the rate of organic matter burial in lakes, it remains unclear how much of this increase is attributed to an increase in MAR. For example, Anderson et al. (2020) evaluated the temporal dynamics of global carbon storage in inland water bodies, and reported that carbon burial rates have nearly tripled within the last

100 years. As a follow up, it would be interesting to disentangle how much of this recent increase in carbon sequestration was driven by changes in MAR and how much is attributable to changes in carbon concentration in the sediments. It is also interesting to compare the rates of change of multiple nutrients. Whereas carbon storage has increased globally 3-fold over the last 100 years, global nitrogen and phosphorus use have increased about 20-fold (Anderson et al. 2020). Our findings show that global MAR values have increased by 3-fold. The disconnect between nutrient use and response, measured as burial rate in lake sediments, could be explained by a variety of factors including: a) nutrient is stored on the landscape, b) inefficient nutrient uptake by primary producers and consumption by consumers, and/or c) heterogeneity in sediment accumulation among sites.

Our dataset is also informative for watershed-scale erosion models aiming to calculate sediment yields (Ranzi et al, 2012; Biswas and Pani, 2015). While many attributes of the watershed are required for estimating total watershed sediment delivery using the revised universal soil loss equation (RUSLE) (Renard et al, 2011), the presence of lakes within the watershed, and their role as sinks for total sediment yield must also be considered. With our dataset, upstream lakes present within a watershed of interest could be identified and accounting for their sediment mass accumulation rate when considering the total watershed erosive yield could lead to more accurate estimates. While the comparison of watershed total sediment delivery and lake sediment MAR remains challenging (Pope et al. 2016), we believe our dataset can provide insights for such investigations, especially when considering analyses at a regional or global scale.

Conclusions

Since about AD 1850, global lake sedimentation rates, measured as SAR or MAR, have increased three- to four-fold, showing a pronounced acceleration between 1930 and 1980. Increases in SAR and MAR are primarily attributed to modifications of the natural landscape, with the development of agriculture and urban areas. Our analyses provide valuable information for future paleolimnological field studies, enabling estimation of recent sediment accumulation rates in different regions of the world. Finally, this large-scale analysis of lake sedimentation rates bridges two important metrics of sedimentation, SAR and MAR, and lays the groundwork for future modeling efforts in global carbon storage and landscape erosion.

Acknowledgments

This work was supported by a Fonds de Recherche du Québec, Nature et Technologie (FRQNT) Fellowship and an Excellence Award from the Department of Biology at McGill University to AB. We also acknowledge funding from an FRQNT Team grant awarded to IGE and PF (and Dermot Antoniades and Paul del Giorgio), as well as Canada Research Chairs awarded to IGE and PF. We thank the Department of Biology for funding an internship for AB to visit JPJ in Jena, Germany where this work was further developed. We are grateful for thoughtful feedback from the Gregory-Eaves lab, Bernhard Lehner and Brian Leung, and to Florence Tan for early comments and guidance with GIS.

References

Anderson NJ, Heathcote AJ, Engstrom DR (2020) Anthropogenic alteration of nutrient supply increases the global freshwater carbon sink. Sci Adv 6: eaaw2145

Anderson-Teixeira K, Snyder PK, Twine TE, Cuadra SV, Costa MH, DeLucia EH (2012) Climate-regulation services of natural and agricultural ecoregions of the Americas. Nat Clim Change 2: 177-181

Appleby P, Oldfield F (1978) The calculation of lead-210 dates assuming a constant rate of supply of unsupported 210Pb to the sediment. Catena 5: 1-8

Barnett V, Lewis T (1994) Outliers in statistical data. Wiley, Chichester

Bergamaschi BA, Bernknopf R, Clow D, Dye D, Faulkner S, Forney W, Gleason R, Hawbaker T, Liu J, Liu S, Prisley S, Reed B, Reeves M, Rollins M, Sleeter B, Sohl T, Stackpoole S, Stehman S, Striegl RG, Wein A, Zhu Z (2010) A method for assessing carbon stocks, carbon sequestration, and greenhouse-gas fluxes in ecosystems of the United States under present conditions and future scenarios. Sci Inv Rep 2010-5233. https://doi.org/10.3133/sir20105233

Biswas SS, Pani P (2015). Estimation of soil erosion using RUSLE and GIS techniques: a case study of Barakar River basin, Jharkhand, India. Model. Earth Syst. Environ. 1, 42

Bhaduri B, Harbor J, Engel B, Grove M (2000) Assessing watershed-scale, long-term hydrologic impacts of land-use change using a GIS-NPS model. Environ Manage 26: 643-658

Brothers S, Vermaire JC, Gregory-Eaves I (2008) Empirical models for describing recent sedimentation rates in lakes distributed across broad spatial scales. J Paleolimnol 40: 1003-1019

Couillard Y, Courcelles M, Cattaneo A, Wunsam S (2004) A test of the integrity of metal records in sediment cores based on the documented history of metal contamination in Lac Dufault (Québec, Canada). J Paleolimnol 32: 149-162

Davis RB, Hess CT, Norton SA, Hanson DW, Hoagland KD, Anderson DS (1984) 137Cs and 210Pb dating of sediments from soft-water lakes in New England (USA) and Scandinavia, a failure of 137Cs dating. Chem Geol 44: 151-185

Dean WE (1974) Determination of carbonate and organic matter in calcareous sediments and sedimentary rocks by loss on ignition; comparison with other methods. J Sediment Res 44: 242-248

Downing J, Prairie Y, Cole J, Duarte C, Tranvik L, Striegl R, McDowell W, Kortelainen P, Caraco N, Melack J (2006) The global abundance and size distribution of lakes, ponds, and impoundments. Limnol Oceanogr 51: 2388-2397

Dunlap RE (1991) Trends in public opinion toward environmental issues: 1965–1990. Soc Natur Resour 4: 285-312

Ellis EC (2011) Anthropogenic transformation of the terrestrial biosphere. Philos Trans A Math Phys Eng Sci 369: 1010-1035

Engstrom DR, Fitzgerald WF, Cooke CA, Lamborg CH, Drevnick PE, Swain EB, Balogh SJ, Balcom PH (2014) Atmospheric Hg emissions from preindustrial gold and silver extraction in the Americas: A reevaluation from lake-sediment archives. Environ Sci Technol 48: 6533-6543

Engstrom DR, Rose NL (2013) A whole-basin, mass-balance approach to paleolimnology. J Paleolimnol 49: 333-347

Gagnon-Poiré A, Brigode P, Francus P, Fortin D, Lajeunesse P, Dorion H, Trottier A-P (2021) Reconstructing past hydrology of eastern Canadian boreal catchments using clastic varved sediments and hydro-climatic modeling: 160 years of fluvial inflows. Clim Past 17: 653-673

Gälman V, Rydberg J, de-Luna S, Bindler R, Renberg I (2008) Carbon and nitrogen loss rates during aging of lake sediment: Changes over 27 years studied in varved lake sediment. Limnol Oceanogr 53: 1076-1082

Grill G, Lehner B, Lumsdon AE, MacDonald GK, Zarfl C, Liermann CR (2015) An index-based framework for assessing patterns and trends in river fragmentation and flow regulation by global dams at multiple scales. Environ Res Lett10: 015001

Guy HP, Ferguson GE (1963) Sediment in small reservoirs due to urbanization. T Am Soc Civ Eng 128

Håkanson L, Jansson M (1983) Principles of Lake Sedimentology. Springer-Verlag, Berlin, pp. 73-75

Heiri O, Lotter AF, Lemcke G (2001) Loss on ignition as a method for estimating organic and carbonate content in sediments: reproducibility and comparability of results. J Paleolimnol 25: 101-110.

Hinderer M, Einsele G (2001) The world's large lake basins as denudation-accumulation systems and implications for their lifetimes. J Paleolimnol 26: 355-372

Hobbs WO, Engstrom DR, Scottler SP, Zimmer KD, Cotner JB (2013) Estimating modern carbon burial rates in lakes using a single sediment sample. Limnol Oceanogr Methods 11: 316-326

Issaka S, Ashraf MA (2017) Impact of soil erosion and degradation on water quality: a review. Geol Ecol Landscapes 1: 1-11

Jenny J, Normandeau A, Francus P, Taranu ZE, Gregory-Eaves I, Lapointe F, Jautzy J, Ojala AE, Dorioz J, Schimmelmann A (2016) Urban point sources of nutrients were the leading cause for the historical spread of hypoxia across European lakes. Proc Nat Acad Sci USA 113: 12655-12660

Jenny J, Koirala S, Gregory-Eaves I, Francus P, Niemann C, Ahrens B, Brovkin V, Baud A, Ojala AEK, Normandeau A, Zolitschka B, Carvalhais N (2019) Human and climate global-scale imprint on sediment transfer during the Holocene. Proc Natl Acad Sci USA 116: 22972-22976

John B (2004) A comparison of two methods for estimating the organic matter content of sediments. J Paleolimnol 31: 125-127

Keatley BE, Bennett EM, MacDonald GK, Taranu ZE, Gregory-Eaves I (2011) Land-use legacies are important determinants of lake eutrophication in the anthropocene. Plos One 6: e15913

Kim S, Jang T, Kang M, Im S, Park S (2014) GIS-based lake sediment budget estimation taking into consideration land use change in an urbanizing catchment area. Environ Earth Sci 71: 2155-2165

Klaminder J, Appleby P, Crook P, Renberg I (2012) Post-deposition diffusion of 137Cs in lake sediment: Implications for radiocaesium dating. Sedimentology 59: 2259-2267

Klein Goldewijk K (2016) A historical land use data set for the Holocene; HYDE 3.2. 18: 1574

Last WM, Smol JP (2006) Tracking Environmental Change Using Lake Sediments, Volume 2: Physical and Geochemical methods. Kluwer Academic Publishers, Dordrecht, pp. 1-5

Lehman JT (1975) Reconstructing the rate of accumulation of lake sediment: The effect of sediment focusing. Quatern Res 5: 541-550

Lehner B, Grill G (2013) Global river hydrography and network routing: baseline data and new approaches to study the world's large river systems. Hydrol Process 27: 2171-2186

Lehner B, Verdin K, Jarvis A (2006) HydroSHEDS technical documentation, version 1.0. World Wildlife Fund US, Washington, DC: 1-27

Maier DB, Rydberg J, Bigler C, Renberg I (2013) Compaction of recent varved lake sediments. GFF 135: 231-236

Mann HB (1945) Nonparametric Tests Against Trend. Econometrica 13: 245-259.

Messager ML, Lehner B, Grill G, Nedeva I, Schmitt O (2016) Estimating the volume and age of water stored in global lakes using a geo-statistical approach. Nat Commun 7: 13603

Miller RG (1981) Normal Univariate Techniques. In: Miller RG (ed) Simultaneous Statistical Inference. Springer New York, New York, NY, pp. 37-108

Muggeo VMR (2003) Estimating regression models with unknown break-points. Statist Med 22: 3055-3071

Neff J, Ballantyne A, Farmer G, Mahowald N, Conroy J, Landry C, Overpeck J, Painter T, Lawrence C, Reynolds R (2008) Increasing eolian dust deposition in the western United States linked to human activity. Nat Geosci 1: 189-195

Olson DM, Dinerstein E (2002) The Global 200: Priority ecoregions for global conservation. Ann Mo Bot Gard: 199-224

Pachauri RK, Allen MR, Barros VR, Broome J, Cramer W, Christ R, Church JA, Clarke L, Dahe Q, Dasgupta P (2014) Climate change 2014: synthesis report. Contribution of Working Groups I, II and III to the fifth assessment report of the Intergovernmental Panel on Climate Change. IPCC, Geneva

Pinheiro J, Bates D, DebRoy S, Sarkar D, Heisterkamp S, Van Willigen B, Maintainer R (2017) Package 'nlme'. Linear and nonlinear mixed effects models, version 3

Pope IC, Odhiambo BK (2014). Soil erosion and sediment fluxes analysis: a watershed study of the Ni Reservoir, Spotsylvania County, VA, USA. Environ Model Assess, 186(3), 1719-1733

Rakap S, Rakap S, Evran D, Cig O (2016) Comparative evaluation of the reliability and validity of three data extraction programs: UnGraph, GraphClick, and DigitizeIt. Comput Hum Behav 55: 159-166

Ranzi R, Le TH, Rulli MC (2012). A RUSLE approach to model suspended sediment load in the Lo river (Vietnam): Effects of reservoirs and land use changes. J Hydrol, 422, 17-29

Renard KG, Yoder DC, Lightle DT, Dabney SM (2011). Universal soil loss equation and revised universal soil loss equation. In Morgan, R.P.C. and Nearing, M.A., Eds., Handbook of erosion modelling. Blackwell Publ., Oxford, UK, 137-167

Rodriguez A, McKee B, Miller C, Bost M, Atencio A (2020) Coastal sedimentation across North America doubled in the 20 th century despite river dams. Nat Commun 11: 1-9

Rose NL, Morley D, Appleby PG, Battarbee RW, Alliksaar T, Guilizzoni P, Jeppesen E, Korhola A, Punning J (2011) Sediment accumulation rates in European lakes since AD 1850: trends, reference conditions and exceedence. J Paleolimnol 45: 447-468

Schiefer E, Petticrew EL, Immell R, Hassan MA, Sonderegger DL (2013) Land use and climate change impacts on lake sedimentation rates in western Canada. Anthropocene 3: 61-71

Simmatis B, Baud A, Gregory-Eaves I, Francus P, Smol JP (2020) Subfossil Simuliidae track past river flow into an industrially contaminated lake. J Paleolimnol 64: 179-192

Steffen W, Broadgate W, Deutsch L, Gaffney O, Ludwig C (2015) The trajectory of the Anthropocene: the great acceleration. Anthropocene Rev 2: 81-98

Syvitski J, Waters CN, Day J, Milliman JD, Summerhayes C, Steffen W, Zalasiewicz J, Cearreta A, Gałuszka A, Hajdas I (2020) Extraordinary human energy consumption and resultant geological impacts beginning around 1950 CE initiated the proposed Anthropocene Epoch. Commun Earth Environ 1: 32.

Syvitski JP, Vorosmarty CJ, Kettner AJ, Green P (2005) Impact of humans on the flux of terrestrial sediment to the global coastal ocean. Science 308: 376-380

Taranu ZE, Gregory-Eaves I (2008) Quantifying relationships among phosphorus, agriculture, and lake depth at an inter-regional scale. Ecosystems 11: 715-725

Taranu ZE, Gregory-Eaves I, Leavitt PR, Bunting L, Buchaca T, Catalan J, Domaizon I, Guilizzoni P, Lami A, McGowan S (2015) Acceleration of cyanobacterial dominance in north temperate-subarctic lakes during the Anthropocene. Ecol Lett 18: 375-384

van Rij J, Wieling M, Baayen RH, van Rijn H, van Rij MJ (2016) Package ‘itsadug’

Verpoorter C, Kutser T, Seekell DA, Tranvik LJ (2014) A global inventory of lakes based on high-resolution satellite imagery. Geophys Res Lett 41: 6396-6402

Wallace D, Green SB (2002) Analysis of repeated measures designs with linear mixed models. In: Lawrence Erlbaum Associates Publishers, Mahwah, NJ, US, pp. 103-134.

Wang S, Kang S, Zhang L, Li F (2008) Modelling hydrological response to different land-use and climate change scenarios in the Zamu River basin of northwest China. Hydrol Process 22: 2502-2510

Waters CN, Zalasiewicz J, Summerhayes C, Barnosky AD, Poirier C, Gałuszka A, Cearreta A, Edgeworth M, Ellis EC, Ellis M, Jeandel C, Leinfelder R, McNeill JR, Richter Dd, Steffen W, Syvitski J, Vidas D, Wagreich M, Williams M, Zhisheng A, Grinevald J, Odada E, Oreskes N, Wolfe AP (2016) The Anthropocene is functionally and stratigraphically distinct from the Holocene. Science 351: aad2622

Watson JEM, Dudley N, Segan DB, Hockings M (2014) The performance and potential of protected areas. Nature 515: 67-73

Williamson CE, Saros JE, Vincent WF, Smol JP (2009) Lakes and reservoirs as sentinels, integrators, and regulators of climate change. Limnol Oceanogr 54: 2273-2282

Wood S (2012) mgcv: Mixed GAM Computation Vehicle with GCV/AIC/REML smoothness estimation

Yandell B (2017) Practical Data Analysis for Designed Experiments. Routledge, Philadelphia

Zuur AF, Ieno EN, Walker NJ, Saveliev AA, Smith GM (2009) Limitations of linear regression applied on ecological data. In: Mixed effects models and extensions in ecology with R. Springer, New York, pp 11-33

Tables Chapter I

Table I.1. Summary of the breakpoint results based on MAR data (z-transformed by lake), where analyses were performed on separate, ecoregion-specific data-frames. Trend's analysis in these breakpoint analyses demarcating the acceleration onset are based on the results extracted from general additive mixed effect models (Figure A.4)

Ecoregion	**MAR Acceleration onset**	**Breakpoint sig. (*p* value)**
Temperate Broadleaf and Mixed Forests (n=32)	1930	4.38e-36
Temperate Grasslands, Savannas and Shrublands (n=5)	1934	2.91e-10
Temperate Conifer Forests (n=22)	1951	4.41e-16
Tundra (n=12)	1963	6.30e-08
Boreal Forests/Taiga (n=7)	-	-
Deserts and Xeric Shrublands (n=7)	1989	1.85e-03

Figures Chapter I

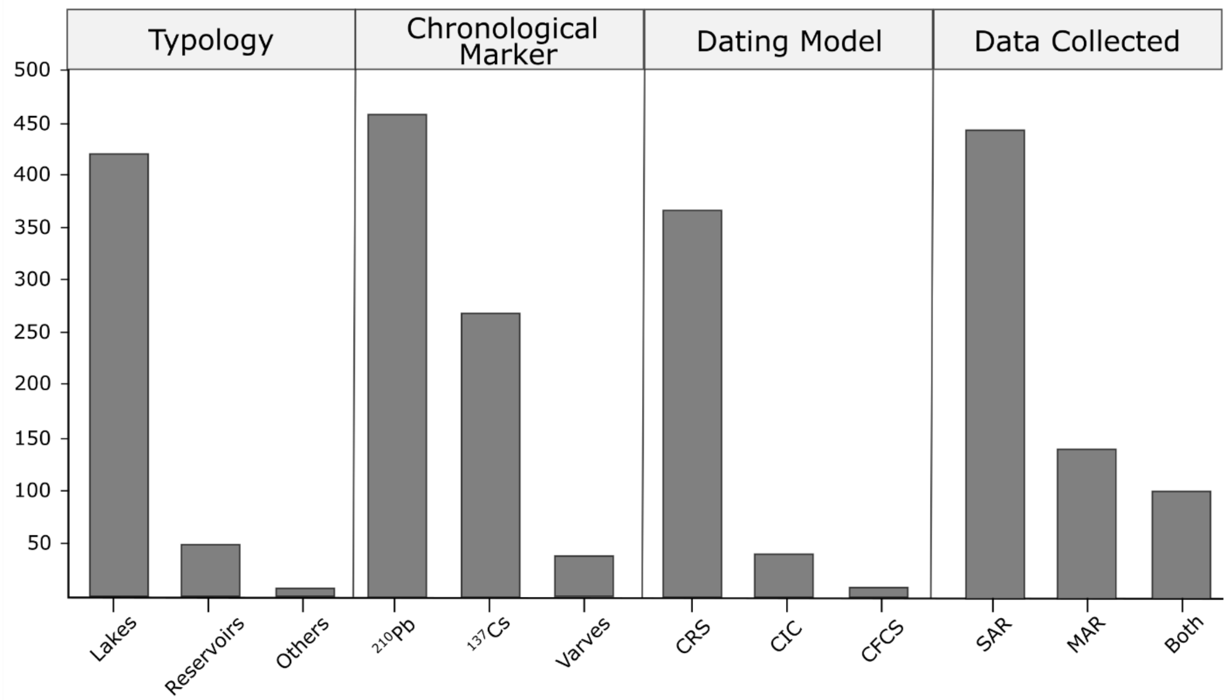

Figure I.1. Bar plots highlighting the distribution of the data collected from 304 source articles published in the *Journal of Paleolimnology* between 1988 and 2016.

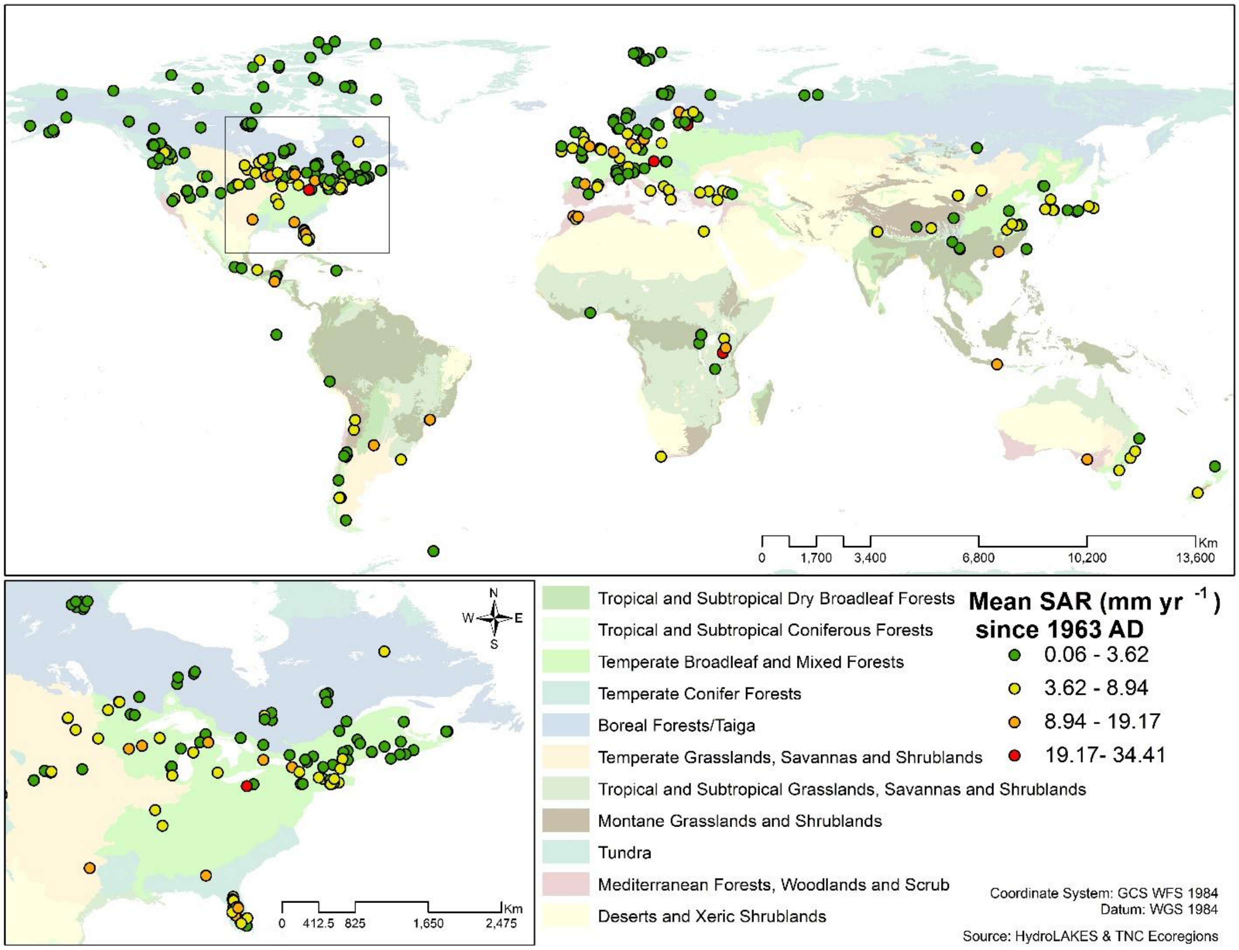

Figure I.2. Map showing the distribution in mean sediment accumulation rate (SAR; mm yr^{-1}) since 1963 (±10 years), showing enlarged area for North America to accommodate the high density of lakes in this region. Mean SAR classes were defined following ArcMap's default Jenks natural breaks optimization

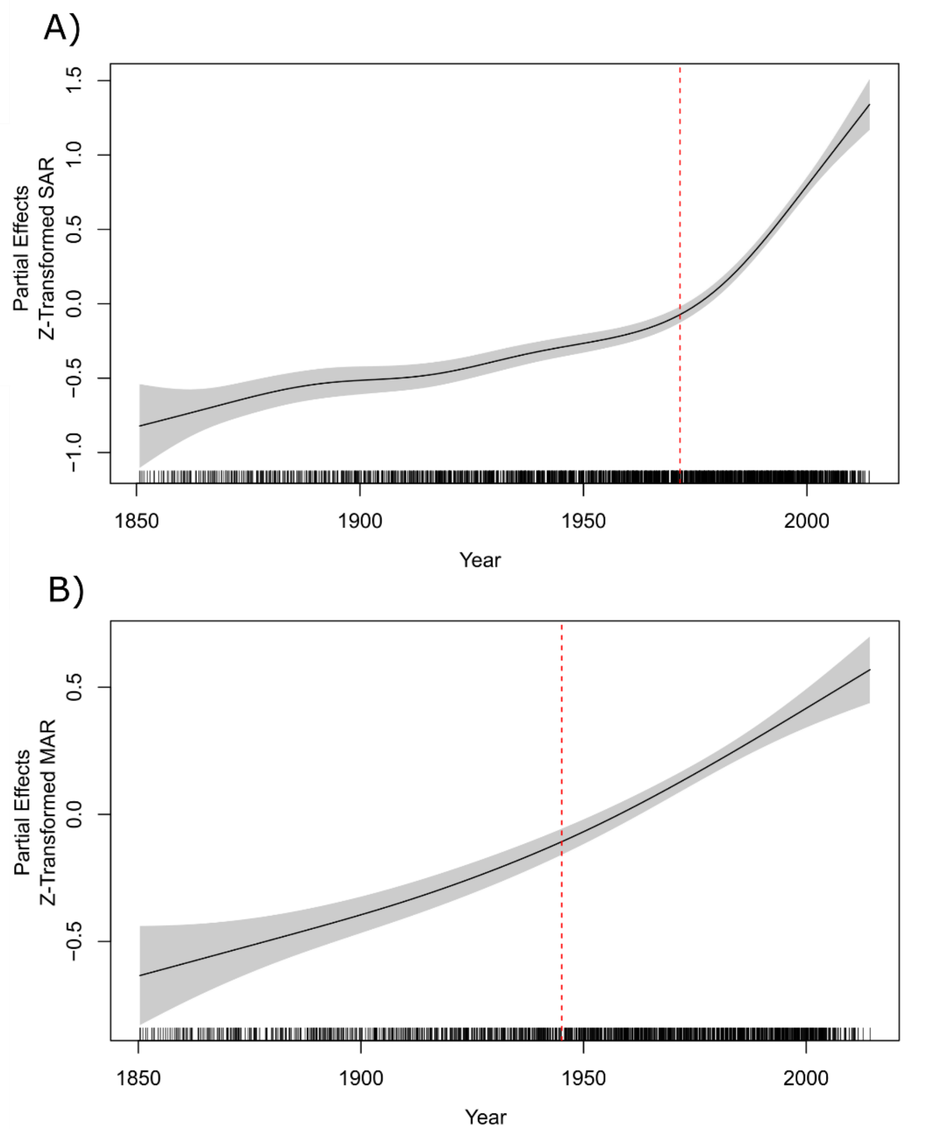

Figure I.3. A) Fitted general additive model for z-transformed Sediment Accumulation Rate (SAR) as a function of time from 1850 to 2015; n = 258, pseudo-r^2 = 0.28, e.d.f =4.94, $F(1, 2516)$ = 164.1, p <.001. Red dashed line at ~1966 indicates the onset of a SAR acceleration, determined by the breakpoint analysis. **B**) Fitted general additive model for z-transformed Mass Accumulation Rate (MAR) as a function of time from 1850 to 2015; n = 94, pseudo-r^2 = 0.14, e.d.f =3.073, $F(1,1223)$ =66.46, p <.001. Red dashed line at ~1941 indicates the onset of MAR acceleration determined by the breakpoint analysis, although graphically we observe that this transition is more gradual

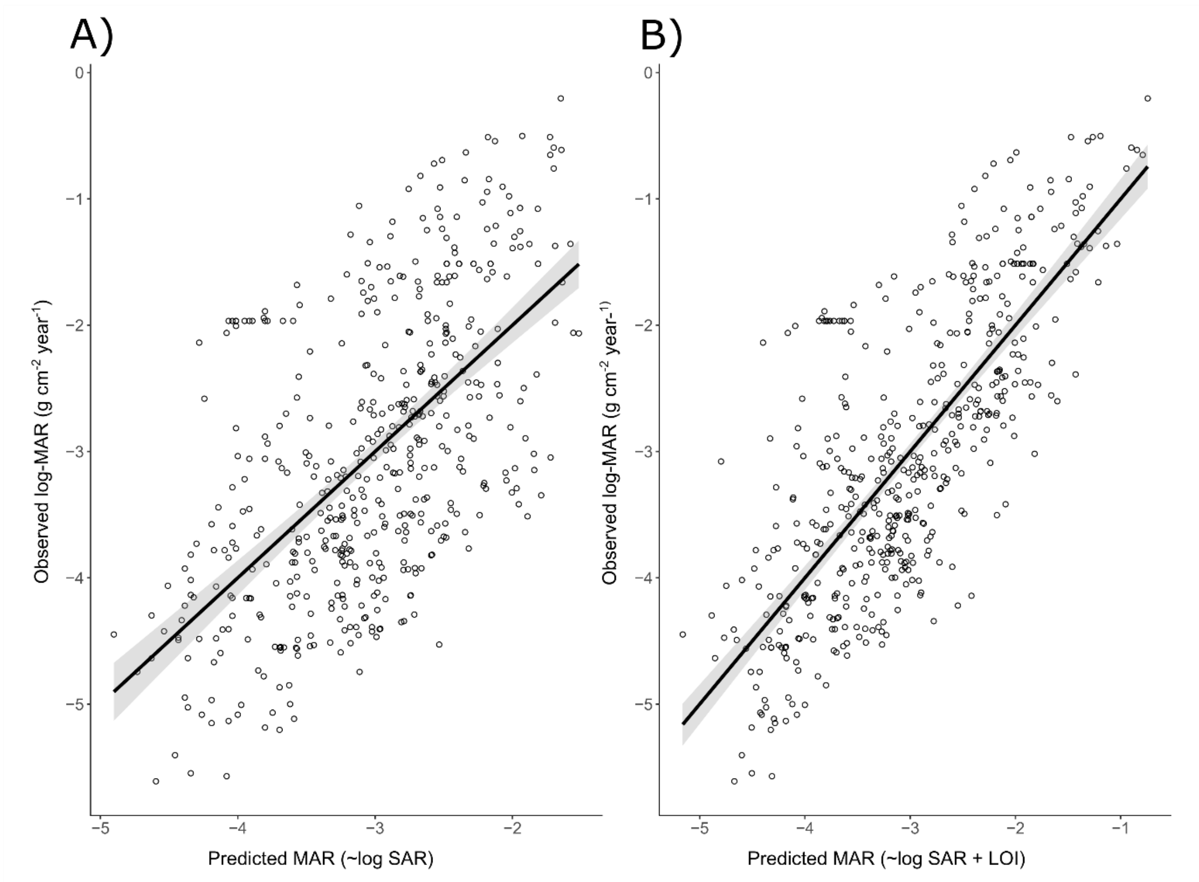

Figure I.4. Fitted linear models evaluating the fit between observed log-MAR and predicted MAR using **A**) SAR estimates only (R^2 = 0.37) and **B**) using SAR and Loss-on-Ignition (LOI) to account for sediment transformation post deposition (R^2 = 0.60)

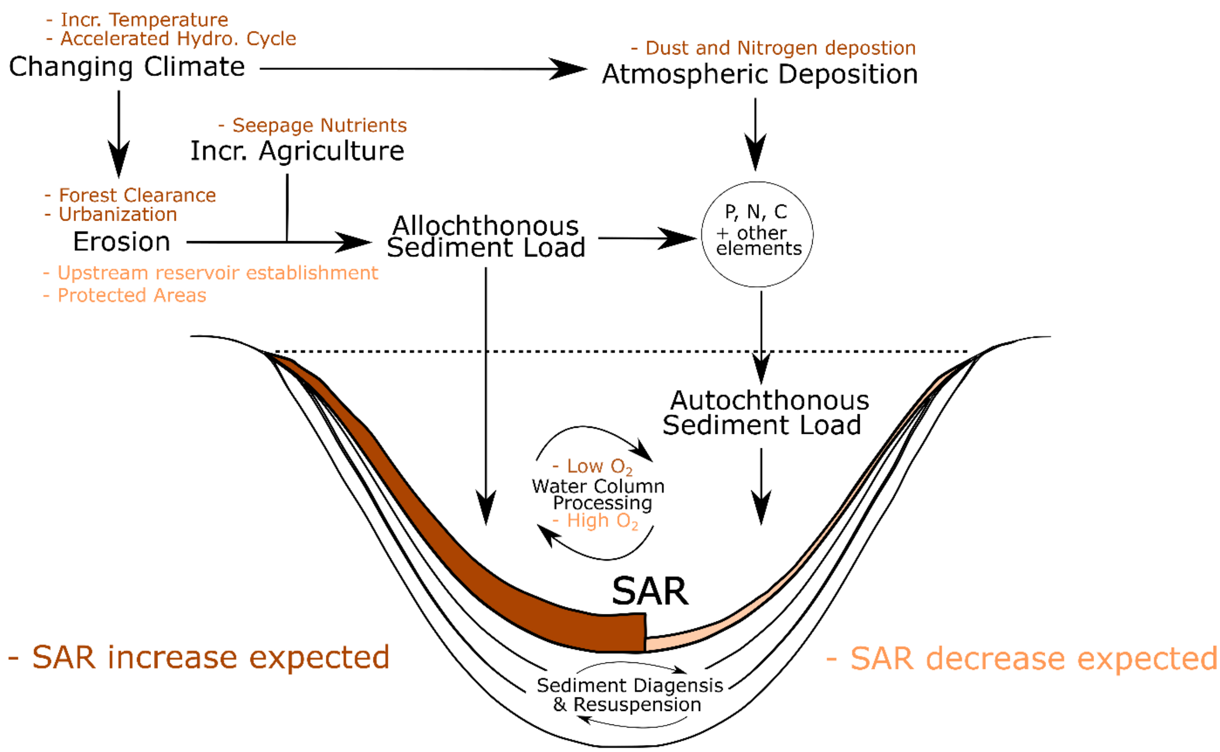

Figure I.5. Conceptual diagram summarizing the main mechanisms that influence a lake's sedimentation rate (SAR), which are the product of both allochthonous and autochthonous processes. Processes leading to an increase in sediment accumulation are shown in dark brown whereas conditions leading to a decrease in sediment accumulation appear in light orange

Appendices Chapter I

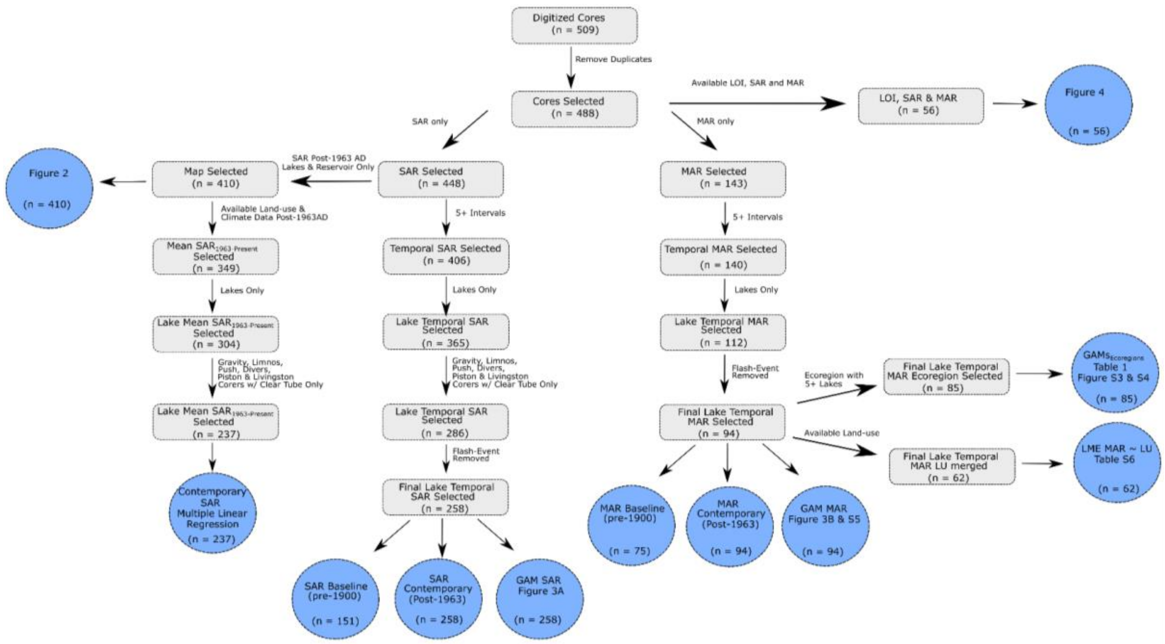

Figure A.1. Graphical summary highlighting the steps taken throughout the analysis. The grey rectangles account for subsetted dataset, linked with an arrow highlighting the step taken from one to another. The blue circles represent figure and estimates used in the manuscript. For each the number of sites is accounted for in parentheses.

Table A.2. Summary of the predictive factors investigated in this study, along with their source.

Note: pixel size for Cropland density and Population Count is $9km^2$

Variable (unit)	**Source**	Min	**Mean**	Max
State Variables				
Geospatial Coordinates (Lat ° Long °)	Source Article (Google EarthPro)	-60.72° -159.43°	**43.15°** **-32.48°**	83° 174.76°
Lake surface area (ha)	Source Article	0.12	**1.28×10^4**	3.17×10^6
Lake maximum depth (m)	Source Article	0.6	**30**	1637
Lake Altitude (m a.s.l)	Source Article (GoogleEarthPro)	-47	**471**	4724
Watershed area (km^2)	Source Article (GIS-inferred)	0.005	**7.55×10^3**	7.66×10^5
Watershed slope (°)	Source Article (GIS-inferred)	-1	**4.6**	23.2
Temporal Variables				
Cropland density (km^2/ $9km^2$ pixel)	Hyde 3.2 (1800 – 2015)	0	**6.8**	62.26
Population count (inhabitants/ $9km^2$ pixel)	Hyde 3.2 (1800 – 2015)	0	**4987**	1.19×10^6
Mean monthly temperature (°C)	NCDC (1900 – 2014)	-27.32	**6.46**	29.2
Total monthly precipitation (mm)	NCDC (1900 – 2014)	0	**78.45**	366.68

As presented in the main text, we also developed a multiple linear regression model evaluating the drivers responsible for variation in mean SAR (averaged between 1850AD to present). The rationale for this equation is to enable investigators to predict, using the equation, the necessary expected core length to reach pre-industrial conditions. Of the variables evaluated (presented in Table A.2), log-transformed average cropland density (total cropland area, in km^2 per *9 km^2* gridcell, averaged between 1850 to present) was found to be the strongest predictor, accounting for 32% (p-value = 3.61e-6) of the variation in log-transformed mean SAR averaged between 1850 to present. Additional significant parameters explaining variation in mean SAR included annual mean of mean monthly temperature averaged between 1850 to present (explaining 6% of the variation, p-value = 4.83e-7), square-root transformed altitude (2%, p-value = 0.0028) and annual sum of mean monthly Precipitation averaged between 1850 to present (1%, p-value =0.041). Altogether, these variables accounted for 38% of the total variance in log-transformed mean SAR (1850 to present) and yielded the following predictive equation:

Log(Mean $SAR_{1850\text{-}Present}$) (mm yr^{-1}) = 0.50 + 0.15 × log(Mean $Cropland_{1850\text{-}Present}$ + 1) (km^2) + 0.012 × Mean $Temperature_{1850\text{-}Present}$ (ºC) – 2.8e-3 × $Altitude^{1/2}$ (m. asl) – 7.7e-4 × Mean $Precipitation_{1850\text{-}Present}$ (mm)

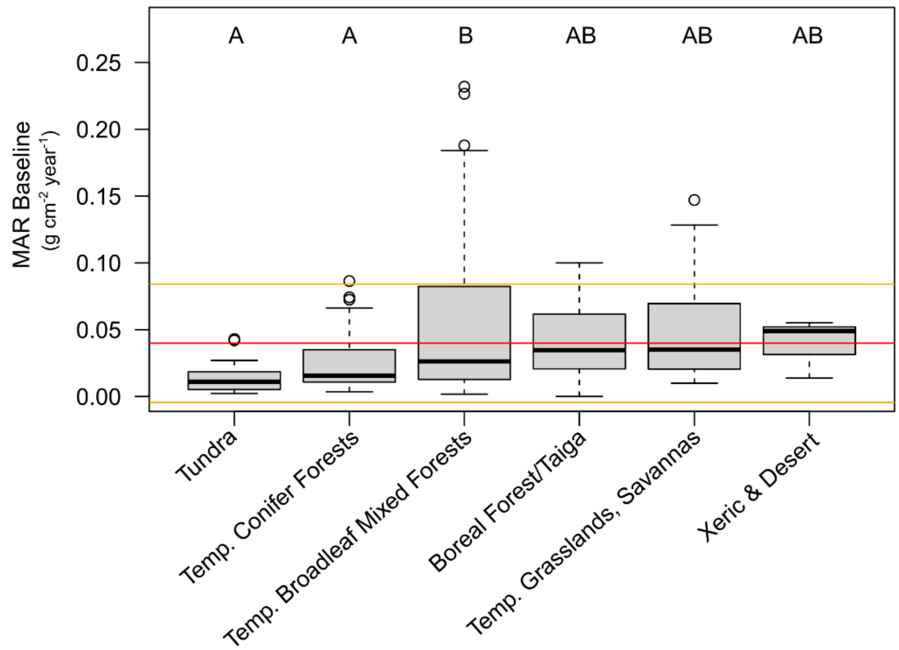

Figure A.3. Distribution of lake Mass Accumulation Rate (MAR) baseline values (pre-1900 AD) from across selected ecoregion with more than three lakes. The red horizontal line represents the mean baseline MAR estimate of 0.040 g cm^{-2} yr^{-1} reported in the manuscript while the two orange lines account for one standard deviation variation associated with this estimate. The letters account for Tukey post-hoc test where A and B are significantly different from one another while AB are not significantly different from A nor B.

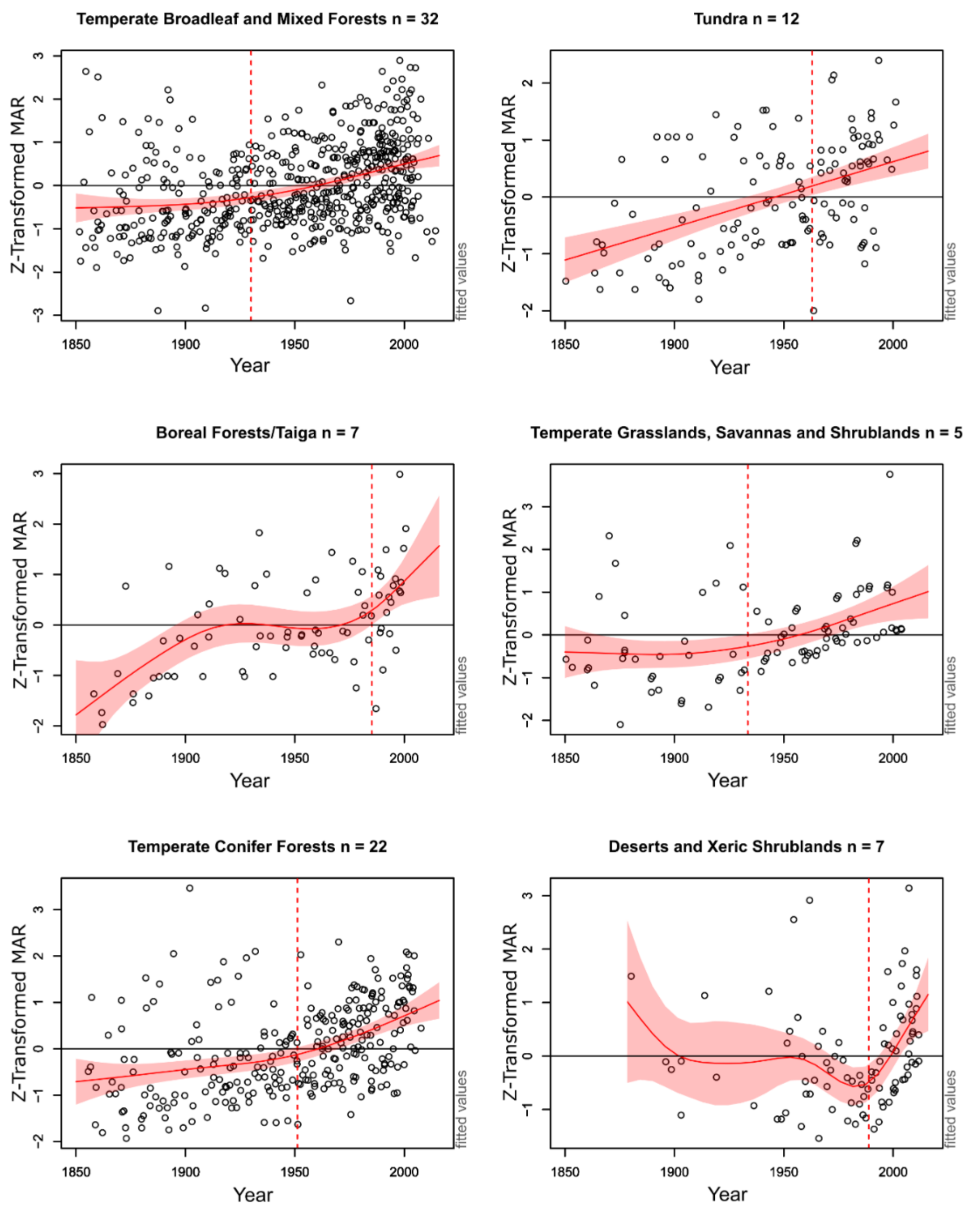

Figure A.4. Multi-panel showing the temporal variation in z-transformed sediment Mass Accumulation Rate (MAR) across different ecoregions, where each individual lake core measurement is shown as a black dot, all data beginning in 1850 AD are included. The general trend across all lake records was modelled by a separate general additive model per ecozone (red). Dashed horizontal red line indicates the onset of MAR acceleration across each ecozone; see Table I.1 for ecoregion-specific breakpoints and associated p-values

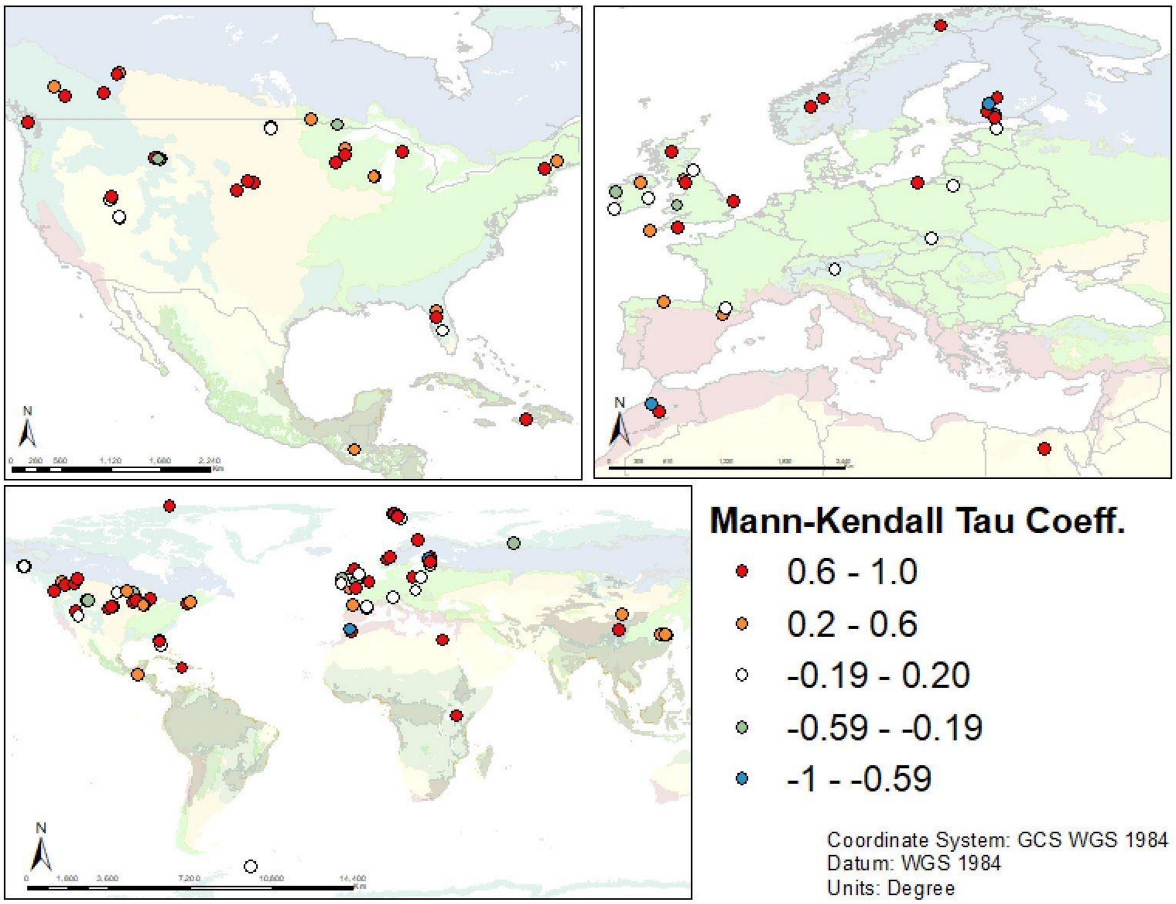

Figure A.5. Global distribution of Mann-Kendall (MK) tau coefficients demonstrating the spatial variation in MAR trends (based on 1850 AD to present records). A MK Tau coefficient lower than zero indicates a decreasing monotonic MAR trend while value above zero indicates an increasing monotonic MAR trend. Most lakes show a positive tau coefficient, which indicates that most lakes have recorded a temporal increase in MAR rates.

Table A.6. Results of linear mixed model testing the effect of land-use change defined as Population (inhabitants/pixel) and Cropland densities (km^2 of cropland/pixel) on Mass Accumulation Rates since 1850 AD (MAR). Population and Cropland were log-transformed(x+1) to account for sites that had no cropland nor inhabitants. MAR estimates were log-transformed.

Effect	Estimate (Std. Error)	Degree of Freedom	T-value	P-value
Fixed Effects				
Marginal R^2 = 0.42				
(Intercept)	-1.894 (0.11)	377	-17.26	<.0001
log-Population	0.211 (0.040)	377	5.23	<.0001
Log-Cropland	0.169 (0.082)	377	2.05	0.041
Random effects (Proportion of variance explained by LakeID and Ecoregions = 0.51)				
LakeID	0.163			
Ecoregion	0.0370			
Residual	0.0327			
Overall model: Conditional R^2 = 0.92				

Connecting statement between Chapters I and II

The results from this global synthesis of lake sedimentation rates presented in Chapter I highlighted a significant association between human development, through the intensification of agriculture and urban development, and lake sediment accumulation rates. Our results also demonstrated the marked acceleration in sedimentation rate that was recorded during the 1940s-1950s whereby it is estimated that lakes are currently accumulating 3 - 4x more sediment than they did since the end of the Holocene period (based on Jenny et al., 2019). Our study also demonstrated for the first time that diagenetic processes (i.e., compaction associated with sediment transformation and degradation) yielded inflated estimates of sediment accumulation rates at the top of sediment cores but could be partially accounted for by including data on sediment organic matter. Finally, my first chapter also demonstrated that across the three chronological models, the C.R.S. model was the most widely applied (> 75%) but that motivation for its selection over other chronological models relied on vague descriptions of how the C.R.S. model assumptions fit better than alternatives.

In my 2nd chapter, I developed an objective framework to consider the applicability and selection of the three different chronological models based on the quantitative assessment of their unique assumptions with the measured radioisotopes abundances. This 2nd chapter also served to gain a greater understanding of the spatial and temporal patterns of lake sedimentation rates across Eastern Canada and test whether the trends observed globally were conserved when investigating a more localized geographic region. In our statistical analyses of the sedimentation rate data, we considered explanatory variables specific to the region by collecting population counts obtained via historical Canadian census, and historical climatic data using archived meteorological station data.

CHAPTER II - A framework for ^{210}Pb model selection and its application to 37 cores from Eastern Canada to identify the dynamics and drivers of lake sedimentation rates

Alexandre Baud[1,2], Candice Aulard[2,3], Hamid Ghanbari[2,4], Maxime Fradette[5], Dermot Antoniades[2,4], Paul del Giorgio[2,3], Yannick Huot[2,5], Pierre Francus[6,7], John Smol[8] and Irene Gregory-Eaves[1,2]

[1]Biology Department, McGill University, Montréal, Québec, H3A 1B1, Canada

[2]Group for Interuniversity Research in Limnology and Aquatic Environments (GRIL);

[3]Département des sciences biologiques, Université du Québec à Montréal, Montréal, Québec, H2X 3X8, Canada

[4]Département de géographie, Université Laval, Québec City, Québec G1V 0A6, Canada

[5]Département de géomatique appliquée, Université de Sherbrooke, Sherbrooke, Québec, J1K 2R1

[6]Centre Eau Terre Environnement, Institut National de la Recherche Scientifique (INRS), Québec City, Québec, G1K 9A9, Canada

[7]GEOTOP, Geochemistry and Geodynamics Research Centre, Université du Québec à Montréal, Montréal, Québec H3C 3P8, Canada

[8]Biology Department, Queen’s University, Kingston, Ontario, K7L 3N6, Canada

Manuscript published in *Earth Surface Processes and Landforms* in May 2022

Abstract

Lake sedimentation rate represents a synthetic metric of ecosystem functioning. Many localized studies have reported a significant association between land use/land cover changes and lake sediment mass accumulation rates, with a few global syntheses echoing these findings at larger scales. In the literature, studies evaluating lead-210 (^{210}Pb) for establishing sediment chronologies will report at least one of three dating models, but the constant rate of supply (C.R.S.) model is the most widely used. However, it is often unclear how or why this model is selected, despite its influence on the interpretation of many subsequent analyses about ecosystem dynamics and functioning. It would thus be advantageous to design an objective and semi-automated way of choosing among dating models. We measured radioisotopic activities in 37 sediment cores across four ecozones of eastern Canada and developed an approach to assess model fit for the three commonly applied dating models. The derived chronologies were then used to evaluate the spatial and temporal variation in sedimentation rates across four ecozones in Canada (covering a surface area of 2.2×10^6 km^2). We observed a recent increase in lake sedimentation rates across most lakes, as has been observed globally, albeit with significant differences in the magnitude of sedimentation rates across ecozones. Across all lakes, we found that regional human population counts and mean annual air temperatures were significant temporal predictors of variation in mass accumulation rates. Overall, this analytical framework offers an objective approach for assessing fit and selecting among sediment age models, which contributes to a more robust quantification of sedimentation rates. With this first application, we provide a quantitative assessment of how lake

sedimentation rates have varied across a northern lake-rich region and have responded to environmental change.

Introduction

Lakes are critical ecosystems, acting as hotspots of biogeochemical cycling and biodiversity (Schallenberg et al., 2013). Using proxies of past conditions preserved in lake sediments, paleolimnologists can reconstruct shifts in lake ecosystem properties and of their surrounding watersheds, on scales spanning decades to millennia (Last et al., 2003; Korosi et al., 2013). While paleolimnology can provide insights and context for local and regional environmental changes over extended timescales, the study of lake sediment cores also provides key insights into ecosystem functioning (Millet et al., 2010; Winegardner et al., 2017). In particular lake sediment mass accumulation rates (MAR) are reflective of both the export of materials from the watershed and of material processing and burial within lakes, and in turn strongly influence the biogeochemical functioning of lakes. Several authors have recently evaluated the temporal change in lake sedimentation regimes and the factors controlling them across large regions. For example, sedimentation rates have increased globally during the mid to late Holocene, coincident with forest clearance and the onset of European-style agriculture (Jenny et al., 2016). Considering a more recent time frame, Baud et al. (2021) found global sedimentation rates to have increased 3- to 4-fold since ca. 1850 CE, associated with further expansion of agriculture and urbanization.

The development of reliable sediment chronologies is critical to establishing sedimentation rates, which in the absence of annual laminae (i.e., varves) are most often derived through the quantification and analysis of naturally occurring radioisotopes, such as radioisotopic lead (^{210}Pb) for recent sediments. ^{210}Pb has a half-life of 22.23 years (DDEP, 2010), and thus is an obvious candidate for the chronological dating of recent sediments. While the account of the lead radioisotopic decay series has been described elsewhere (Goldberg, 1963; Krishnaswami, 1978; Appleby and Oldfield, 1983), it is important to note that radioactive lead is part of the natural decay series of uranium. ^{210}Pb activities in sediment records originate from two components: 1) a supported ^{210}Pb component, derived from the in situ radioactive decay series of uranium-238 (^{238}U) in soils and from the transfer of radon-222 (^{222}Rn) via surface run-off or groundwater contribution; and 2) an unsupported ^{210}Pb fraction, derived from ^{222}Rn that first diffuses from the Earth's surface into the atmosphere and subsequently decays into ^{210}Pb (Ghaleb, 2009) (Figure II.1). This unsupported ^{210}Pb component is expected to follow a first order-decay rate while the supported ^{210}Pb component is expected to have a constant, near-zero activity. The supported ^{210}Pb fraction is often measured via gamma spectroscopy by quantifying the activity of short-lived daughter products of radium-226 (^{226}Ra) such as lead-214 (^{214}Pb) or bismuth-214 (^{214}Bi) (Martz et al., 1991). With gamma spectroscopy, additional radioisotopes independent of the ^{210}Pb decay series are routinely measured, providing validation for ^{210}Pb dating methods. These radioisotopes include cesium-137 (^{137}Cs) and americium-214 (^{241}Am), both of which are associated with radioactive fallout. Cesium-137 is expected to begin rising in the sedimentary record around 1950, when the first nuclear weapons tests were initiated, and reach peak activities ca. 1963 CE (Pennington et al., 1976), the year of maximum atmospheric nuclear testing (Wright et al., 1999). Likewise, ^{241}Am has been reported to reach maximum abundance around 1963 (Appleby et al., 1991). The meltdown of the Chernobyl reactors (1986 CE) created a second peak in ^{137}Cs, mainly over northern Europe.

Stemming from the behavior of the measured ^{210}Pb activity in sediment cores, different dating models have emerged, each with different assumptions and applications. There are three main models: the Constant Flux Constant Sedimentation model (C.F.C.S.); the Constant Initial Concentration model (C.I.C.); and the Constant Rate of Supply model (C.R.S.). All three models have a central assumption of an unmixed temporal structure of the sediment core where the ^{210}Pb incorporated within it follows its natural accumulated order and is not affected by any subsequent redistribution processes. However, the three models differ in the fraction of ^{210}Pb investigated and its expected decay function, thereby yielding divergent age models (Table II.1). The choice of model therefore has implications for the estimates of the age of individual sediment layers, but perhaps more importantly, may greatly influence not only the sediment mass accumulation rates that are derived from these modeled ages, but also any assessment of potential changes in these accumulation rates that may have occurred over past decades, the latter being a fundamental and yet unresolved issue in contemporary limnology.

When confronted with the outputs from the three dating models for any one sediment core, selecting the model that best reflects the core chronology is not a straightforward procedure. An in-depth evaluation of the sediment properties and possible changes in the sediment stratigraphy, the lake and its watershed and airshed as well as a clear account of historical events (human settlement, known flood events) are often necessary to gain full confidence in the derived chronology. This knowledge, which is also clearly useful for more than just developing a chronology, can be difficult to obtain, especially when considering large numbers of lakes or sites in remote regions. When dealing with model selection, previous regional coring efforts have used independent markers to validate the derived ^{210}Pb-based chronology, including other radioisotopes (e.g., ^{137}Cs and ^{241}Am), modern contaminants, forest fires or pollen markers indicative of recent settlement activities (e.g., the *Ambrosia* (ragweed) rise in eastern North America) (Blais et al., 1995; Smol, 2008).

Most commonly, only peak activities of ^{137}Cs and (more rarely) ^{241}Am are considered when evaluating ^{210}Pb-based chronologies. Given that gamma spectroscopy measures these radioisotopes at the same time as ^{210}Pb activities, many investigators have easy access to these data. Most studies publishing ^{210}Pb profiles measured from gamma spectroscopy will report the use of ^{137}Cs (Turner and Delorme, 1996). However, several papers have emerged over the past few decades highlighting the potential for post-depositional mobility of ^{137}Cs (Davis et al., 1984; Klaminder et al., 2012). Unfortunately, other independent measures can require extensive laboratory processing, or are simply not possible due to shortages of sediment material.

Based on several large, regional paleolimnological studies, a few key observations regarding sediment dating have emerged. For example, in a study of ~30 North American lakes, Binford et al. (1993) compared chronologies derived from the C.I.C. and C.R.S. models with multiple independent markers (^{137}Cs, fly ash, and the *Ambrosia* rise were analyzed in cores from Florida, New-England Adirondack Mountains and Minnesota). While the authors reported having considered both dating models, they later state that they relied exclusively on C.R.S.-derived ages. This choice was mainly motivated by the fact that previous studies had reported variable sedimentation rates and dilution of the ^{210}Pb in surficial sediment by higher sediment accumulation rates (Binford and Brenner 1986). In another study of 22 lake sediment cores from the Canadian Prairies, Turner and Delorme (1996) also considered multiple dating models and generally observed a good agreement (in over 50% of the cores) between the dates derived from C.I.C and C.R.S. models. Having validated their chronologies using *Ambrosia* pollen, the authors also noted that, in some instances, the close agreement in core chronologies between models only held true for the upper most (recent) section of the sediment cores, beyond which the C.R.S. model started to assign much older dates as a function of small increases in core depth. This account of age over-estimation of the C.R.S. model in deeper sediments was also noted in more recent work (Bruel and Sabatier, 2020). It is thus recommended to be careful or to avoid extrapolating C.R.S. age models beyond the point where the ^{210}Pb inventory has reached background activity. As reported from a global synthesis of published sediment chronologies from the *Journal of Paleolimnology*, the C.R.S. model was the most popular dating model, being reported in over 75% of the studies establishing recent sediment radiochronology (Baud et al., 2021).

In this study, we have explicitly applied and compared the three dating models to radioisotopic sediment profiles for 37 lakes spanning four ecozones of eastern Canada to develop a robust and consistent framework for the selection of lake sediment age models. We then applied the resulting framework to estimate mass sedimentation rates for these lakes, to assess both cross lake patterns in sedimentation and potential temporal shifts in these rates. Given the substantial differences in land use, vegetation and climate across these ecozones, we expected both differences in mean mass sedimentation rates as well as variation in recent sediment mass accumulation rates among ecozones. Furthermore, given that human population and land use have emerged as significant predictors of sedimentation rates in a global database (Baud et al., 2021), we tested the hypothesis that catchment-scale human population would be a significant predictor of sedimentation rates across time and among lakes in our four Canadian ecozones.

Methodology and Methods

Core collection and shipment

A total of 37 sediment cores was collected from lakes across four ecozones of Eastern Canada as part of the NSERC LakePulse network. Virtually all lakes greater than $0.1km^2$ and within 1km of a road were considered for selection by the modified stratified design whereby an equal number of lakes would be sampled across different ecozones (CCEA Canada Ecozones V5b, 2014) as well as lake area and human impact classes (Huot et al., 2019). Ecozones are defined as regional delineations of shared geological, climatic and ecological characteristics (Ecological Stratification Working Group, 1996). Logistical considerations meant that full cores were collected once a week, on the day before sample shipment, and thus slightly altered the original stratified design. Sediment cores were retrieved using the NLA Gravity corer (built by Aquatic Research Instruments) from the deepest point of the lake detected, or from the deepest point of one of the lake's sedimentary basins. On the same day as core collection, sodium polyacrylate was slowly added to a small volume of overlying water within the core tube to stabilize the water-sediment interface for shipping (Tomkins et al., 2008). The addition was done in increments (e.g., adding and waiting for stabilization) to limit porewater absorption. Once the sodium polyacrylate had formed a gel, the sediment cores were stored in a cooler at 4°C until shipping (usually within 24 hrs, (NSERC Canadian Lake Pulse Network, 2021)). Additional cores were also collected on the same day and extruded in the field for surface and pre-industrial sediment layers (Top-Bottom), and ^{210}Pb activities from these secondary cores were compared to the full cores. Full sediment cores were shipped on freezer packs to Laval University. Shortly after arrival, these sediment cores were split longitudinally for core scanning. One of the sediment core halves was kept as an archive while the other, "working half" was subsequently subsampled at 1 cm intervals and placed in Whirl-pak sampling bags that were kept frozen until freeze drying.

Gamma Spectroscopy

For each of the 37 full sediment cores, ~15 discrete sediment intervals along the depth of each core were prepared for gamma spectroscopy and analyzed at the Paleoecological Environmental Assessment and Research Laboratory (PEARL) at Queen's University, Canada. Briefly, sediment intervals were freeze-dried, placed into gamma tubes to a height of about 2.5 cm and sealed using 2-ton epoxy over a silicone septum and left to reach equilibrium for three weeks. An Ortec® high purity Germanium gamma spectrometer (Oak Ridge, TN, USA) was then used to measure the gamma activity of the radioisotopes ^{210}Pb, ^{214}Pb, ^{214}Bi and ^{137}Cs. The chronologies for these cores were derived from the measured radioisotopic activity using ScienTissiME 2.1.4 software (http://www.scientissime.net/) (Apr 2017) for the three dating models described above.

Overview of the Three Dating Models (C.F.C.S., C.I.C., C.R.S.)

The *simplest* model of the three is the C.F.C.S. model. It assumes a constant sedimentation rate throughout the entire sediment sequence, such that the activity of unsupported ^{210}Pb is expected to decay as a function of the cumulative dry mass of sediment in a core (Crozaz et al., 1964; Koide et al., 1972). Dates for sediment intervals are derived graphically from the slope of the log-transformed unsupported ^{210}Pb against cumulative dry mass (Sanchez-Cabeza and Ruiz-Fernandez, 2009). This dating model is described as the most appropriate for lakes where erosive processes in the catchment have been steady and in-lake productivity has been constant (Appleby and Oldfield, 1983), as exemplified by many remote and large Alaskan lakes (Rogers et al., 2013).

The C.I.C. model assumes a 1st order decay of the unsupported ^{210}Pb activity. However, the C.I.C. model relies on the assumption that there will be a constant activity of unsupported ^{210}Pb in each sediment layer as it is formed. This model allows for variation in sedimentation rates but assumes that increases in the flux of sedimentary particles from the water column will proportionally increase the ^{210}Pb deposited to the sediment floor, thus yielding constant initial unsupported ^{210}Pb activities irrespective of any variations in sediment accumulation rate (Appleby and Oldfield, 1983).

Finally, the C.R.S. model also assumes a 1st order decay rate but is based on the decay of the total cumulative unsupported ^{210}Pb activity, also known as the total ^{210}Pb inventory (A_0). A_0 is the cumulative, density-corrected unsupported ^{210}Pb measured across sediment intervals (Sanchez-Cabeza and Ruiz-Fernandez, 2009). In this model, the underlying hypothesis is that there is a constant fallout of ^{210}Pb from the atmosphere, yielding a constant rate of supply of unsupported ^{210}Pb to the sediment surface (Appleby and Oldfield, 1983). However, across different layers, the unsupported ^{210}Pb of the initial activity (at time zero) will be inversely proportional to the mass accumulation rate, such that increases in sediment erosion or autochthonous production could result in a dilution of unsupported ^{210}Pb.

<u>Dating Model Selection</u>

To evaluate the performance of the different dating models generated by the ScienTissiME software, we plotted for each lake the pattern of the unsupported ^{210}Pb ($^{210}Pb_{Unsupp.}$) content measured throughout the cores as a function of the expected decaying trends across each model as detailed in Appleby and Oldfield (1983).

For the C.F.C.S. model, the log-transformed unsupported $^{210}Pb_{Unsupp.}$ was plotted against the cumulative dry mass of sediment. As described in Appleby et al. (1983), for the C.F.C.S. model to be considered valid, log-$^{210}Pb_{Unsupp.}$ must follow a linear relationship with cumulative dry mass.

$$\mathrm{Log}(C_{t_x}) = \mathrm{Log}(C_0)\ e^{-\lambda \frac{m}{MAR}} \qquad \text{(Equation 1)}$$

Where *log*(C_{t_x}) is the log-transformed activity of $^{210}Pb_{Unsupp.}$ (Bq kg^{-1}), *log*(C_0) the initial log-transformed activity of $^{210}Pb_{Unsupp.}$, λ the ^{210}Pb disintegration constant (λ = 0.03114 year^{-1}); *m* the cumulative dry mass of the sediment core (g) and *MAR* the sediment mass accumulation rate (g cm^{-2} year^{-1}).

To evaluate performance of the C.I.C. model, we modeled the expected decay of the measured $^{210}Pb_{Unsupp.}$ activity as a function of cumulative dry mass. To allow for the 1st order reaction to reach "background" activity (= where the unsupported ^{210}Pb level reaches the supported ^{210}Pb

activity; ~1900 CE) at the observed cumulative dry mass, we incorporated the measured cumulative dry mass where background is reached (m_{bgd}) as the denominator of the decaying-section of the equation (= exponent denominator) and replaced $\lambda * t_x$ by the ratio of age-background (t_{bgd} = 1900 CE) to ^{210}Pb half-life ($t_{1/2}$=22.23 years).

$$C_{t_x} = C_0 e^{-\lambda t_x} = C_0 e^{-\frac{\frac{t_{bgd}}{t_{1/2}}}{m_{bgd}} \cdot g\ cm^{-2}\ yr^{-1}} \qquad \text{(Equation 2)}$$

The expected decay rate associated with validation of the C.R.S. models followed a similar methodology as for the C.I.C. expected decay profile, but further considered the 1st-order decay rate of the ^{210}Pb inventory, which evaluates the density-corrected cumulative content of $^{210}Pb_{Unsupp.}$: A_0 (Bq m^{-2}). Similar to what has been previously described, the ^{210}Pb inventory was modeled to decay as a function of cumulative dry mass where ^{210}Pb inventory reaches background supported ^{210}Pb.

$$A_{t_x} = A_0 e^{-\lambda t_x} = A_0 e^{-\frac{\frac{t_{bgd}}{t_{\frac{1}{2}}}}{m_{bgd}} \cdot g\ cm^{-2}\ yr^{-1}} \qquad \text{(Equation 3)}$$

To compare models and select the most robust among them, we evaluated the fit (R^2) between observed ^{210}Pb content and predicted ^{210}Pb quantities derived from the expected decaying trends. To remove the scale impact in relation to the different ^{210}Pb quantities evaluated (log($^{210}Pb_{Unsupp.}$) for C.F.C.S., $^{210}Pb_{Unsupp.}$ for C.I.C. and ^{210}Pb Inventory for C.R.S.), we Z-transformed the observed and the predicted ^{210}Pb quantities and calculated the resulting *Z-scaled* Root Mean Squared Error (Z-RMSE). The model returning the greatest R^2 and the lowest Z-RMSE values was then selected. A summary of the steps taken towards model selection is available in the supplementary materials (Figure B.1). Chronologies from selected dating models yielding non-increasing age-depth relationships were rejected, and instead we selected chronologies from the dating model returning the second highest R^2 and second lowest Z-scaled RMSE. Lake sediment cores displaying both a uniform $^{210}Pb_{Total}$ distribution along core depth and the lack of a distinct ^{137}Cs peak should also qualify for rejection because of concerns over potential mixing and/ or re-distribution of $^{210}Pb_{Total}$, thereby violating dating model assumptions. In general, a thorough investigation of the resulting mass accumulation rates should be performed, leading to the potential rejection of the chronology when anomalous MAR estimates have been identified.

General errors and chronological uncertainty

Analytical errors linked with gamma detection of the naturally occurring radioisotopes were reported following the equation provided in Sanchez-Cabeza and Ruiz-Fernandez (2012). This error was propagated to the calculation of age estimates using empirical equations as it is generated in ScienTissiME 2.1.4. Another error in establishing core chronologies using ^{210}Pb is if the uppermost unconsolidated section is not retrieved by the coring device (Crusius and Anderson, 1991) or was potentially influenced by the sodium polyacrylate addition. To evaluate these processes, we compared ^{210}Pb unsupported activities from the first subsampled interval of our full sediment cores (0-1 cm) to the *Top* (0-1 cm) sample collected from the additional sediment cores (Top-Bottom) retrieved the same day and extruded in the field. This comparison yielded a robust correlation coefficient ($R^2 = 0.64$) indicative that the ^{210}Pb activities in the top intervals of the full sediment cores were similar between cores. Due to the large-scale nature of the sampling protocol the full sediment cores were sub-sectioned horizontally every cm in the lab. This coarse subsampling led to a reduction in the number of intervals available for dating model selection in regions of low sedimentation rates, likely reducing the robustness in model selection. For each derived chronology, age estimates were compared to the natural ^{137}Cs maximum abundance found within each sediment core, but with full knowledge that the ^{137}Cs peak may be mobile within the sediment column (see Metadata). To compensate for the coarse subsampling resolution when investigating naturally occurring ^{137}Cs maxima in sediment stratigraphies, we used a spline interpolation to model the raw abundance of ^{137}Cs across sediment intervals. A graphical representation of each radioisotope profile was made against the expected decay profile across each model, and the fit between expected ^{210}Pb, generated from empirical equations, and observed ^{210}Pb activity measured across intervals was compared by linear regression (Figure II.2).

__Sediment Mass Accumulation Rate Calculation__

Lake sediment mass accumulation rates were calculated following model-specific equations. For the C.F.C.S. model, sediment Mass Accumulation Rate ($MAR_{C.F.C.S.}$, g cm^{-2} year^{-1}) was calculated based on the slope of the natural log unsupported ^{210}Pb ($Log(C_{tx})$) regression as a function of cumulative dry mass. Following the parametric equation "y = a + bx", *a* equals log-transformed C_0 and b ($\frac{1}{g\ cm^{-2}}$) is the slope of the log-transformed Cx relationship with cumulative dry mass. MAR can be derived using the following:

$$MAR_{C.F.C.S.} = \frac{-\lambda}{b} \qquad \text{(Equation 4)}$$

For the C.I.C. model, sediment mass accumulation rate ($MAR_{C.I.C.}$, g cm^{-2} year) was calculated from the mass difference between two intervals i and j (m_i and m_j) and the associated elapsed time between the deposition of these two layers ($\Delta t = t_i - t_j$, years)

$$MAR_{C.I.C.} = \frac{m_j - m_i}{\Delta t} \qquad \text{(Equation 5)}$$

For the C.R.S. model, sediment mass accumulation rate ($MAR_{C.R.S.}$, *kg* m^2 $year^{-1}$) was calculated for each interval based on the proportion of unsupported ^{210}Pb (C_{t_x}, Bq kg^{-1}) to cumulative ^{210}Pb inventory from the bottom of the core to interval corresponding to time t_x (Bq m^{-2}).

$$MAR_{C.R.S.} = \lambda \times \frac{A_{t_x}}{C_{t_x}} \qquad \text{(Equation 6)}$$

$MAR_{C.R.S.}$ is obtained by means of a ratio, and low C_i values can be measured when approaching background supported ^{210}Pb activity; as a result, artificially elevated values in $MAR_{C.R.S.}$ can be detected. For this reason, we removed one estimate of $MAR_{C.R.S.}$ associated with lake 08-179 where the specific $MAR_{C.R.S.}$ was 87 times greater than the rest of $MAR_{C.R.S.}$ for this lake.

Census Population Reconstruction

We delineated the hydrologically conditioned watersheds of the lakes using a 20 m flow direction raster layer acquired from the 0.75 arc second Canadian Digital Elevation Model dataset (Government of Canada, 2015). The delineation uses the union of all sub-drainage basins that reach each point along a lakeshore based on the National Hydro Network lakes polygon data (Government of Canada, 2017). We then acquired Census Subdistrict (CSD) boundary files from 1911 CE to 2016 CE (accessible from: http://geo.scholarsportal.info/) along with the relevant microstatistics table files that feature the total population within each CSD (accessible from: http://odesi2.scholarsportal.info/webview/). In an effort to normalize the geographical data and to overcome issues of the Modifiable Areal Unit Problem (MAUP) (Openshaw, 1983), we used the WorldPop UN dataset to redistribute CSD population counts across each CSD. To reduce the error associated with new urban development arising during the 20th century, digitized historical topographic maps were used when available. These historical maps were acquired from national and university libraries (Scholar Geoportal for Ontario, BaNQ for Quebec and from an online repository from the University of Ottawa). These maps were produced from 1909 to 1989 CE at a resolution of 1:63,360 or 1:50,000. These maps were georeferenced using the WGS84 coordinates present on the map. Each “house” on the maps was accounted for by a point feature. We then compared our redistributed population against the georeferenced point feature layer to ensure our population estimates were adequate.

Temporal Temperature and Precipitation reconstruction

Historical (1841 CE – 2017 CE) monthly records of air temperature and precipitation were obtained from Environment and Climate Change Canada using the rclimateca package (Dunnington, 2018). Only stations with at least a complete year of monthly data were selected to create mean annual temperature and total annual precipitation estimates for each station. Rather than assigning air temperature and precipitation estimates based on the nearest station (which can be hundreds of km away), estimates from stations within 75 km of the study site were spatially interpolated, forming rings of raster values (estimated temperature and precipitation) around the input station. This step ensured that the estimated temperatures for any site were reflective of station input data.

Lake Morphometric and Watershed Land Use, Bedrock Geology and Soil Composition

Basic lake morphometric information was recorded across all lakes featured in this study. Lake maximum depth (m) was estimated as the maximum depth measured by the field teams during sampling with aid of bathymetric maps when available. Lake surface area (km^2) was obtained via Canvec/HydroLakes and altitude (m a.s.l.) calculated from The Canadian Digital Elevation Model (CDEM).

Since the methodology developed for the LakePulse pan-Canadian sampling of lakes involved the classification of lakes according to the relative proportion of natural to more intensive land uses (e.g. Agriculture, Urban, Mines; see Huot et al. (2019) for details) in their watersheds, we explored the influence of each of these land-use types on the variation observed in lake sediment mass accumulation rates. A table summarizing data sources included in Huot et al. (2019) is available in the supplementary materials of this study (Table B.1). We simplified the original land use definitions found in *Annual Space-Based Crop Inventory for Canada* (2016) and in *Land Use* (2010) into seven categories (NoData, Water, Natural Landscape, Forestry, Urban, Agriculture, Pasture and Mines). A table summarizing the original class definition and the simplified categories is also available in the appendices for Chapter II (Table B.2).

To investigate the role of watershed soil and geological composition on the variation observed in mass accumulation rates, we acquired bedrock geology from the Geological Survey of Canada (1996) and computed the intersection between the watershed polygons and the bedrock geology polygons. With one of the lakes' watersheds spanning outside of Canada into the USA, "NoData" has been assigned for this portion of the watershed. Soil properties maps generated by the International Soil Reference and Information Centre (ISRIC) were retrieved from *soilgrids.org.* From the available soil horizon depths, we selected the 0-5m depth layer and computed for each watershed the mean abundance of all soil property values.

Statistical analyses

All statistical modelling was performed using R (R Core Team, 2013) and all occurrences of log-transformed variables refer to the common (i.e., base 10) logarithms. Specific packages used include *davies.test::segmented* for the analysis of breakpoints in the regression parameter in the linear predictor (Muggeo, 2003). General additive mixed effects models (GAMMs) were fitted using the r package *mgcv* (Wood, 2012). A random factor was assigned to lake identity (LakeID) to structure errors in the model's residuals. In GAMMs, the estimated degree of freedom (e.d.f.) summarizes the degree of non-linearity of the modelled trends, with values of

1 being linear and with any value above 1 reflecting a departure from linearity. To establish the potential significant differences in lake sediment mass accumulation across different timesteps instructed from Davies' test, we first assessed the normality in the paired MAR differences (pre and post breakpoint) for each of the four ecozones using a Shapiro-Wilk test. Since all ecozone specific Shapiro-Wilk tests returned p-values greater than $p = 0.05$, the paired MAR differences were considered to be normally distributed and the significant difference in means was evaluated using a paired t-test. To establish a predictive model of recent mean lake mass accumulation rates, we selected and averaged MAR estimates ranging from 2000 to 2017 (the latter indicative of the year when the cores were retrieved). Using a post-2000 period was mainly motivated by the limited availability of environmental datasets that are necessary to explore the drivers of recent lake MARs. Lake specific recent mean MARs were then used in a multiple linear regression model. For this predictive model, the explanatory variables that were considered included climatic variables (mean annual air temperature (MAT, °C) and total annual precipitation (mm)), watershed land-use variables (fraction of agriculture in the catchment (%), population count (individuals), soil and bedrock geology fractions (%)), watershed size (km^2), and lake morphological variables (lake depth (m), lake surface area (km^2)).

Results

Assessing the Performance of Dating Models

Across the 37 sediment cores considered, the C.R.S. model returned higher R^2 values for 30 lakes when assessing the fit between observed and predicted values of unsupported ^{210}Pb. The C.I.C. model typically had the lowest fit, while the C.F.C.S. equation performed well in only a handful of lakes (Table II.2). Considering each of the four ecozones separately, the C.R.S. model always returned the highest R^2 for lakes in the Mixedwood Plains region. In contrast, the C.F.C.S. model was selected as having the best fit in several Boreal Shield sites, although the C.R.S. was still deemed appropriate for most lakes in this ecozone. Lakes set in the two Atlantic ecozones (Atlantic Highlands and Atlantic Maritime) also predominantly followed the C.R.S. exponential decay of ^{210}Pb inventory quantities (Table II.2). While the C.R.S. model generally produced a higher R^2 than the other models, for some lakes the C.F.C.S. model and the C.R.S. model generated similar R^2 values (Table II.3, Figure B.2). Lakes with higher proportions of urban land cover in their watersheds tended to display a greater R^2 difference between C.F.C.S. and C.R.S. models. While the agriculture fraction within watersheds was also tested, it was not a significant predictor of this difference. There was no clear spatial distribution signal in the selected chronological model (Figure II.3).

Temporal variation in sediment mass accumulation rates

Using the selected dating model identified for each ecozone, we considered region-specific change in lake MARs. While pre-industrial (pre-1900) lake sediment MARs exhibited similar values across all four ecozones, with estimates ranging from 6.3×10^{-3} to 1.5×10^{-2} g cm^{-2} year^{-1}, there was a marked difference across ecozones, with lakes in the Mixedwood Plains (M.P.) accumulating a greater amount of sediment than lakes in the other 3 ecozones (Figure II.4a). One lake set in the Boreal Shield (B.S.) had highly elevated MAR estimates compared to other lakes in this ecozone. This site is located in the floodplain of Lac St-Jean (QC), and the ^{210}Pb profile suggested numerous rapid-deposit events (see Metadata). Given that this lake (Lac à la

Croix, 06-103) was not representative of its region's sedimentation rate patterns, it was removed from the dataset for any further analysis. Region-specific modelled trends provided evidence of non-linear variation in MARs across three of the four ecozones evaluated, with GAM-estimated degree of freedom (e.d.f.) values ranging from 1.12 - 1.49 (Figure II.4b). The Atlantic Maritime (A.M.) and Atlantic Highlands (A.H.) as well as the Mixedwood Plains displayed nearly constant rates of sedimentation prior to the 1940s. Between 1947 and 1956, rates of sedimentation accelerated across these three ecozones (supported by the Davies test results, Figure II.4b). In the case of the Boreal Shield, the GAM did not detect any support for nonlinear temporal variation of MAR.

Considering the continuous temporal variation observed for MAR and the marked acceleration in lake MAR as evidenced from the Davies test (Figure II.4a and b), we considered a former timestep defined as *pre-1955 CE*, which includes MAR estimates prior to the acceleration recorded across Eastern Canada. A second timestep – post-2000 CE, reflective of the last ~20 years of MAR – was also considered as it is the focus of a subsequent analysis in this study where we evaluate the predictors of recent lake MARs. As described previously, using a post-2000 timestep was partly motivated by the limited availability of environmental datasets which are necessary to explore the drivers of recent lake MARs. Shapiro-Wilks tests of normality demonstrated the normal distribution of the paired MAR differences in all four ecozones. Paired t-tests for each of the four ecozones evidenced significant differences in lake sediment mass accumulation rates (Figure II.5). For both the Atlantic Highlands and Maritimes regions, mean MAR between time steps doubled: A.H. $t(10) = -3.17$, $p = 1.0 \times 10^{-3}$; A.M. $t(5) = -$

3.30, $p = 2.1 \times 10^{-2}$. For the Mixedwood Plains, mean MAR quadrupled: $t(7) = -2.42$, $p = 4.6 \times 10^{-2}$. In contrast, the change in mean MAR across the two time periods in the Boreal Shield was more modest, but paired t-tests still detected a significant difference in lake MARs across the two timesteps considered (B.S. $t(8) = -2.72$, $p = 2.6 \times 10^{-2}$).

Temporal drivers responsible for increased lake sediment mass accumulation rates

We applied a linear mixed effects model, correlating our estimates of mass accumulation rates year by year with population counts (number of individuals; measured approximately every 5 years), climate estimates (Mean Annual air Temperature (MAT, °C) and total annual precipitation (mm)) linearly approximated to the same year as the MAR estimate, to evaluate the temporal drivers of variation and the spatial component of the dataset as accounted for by using LakeID as a random effect. We found that mass accumulation rates (log-transformed) were positively related to log(x+1) transformed population count in the watershed (Slope = 0.177 (± 0.046), D.F. = 146, p-value = < 0.001). MAT (°C) was also found to be positively related to log-transformed lake MAR, but its contribution to the model was smaller than that of population count (Slope = 0.0912 (± 0.046), D.F. = 146, p-value = 0.0515). Overall, our regression model, which considered ~120 years of sedimentation rates for 37 sediment cores, was capable of accounting for 22% of the variation in its fixed effects. We also tested mean total annual precipitation (derived from Environment and Climate Change Canada monitoring stations) as a predictor for temporal variation in MAR, but it was not a significant parameter in the linear mixed effects model. However, LakeID as a random factor explained a large proportion (49%) of the residual variation (Table II.4).

Predictive model for recent lake sediment average mass accumulation rates

Through multiple linear regression, we investigated the cross-lake variation in modern mean MAR post-2000 CE (all MAR estimates from a single lake averaged between 2000 – 2017 and expressed $MAR_{2000\text{-Present}}$, g cm^{-2} year^{-1}) to identify significant predictors of this variation. Anthropogenic indicators, specifically the fraction of agriculture expressed in percent (p-value = 2.5×10^{-4}) and log-transformed human population count (number of individuals) (p-value = 1.1×10^{-4}) in lakes' watersheds averaged between 2000 and 2016 explained the greatest amount of variation in recent lake sediment mass accumulation rates. Another variable that accounted for a significant portion of the variation was mean total annual precipitation (over the post-2000 CE period; p-value = 2.4×10^{-4}). Altogether these variables accounted for 57% of the variation observed in average recent lake sediment mass accumulation rates (post-2000 CE) (Figure II.6). Additional variables, such as the proportion of sand in the lake watershed and log-transformed lake maximum depth, were also found to be weakly significant (p-value < 0.1) but were omitted from the regression equation to prevent over-fitting of the model. The final model is expressed as:

$$\mathrm{Log}(\text{Mean MAR}_{2000\text{-Present}})\ (\text{g cm}^{-2}\ \text{year}^{-1}) = -\ 8.86 + 4.3 \times \text{Mean Agriculture}_{2000\text{-Present}}\ (\%) + 0.22 \times \mathrm{Log}(\text{Population Count}_{2000\text{-Present}} + 1)\ (\text{individuals}) + 0.0036 \times \text{Mean Precipitation}_{2000\text{-Present}}\ (\text{mm})$$

(Equation 6)

Discussion

The need for a reproducible establishment of lake sediment chronologies

Developing a robust chronology and calculating mass sediment accumulation data are critical steps in most paleolimnological and biogeochemical lake studies. The new insights gained from our inter-regional study of lake core dating and sedimentation rates are methodological and data-driven. On the methodological front, we present a robust empirical framework for evaluating the three most commonly used chronological dating models. Applying this new framework whereby we fit model-specific empirical equations and compared the outcomes statistically to 37 sediment core records from across 4 ecozones, we clearly showed substantial spatio-temporal variation, for which we identified significant predictors.

Earlier work had shown that the C.R.S. model dating results are those most frequently reported in the literature, but it is not always clear why this approach was adopted. The difficulty of dating model selection becomes even greater when the number of sediment cores to be dated increases, or with growing spatial coverage. However, this challenge can now be met with the approach we have described for assessing how closely the measured isotopic activities are in accordance with the specific assumptions of each chronological model. This standardized method of evaluating different chronologies will further facilitate identification of the most reliable chronological dating model where model assumptions are respected. Interestingly, Barsanti et al. (2020) recently conducted an interlaboratory calibration exercise with 14 different laboratories worldwide to evaluate a single lake sediment isotopic profile and no consensus was reached with regard to dating model selection: seven laboratories selected the C.R.S. model, five adopted the C.F.C.S. model, another one chose the C.I.C model, and finally the last group selected a modified version of the C.F.C.S. model. Clearly, there is a need to standardize approaches to model selection.

From a mathematical perspective, there is a greater probability of obtaining a better R^2 value when considering the C.R.S. or the C.F.C.S. model assumption over the C.I.C. model. Specifically, the C.F.C.S. model is based on analyses of log-transformed ^{210}Pb activity, which reduces to some extent the stochastic nature of radioisotopic measurements in sediment and thus one can expect a stronger fit relative to C.I.C. model results. For the C.R.S. model, the analyses are based on the cumulative ^{210}Pb inventories and it is thus less sensitive to inter-sample variation that could be apparent with C.I.C. models. Independent of the dating model, the establishment of a robust chronology also depends on the number of sediment intervals with measurable $^{210}Pb_{unsupp.}$ exceeding equilibrium with $^{210}Pb_{supp.}$. For this reason, it is recommended to adjust sediment core subsampling according to empirical regional sedimentation rates.

Distribution of assigned chronological model across ecoregions

The selection of chronological dating models across the 37 sediment cores using our framework was in line with findings from the literature, where the C.R.S. model was selected the most frequently (Dillon et al., 1986; Appleby, 2002). Our observation that the C.R.S. model was the most appropriate for 100% of lakes studied from the Mixedwood Plains suggests that changes in sedimentation rate are common in this region, which is a plausible hypothesis as this ecozone is the most densely populated region of Canada. In the Atlantic Highlands and Atlantic Maritimes, a majority of cores (> 80%) displayed ^{210}Pb activities best modeled following the C.R.S. model assumptions *and* showed increased sedimentation rates. Increased sedimentation rates were not unexpected, either, given the long history of settlement in the area. By contrast, 30% of the cores from the Boreal Shield had ^{210}Pb activities that matched most strongly with the C.F.C.S. model's assumption (i.e., a consistent a log-linear decay of ^{210}Pb activities with cumulative dry mass). The C.F.C.S. model was designed for lakes where erosive processes in the catchment are steady and in-lake productivity is constant (Appleby and Oldfield, 1983), which aligns with the more pristine and remote settings of many lake-watershed ecosystems in the Boreal Shield. It is also interesting that while only one of the 37 sediment cores followed the C.I.C. model's assumptions, dates generated by this model could not be applied due to non-decreasing age with depth. While Appleby and Oldfield (1992) described an example where the chronological C.R.S. model was invalidated due to discontinuity within the sediment stratigraphy, the lake in our study for which C.I.C. was selected was not one exhibiting the most drastic stratigraphic changes. We thus recommend a careful contextualization of stratigraphical facies with radioisotope profiles (^{210}Pb, ^{137}Cs and ^{241}Am).

One of the challenges with developing an empirical means to estimate chronologies from ^{210}Pb is the establishment of the expected ^{210}Pb decay trend. We must assume the age associated with the sediment cumulative dry mass where unsupported ^{210}Pb activity has reached supported ^{210}Pb activity (= t_{bgd}) (see Equations 2- 3). Depending on lake location, one can often detect 4-5 half-lives before reaching the supported ^{210}Pb activity. However, at high latitudes, where the flux of atmospheric ^{210}Pb can be lower (Baskaran and Naidu, 1995; Tomkins et al. 2009) or at locations where elevated autochthonous production leads to the dilution of unsupported ^{210}Pb in the sediment (Binford and Brenner, 1986; Arias-Ortiz et al., 2018), the number of half-lives detected can decrease on the order of 1-3 half-lives. In our study, the estimated age of background was selected to be 110 years, which corresponds to 5 half-lives. Results of the sensitivity analysis (Figure B.3) demonstrated that the model selection we present in this manuscript was consistent across the range of naturally expected values for t_{bgd} (80 – 130 years) and did not elicit any analytical artifacts as can be seen outside of this range.

While we have highlighted the models with the best fit, it should be noted that in many cases the R^2 values were very close across dating models for the same core (Figure B.2). In such cases there was an important overlap between dating models, at least for the uppermost section of the cores (see Metadata) prior to C.R.S. model yielding older age estimates for bottom samples. While this phenomenon has been described elsewhere (Turner al., 1995; Bruel and Sabatier, 2020), our results further reinforce the need to cautiously consider these older dates and evaluate different dating models. With only a few lakes not returning C.R.S. as the best dating model, we did not observe striking regional differences when using MAR estimates derived solely from the C.R.S. models (Figure B.4).

Temporal drivers of sediment mass accumulation rate across Eastern Canada

Mass accumulation rates across ecozones generally matched previous estimates from the literature and varied substantially across lakes within regions and also across ecozones. Set in similar geological environments rich in granite and gneiss, with cool and moist climates, the Atlantic Highlands and Atlantic Maritimes had similar MAR estimates. Greater proportions of sand in these lakes' watersheds were found to negatively influence MARs, and the contemporary anthropogenic development experienced predominantly in the coastal lowland areas of these regions could be at play. The lakes from the Boreal Shield are in a different geological and hydrological region defined by a strong continental climate and Precambrian granitic bedrock and, surprisingly, were not characterized by lower mean mass accumulation rates. Lakes from the Boreal Shield also experienced less development of anthropogenic land use within their watersheds (Huot et al., 2019). In contrast, lakes from the Mixedwood Plains which are associated with a warmer climate and lie in watersheds with fertile soils, along with more extensive anthropogenic development, accumulated a significantly greater mass of sediment than the three other ecozones. When breaking down the temporal variation into two timeframes (pre-1955 and post-2000 CE), it is apparent that all 37 lakes accumulated comparable amounts of sediment prior to the 20th century. With all four ecozones having similar baseline mass accumulation rates, ranging from ~ 6.3×10^{-3} to 1.5×10^{-2} g cm^{-2} year^{-1}, it is lakes from the Mixedwood Plains that have recorded the largest recent increases in sediment MAR.

From the ecozone-specific General Additive Models, we can conclude that MAR estimates in the Boreal Shield exhibited a linear temporal increase while the other 3 ecozones displayed non-linear temporal variation in MARs with GAM e.d.f. values ranging from 1.12 to 1.49. Another commonality found across these three ecozones was the timing of the MAR acceleration onset. Lakes in the Mixedwood Plains and Atlantic Highlands ecozones were first to experience MAR acceleration with estimated onset occurring around 1947 and 1949, respectively. Lakes in the Atlantic Highlands closely followed with a recorded MAR onset around 1958. These reported onsets of MAR acceleration values are similar to those identified from global lake sediment assessments. For example, in Baud et al. (2021), an onset of global MAR acceleration was identified around 1941 and was explained by widespread increases in anthropogenic landscape transformations and application of fertilizer. Echoing these findings, our results from the linear mixed effects model detected significant associations between sediment MAR and anthropogenic land-use variables, where percent agriculture and population count in lake watersheds were found to be significant predictors. While climate accounted for some variation in sediment mass accumulation rates when evaluating recent average MAR, it did not account for a significant part of the variation when assessing the temporal variation in MAR. The lack of historical climate data that are distributed in sufficiently close proximity to our sites in Eastern Canada may be part of the problem. Indeed, only a few stations in the Boreal Shield region were available, limiting the scope of the analysis. When considering additional variables, such as the geological characteristics of the watershed or lake morphometric variables (lake area, lake maximum depth), the fraction of sand present in the lake watershed and log-transformed lake maximum depth were only marginally significant (p-value < 0.1).

Data Availability Statement

Radioisotopic activity profiles and associated ^{210}Pb dates derived from the 37 sediment cores , as well as human population and climatic data are available from the open science platform Zenodo accessible at https://zenodo.org/record/7372968 . Land use, bedrock geology and soil composition information layers will be available from the LakePulse website (https://lakepulse.ca/)

Conclusion

We generated a framework to examine ^{210}Pb activities to enable dating model selection following a repeatable and quantifiable approach. Using this approach, the C.R.S. dating model was selected as the most robust model for a majority of sites. We identified heterogeneity across ecozones of eastern Canada in terms of the amount of sediment that lakes accumulate. Mixedwood Plains lakes accumulated on average 4 times more sediment than any of the three other ecozones. While all four ecozones of Eastern Canada have recorded temporal increases in lake sediment MAR since 1880 CE, it is the Mixedwood Plains ecozone that recorded the greatest increase with over a 4-fold increase from baseline rates. We conclude that the likely influence of population size in the watershed and increasing temperatures were significant predictors for this MAR temporal variation. We also found that current mean lake sediment MAR can be predicted using anthropogenic land-use variables (population count and percent agriculture) along with precipitation within the watershed. Bridging the analytical model selection and the derived implication for lake sedimentation provides a comprehensive approach for dealing with sedimentation rate variations, which in turn is critical for the establishment of mass-balance models evaluating sediment constituents such as carbon and heavy metals.

References

Appleby, P. G. and Oldfield, F. (1978). The calculation of lead-210 dates assuming a constant rate of supply of unsupported 210Pb to the sediment. *Catena*, 5(1), 1-8.

Appleby, P. (2002). Chronostratigraphic techniques in recent sediments. In: Last, W. and Smol, J.P. Editors. Tracking environmental change using lake sediments: Vol 1. Basin analysis, coring, and chronological techniques. (pp. 171-203) *Springer*.

Appleby, P. and Oldfield, F. (1983). The assessment of ^{210}Pb data from sites with varying sediment accumulation rates. *Hydrobiologia*, 103(1), 29-35.

Appleby, P., Richardson, N. and Nolan, P. (1991). ^{241}Am dating of lake sediments. *Hydrobiologia*, 214(1), 35-42.

Arias-Ortiz, A., Masqué, P., Garcia-Orellana, J., Serrano, O., Mazarrasa, I., Marbà, N., Lovelock, C.E., Lavery, P.S. and Duarte, C.M., (2018). Reviews and syntheses: ^{210}Pb-derived sediment and carbon accumulation rates in vegetated coastal ecosystems–setting the record straight. *Biogeosciences*, 15(22), 6791-6818.

Barsanti, M., Garcia-Tenorio, R., Schirone, A., Rozmaric, M., Ruiz-Fernández, A.C., Sanchez-Cabeza, J.A., Delbono, I., Conte, F., Godoy, J.D.O., Heijnis, H. and Eriksson, M., (2020). Challenges and limitations of the ^{210}Pb sediment dating method: Results from an IAEA modelling interlaboratory comparison exercise. *Quaternary Geochronology*, 59, 101093.

Baskaran, M. and Naidu, A. (1995). ^{210}Pb-derived chronology and the fluxes of ^{210}Pb and ^{137}Cs isotopes into continental shelf sediments, east Chukchi Sea, Alaskan Arctic. *Geochimica Et Cosmochimica Acta*, 59(21), 4435-4448.

Baud A., Jenny J.P., Francus P. and Gregory-Eaves I. (2021) Global spatio-temporal analyses identify an acceleration of lake sedimentation rates associated with modern land-use change. Journal of Paleolimnology.

Binford, M. W. and Brenner, M. (1986). Dilution of ^{210}Pb by organic sedimentation in lakes of different trophic states, and application to studies of sediment-water interactions. *Limnology and Oceanography*, 31(3), 584-595.

Binford, M. W., Kahl, J. S. and Norton, S. A. (1993). Interpretation of ^{210}Pb profiles and verification of the CRS dating model in PIRLA project lake sediment cores. *Journal of Paleolimnology*, 9(3), 275-296.

Blais, J. M., Kalff, J., Cornett, R. J. and Evans, R. D. (1995). Evaluation of ^{210}Pb dating in lake sediments using stable Pb, ambrosia pollen, and ^{137}Cs. *Journal of Paleolimnology*, 13(2), 169-178.

Bruel, R. and Sabatier, P. (2020). Serac: A package for ShortlivEd RAdionuclide chronology of recent sediment cores. *Journal of Environmental Radioactivity*, 225, 106449.

Canadian Council on Ecological Areas (2014) Canada Ecozones. Version 5b [shapefile].

Center for Agroclimate, Geomatics and Earth Observation, Science and Technology Branch, Agriculture and Agri-Food Canada. Annual space-based crop inventory for Canada, Albers conic equal area, 30m [GeoTIFF].

Center for Mapping and Earth Observation, Natural Resources Canada. (2017). CanVec manmade features, NAD83 CSRS, 50k [shapefile].

Center for Mapping and Earth Observation, Natural Resources Canada. CanVec resource management features, NAD83 CSRS, 50k [shapefile].

Crozaz, G., Picciotto, E. and De Breuck, W. (1964). Antarctic snow chronology with Pb^{210}. Journal of *Geophysical Research*, 69(12), 2597-2604.

Crusius, J. and Anderson, R. F. (1991). Core compression and surficial sediment loss of lake sediments of high porosity caused by gravity coring. *Limnology and Oceanography*, 36(5), 1021-1030.

Davis, R. B., Hess, C. T., Norton, S. A., Hanson, D. W., Hoagland, K. D. and Anderson, D. S. (1984). ^{137}Cs and ^{210}Pb dating of sediments from soft-water lakes in New England (USA) and Scandinavia, a failure of ^{137}Cs dating. *Chemical Geology*, 44(1-3), 151-185.

DDEP – DATA DECAY EVALUATION PROJECT. LNELNHB/ CEA. (August 2010). Table de radionucléides 210Pb. Retrieved from http://www.nucleide.org/DDEP_WG/DDEPdata.htm

Dillon, P., Scholer, P. and Evans, H. (1986). ^{210}Pb fluxes in acidified lakes. Sediments and water interactions (pp. 491-499) *Springer*.

Ecological Stratification Working Group (Canada), Center for Land, Biological Resources Research (Canada), & Canada. State of the Environment Directorate. (1996). A national ecological framework for Canada. Centre for Land and Biological Resources Research; Hull, Quebec: State of the Environment Directorate.

Ghaleb, B. (2009). Overview of the methods for the measurement and interpretation of short-lived radioisotopes and their limits. Paper presented at the IOP Conference Series: *Earth and Environmental Science*, 5(1) 012007.

Goldberg, E. (1963). Geochronology with ^{210}Pb radioactive dating. *International Atomic Energy Agency*, Vienna, 121, 130.

Jenny, J.P., Normandeau, A., Francus, P., Taranu, Z.E., Gregory-Eaves, I., Lapointe, F., Jautzy, J., Ojala, A.E., Dorioz, J.M., Schimmelmann, A. and Zolitschka, B. (2016). Urban point sources of nutrients were the leading cause for the historical spread of hypoxia across European lakes. *Proceedings of the National Academy of Sciences of the United States of America*, 113(45), 12655-12660. doi:10.1073/pnas.1605480113 [doi]

Klaminder, J., Appleby, P., Crook, P. and Renberg, I. (2012). Post-deposition diffusion of ^{137}Cs in lake sediment: Implications for radiocaesium dating. *Sedimentology*, 59(7), 2259-2267.

Koide, M., Soutar, A. and Goldberg, E. D. (1972). Marine geochronology with ^{210}Pb. *Earth and Planetary Science Letters*, 14(3), 442-446.

Korosi, J. B., Ginn, B. K., Cumming, B. F. and Smol, J. P. (2013). Establishing past environmental conditions and tracking long-term environmental change in the Canadian maritime provinces using lake sediments. *Environmental Reviews*, 21(1), 15-27.

Krishnaswami, S. and Lal, D. (1978). Radionuclide limnochronology. *Lakes* (pp. 153-177) Springer.

Last, W. M. and Smol, J. P. (2002). Tracking environmental change using lake sediments: Volume 2: Physical and geochemical methods *Springer Science & Business Media*.

Martz, D. E., Langner, G. H., Jr, and Johnson, P. R. (1991). Half-lives of ^{214}Pb and ^{214}Bi. *Health Physics*, 61(4), 511-518. doi:10.1097/00004032-199110000-00006 [doi]

Millet, L., Giguet-Covex, C., Verneaux, V., Druart, J., Adatte, T. and Arnaud, F. (2010). Reconstruction of the recent history of a large deep prealpine lake (lake bourget, france) using subfossil chironomids, diatoms, and organic matter analysis: Towards the definition of a lake-specific reference state. *Journal of Paleolimnology*, 44(4), 963-978.

Muggeo, V. M. R. (2003). Estimating regression models with unknown break-points. *Statistics in Medicine*, 22(19), 3055-3071. doi:10.1002/sim.1545

NSERC Canadian Lake Pulse Network. (2021). NSERC Canadian Lake Pulse Network field manual 2017 – 2018 - 2019 surveys (M-P. Varin, M. Beaulieu, & Y. Huot, Eds.). Université de Sherbrooke. https://doi.org/10.17118/11143/18662

Openshaw, S. (1983). The modifiable areal unit problem. *Concepts and techniques in modern geography* 38, GeoBooks, Norwich, England.

Pennington, W., Cambray, R., Eakins, J. and Harkness, D. (1976). Radionuclide dating of the recent sediments of Blelham Tarn. *Freshwater Biology*, 6(4), 317-331.

Rogers L.A., Schindler D.E., Lisi P.J., Holtgrieve G.W., Leavitt P.R., Bunting L., Finney B.P., Selbie D.T., Chen G., Gregory-Eaves I., Lisac M.J. and Walsh P.B. (2013) Centennial-scale fluctuations and regional complexity characterize Pacific salmon population dynamics over the past five centuries. *Proceedings of the National Academy of Sciences of the United States of America,* 110: 1750-1755.

Sanchez-Cabeza, J. and Ruiz-Fernández, A. (2012). ^{210}Pb sediment radiochronology: An integrated formulation and classification of dating models. *Geochimica Et Cosmochimica Acta*, 82, 183-200.

Schallenberg, M., de Winton, M. D., Verburg, P., Kelly, D. J., Hamill, K. D. and Hamilton, D. P. (2013). Ecosystem services of lakes. Ecosystem Services in New Zealand: Conditions and Trends. Manaaki Whenua Press, Lincoln, New-Zealand 203-225.

Team, R. C. (2013). R: A language and environment for statistical computing.

Tomkins, J. D., Antoniades, D., Lamoureux, S. F. and Vincent, W. F. (2008). A simple and effective method for preserving the sediment–water interface of sediment cores during transport. *Journal of Paleolimnology*, 40(1), 577-582.

Tomkins, J. D., Lamoureux, S. F., Antoniades, D. and Vincent, W. F. (2009). Sedimentary pellets as an ice-cover proxy in a high arctic ice-covered lake. *Journal of Paleolimnology*, 41(1), 225-242.

Turner, L. and Delorme, L. (1996). Assessment of ^{210}Pb data from Canadian lakes using the CIC and CRS models. *Environmental Geology*, 28(2), 78-87.

Winegardner, A. K., Legendre, P., Beisner, B. E. and Gregory-Eaves, I. (2017). Diatom diversity patterns over the past c. 150 years across the conterminous United States of America: Identifying mechanisms behind beta diversity. *Global Ecology and Biogeography*, 26(11), 1303-1315.

Wood, S. (2012). Mgcv: Mixed GAM computation vehicle with GCV/AIC/REML smoothness estimation.

Wright, S., Howard, B., Strand, P., Nylén, T. and Sickel, M. (1999). Prediction of ^{137}Cs deposition from atmospheric nuclear weapons tests within the Arctic. *Environmental Pollution*, 104(1), 131-143.

Tables Chapter II

Table II.1. Summary of dating models highlighting the key assumption and equations across each of the three main dating models. See symbols and abbreviation table.

Model	Assumption	Equations
Constant Flux Constant Sedimentation model (C.F.C.S.)	• Assumes a constant sedimentation rate along the entire core • Activity of unsupported ^{210}Pb is expected to decay as a function of the cumulative dry mass of the sediment in the core	$\mathrm{Log}(C_{t_x}) = \mathrm{Log}(C_0)\ e^{-\lambda \frac{m}{MAR}}$ $MAR_{C.F.C.S.} = \frac{-\lambda}{b}$
Constant Initial Concentration model (C.I.C.)	• Assumes a constant activity of unsupported ^{210}Pb in each sediment layer as it is formed • Increases in the flux of sedimentary particles from the water column will proportionally increase amounts of unsupported ^{210}Pb deposited to the sediment floor	$C_{t_x} = C_0 e^{-\lambda t_x}$ $MAR_{C.I.C.} = \frac{m_j - m_i}{\Delta t}$
Constant Rate of Supply model (C.R.S.)	• Assumes a constant fallout of ^{210}Pb from the atmosphere, yielding a constant rate of supply of unsupported ^{210}Pb to the sediment surface • Unsupported ^{210}Pb of the initial activity (at time zero) will be inversely proportional to the mass accumulation rate, such that increases in burial driven by sediment erosion or autochthonous production results in dilution of unsupported ^{210}Pb	$A_{t_x} = A_0 e^{-\lambda t_x}$ $MAR_{C.R.S.} = \lambda \times \frac{A_{t_x}}{C_{t_x}}$

Symbols used in tables: $\boldsymbol{\lambda}$, ^{210}Pb disintegration constant (λ = 0.03114 year^{-1}); $\boldsymbol{m}$, Cumulative dry mass of sediment (g); $\boldsymbol{MAR}$, Sediment mass accumulation rate (g cm^{-2} year^{-1}); $\mathbf{b}$, Slope of log-transformed C_{t_x} with cumulated dry mass ($\frac{1}{g\ cm^{-2}}$); $\boldsymbol{C_{t_x}}$, Unsupported ^{210}Pb activity at time t_x (Bq kg^{-1}); $\boldsymbol{t_x}$, Time *x* (in years); $\boldsymbol{\Delta t}$, Elapsed time between the deposition of two intervals ($\Delta t = t_i - t_j$, years); $\boldsymbol{A_{t_x}}$, ^{210}Pb$_{unsupp.}$ accumulated below interval corresponding to time t_x (Bq m^{-2});

Table II.2. Distribution of the selected dating model percentage across the four Eastern Canadian ecozones. Lakes sample size across ecozone is indicated between parentheses.

Ecozone	C.F.C.S.	C.I.C.	C.R.S.
Atlantic Highlands (11)	9%	9%*	82%
Atlantic Maritime (7)	14%	0%	86%
Boreal Shield (10)	30%	0%	70%
Mixedwood Plains (8)	0%	0%	100%

*Despite the C.I.C. model being selected for one of the lakes (17-067) in the Atlantic Highlands, dates for this core could not be derived using the C.I.C. equation as it generated non-decreasing age with depth (see metadata). For core 17-067, we thus generated dates using the C.R.S. model which returned similar R^2 to that of the C.I.C. model (see Figure B.4).

Table II.3. Summary of the linear model R^2 for the three dating models tested (n=111). The *Estimate* parameter accounts for the mean R^2 value obtained across all 37 lakes.

Dating Model	Mean R^2	Standard Error of R^2	p-value
C.F.C.S.	0.788	0.035	< 0.001
C.I.C.	0.667	0.039	0.002
C.R.S.	0.944	0.039	< 0.001

Table II.4. Summary of the linear mixed effects model assessing the temporal variation in log-transformed Mass Accumulation Rate (MAR) across the 37 cores. t-value refers to the t statistics. LLR refers to the log-likelihood ratio.

Effect	Estimate (Std. Error)	Degree of Freedom	t-value	LLR	p-value
(Marginal R^2 = 0.222, Conditional R^2 = 0.696)					
Intercept	-5.29 (0.30)	146	-17.52		
Log(Population+1) (numbers of individuals)	0.177 (0.046)	146	3.84	17.17	0.0002
MAT (°C)	0.0912 (0.046)	146	1.96	3. 85	0.0515
Random effects (Proportion of variance explained by LakeID = 0.710)					
LakeID	0.714 (0.51)			116.12	< .001
Residual	0.571 (0.32)				

Figures Chapter II

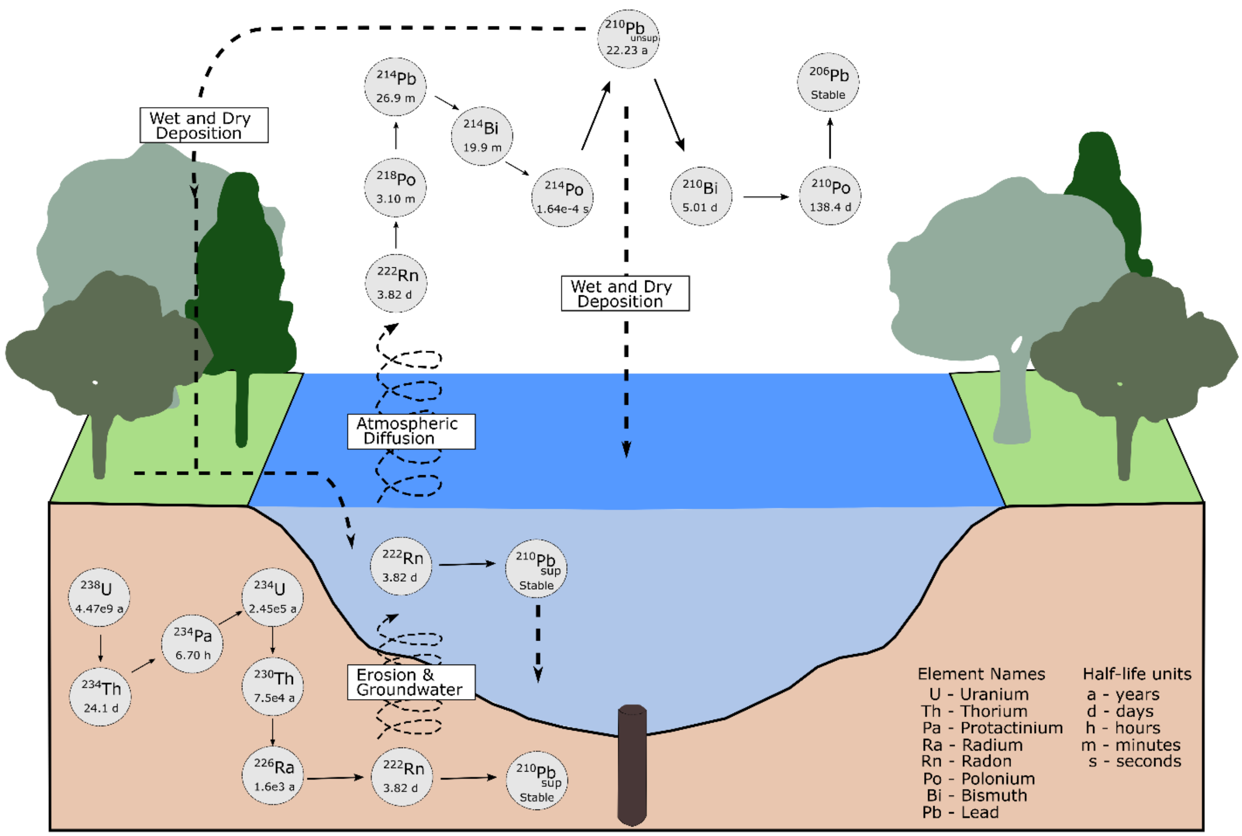

Figure II.1. The ^{238}U (uranium) decay series accounting for the deposition of supported ^{210}Pb and unsupported ^{210}Pb into lake sediments via wet and dry deposition on the landscape. Solid lines represent the radionuclide transitions while curved dashed lines account for the transfer of ^{222}Rn from the lithosphere into lakes via erosion and from lakes into the atmosphere via diffusion.

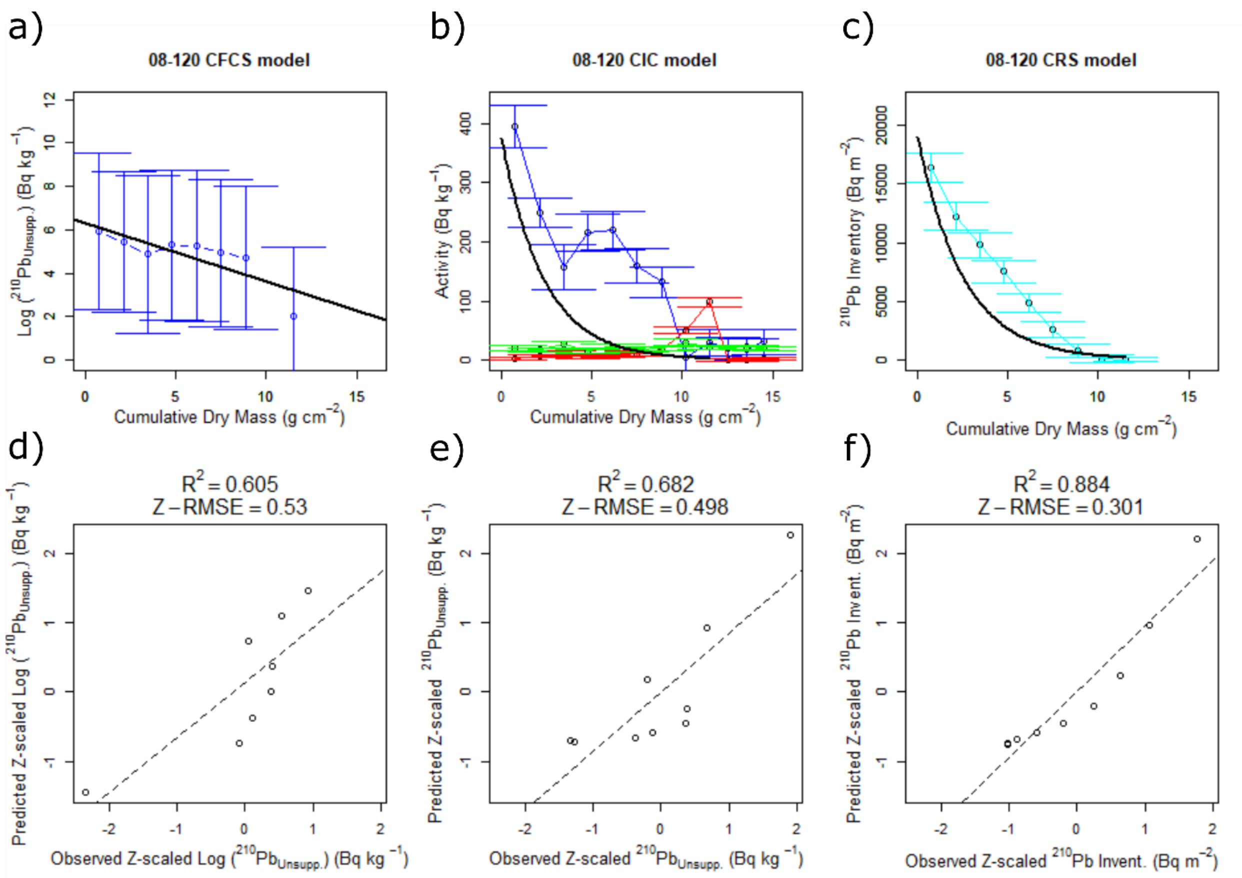

Figure II.2. Multi-panel plot summarizing the empirical ^{210}Pb dating model fitting (detailed in Appleby and Oldfield (1983), and evaluation using linear regression for lake 08-120 (Lac des Chicots – Ste Therese, QC). a) Log-transformed $^{210}Pb_{Unsupp}$, with error bars in blue as a function of cumulative dry mass. The black line represents the best linear model fit. b) Graphical representation of the measured ^{210}Pb (Bq kg^{-1}) in blue with corresponding errors as a function of cumulative dry mass. The red line is the ^{137}Cs activities (Bq kg^{-1}) and the ^{214}Bi activities are in green. The black line is the expected decay curve for $^{210}Pb_{Unsupp.}$ c) Graphical representation of the observed ^{210}Pb inventory and corresponding errors in cyan, as a function of cumulative dry mass. The black line is the expected decay curve for ^{210}Pb inventory. d) Linear regression evaluating the fit of the predicted log Z-transformed $^{210}Pb_{Unsupp.}$ activities (Bq kg^{-1})

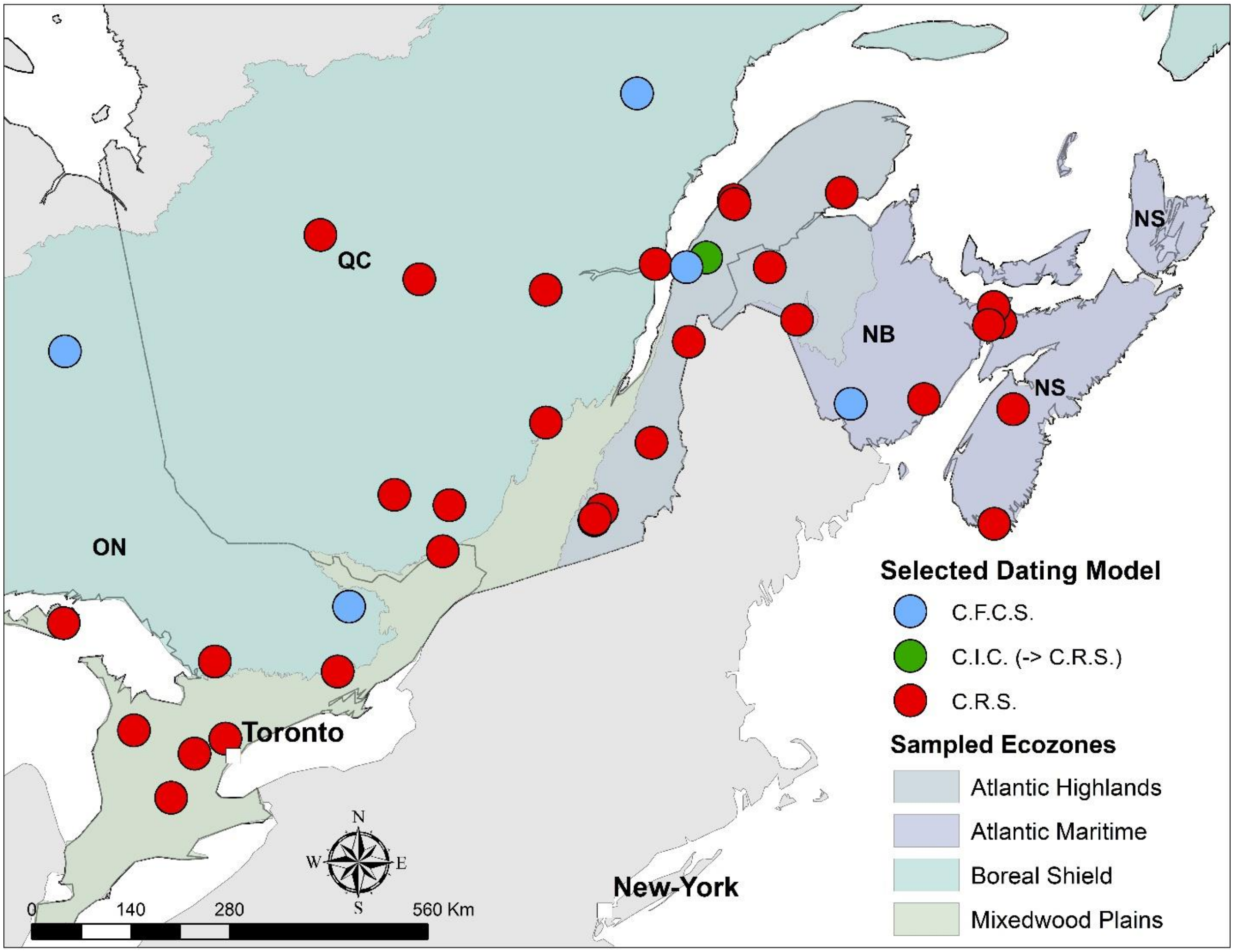

Figure II.3. Map showing the distribution of the selected dating models across the four sampled Eastern Canadian ecozones.

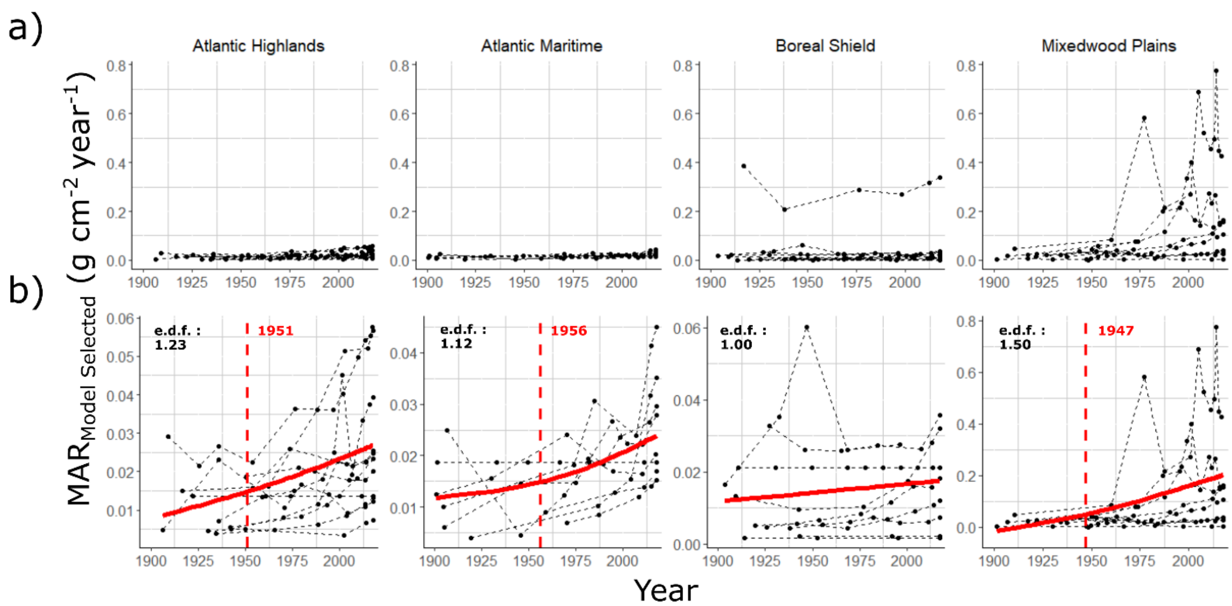

Figure II.4. Temporal variation in sediment dry weight mass accumulation rate across the four ecozones of Eastern Canada as determined from dating model selection. a) The upper panels display the raw measured sedimentation rates across the 37 lakes. b) The lower panels show the general additive model (GAMM) trends of ecozone-specific MAR temporal variation. The estimated degrees of freedom (e.d.f.) associated with the GAMM is also reported, as is the estimated onset of the MAR acceleration across each ecozone based on a breakpoint analysis. Note: One lake (06-103) for the Boreal Shield was identified as having anomalously high MAR and was also found to be a site in a floodplain, and was thus removed from GAMM analyses and all subsequent analyses.

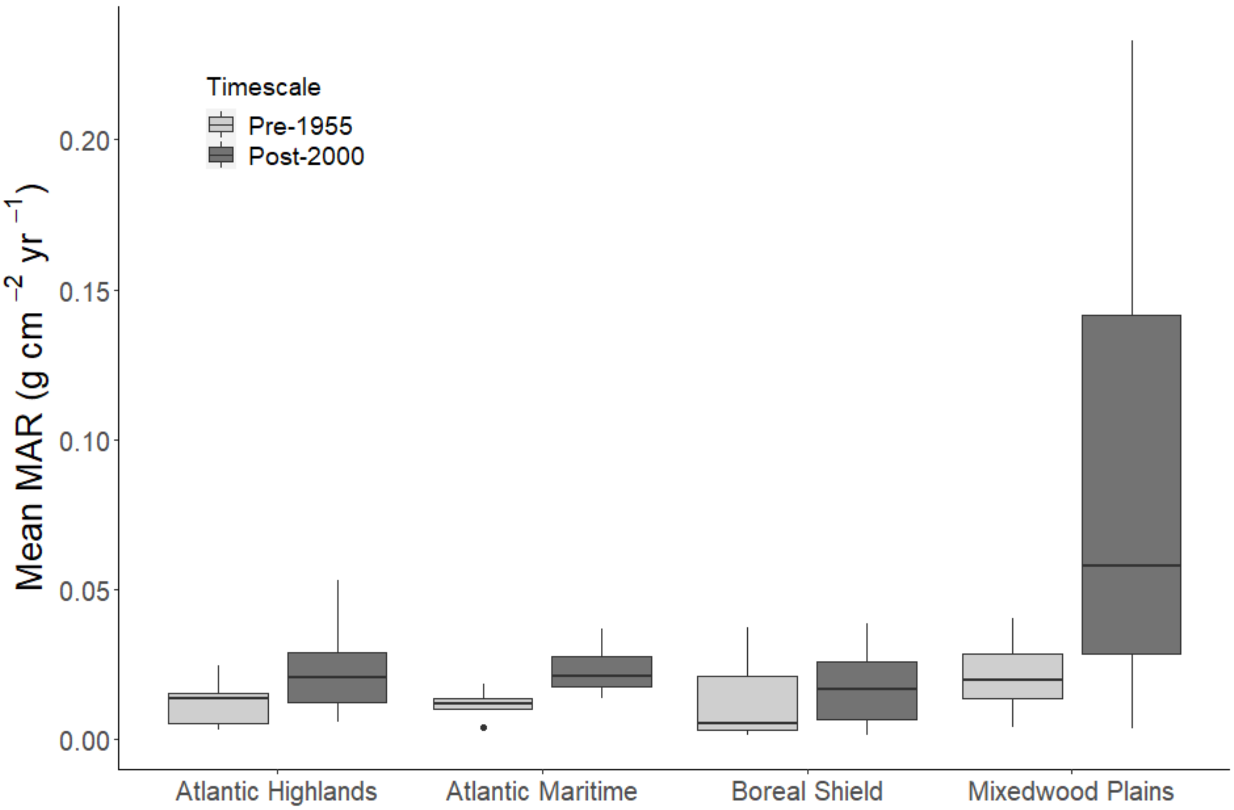

Figure II.5. Mean Mass Accumulation Rate (MAR: g cm^{-2} year^{-1}) across the four sampled Eastern Canadian ecozones for two timesteps: "Pre-1955" ($n_{MARPre\text{-}1955}$ = 34), "and "Post-2000" ($n_{MARPost\text{-}2000}$ = 36). While pre-1955 includes MAR estimates prior to the acceleration recorded across Eastern Canada, we also considered a post-2000 timestep, reflective of the recent MAR estimates. This timestep was considered as it is the focus of a predictive model assessing the drivers of recent lake MARs. Using this former timestep was also motivated by the limited availability of contemporary environmental datasets which are necessary to explore the drivers of recent lake MARs.

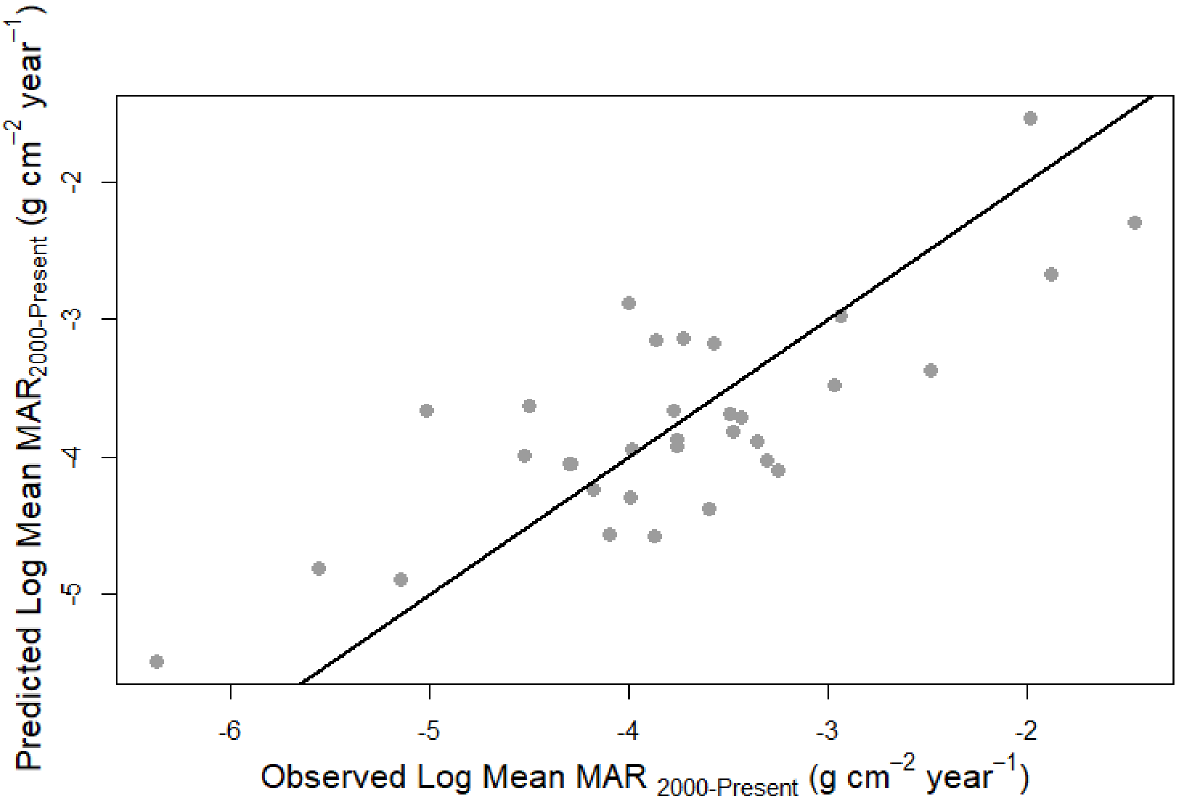

Figure II.6. Observed versus predicted log-transformed Mean Mass Accumulation Rate (post-2000 CE, from equation 6).

Appendices Chapter II

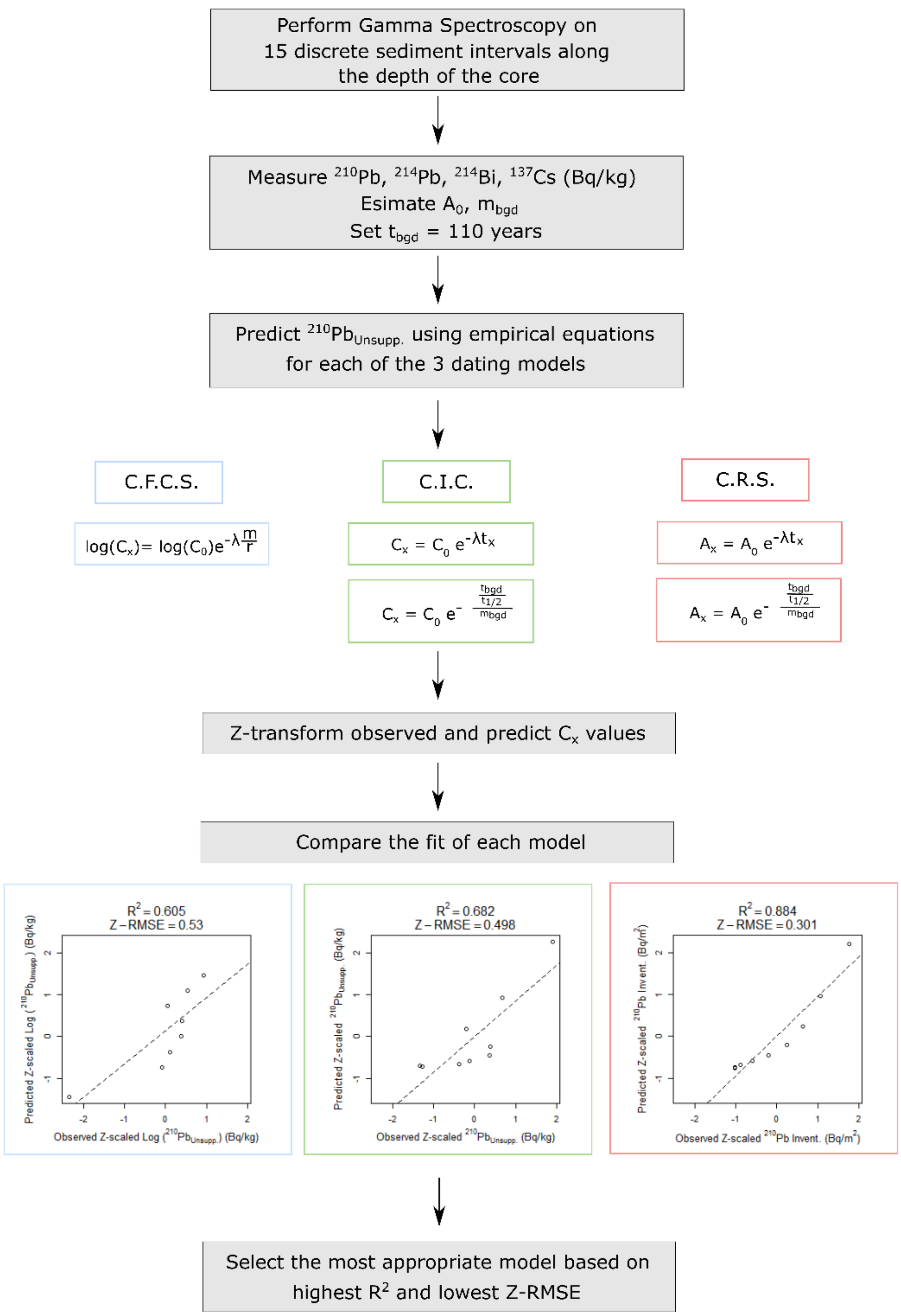

Figure B.1. Model selection framework for comparing the ^{210}Pb quantities across 3 dating models using empirical equations from Appleby and Oldfield (1983).

Table B.2. Land use, human impact value and data sources. Updated from Huot et al. (2019).

Land Use type	Human impact value	Data source
Urban	1	AAFC Annual Crop inventory 2017; AAFC Land Use 2010; NRCan CanVec Manmade features; USDA NASS Cropland Data Layer 2017; NALCMS Landcover 2010
Mines/Excavation	1	NRCan CanVec Resource Management Features
Agriculture	1	AAFC Annual Crop inventory 2017; AAFC Land Use 2010; USDA NASS Cropland Data Layer 2017; NALCMS Landcover 2010
Pasture	0.5	AAFC Annual Crop inventory 2017; AAFC Land Use 2010; USDA NASS Cropland Data Layer 2017
Recent clearcuts (2012 to 2017)	0.5	Year of gross forest cover loss event (2012 to 2017) from: Hansen et al. 2013; NRCan Natural Burned Area Composite (2010 to 2017)
Natural landscapes	0	NRCan EOSD forest cover map, AAFC Annual Crop inventory 2017; AAFC Land Use 2010; USDA NASS Cropland Data Layer 2017; NALCMS Landcover 2010

Table B.3. Class definition and simplified land use categories

Class	Definition	Category simplified
0	No Data	NA
1	Water	Water
10	Exposed Land / Barren / Rock / Snow / Ice	Natural Landscape
20	natural landscape (unclassified)	Natural Landscape
21	Bryoids	Natural Landscape
22	Shrubland	Natural Landscape
23	Herb / Grassland	Natural Landscape
24	Coniferous	Natural Landscape
25	Broadleaf	Natural Landscape
26	Mixedwood	Natural Landscape
27	Forest (undifferentiated)	Natural Landscape
30	Wetland	Natural Landscape
40	Forest Loss (2012-2017)	Forestry
100	Urban / Developed	Urban
101	Sod	Urban
200	Greenhouses	Agriculture
201	Agriculture (undifferentiated)	Agriculture
202	Pasture / Forages	Pasture
203	Too Wet to be Seeded	Agriculture
204	Fallow	Agriculture
205	Cereals	Agriculture
206	Barley	Agriculture
207	Other Grains	Agriculture
208	Millet	Agriculture

209	Oats	Agriculture
210	Rye	Agriculture
211	Spelt	Agriculture
212	Triticale	Agriculture
213	Wheat	Agriculture
214	Switchgrass	Agriculture
215	Sorghum	Agriculture
216	Winter Wheat	Agriculture
217	Spring Wheat	Agriculture
218	Corn	Agriculture
219	Tobacco	Agriculture
220	Ginseng	Agriculture
221	Oilseeds	Agriculture
222	Borage	Agriculture
223	Camelina	Agriculture
224	Canola / Rapeseed	Agriculture
225	Flaxseed	Agriculture
226	Mustard	Agriculture
227	Safflower	Agriculture
228	Sunflower	Agriculture
229	Soybeans	Agriculture
230	Pulses	Agriculture
231	Peas	Agriculture
232	Beans	Agriculture
233	Lentils	Agriculture
234	Vegetables	Agriculture
235	Tomatoes	Agriculture
236	Potatoes	Agriculture

237	Sugarbeets	Agriculture
238	Other Vegetables	Agriculture
239	Fruits	Agriculture
240	Berries	Agriculture
241	Blueberry	Agriculture
242	Cranberry	Agriculture
243	Other Berry	Agriculture
244	Orchards	Agriculture
245	Other Fruits	Agriculture
246	Vineyards	Agriculture
247	Hops	Agriculture
248	Herbs	Agriculture
249	Nursery	Agriculture
250	Buckwheat	Agriculture
251	Canaryseed	Agriculture
252	Hemp	Agriculture
253	Vetch	Agriculture
254	Other Crops	Agriculture
300	mines/excavation	Mines

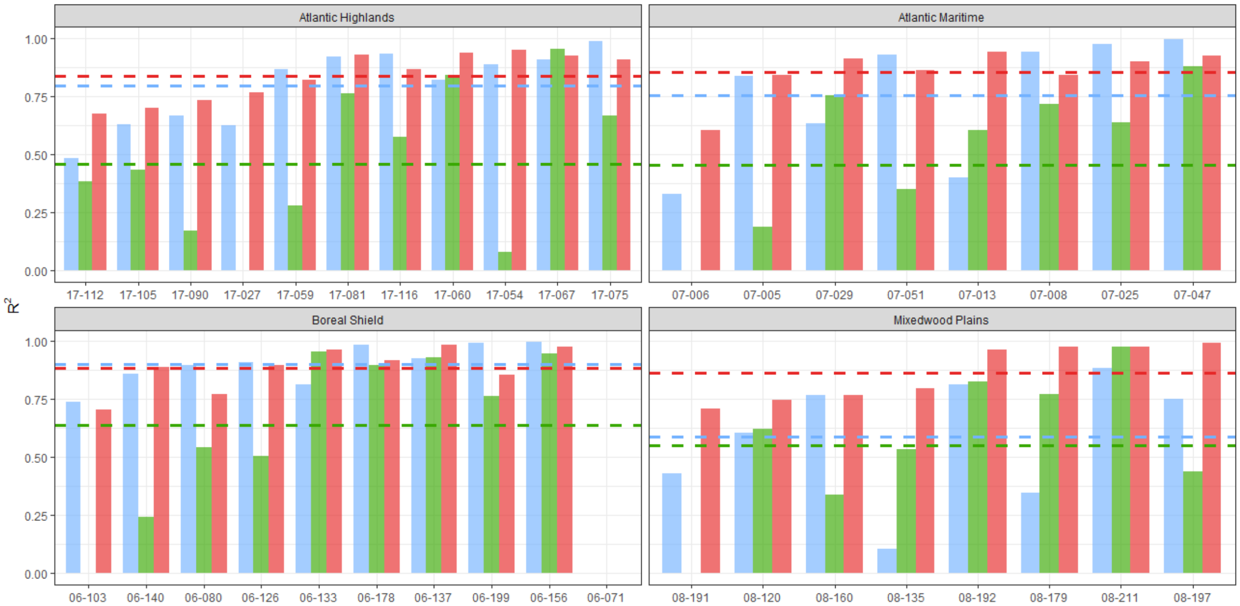

Figure B.4. Distribution of predicted and observed R^2 fit across different dating model for all lakes, by ecozone. In blue is the C.F.C.S., green is C.I.C. and red C.R.S. model fit. Lakes are ordered by increasing selected R^2. The colored horizontal dashed lines indicate the mean R^2 for each dating model across each ecozone.

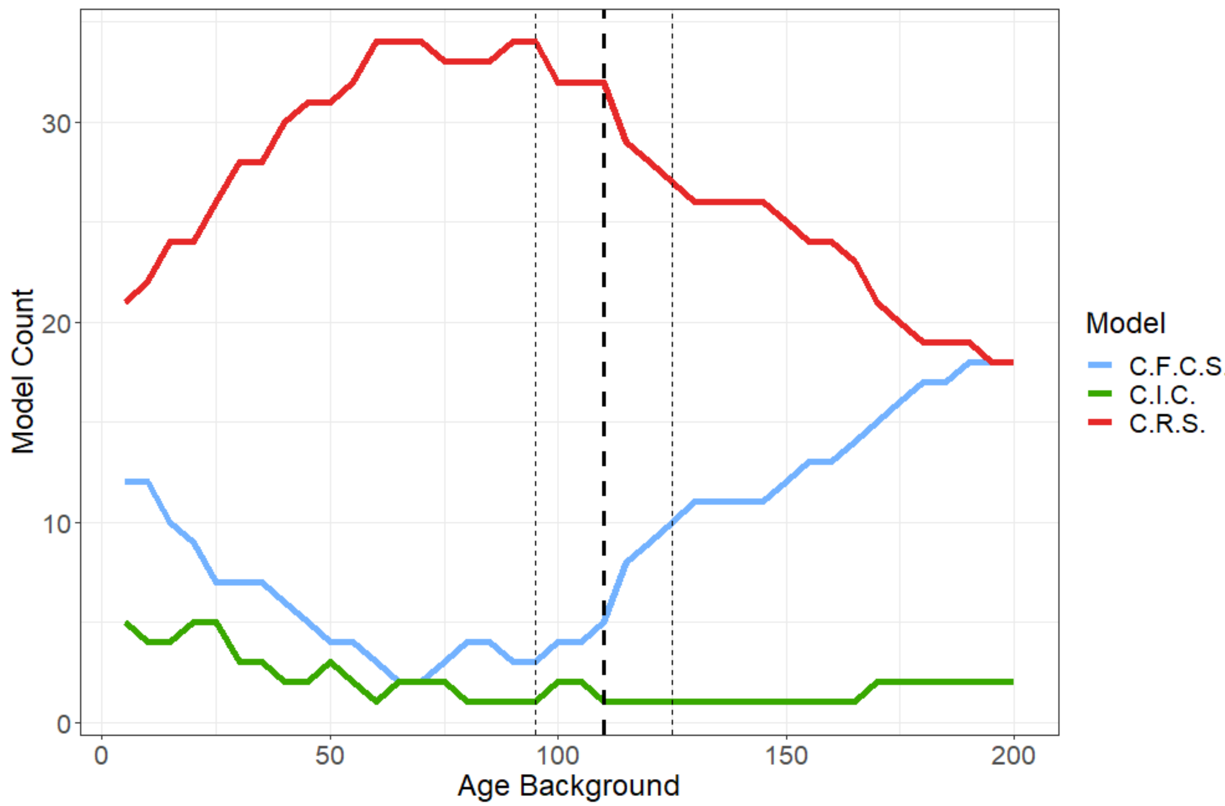

Figure B.5. Sensitivity analysis of Age background (= t_{bgd}) parameter used for dating model selection. While t_{bgd} must have environmental significance in accordance with the natural decay of ^{210}Pb (80 – 130 years), represented here by the thin dashed vertical lines, this figure shows the mathematical bias that exists when investigating t_{bgd} outside of this range as well as the model selection stability present within this natural range. The selected t_{bgd} of 110 years is indicated by the thicker dashed line.

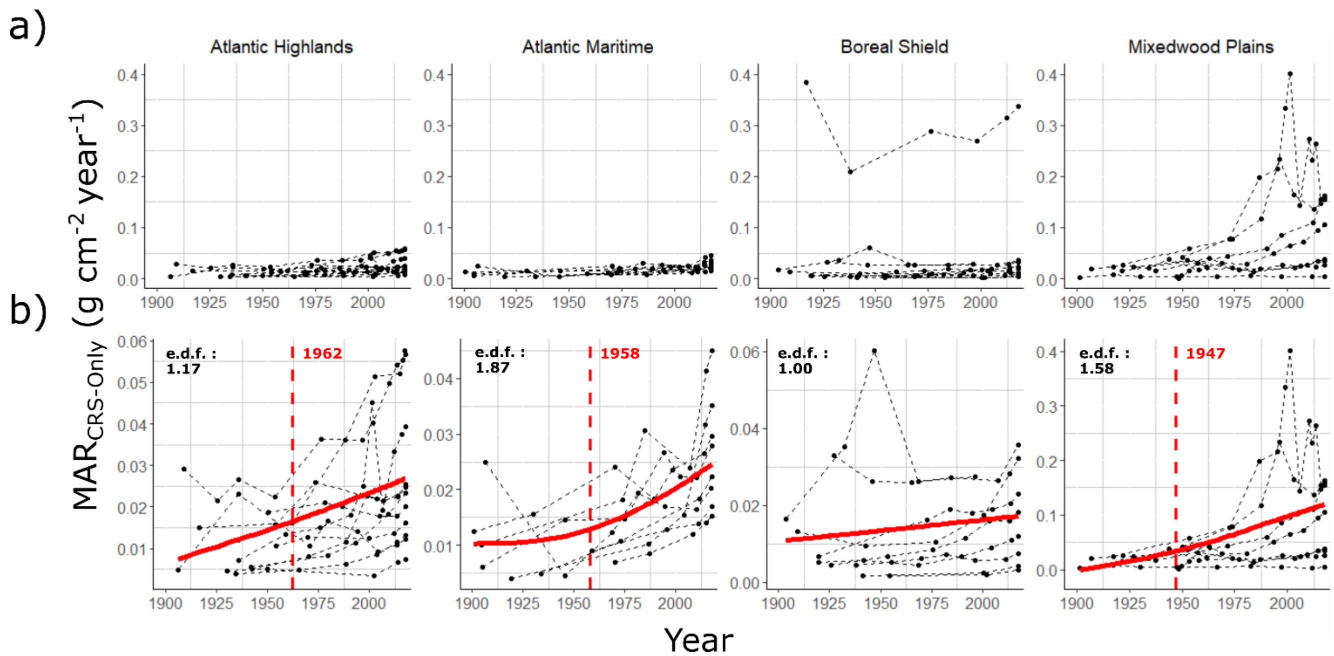

Figure B.6. Temporal variation in sediment dry weight mass accumulation rate across the four ecozones of Eastern Canada as determined using only the C.R.S. dating model. The upper panel displays the raw measured sedimentation rates across the 37 lakes. In the lower panel are reported the general additive mixed model (GAMM) trends of ecozone specific MAR temporal variation. The estimated degrees of freedom (e.d.f.) associated with the GAMM is also reported, as is the estimated onset of the MAR acceleration across each ecozone based on a breakpoint analysis. Lake 06-103 from the Boreal Shield was identified as having anomalously high MAR and was also found to be a site in a floodplain, and thus was removed from our GAMM analyses and all subsequent analyses.

Connecting statement between Chapters II and III

The framework developed for my 2nd Chapter led to the successful establishment of lake sediment chronologies for the 37 sediment cores collected across Eastern Canada. In agreement with past research (summarized in Baud et al. 2021), the ^{210}Pb found within the cores were most in agreement with the C.R.S. assumptions. Similar to results from my first chapter, we found that lake sedimentation rates have been increasing since the start of the Industrial Revolution and that these increases were often correlated with human development in lake watersheds. In addition, we detected patterns in lake sedimentation rates that varied by terrestrial ecoregions of Eastern Canada. The establishment of these chronologies and apparent ecoregion variation were foundational in analyzing spatio-temporal geochemical patterns based on the sediment core archives in my 3rd chapter. The datasets that were assembled in Chapter II (i.e., population counts and climate time series within the watershed of the lakes considered) were also critical in identifying predictors of geochemical composition across the ecoregions sampled. This connecting statement also marks the transition from the study of the physical responses of lake sediments, mainly measured as variation in sedimentation rates, to the geochemical responses of lake sediments. In chapter III, we used the 37 sediment cores collected across Eastern Canada mentioned in Chapter II and inferred via micro X-ray fluorescence the relative abundance of various geochemical elements present in these sediment archives. Specifically, this chapter investigated the spatial and temporal distribution associated with different sediment constituents and considered their sources.

CHAPTER III - Geochemical changes in Eastern Canadian lake sediment cores spanning the last ~150 years highlight a relative shift towards increased metals and erosive materials

Alexandre Baud[1, 2, *], Pierre Francus[3, 4], John P. Smol[5], Dermot Antoniades[2, 6] and Irene Gregory-Eaves[1, 2]

[1]Department of Biology, McGill University, Montréal, Québec, H3A 1B1, Canada

[2]Group for Interuniversity Research in Limnology and Aquatic Environments (GRIL)

[3]Centre Eau Terre Environnement, Institut National de la Recherche Scientifique (INRS), Québec City, Québec, G1K 9A9, Canada

[4]GEOTOP, Geochemistry and Geodynamics Research Centre, Université du Québec à Montréal, Montréal, Québec H3C 3P8, Canada

[5] Paleoecological Environmental Assessment and Research Lab (PEARL), Department of Biology, Queen's University, Kingston, Ontario, K7L 3N6, Canada

[6]Département de géographie, Université Laval, Québec City, Québec G1V 0A6, Canada

Manuscript with minor revision in *CATENA* in December 2022

Abstract

Since the start of the Industrial Revolution, the chemical cycling of numerous elements has been fundamentally altered. Using ^{210}Pb-dated sediment cores from 37 Eastern Canadian lakes situated in 4 ecoregions, we quantified the geochemical change experienced across this region since ca. 1850 CE using high-resolution computed X-ray Tomography and micro-X-ray fluorescence (µ-XRF) ITRAX scanners. Independent calibrations of µ-XRF ITRAX intensities using ICP-MS and -AES found strong correlations for numerous elements. Using relative abundance measures and absolute concentration estimates, we observed that most of our study lakes recorded temporal enrichments of metals, with several sites exceeding Canadian sediment quality guidelines. Using principal component analysis, we identified that parameters commonly associated with erosion (strontium and titanium), organic matter (molybdenum and incoherence:coherence ratio), and metals (zinc and lead) were key variables structuring within and among-lake variation since ca. 1850 CE. Calcium was identified as an additional variable, particularly for lakes in the Mixedwood Plains (MWP) ecozone, which may be linked to catchment activities including land-use changes. Temporally, many lakes shifted towards greater accumulation of inorganic sediment, coeval with higher Pb and Zn concentrations, reaching maxima ca. 1970 CE before decreasing rapidly. These results suggest that most lakes in the region were subjected to environmental pollution but that controls on key atmospheric pollutants in North America were effective across a large part of the country.

Introduction

Under the pressures of human activities, the cycling of numerous geochemical elements has been dramatically modified over the last century (Syvitski et al., 2005; Davidson, 2009; Boden et al., 2017; Hoesly et al., 2018; Masson-Delmotte et al., 2021). Lake sediments offer an excellent record of long-term changes that can be used to better understand the magnitude and timing of geochemical alterations linked to local activities (Punning et al., 2007; Walling, 2009), as well as those originating hundreds to thousands of kilometers away (Last and Smol, 2002; Roberts et al., 2018; Lepak et al., 2020). While numerous geochemical studies of sediment cores have been published, disentangling anthropogenic contributions from natural sources remains a challenge. Regional-scale investigations of the spatio-temporal distributions of geochemical changes can provide a more complete picture of environmental change, highlighting potential spatial heterogeneity and diverging sources of contamination. Most such investigations have relied on the study of surficial or so-called "top-bottom" or "before and after" sediment studies (Semkin and Kramer, 1976; Camarero, 2003), which have the benefit of providing insights into the regional variability across a large number of lakes. However, such studies often lack the temporal component necessary to contextualize variation in elemental deposition through time. Analysis of complete time series of elemental deposition is especially important when considering the influence of environmental legislation and regulations. Moreover, climate change has the potential to alter long-range atmospheric deposition patterns (Hole and Engardt, 2008), modify the remobilization of legacy contamination (Schiedek et al., 2007; Jarsjö et al., 2020), and alter transport pathways of metals from watersheds (Kimball and Runkel, 2002). It is thus important to consider how a suite of elements has jointly responded to modifications linked with climate change, land-use change and other contemporary stressors.

Until recently, geochemical measurements were mainly generated using discrete sediment intervals analyzed via inductively coupled plasma mass spectroscopy (ICP-MS) or inductively coupled plasma atomic emission spectroscopy (ICP-AES), which require labor-intensive processing and the use of concentrated acids. With the emergence of new analytical instruments geared towards the study of lacustrine and marine sediments (e.g., micro–X-Ray Fluorescence and Computed Tomography scanners), the physical and geochemical composition of sediment can now be measured rapidly and at high resolution (Rothwell, 2015), allowing for broader sampling strategies and regional insights into geochemical variation. The micro–X-Ray Fluorescence (µ-XRF) scanner can generate proxies for a wide range of sediment sources such as detrital inputs through measures of titanium (Ti), rubidium (Rb), strontium (Sr) and aluminum (Al) (Boës et al., 2011). Scans from µ-XRF have also widely been used to study metal pollution (Pb, Zn, Cu, Ni, Cd) in sediments (Fielding et al., 2020), although not all heavy metals are well detected, especially when they occur in trace amounts. Of the elements that can be quantified, some are indicative of potentially biogenic sediment fractions such as calcium (Ca), silicon (Si), and bromine (Br) (Kalugin et al., 2007; Davies et al., 2015). Other elements, such as iron (Fe) and manganese (Mn), or rather the elemental ratio of Mn/Fe, have been used to track redox conditions at the water-sediment interface (Naeher et al., 2013), however it should be noted that concerns about post-deposition mobility of the Mn/Fe ratio have been raised (Makri et al., 2021). Another insightful ratio provided by the µ-XRF scanner is the molybdenum incoherent : coherent scattering ratio, which has been proposed as a robust proxy for sediment organic content (Woodward and Gadd, 2019).

This study quantifies lake sedimentary geochemical change across broad regions of Eastern Canada by employing a comprehensive definition of sediment geochemical composition measured via a µ-XRF scanner which generates high-resolution time series. Specifically, our goal was to identify elements demonstrating important spatio-temporal variation induced by large-scale patterns of environmental change and relate them to watershed properties and climate variables. Metals were expected to be a significant feature of geochemical change due to the mining legacies in many regions of Eastern Canada. Additionally, erosive materials and detrital inputs are also expected to play a significant role in shaping in geochemical change when considering the important hydrological modifications and land-use conversions that have taken place throughout the last ~150 years (Grill et al., 2015; Jenny et al., 2019).

Methods

Core collection and processing

A total of 37 sediment cores were collected during the summer of 2017 as part of the LakePulse field campaign (Huot et al., 2019) (Table CB.1), which spanned four ecozones of Eastern Canada: the Atlantic Highlands (#17), Atlantic Maritime (#07), Boreal Shield (#06) and Mixedwood Plains (#08) (Figure III.1). Lake selection was based on a stratified design where lakes accessible within 1 km of a road were randomly selected across a gradient of lake size and human impact (defined based on watershed land-use; Huot et al., 2019). Lake sediment cores were retrieved using a NLA gravity corer (Blomqvist, 1991) from the lake's deepest point or from a profundal basin. After retrieval, the length of the sediment cores was recorded and the sediment-water interface was stabilized using sodium polyacrylate (Tomkins et al., 2008), which was added in increments to limit porewater migration within the core. Cores were sent by courier to the Institut National de Recherche Scientifique (INRS) where Computed-Tomography (Goldschmidt)-scans using a Siemen SOMATOM Definition AS+ 128 were performed. Density values organized in axial slices (i.e., orthogonal to core axis) were extracted as Hounsfield units (Hounsfield, 1980) over a circular section of approximately 20 cm^2 centered in the middle of the sediment (i.e., integrating >70% of the sedimentary material) and averaged across each axial slice. The cores were then split longitudinally, and their length measured again using a measuring tape. Core halves were then scanned using a non-destructive Cox Analytics μ-XRF ITRAX scanner, set up with a molybdenum-anode X-ray tube at 40 kV and 10 mA at 0.1-mm resolution for 20 s per interval (Rothwell and Rack, 2006). After scanning, the working half of each core was subsampled at 1 cm resolution using non-metallic equipment. For a subset of subsamples, an aliquot for metal analyses was collected while the rest of the sample was kept in a Whirlpak bag. All samples were weighed to record the total mass of the sediment present for each 1 cm interval. Sediment was kept frozen until being freeze-dried.

For each of the 37 sediment cores, approximately 15 discrete intervals were collected along the depth of the sediment core and packed in tubes for dating via gamma spectrometry using a Ortec high-purity Germanium gamma spectrometer (Oak Ridge, TN, USA). Radionuclide profiles for lead-210 (^{210}Pb), lead-214 (^{214}Pb) and cesium-137 (^{137}Cs) were recorded and dated using one of the three dating models (Constant Flux Constant Sedimentation (C.F.C.S.), Constant Initial Concentration (C.I.C.) and Constant Rate of Supply (C.R.S.), as described in Baud et al. (2022).

μ-XRF ITRAX processing and evaluation

Upon completion of the μ-XRF ITRAX scans, the sum spectra were re-evaluated using a protocol adapted from the QSpec Guide (Cuven et al., 2007). This step involves fine-tuning of the detector and X-ray tube parameters, which reduces the overall mean squared error (MSE) associated with each spectrum. To discriminate between materials used in sediment core transport (in our case sodium polyacrylate) and sedimentary material, we used the Mahalanobis distance of each point to the centroid using the mahalanobisQC function in R. Consecutive points from the start and end of the scans, with a significance level (p-value < 0.0001), were considered as outliers and removed from the dataset (Figure CB.2 & CB.3).
To evaluate the quantitative nature of μ-XRF ITRAX intensities across different sediment cores, we performed ICP-MS and ICP-AES on 105 discrete samples from a subset of lake sediment cores (n=7) were identified during exploratory data analyses as displaying important range of variation in elemental abundances. We assessed multiple normalization procedures from published literature including: counts-per-second correction; counts-per-second & density correction (i.e., inferred from tomography scanner) and multivariate log-ratio transformations (Weltje et al., 2015) and compared the resulting ordination patterns with original ICP-MS/AES measures (See full details in Appendix CA).

External environmental datasets

The hydrologically-conditioned watershed for each of the 37 lakes was delineated using a 20 m flow direction raster layer acquired from the Canadian Digital Elevation Model dataset (Government of Canada, 2015). These watersheds served as the geographical areas from which to extract the temporal variation in human population using Canadian Census Data (http://geo.scholarsportal.info/) and in climate (total annual precipitation (mm) and mean annual air temperature (MAT ºC) (https://climate.meteo.gc.ca/). Additional datasets for soil properties were accessed from SoilGrids, a system for global digital soil mapping (SoilGrids.org). These datasets featured information related to broad categories of soil characteristics such as mean bulk density of the fine earth fraction (bdod_mean), mean volumetric fraction of coarse fragments (> 2 mm) (cfvo_mean), and the proportion of clay, silt and sand, as well as mean soil pH and cation exchange capacity. From this dataset, null pixels (fresh water, permanent ice or snow, bare rocks, urban areas) were excluded when calculating watershed estimates for each soil property. Only properties from the surficial soil layer (0 – 5 cm) were selected for our analysis.

Statistical analyses

All statistical analyses were performed using R v4.0 (R Core Team, 2021). A principal component analysis (PCA) was computed to explore the variance in geochemical composition within and across all sediment cores. Elemental abundances derived from µ-XRF ITRAX intensities were scaled prior to developing the PCA using the vegan::rda() function. To account for the widely different sedimentation rates that were found across the Eastern Canadian landscape, and to give equal weight to every lake, original lake core datasets were pared down to time series with the same number of intervals equally spaced between ~1850 and 2017 CE. The predictor variables accounting for the most variation were selected on the basis that elemental intensities had high and significant correlation coefficients ($R^2 > 0.5$) with concentrations derived from ICP-MS/AES measurements. We then used a stepwise backward model fitting procedure where variables were omitted from the PCA if they did not improve the variance explained or were found to be correlated to another variable explaining more variation. Finally, Fe and Mn were omitted because of their potential for post-depositional mobility. The number of significant PC axes was determined using the broken-stick method (Jackson, 1993). For each lake and ecozone, a bidimensional elliptical confidence interval was delineated from the ordination space defined within the PCA using a custom function adapted from SIBER package in R (Jackson et al., 2011). These lake-specific delineations enabled the visualization of *geochemical dispersion,* analogous to the magnitude and direction of the geochemical change captured from one lake sediment core from ca. 1850 CE onwards. Ecozone-specific ellipses served to represent *geochemical coverage*, analogous to the heterogeneity in the geochemical nature of sediment cores within a region. To evaluate the timing associated with the greatest amount of geochemical change experienced throughout Eastern Canada, we modeled the temporal variation of the significant principal comment (PC) axes using general additive mixed-effect models (GAMMs) using the R-package mgcv (Wood et al., 2016). To test the significance of the environmental factors on the observed variation in sediment geochemistry, we used redundancy analysis (RDA) (Legendre et al., 2011), ensuring no predictor variables were significantly correlated using Variance Inflation Factors (VIF) (Gross, 2003) and selected significant variables using forward selection. Variance partitioning using the varpart package in R (Peres-Neto et al., 2006) was used to further differentiate between the sources of explained variance. To capture the influence of land-use and soil properties on the spatial distribution of regional elemental abundance, we considered a reduced µ-XRF ITRAX dataset where intensities were averaged across each element for each lake. The same procedure (averaging time series from ca. 1850 – 2017 CE) was also performed for our reconstructed precipitation, temperature, and population datasets. The µ-XRF ITRAX dataset was Hellinger transformed and environmental datasets were standardized (scaled to zero mean and unit variance) prior to performing RDA.

Results

Comparison of µ-XRF ITRAX intensities with ICP-MS/AES concentration data

We detected strong correlation coefficients between µ-XRF ITRAX raw re-evaluated intensities and ICP-MS/AES concentrations for most of the available elements (Figure III.2, see full details in Appendix A, Table CA.1; Figure CA.2). We also found that the raw re-evaluated intensity data yielded ordination patterns similar to those observed for ICP-MS/AES measures (Figure CA.3, Table CA.4). We thus chose to conduct all further analyses of the µ-XRF ITRAX data using raw re-evaluated intensities to take advantage of the high temporal resolution offered by these time series.

Spatio-temporal dynamics of lake sediment geochemistry from Eastern Canada

We summarized the major axes of geochemical change across the 37 lake sediment records by applying a PCA to the raw re-evaluated intensity data from the XRF µ-ITRAX. Stepwise backward variable selection in the PCA retained *Inc.Coh*, Ca, Sr, Ti, Zn and Pb, accounting for a significant portion of the variation observed in the geochemical dataset from the two first PC axes (i.e., 70%; Figure III.3A). The first PC component most closely tracked variation in the organic (vs. inorganic) fraction of the sediment cores, where *Inc.Coh*, Sr and Ti accounted respectively for 25.1%, 23.1% and 22.8% of the variance explained (Figure III.3B). Lakes with relatively higher organic content plotted on the left-hand side of the ordination (most lakes ordinated there). Samples on the right-hand side of the ordination were dominated by inorganic terrigenous input, with higher abundances of Sr and Ti (Figure III.3A). The second PC axis was driven largely by the fraction of heavy metals, where Pb and Zn accounted for 28.6% and 23.1% of the variance explained, respectively (Figure III.3C). The calcium gradient also strongly contributed to PC2, accounting for 24.5% of the variation on this axis. Samples with high Ca contents plotted on the upper half of the ordination (Figure III.3A), while lake sediment dominated by Pb and Zn plotted on the lower half of the biplot.

The four ecoregion-level ellipses based on 95% confidence intervals showed substantial overlap, which was particularly evident for three of the four ecozones (Boreal Shield (#06), Atlantic Maritime (#07) and Atlantic Highlands (#17)), indicating that a high degree of similarity in geochemical composition is present between the cores of these ecoregions. However, one lake in the Atlantic Maritime ecozone ordinated more strongly along the Pb and Zn loadings, reflective of a greater abundance in these variables. In contrast, lake sediments from the

Mixedwood Plains occupied a much larger gradient of geochemical compositions, especially in calcium which was more abundant than in other ecoregions. Some lakes in the Mixedwood Plains also contained high concentrations of metals (Pb and Zn).

When investigating the temporal variation of the 37 lakes sampled, the GAMMs based on the PCA axes revealed a general signature of gradual enrichment in inorganic sedimentary materials across the last ~150 years (Figure III.4A). PC1 varied from negative values early in the records (indicative of organic-rich sediment) to positive PC1 values, highlighting the fact that lakes became richer in inorganic sediment. This increase in the fraction of inorganic material was further reinforced when observing the geochemical temporal variation observed along PC2 (Figure III.4B). PC2 varied from early positive to recent negative values, which reflected a shift towards a greater abundance of heavy metals starting in the early 20th century. PC2 reached a minimum (indicative of maximum metal abundance) around the year 1970 CE, before showing a significant decline (Figure III.4B).

<u>Investigating the influence of land use, soil composition and climate on lake sediment geochemical composition</u>

The Redundancy analysis (RDA) produced an ordination of sites similar to that identified in the PCA (Figure III.5). The RDA also served to highlight the influential role of total agricultural fraction (%) (F-statistic = 6.22, p-value = 0.002), estimated soil pH (F-statistic = 9.08, p-value = 0.001), soil volumetric fraction of coarse fragments (vol‰) (F-statistic = 3.26, p-value = 0.025), and mean population counts (inhabitants) F-statistic = 5.65, p-value = 0.006) (Figure III.5A) with none of these variables displaying VIF values greater than the threshold value (VIF > 5) (Gareth et al., 2013). Together, these variables accounted for 34% of the variance explained across the 37-lake mean elemental sediment geochemistry dataset. While the organic content of the sediment (*Inc:Coh* ratio) co-varied strongly with the coarse soil fraction, lakes that had a greater fraction of heavy metals (namely Pb and Zn) co-varied with increased population in their watersheds. Titanium, a measure of allochthonous contribution, also co-varied with the mean population of lake watersheds. Calcium content of lake sediment was best explained by both the proportion of agriculture present within the lakes' watersheds and the average watershed soil pH. Calcium was the element responsible for the greatest degree of separation within the ordination plane from the RDA. These overarching effects of soil and land use were also apparent in the variance partitioning, where soil composition accounted for 8% of the variation but also explained an additional 9% of the variation that was shared with land use (Figure III.5B). Land use, which considers lake watershed population (inhabitants) and proportion of agriculture, accounted for an additional 19% of the variance in sediment geochemistry. Echoing results from the RDA, variance partitioning analysis accounted for 36% of the total variance. While climatic variables were considered as potential predictors for the most parsimonious RDA model, neither mean temperature nor mean annual precipitation explained significant independent portions of the variance. However, these variables (mean annual temperature and total annual precipitation) were found to be significant predictors of lake sediment geochemical change when considering the data at its fullest temporal resolution (1911-2016 CE) (Figure CB.4) (F-statistic = 47.40, p-value = < 0.001; F-statistic =24.30, p-value < 0.001). With the temporal RDA model, the watershed population time series was also found to be a significant predictor (F-statistic = 16.07, p-value = < 0.001). Together, these three variables (temperature, precipitation and population) accounted for a total of 9.2% of the variance explained in the temporal lake sediment geochemical change (note: other variables measured at only one time point (e.g., soil pH) could not be included in this model).

Contextualizing sediment concentrations to environmental sediment quality guidelines

When comparing the elemental concentrations measured by ICP-MS on discrete samples to published Canadian sediment quality guidelines (CCME, 1999), we observed that, for all seven lakes assessed, at least five elements (As, Cd, Cr/Cu, Pb and Zn) exhibited values greater than the recommended Interim Freshwater Sediment Quality Guidelines (ISQG) in at least one sample (Table III.1). Four of the seven lakes had elemental concentrations greater than the ISQG for all elements with available guidelines. When assessing the temporal variation of these elements with respect to published environmental guidelines (Figure CB.5), some sites were clearly identified as having been subjected to considerable enrichment in metallic species. These sites included Stoco Lake, Ontario (08-160) where arsenic concentrations reached peak levels during the 1950s that were 22 times greater than the Probable Effect Level (PEL). This exercise also identified at least one lake with high pre-industrial concentrations for some of its elements. Silver Lake, NB (07-008), located in Sackville (New Brunswick), displayed cadmium and zinc concentrations having exceeded the PEL for centuries prior to the 1700s. The six other lakes showed more characteristic “hockey-stick trends” where metal concentrations have been increasing since the late-1800s (Figure CB.5).

Discussion

Temporal enrichment in sediment metal content

From the 37 full sediment records examined, most lakes were found to have experienced a considerable temporal enrichment in metal content. While our ICP-MS results are based on a smaller subset of lakes (n= 70 samples across 7 lakes), it was apparent that the concentration of numerous metal species (e.g., As, Pb, Zn) started increasing during the late 1800s. In fact, in all seven lakes, levels exceeding the ISQGs, and in some cases exceeding the PELs, were detected, particularly for Pb and Zn. Silver Lake, NB (07-008) and Stoco Lake, ON (08-160) exhibited particularly elevated concentrations for several metal species. These findings were echoed in the PCA and RDA ordinations which visualized the geochemical variation of our 37 lakes based on the raw re-evaluated µ-XRF ITRAX data, and identified that these two sites demonstrated a clear enrichment in metals when compared to other lakes. The causes for these elevated concentrations are likely to have different origins. In the case of Silver Lake (07-008), we found that even pre-industrial baseline concentrations for several elements were elevated as Cd and Zn concentrations have exceeded PEL concentrations for centuries prior to the 1700s (Figure CB.5). Contrastingly, the elevated concentrations recorded in Stoco Lake (08-160) are thought to stem from a mining operation in the vicinity of the lake (Simmatis et al., 2020).

To further contextualize our results, we compared Pb, As, Cu and Zn concentrations to published values from Davidson et al. (2021), who analyzed contaminated and reference lake sediment from Boat Harbour which received pulp mill effluent (Nova Scotia, Canada). They found that all four elements exceeded the ISQG concentration in both contaminated and reference systems, and that Zn concentrations exceeded the PEL in the contaminated site and As in the reference site. Other accounts of environmental exceedance have been reported in sites in western Canada. For example, Sanei et al. (2010) investigated metal species concentrations in lakes distributed across the Wabamun area (Alberta) and reported that, for many of the lakes considered (n = 10), the mean post-1956 concentrations of As, Cr, Cu, and Zn exceeded the Canadian sediment quality guidelines for the protection of aquatic life, which was attributed to coal-fired power plants in the region. While sedimentary quality guidelines are important and must be considered when evaluating the distribution of metals in specific locations, our work emphasizes the value of having historical estimates of elemental concentrations to properly contextualize the potential presence of environmental contamination.

Landscape heterogeneity of Eastern Canada

The PCA showed substantial spatial and temporal variation in sediment geochemistry across the eastern Canadian landscape. When considering ecozone-specific ellipses delineated from the PCA, we observed important overlaps in the sediment composition of lakes from the Atlantic Maritime, Atlantic Highlands, and Boreal Shield ecozones. These lakes had notably higher molybdenum incoherence to coherence ratios (*Inc.Coh* ratio), a proxy that has often been described as a measure of the sediment organic content. Despite several lakes from the Mixedwood Plains having high *Inc.Coh,* most lakes within this ecozone had greater inorganic content, especially in carbonates as represented by elevated Ca abundances. Our results echo earlier reports that the µ-XRF ITRAX scanner is a powerful tool for discerning variation in organic to inorganic sediment. For example, Barreiro-Lostres et al. (2015) identified clear distinctions between terrigenous material (Sr, Ti, Rb) and organic sediment (Inc.Coh). Similarly, Makri et al., (2021) used TIC, TOC, calcium, iron, and manganese inferred from µ-XRF ITRAX to investigate mixing regimes in Lake Moossee since Late-glacial times, and were able to explain 70% of variance in geochemistry with their ordination analyses; these results allowed them to discriminate distinct sediment stratigraphical units.

Accounting for over 30% of variance explained in mean lake sediment geochemistry, the RDA yielded insights into our understanding of the potential drivers leading to geochemical heterogeneity represented within our eastern Canadian core collection. The greater sediment organic content found in most lakes was best explained by the coarse volumetric fraction of the catchment soil, while carbonate-rich sediments were associated with soils of greater pH values. We suggest that the greater calcium content is due to the carbonate-rich surficial deposits associated with the Late Pleistocene Champlain Sea that covered this region (Venture and Warkentin, 1965). As such, the Champlain Sea gave rise to the productive soil of the St. Lawrence lowlands, which is also observed within the RDA, where the proportion of agriculture was also highly correlated to soil pH and inferred calcium concentration from lake sediments in the region. We suggest that current land-use distribution, at least in part, reflects the geological underpinning of the landscape. The RDA also revealed the higher loading of Pb and Zn with greater population sizes within watersheds, which could be associated with increased vehicle exhaust and urban stormwater run-off (Müller et al., 2020; Silva et al., 2020). However, Ti (a marker of sediment allochthonous contribution) was also associated with population size. It is possible that the association of greater Ti and population is linked to the greater hydrological control of lakes in regions with higher population counts and/or with important land use conversion, especially forest clearing which has the potential to increase soil erosion (Borrelli et al., 2017).

Lake sediment geochemical change

We observed a marked shift towards greater inputs of inorganic material through time when considering the geochemical changes experienced by lake sediments across Eastern Canada. This pattern was visible from the relative change from high organic carbon content (inferred from *Inc.Coh*) towards more elevated abundances of titanium, strontium and other metals such as lead and zinc (Figure III.4). This shift is likely the result of a greater contribution of soil erosion within watersheds associated with the intensification of land-use conversion from forest to urban and suburban areas in Eastern Canada, which continued to increase greatly in the early 1900s (Lemon, 1977; Drushka, 2003). Land-cover changes have been the driving factor for increased soil erosion on a global scale (Jenny et al., 2019). The change towards a greater inorganic content was also supported by the temporal variation in elements such as Pb and Zn (which corresponded to negative PC2 values) (Figure III.4). The timing of this variation is especially interesting, recording an increase during the early 1900s, then reaching a maximum ca. 1970 CE, before rapidly decreasing until the present. This timing coincides with the successful effort to phase out leaded gasoline (Nriagu, 1990) and to a broader and heightened environmental consciousness. For example, the Canadian Clear Air Act (1971) and the American Clean Water Act (1972) coincided with the largest improvements recorded since Canadian air monitoring began in the 1950s. The timing would thus imply that atmospheric deposition, associated with lead and zinc emissions from industrial sites, are the likely source of the recorded enrichment of these metals. The RDA supports the idea that greater metal content is associated with human populations. However, it is difficult to attribute the exact source of this environmental pollution, as many factors may mitigate pollution effects and we can thus only speculate on the source of metal loading. Whilst several previous publications investigating single sites have reported increases in Pb content between ca. 1930 – 1980, our study demonstrates the ubiquity of these trends in lakes across the four ecozones in northeast Canada. Past work using Pb isotopes showed that Pb-bearing compounds could travel over hundreds of kilometers before being deposited in lake sediments (France and Blais, 1998). Despite having observed a trend of decreasing metals across Eastern Canada, we acknowledge that this pattern of environmental recovery is not necessarily observed for every location in Canada, let alone the world (Odumo et al., 2018; Jasiak et al., 2021), and that atmospheric transport and deposition of pollutants may have resulted in different trajectories elsewhere.

Limitations and future considerations

Given the strong coherence between the concentrations measured via ICP-MS/AES and the intensities yielded by the µ-XRF ITRAX scanner, we concluded that the very high-resolution data acquired by the scanner were a reliable source of information for resolving questions of temporal geochemical dynamics. µ-XRF ITRAX's high temporal resolution data can be especially insightful when used to complement ICP-MS/AES concentrations, which are often measured at coarser temporal resolution and thus may fail to capture some of these dynamics. For example, the µ-XRF ITRAX-generated data demonstrated a recent (ca. 1980 – 2017 CE) decrease in Pb that was not captured in the ICP-MS analyses because of coarser sample resolution. Lakes may also differ greatly in sediment accumulation rates, with rates varying by orders of magnitude despite being located in the same region. Indeed, for some of the cores considered here, 1 cm of sediment accumulation corresponded to 2 – 50 years at the top of the core (Baud et al., 2022). Where sediment cores must be subsampled into discrete vertical intervals, varying sedimentation rates can have important repercussions on subsequent analyses, leading to intervals encapsulating widely different temporal ranges. For lakes with low sedimentation rates, this will ultimately restrict analyses to very thin intervals. While this issue can be mitigated by using the sub-millimetric resolution of the µ-XRF ITRAX scanner, future large-scale sampling campaigns should aim to dedicate substantial resources and adapt to higher subsampling resolution in regions with low sedimentation rates. With proxies accounting for various sources of sediment, the µ-XRF ITRAX is a great tool to reconstruct the relative temporal geochemical change experienced by lakes across the landscape. Using ordination analyses, where each element is allowed to vary as a function of its counterparts' elements, one can clearly visualize lake trajectories as well as lake geochemical change while considering the natural variability within a study region (Figure CB.6). Given the many factors influencing lake sediment composition, it can be challenging to identify point or non-point sources of geochemical change, because lakes accumulate matter originating directly from their watershed, from the atmosphere, and from within the lake. However, with the application of more proxies to the sediment record, further insights can be gained.

Conclusions

Our analyses of multiple lake sediment cores from Eastern Canada revealed robust relationships between data derived from μ-XRF ITRAX scanning, expressed as intensities, and independent ICP-MS and ICP-AES data, expressed as absolute concentrations (in mg/kg). Considering elemental intensities, we observed that a significant amount of variation in sediment geochemistry could be explained by erosion proxies (Ti, Sr), sedimentary organic content productivity (*Inc.Coh*), and local and atmospheric pollution (Pb, Zn) when considering our full network of 37 sediment cores. The geological origins of the watersheds explained a significant portion of this variation, but contemporary land-use variables, reflecting the presence of agriculture and human population, were stronger at explaining the spatial pattern of elemental concentrations. In addition, we observed exceedance of environmental sedimentary guidelines for a number of sites, with lakes generally showing an increase in the combined contents of Pb and Zn. Metal contents were found to have reached a maximum ca. 1970 CE before declining, suggesting that environmental regulations aimed to reduce the emission of metals were likely effective, at least in our studied region of Eastern Canada.

Acknowledgements

This research was supported by an FRQNT Team Research Grant awarded to IGE, PF, DA and JPS. In addition, the collection of the sediment cores and associated environmental data was made possible through the NSERC Canadian Lake Pulse network, of which IGE, DA and JPS are co-PIs. We are also grateful to FRQNT for providing AB with a Doctoral scholarship and the Canada Research Chairs program for providing funding to IGE, PF, DA and JPS. We would also like to acknowledge lab support by Michelle Gros and Chris Grooms, and the LakePulse field teams and director, Dr. Yannick Huot. Feedback by members of the Gregory-Eaves' lab also helped improve the quality of this manuscript.

Data Availability Statement

Measured ITRAX intensities, elemental concentrations obtained via ICP-MS/AES and density profiles obtained via computed-tomography scanner will be made available the open science platform Zenodo accessible at https://zenodo.org/.

References

Barreiro-Lostres, F., Brown, E., Moreno, A., Morellón, M., Abbott, M., Hillman, A., Giralt, S., Valero-Garcés, B., 2015. Sediment delivery and lake dynamics in a Mediterranean mountain watershed: Human-climate interactions during the last millennium (El Tobar Lake record, Iberian Range, Spain). Sci. Total Environ., 533, 506-519. https://doi.org/10.1016/j.scitotenv.2015.06.123

Baud, A., Aulard, C., Ghanbari, H., Fradette, M., Antoniades, D., Del Giorgio, P., Huot, Y., Francus, P., Smol, J., Gregory-Eaves, I., 2022. A framework for 210Pb model selection and its application to 37 cores from Eastern Canada to identify the dynamics and drivers of lake sedimentation rates. Earth Surf. Process Landf. https://doi.org/10.1002/esp.5391

Blomqvist, S., 1991. Quantitative sampling of soft-bottom sediments: problems and solutions. Mar. Ecol. Prog. Ser., 72, 295-304

Boden, T., Andres, R., Marland, G., 2017. Global, regional, and national fossil-fuel co2 emissions (1751-2014)(v. 2017), Environmental System Science Data Infrastructure for a Virtual Ecosystem (ESS-DIVE) (United States); Carbon Dioxide Information Analysis Center (CDIAC), Oak Ridge National Laboratory (ORNL), Oak Ridge, TN (United States).

Boës, X., Rydberg, J., Martinez-Cortizas, A., Bindler, R., Renberg, I., 2011. Evaluation of conservative lithogenic elements (Ti, Zr, Al, and Rb) to study anthropogenic element enrichments in lake sediments. J. Paleolimnol., 46, 75-87. https://doi.org/10.1007/s10933-011-9515-z

Borrelli, P., Robinson, D.A., Fleischer, L.R., Lugato, E., Ballabio, C., Alewell, C., Meusburger, K., Modugno, S., Schütt, B., Ferro, V., Bagarello, V., Van Oost, K., Montanarella, L., Panagos, P., 2017. An assessment of the global impact of 21st century land use change on soil erosion. Nature Communications, 8, 2013. 10.1038/s41467-017-02142-7

Camarero, L., 2003. Spreading of trace metals and metalloids pollution in lake sediments over the Pyrenees, Journal de Physique IV (Proceedings). EDP sciences, pp. 249-253. https://doi.org/10.1051/jp4:20030289

Cuven, S., Francus, P., Crémer, J.-F., 2007. Protocoles d'utilisation et essais de calibration du scanner de microfluorescence X de type «ITRAX TM Core Scanner».

Davidson, E.A., 2009. The contribution of manure and fertilizer nitrogen to atmospheric nitrous oxide since 1860. Nat Geosci, 2, 659-662. https://doi.org/10.1038/ngeo608

Davidson, K.B., Holmes, B.E., Spooner, I.S., Dunnington, D.W., Walker, T.R., Lake, C.B., Su, C.-C., 2021. Application of the paleolimnological method to assess metal contaminant distribution (As, Cu, Pb, Zn) in pulp mill stabilization basin sediments, Nova Scotia, Canada. Environ. Sci. Pollut. Res., 28, 51342-51355. https://doi.org/10.1007/s11356-021-14212-x

Davies, S.J., Lamb, H.F., Roberts, S.J., 2015. Micro-XRF core scanning in palaeolimnology: recent developments. Springer

Drushka, K., 2003. Canada's forests: a history. McGill-Queen's Press-MQUP. 0773526617

Fielding, J.J., Croudace, I.W., Kemp, A.E., Pearce, R.B., Cotterill, C.J., Langdon, P., Avery, R., 2020. Tracing lake pollution, eutrophication and partial recovery from the sediments of Windermere, UK, using geochemistry and sediment microfabrics. Sci. Total Environ., 722, 137745. https://doi.org/10.1016/j.scitotenv.2020.137745

France, R.L., Blais, J.M., 1998. Lead concentrations and stable isotopic evidence for transpolar contamination of plants in the Canadian High Arctic. Ambio, 506-508

Gareth, J., Daniela, W., Trevor, H., Robert, T., 2013. An introduction to statistical learning: with applications in R. Spinger

Goldschmidt, V.M., 1954. Geochemistry. LWW. 0038-075X

Government of Canada., 2015. Canadian Digital Elevation Model. Government of Canada. Accessible from: https://open.canada.ca/data/en/dataset/7f245e4d-76c2-4caa-951a-45d1d2051333

Grill, G., Lehner, B., Lumsdon, A.E., MacDonald, G.K., Zarfl, C., Liermann, C.R., 2015. An index-based framework for assessing patterns and trends in river fragmentation and flow regulation by global dams at multiple scales. Environ. Res. Lett., 10, 015001. http://dx.doi.org/10.1088/1748-9326/10/1/015001

Gross, J., 2003. Variance inflation factors: R News, v. 3.

Hoesly, R.M., Smith, S.J., Feng, L., Klimont, Z., Janssens-Maenhout, G., Pitkanen, T., Seibert, J.J., Vu, L., Andres, R.J., Bolt, R.M., 2018. Historical (1750–2014) anthropogenic emissions of reactive gases and aerosols from the Community Emissions Data System (CEDS). Geosci. Model Dev., 11, 369-408. https://doi.org/10.5194/gmd-11-369-2018

Hole, L., Engardt, M., 2008. Climate change impact on atmospheric nitrogen deposition in northwestern Europe: a model study. Ambio, 9-17. https://doi.org/10.1579/0044-7447(2008)37[9:CCIOAN]2.0.CO;2

Hounsfield, G.N., 1980. Computed medical imaging. Medical Physics, 7, 283-290. https://doi.org/10.1118/1.594709

Huot, Y. et al., 2019. The NSERC Canadian Lake Pulse Network: A national assessment of lake health providing science for water management in a changing climate. Sci Total Environ, 695, 133668. 10.1016/j.scitotenv.2019.133668

Jackson, A., Inger, R., Parnell, A., Bearhop, S., 2011. Comparing isotopic niche widths among and within communities: Bayesian analysis of stable isotope data. J. Anim. Ecol., 80, 595-602. https://doi.org/10.1111/j.1365-2656.2011.01806.x

Jackson, D.A., 1993. Stopping rules in principal components analysis: a comparison of heuristical and statistical approaches. Ecology, 74, 2204-2214

Jarsjö, J., Andersson-Sköld, Y., Fröberg, M., Pietroń, J., Borgström, R., Löv, Å., Kleja, D.B., 2020. Projecting impacts of climate change on metal mobilization at contaminated sites: Controls by the groundwater level. Sci. Total Environ., 712, 135560. https://doi.org/10.1016/j.scitotenv.2019.135560

Jasiak, I., Wiklund, J., Leclerc, E., Telford, J., Couture, R., Venkiteswaran, J., Hall, R., Wolfe, B., 2021. Evaluating spatiotemporal patterns of arsenic, antimony, and lead deposition from legacy gold mine emissions using lake sediment records. Appl. Geochem., 134, 105053. https://doi.org/10.1016/j.apgeochem.2021.105053

Jenny, J.P. et al., 2019. Human and climate global-scale imprint on sediment transfer during the Holocene. Proc Natl Acad Sci U S A, 116, 22972-22976. 10.1073/pnas.1908179116

Kalugin, I., Daryin, A., Smolyaninova, L., Andreev, A., Diekmann, B., Khlystov, O., 2007. 800-yr-long records of annual air temperature and precipitation over southern Siberia inferred from Teletskoye Lake sediments. Quaternary Research, 67, 400-410. https://doi.org/10.1016/j.yqres.2007.01.007

Kimball, B., Runkel, R., 2002. Evaluating Remedial Alternatives for an Acid Mine Drainage Stream: Application of a Reactive Transport. Model Environ. Sci. Technol, 36, 1093-1101. https://doi.org/10.1021/es0109794

Last, W.M., Smol, J.P., 2002. Tracking environmental change using lake sediments: volume 2: physical and geochemical methods. Springer Science & Business Media. 1402006284

Legendre, P., Oksanen, J., ter Braak, C.J., 2011. Testing the significance of canonical axes in redundancy analysis. Methods Ecol. Evol., 2, 269-277. https://doi.org/10.1111/j.2041-210X.2010.00078.x

Lemon, J.T., 1977. George A. Nader, Cities of Canada. Macmillan of Canada. 1469-8706

Lepak, R.F., Janssen, S.E., Engstrom, D.R., Krabbenhoft, D.P., Tate, M.T., Yin, R., Fitzgerald, W.F., Nagorski, S.A., Hurley, J.P., 2020. Resolving Atmospheric Mercury Loading and Source Trends from Isotopic Records of Remote North American Lake Sediments. Environ Sci Technol, 54, 9325-9333. 10.1021/acs.est.0c00579

Makri, S., Wienhues, G., Bigalke, M., Gilli, A., Rey, F., Tinner, W., Vogel, H., Grosjean, M., 2021. Variations of sedimentary Fe and Mn fractions under changing lake mixing regimes, oxygenation and land surface processes during Late-glacial and Holocene times. Sci Total Environ, 755, 143418. 10.1016/j.scitotenv.2020.143418

Masson-Delmotte, V., Zhai, P., Pirani, A., Connors, S.L., Péan, C., Berger, S., Caud, N., Chen, Y., Goldfarb, L., Gomis, M., 2021. Climate change 2021: the physical science basis. Contribution of working group I to the sixth assessment report of the intergovernmental panel on climate change, 2. doi:10.1017/9781009157896.

Müller, A., Österlund, H., Marsalek, J., Viklander, M., 2020. The pollution conveyed by urban runoff: A review of sources. Sci. Total Environ., 709, 136125. https://doi.org/10.1016/j.scitotenv.2019.136125

Naeher, S., Gilli, A., North, R.P., Hamann, Y., Schubert, C.J., 2013. Tracing bottom water oxygenation with sedimentary Mn/Fe ratios in Lake Zurich, Switzerland. Chem. Geol., 352, 125-133. https://doi.org/10.1016/j.chemgeo.2013.06.006

Nriagu, J.O., 1990. The rise and fall of leaded gasoline. Sci. Total Environ., 92, 13-28. https://doi.org/10.1016/0048-9697(90)90318-O

Odumo, B.O., Nanos, N., Carbonell, G., Torrijos, M., Patel, J.P., Rodríguez Martín, J.A., 2018. Artisanal gold-mining in a rural environment: Land degradation in Kenya. LDD, 29, 3285-3293. https://doi.org/10.1002/ldr.3078

Peres-Neto, P.R., Legendre, P., Dray, S., Borcard, D., 2006. Variation partitioning of species data matrices: estimation and comparison of fractions. Ecology, 87, 2614-25. 10.1890/0012-9658(2006)87[2614:vposdm]2.0.co;2

Punning, J.-M., Boyle, J., Terasmaa, J., Vaasma, T., Mikomägi, A., 2007. Changes in lake-sediment structure and composition caused by human impact: repeated studies of Lake Martiska, Estonia. The Holocene, 17, 145-151. https://doi.org/10.1177/0959683607073297

R Core Team., 2021. R: A language and environment for statistical computing. R Foundation for Statistical Computing. http://www.R-project.org/

Roberts, N. et al., 2018. Europe's lost forests: a pollen-based synthesis for the last 11,000 years. Sci Rep, 8, 716. 10.1038/s41598-017-18646-7

Rothwell, R.G., 2015. Twenty years of XRF core scanning marine sediments: What do geochemical proxies tell us?, Micro-XRF studies of sediment cores. Springer, pp. 25-102.

Rothwell, R.G., Rack, F.R., 2006. New techniques in sediment core analysis: an introduction. Geological Society, London, Special Publications, 267, 1-29. https://doi.org/10.1144/GSL.SP.2006.267.01.01

Sanei, H., Goodarzi, F., Outridge, P., 2010. Spatial distribution of mercury and other trace elements in recent lake sediments from central Alberta, Canada: An assessment of the regional impact of coal-fired power plants. Int. J. Coal Geol., 82, 105-115. https://doi.org/10.1016/j.coal.2010.01.010

Schiedek, D., Sundelin, B., Readman, J.W., Macdonald, R.W., 2007. Interactions between climate change and contaminants. Mar. Pollut. Bull., 54, 1845-1856. https://doi.org/10.1016/j.marpolbul.2007.09.020

Semkin, R., Kramer, J., 1976. Sediment geochemistry of Sudbury-area lakes. Canadian Mineralogist, 14, 73-90

Silva, L.F.O., Pinto, D., Neckel, A., Oliveira, M.L.S., 2020. An analysis of vehicular exhaust derived nanoparticles and historical Belgium fortress building interfaces. Geoscience Frontiers, 11, 2053-2060. https://doi.org/10.1016/j.gsf.2020.07.003

Simmatis, B., Baud, A., Gregory-Eaves, I., Francus, P., Smol, J.P., 2020. Subfossil Simuliidae track past river flow into an industrially contaminated lake. J. Paleolimnol., 64, 179-192. https://doi.org/10.1007/s10933-020-00130-4

Syvitski, J.P., Vorosmarty, C.J., Kettner, A.J., Green, P., 2005. Impact of humans on the flux of terrestrial sediment to the global coastal ocean. Science, 308, 376-80. 10.1126/science.1109454

Tomkins, J.D., Antoniades, D., Lamoureux, S.F., Vincent, W.F., 2008. A simple and effective method for preserving the sediment–water interface of sediment cores during transport. J. Paleolimnol., 40, 577-582. https://doi.org/10.1007/s10933-007-9175-1

Venture, R.L., Warkentin, B., 1965. Chemical properties of Champlain Sea sediments. CaJES, 2, 299-308

Walling, D.E., 2009. The impact of global change on erosion and sediment transport by rivers: current progress and future challenges. 978-92-3-104135-8

Weltje, G.J., Bloemsma, M., Tjallingii, R., Heslop, D., Röhl, U., Croudace, I.W., 2015. Prediction of geochemical composition from XRF core scanner data: a new multivariate approach including automatic selection of calibration samples and quantification of uncertainties, Micro-XRF studies of sediment cores. Springer, pp. 507-534.

Wood, S.N., Pya, N., Säfken, B., 2016. Smoothing parameter and model selection for general smooth models. J. Am. Stat. Assoc., 111, 1548-1563. https://doi.org/10.1080/01621459.2016.1180986

Woodward, C., Gadd, P., 2019. The potential power and pitfalls of using the X-ray fluorescence molybdenum incoherent: Coherent scattering ratio as a proxy for sediment organic content. Quat. Int., 514, 30-43. https://doi.org/10.1016/j.quaint.2018.11.031

Tables Chapter III

Table III.1. Summary of the elemental range concentrations (µg/kg) derived from ICP-MS measurements performed on seven lakes (n = 70). For each element the sediment quality guidelines for the Protection of Aquatic Life are presented, as available from the Canadian Council of Ministers of the Environment (CCME, 1999) for both Interim Freshwater Sediment Quality Guidelines (ISQG, dry weight) and Probable Effect Levels (PEL, dry weight). One star (*) indicates that elemental concentration levels exceeded ISQG, while two stars (**) indicate PEL exceedance.

LakeID	**As** (µg/kg) ISQG > 5.9 x 10^3 PEL > 1.7 x 10^4	**Cd** (µg/kg) ISQG > 6.0 x10^2 PEL > 3.5 x10^3	**Cr** (µg/kg) ISQG > 3.7 x10^4 PEL > 9.0 x10^4	**Cu** (µg/kg) ISQG > 3.6 x10^4 PEL > 2.0 x10^5	**Pb** (µg/kg) ISQG > 3.5 x10^4 PEL > 9.1 x10^4	**Zn** (µg/kg) ISQG > 1.2 x10^5 PEL > 3.2 x10^5
06-133	1.6 x10^3 - 1.9 x10^4 **	6.6 x10^2 - 5.4 x10^3 **	9.7 x10^3 - 4.4 x10^4 *	1.6 x10^4 - 6.4 x10^4 *	1.7 x10^3 - 1.5 x10^5 **	8.1 x10^4 - 2.7 x10^5 *
06-137	2.5 x10^3 - 8.2 x10^3 *	3.2 x10^2 - 1.4 x10^3 *	5.6 x10^4 - 6.5 x10^4 *	2.4 x10^4 - 3.0 x10^4 -	1.0 x10^4 - 7.3 x10^4 *	1.0 x10^5 - 1.9 x10^5 *
07-008	7.8 x10^3 - 1.8 x10^4 **	4.5 x10^3 - 2.1 x10^4 **	3.1 x10^4 - 6.6 x10^4 *	1.2 x10^4 - 3.9 x10^4 *	2.9 x10^4 - 8.5 x10^4 *	3.6 x10^5 - 8.0 x10^5 **
07-029	6.3 x10^3 - 1.6 x10^4 *	5.0 x10^2 - 1.1 x10^3 *	2.5 x10^4 - 6.2 x10^4 *	2.1 x10^4 - 1.5 x10^5 *	1.8 x10^4 - 9.4 x10^4 **	9.5 x10^4 - 2.2 x10^5 *
08-160	1.1 x10^5 - 3.88 x10^5 **	1.6 x10^3 - 4.6 x10^3 **	6.0 x10^4 - 7.3 x10^4 *	3.4 x10^4 - 8.0 x10^4 *	5.5 x10^4 - 1.3 x10^5 **	3.3 x10^5 - 1.2 x10^6 **
08-179	6.1 x10^3 - 7.8 x10^3 *	7.3 x10^2 - 1.1 x10^3 *	2.3 x10^4 - 2.6 x10^4 -	1.5 x10^4 - 2.3 x10^4 -	4.8 x10^4 - 1.2 x10^5 **	1.1 x10^5 - 1.9 x10^5 *
08-211	2.7 x10^3 - 2.3 x10^4 **	5.2 x10^2 - 5.6 x10^3 **	1.1 x10^4 - 2.9 x10^4 -	1.7 x10^4 - 7.7 x10^4 *	5.8 x10^3 - 3.2 x10^5 **	5.0 x10^4 - 3.9 x10^5 **

Figures Chapter III

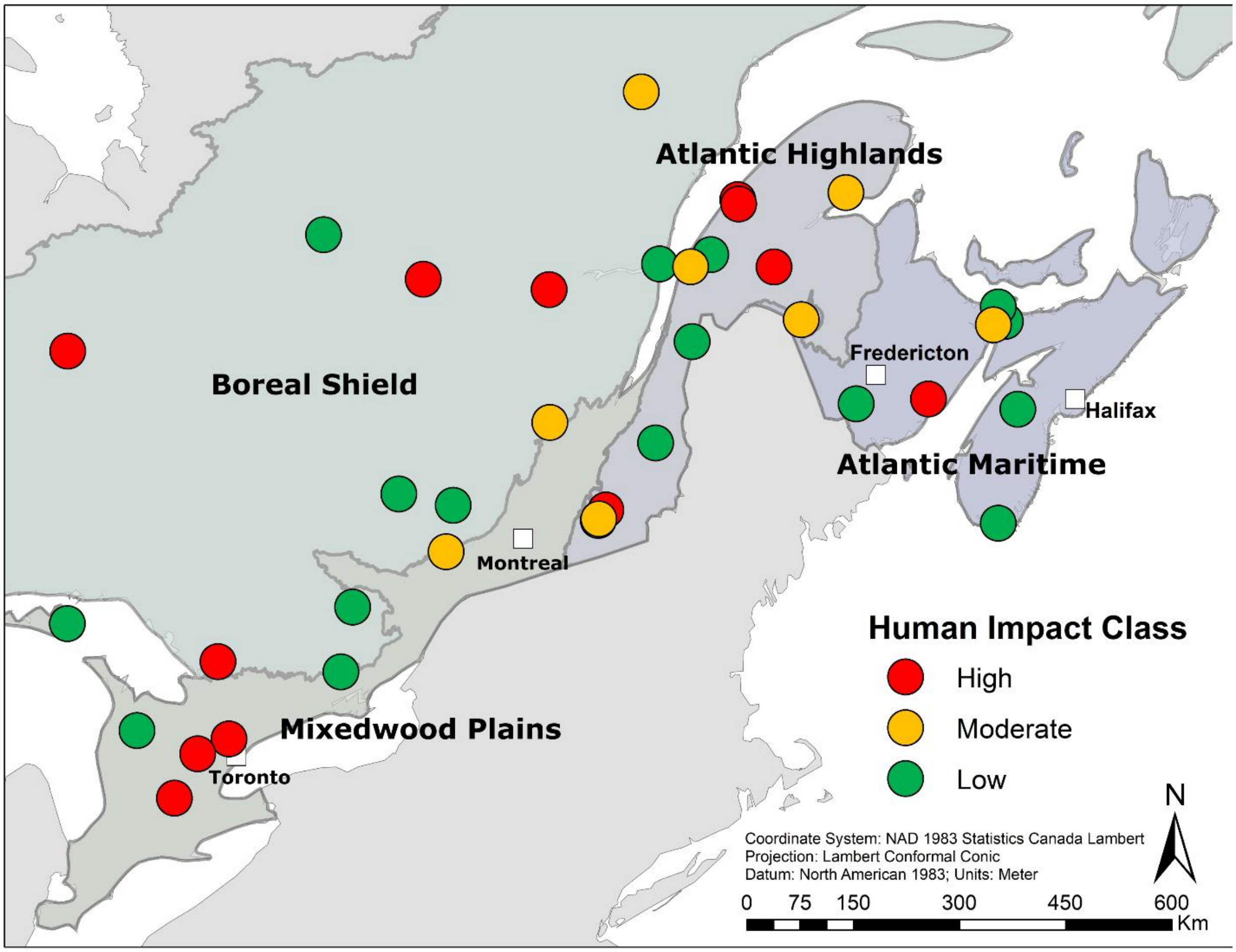

Figure III.1. Map showing the distribution of the 37 lakes sampled across four ecozones of Eastern Canada (Boreal Shield (#06), Mixedwood Plains (#08), Atlantic Highlands (#17) and Atlantic Maritime (#07)).These lakes were selected and sampled along a gradient of human impact, represented by the symbol color, where green is low impact, orange is moderate impact, and red is high impact, using ecozone-specific thresholds (as described in Huot et al., 2019).

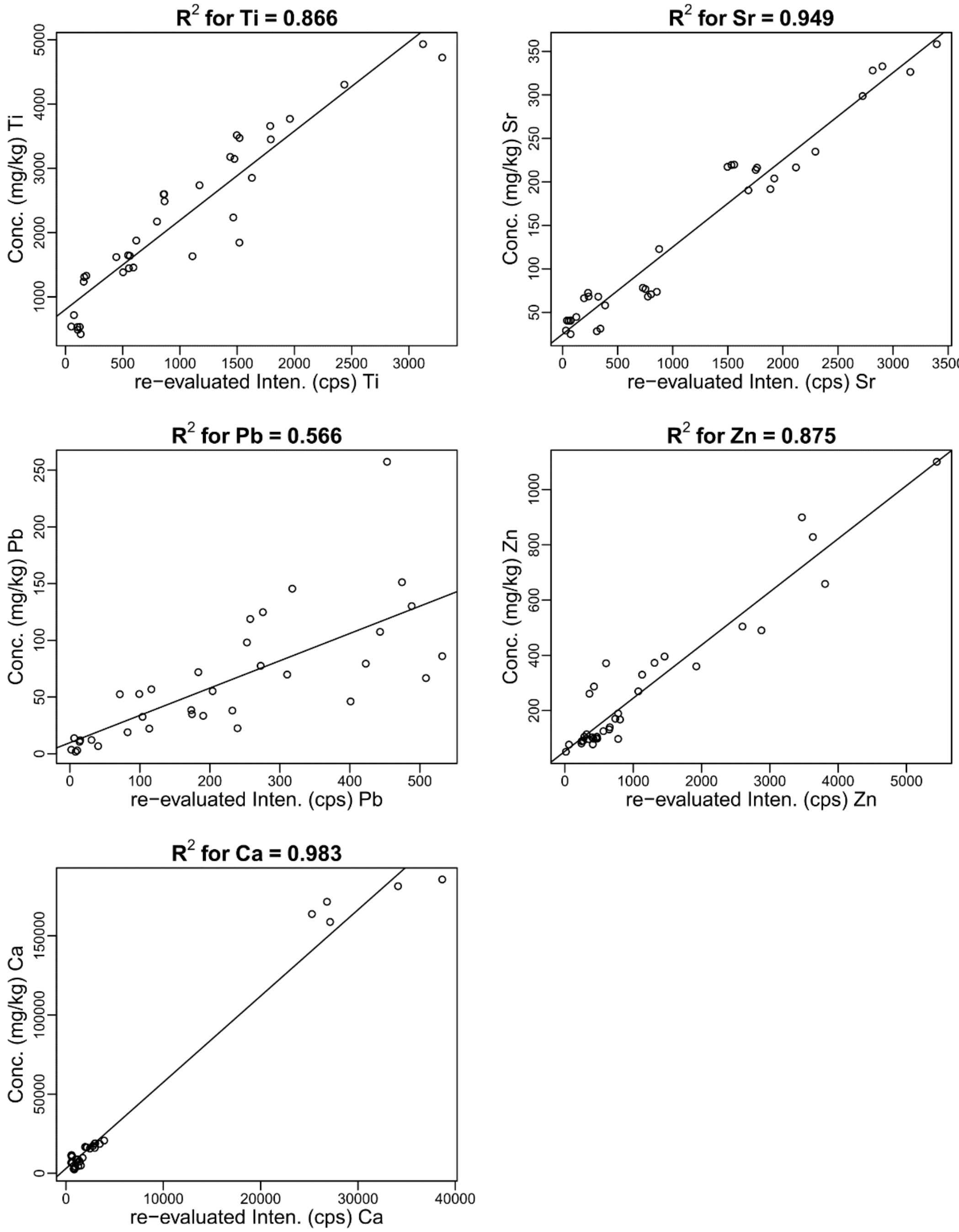

Figure III.2. Graphical representations summarizing the fit of the bootstrapped relationship between ICP-derived concentrations and raw re-evaluated ITRAX intensities measured in counts per second (cps)

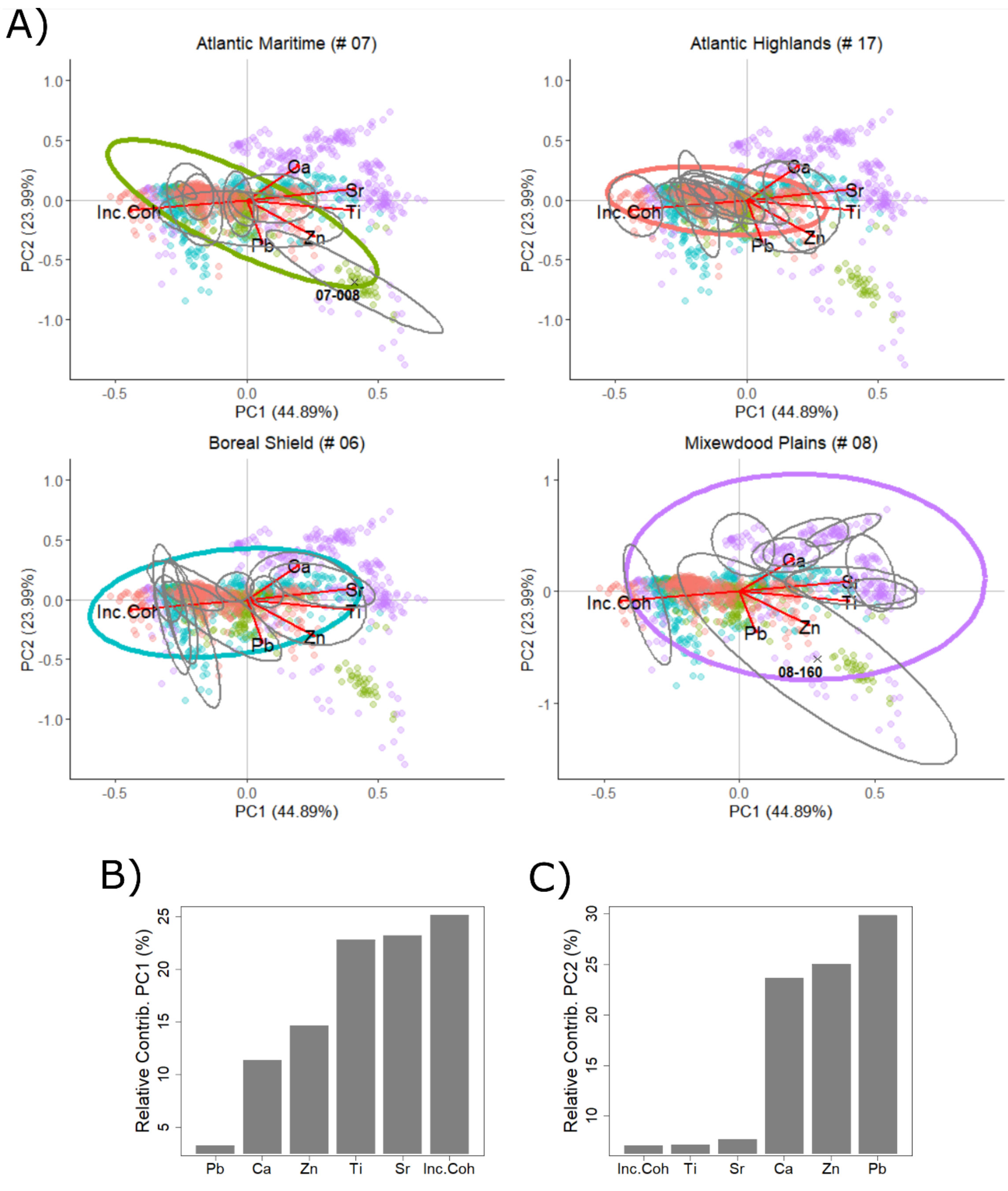

A)
Atlantic Maritime (# 07)
Atlantic Highlands (# 17)
Boreal Shield (# 06)
Mixewdood Plains (# 08)
PC1 (44.89%)
PC2 (23.99%)
Inc.Coh
Ca
Sr
Ti
Zn
Pb
07-008
08-160
B)
C)
Relative Contrib. PC1 (%)
Relative Contrib. PC2 (%)

Figure III.3. A) PCA ordinations showing lake and ecozone-specific 95% confidence interval ellipses using Ca, Sr, Ti, Zn, Pb and *Inc.Coh* as loadings for all 37 lakes sampled (i.e., all lakes included in single analysis). The lakes' 95% confidence interval ellipses appear in grey and are represented as a function of ecozones. For two of the lakes mentioned in the text, the centroid and LakeID are labeled. Thicker colored lines indicate the ecozone-based 95% confidence interval ellipses, with Atlantic Maritimes in green, Atlantic Highlands in red, Boreal Shield in blue and Mixedwood Plains in purple. B and C) Barplots representing the percent relative contribution of each variable to PC1 and PC2 loadings, respectively.

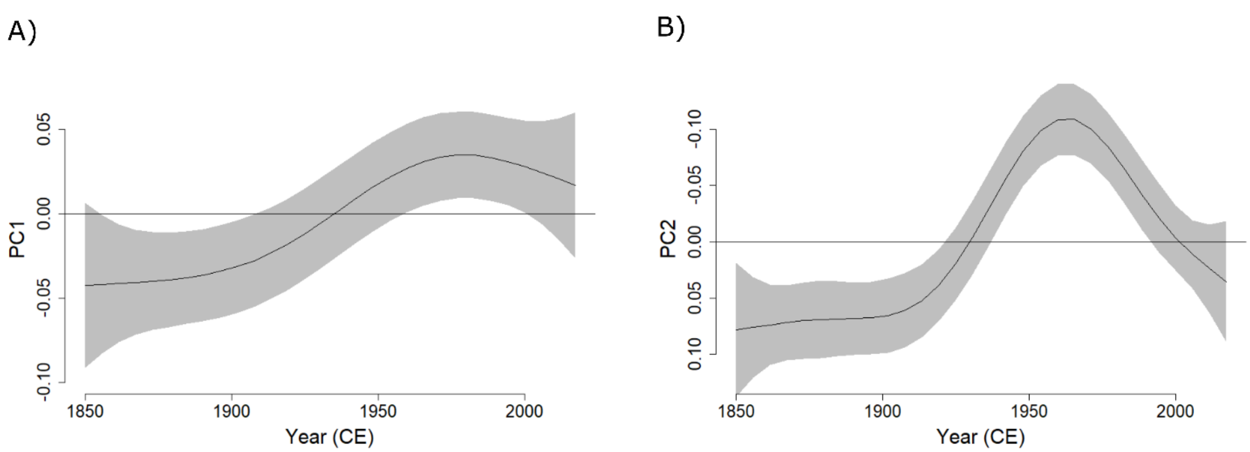

Figure III.4. Principal Component (PC) scores across all cores shown as GAMMs fitted values excluding random effects for PC axis 1 (A) and PC axis 2 (B), plotted as a function of Year (CE). Note that the y-axis for PC2 has been reversed to demonstrate the highlight temporal enrichment in heavy metals observed in during the 1950-1980s.

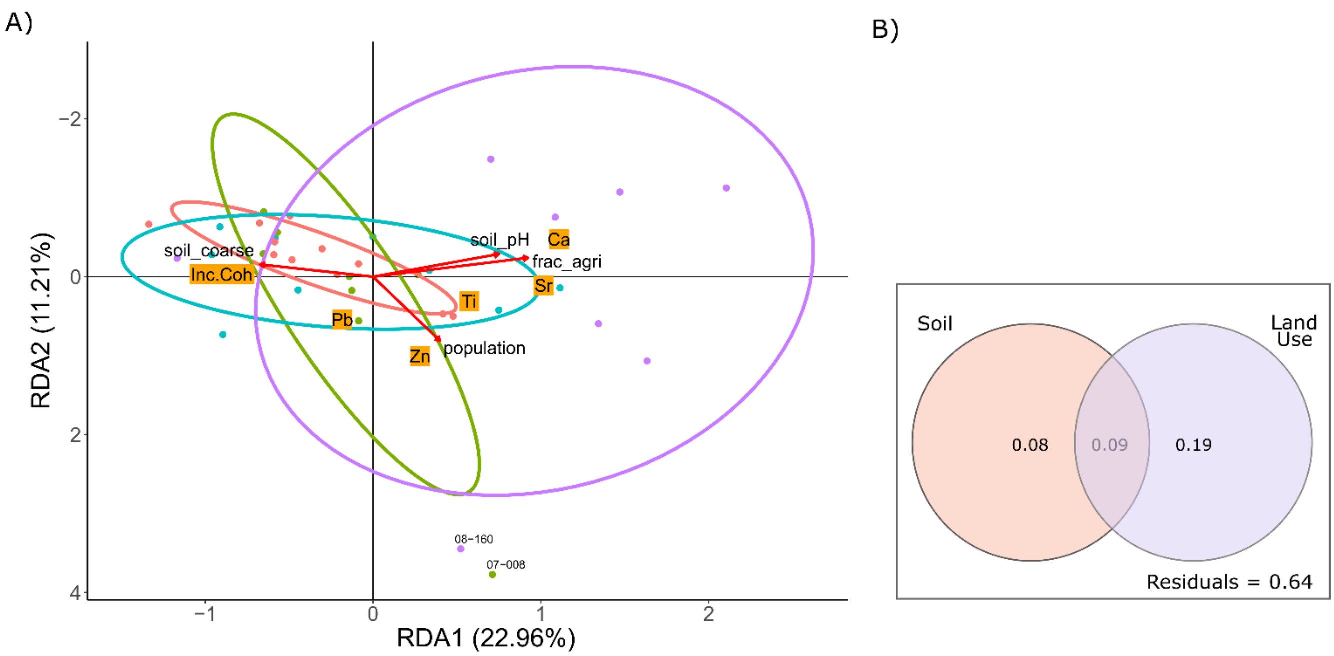

Figure III.5. A) Redundancy Analysis (RDA) evaluating the standardized geochemical intensities of all selected elements (Ca, Sr, Ti, Zn, Pb and *Inc.Coh*). Mixedwood Plains is in purple, Boreal Shield in blue, Atlantic Maritimes in green, and Atlantic Highlands in red. B) Variance partitioning evaluated the contribution of soil and land-use variables to the distribution of mean elemental abundances.

Appendices Chapter III

Appendix CA: Assessment of coherence between ICP-MS/AES concentrations and µ-XRF ITRAX intensities

From the 37 sediment cores collected, seven cores showing important variation in elemental abundances were selected for a calibration exercise between µ-XRF ITRAX intensities and ICP-MS/AES concentrations. In preparation, 0.25 g of dry mass from selected subsamples for ICP-MS/AES analyses underwent a total digestion method that consisted of treating samples with a sequence of concentrated nitric acid, perchloric acid and hydrofluoric acid. These acids completely dissolved the organic matrix over a 72-hour period. For comparative purposes, mean elemental intensities from the µ-XRF ITRAX counts were integrated over 1 cm to develop parallel companion intervals that also were selected for ICP-MS/AES. Using bootstrapped regression from the boot package in R (Canty and Ripley, 2017), we then evaluated the coherence of the ICP-MS/AES data with one of four normalization methods of the 1 cm integrated µ-XRF ITRAX counts following recommendations from Gregory et al. (Gregory et al., 2019), namely: 1) re-evaluated fluorescence; 2) counts per second (cps)-normalized re-evaluated fluorescence; 3) cps-density normalized re-evaluated fluorescence; and 4) Multivariate Log-ratio Calibration (MLC) (Weltje et al., 2015). Across each method, the coefficients of determination (R^2) were determined using the 95% confidence interval of the bootstrapped regression from the boot:boot.ci() R function for all available elements (Al, Ca, Cr, Cu, Fe, K, Mn, P, Pb, S, Sr, Ti, V, Zn, Zr). Elements displaying poor fit ($R^2 < 0.50$) were not considered further. To visualize and compare the influence of each of the four different normalization methods on the ordination of elemental abundances, we performed principal component analyses (PCA) using the vegan library (Oksanen et al., 2013). We also quantified the degree of similarity between PCAs derived from each of elemental datasets generated across the different calibration methods and the measured elemental concentrations derived from ICP-MS/AES by calculating their RV coefficient across each pair of datasets.

When considering the 4 normalization methods that we evaluated, the μ-XRF ITRAX raw re-evaluated normalization method was the one that generally displayed the strongest relationships between intensities and absolute concentrations (mg/kg) from ICP-MS/AES measurements (Table CA.1, Figure CA.2). Exceptions to this were Al, P, Zr and Cu, which were elements that consistently had R^2 below 0.50 and thus were not considered further. In most cases, accounting for the total counts per second (cps) did not improve the relationships between μ-XRF ITRAX and ICP-MS/AES. Similarly, cps-density normalized intensities were found to yield R^2 values that were very close to those observed for raw re-evaluated and cps-normalized intensities. MLC provided improvement for a few elements, namely Al, Cu and Pb, Zr, but R^2 for most other elements were lower than the ones yielded from the raw re-evaluated μ-XRF ITRAX. Overall, we observed that, regardless of the processing method used, no significant improvements were made to the original fit between raw re-evaluated intensities and ICP-MS/AES absolute concentrations. When comparing the four different normalization methods using PCA ordinations, patterns from the original ICP-MS/AES ordinations were highly conserved across at least three of the four calibration methods (Figure CA.3). The RV coefficients measured when comparing the degree of similarity between each dataset were found to be consistently very high, except for the MLC-transformed dataset where the RV coefficients were lower (RV = 0.51 - 0.98; Table CA.4). The results from our evaluation of the four normalization procedures highlighted the strong fit between raw re-evaluated µ-XRF ITRAX intensities and absolute concentrations obtained from ICP-MS/AES analyses. Since our goal was to investigate the relative geochemical change experienced by lakes across Eastern Canada, we decided to use elemental intensities, especially considering the important degree of similarity between this dataset and the measured ICP-MS/AES concentrations.

Table CA.1. Summary table of the four methods' processing steps. Coefficients of determination (R^2) calculated via bootstrapping for all considered elements are summarized within their respective geochemical classification (Goldschmidt, 1954) : Lithophile (light orange); Chalcophile (light yellow); Biophile (light green) and Siderophile (light grey).

	Re-evaluated	**cps-corrected**	**cps-density corrected**	**MLC**
Element	Initial re-evaluation of sum spectra	Initial re-evaluation of sum spectra and normalization to total counts per second	Initial re-evaluation of sum spectra and normalization to total counts per second and density from CT-scan	Multivariate log-ratio transformation
Al	0.153	0.112	0.182	0.127
K	0.749	0.754	0.76	0.501
Ti	0.863	0.879	0.874	0.764
Sr	0.95	0.925	0.913	0.751
Zr	0.21	0.243	0.24	0.08
Cr	0.704	0.687	0.662	0.41
Cu	0.215	0.275	0.218	0.489
Pb	0.566	0.513	0.399	0.746
Zn	0.872	0.835	0.799	0.631
Ca	0.983	0.971	0.968	0.869
P	0.045	0.042	0.06	0.095
S	0.401	0.384	0.365	0.38
V	0.75	0.727	0.741	0.374
Fe	0.851	0.822	0.801	0.773
Mn	0.778	0.754	0.736	0.761

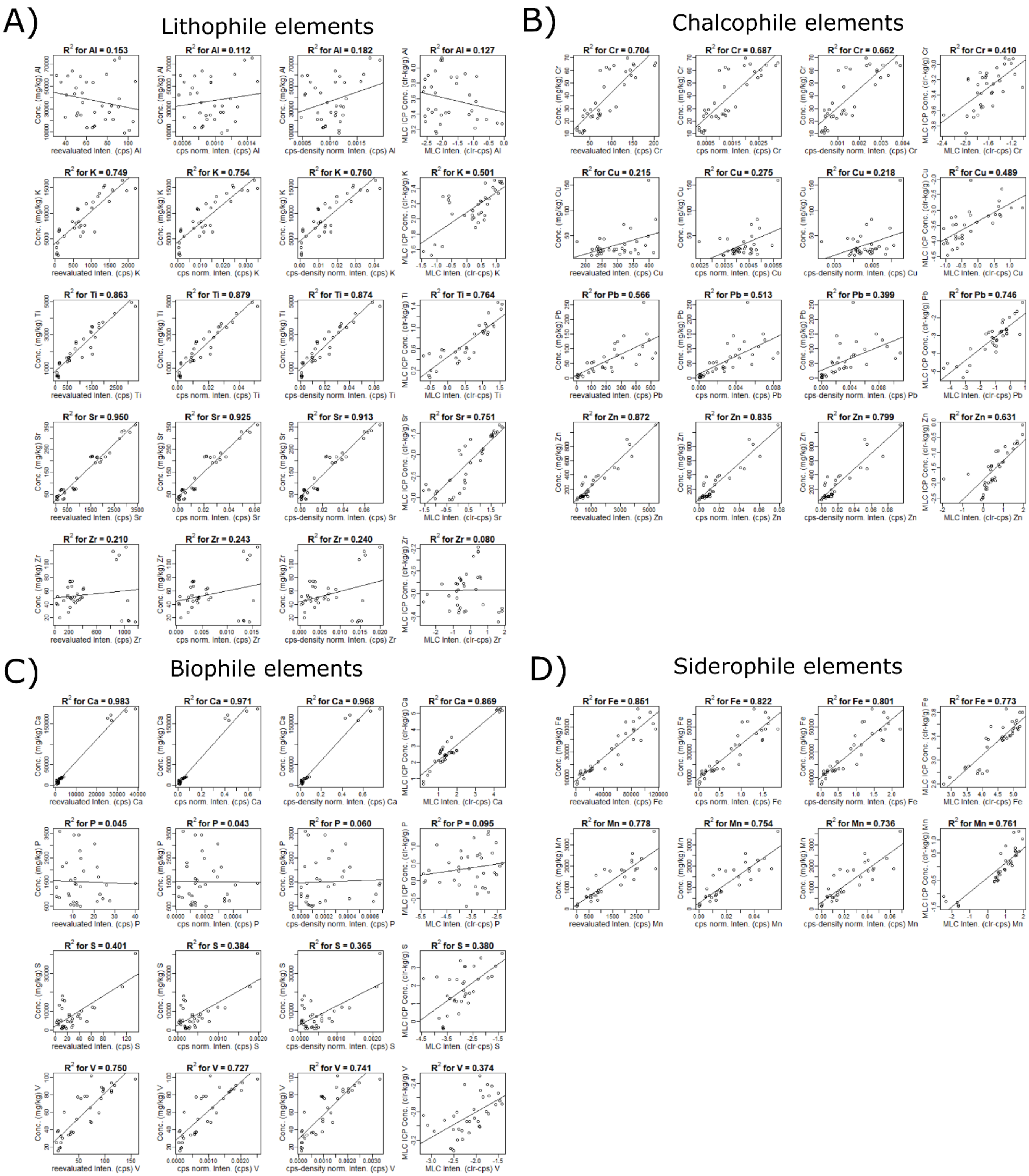

Figure CA.2. Graphical representations summarizing the fit of the bootstrapped relationship between ICP-MS/AES concentrations and ITRAX intensities performed for different groups of elements following Goldschmidt's classification. A) Lithophile elements (Al, K, Ti, Sr and Zr); B)

Chalcophile elements (Cr, Cu, Pb and Zn); C) Biophile elements (Ca, P, S and V); and D) Siderophile elements (Fe and Mn). Across the groups, each column represents a different data processing methodology, with from left to right: the raw re-evaluated ITRAX intensities (counts per second = cps); cps-normalized; cps-density normalized and multi log-ratio calibration (MLC), where concentrations and intensities were center-log transformed (clr).

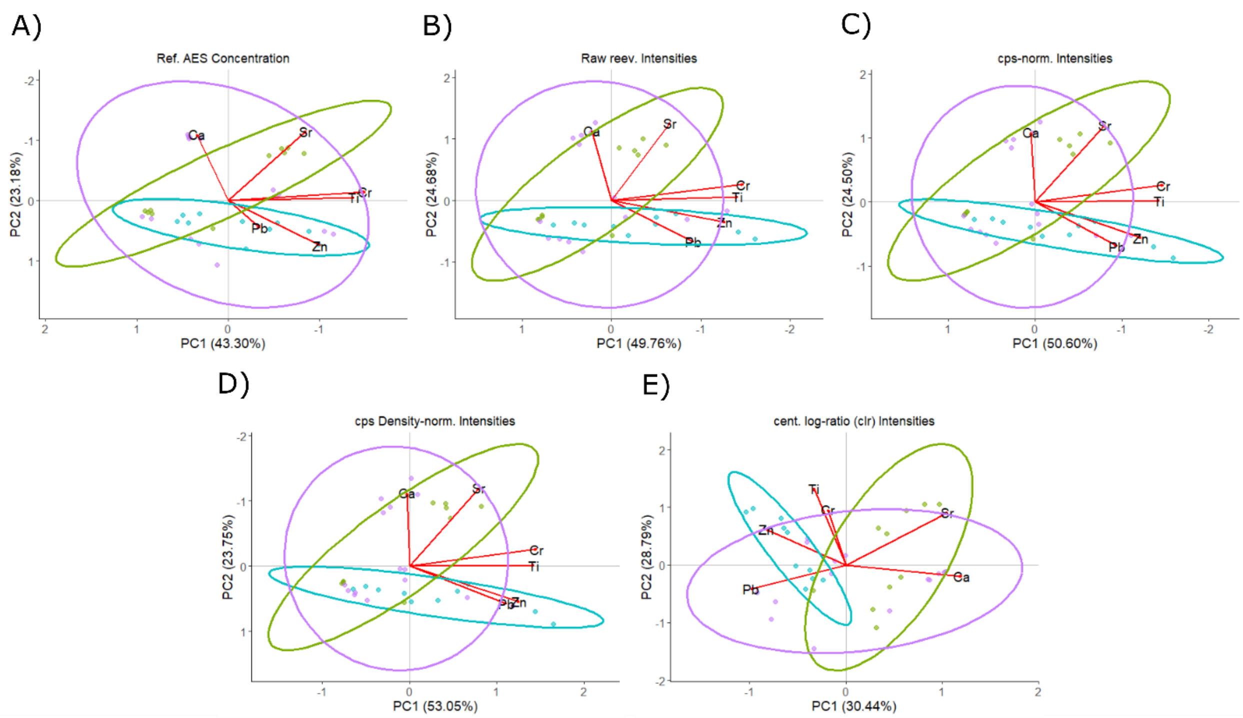

Figure CA.3. Principal component analysis (PCA) ordinations using Ca, Sr, Cr, Ti, Zn and Pb as loadings for the subset of seven lakes with the ICP-AES measurements (n=35). A) Reference ICP-AES concentrations (mg kg^{-1}); B) Raw re-evaluated intensities; C) Normalized intensities corrected for cps; D) Normalized intensities corrected for cps and CT-density; E) Multivariate log-ratio predicted concentrations (MLC; clr-mg kg^{-1}). The colors represent lake ecozones, with Atlantic Maritimes in green, Boreal Shield in blue and Mixedwood Plains in purple. The ellipses represent the 95% confidence interval of lakes across each of the three ecozones. Note: There is no ellipse for the Atlantic Highlands since no ICP-AES measurements were performed for lakes in this ecozone as these lakes exhibited a smaller range of variation in elemental abundance than that captured in lakes of neighboring ecozones.

Table CA.4. Summary table for the RV coefficient when evaluating the correlation in the ordination pattern using predicted geochemical concentrations across the different processing techniques.

	ICP-AES	Raw re-ev.	cps-norm.	cps density-norm.	MLC
ICP-AES	-				
Raw re-ev.	0.980	-			
cps-norm.	0.964	0.997	-		
cps density-norm.	0.961	0.995	0.997	-	
MLC	0.512	0.508	0.501	0.503	-

References

Canty, A., Ripley, B., 2017. boot: Bootstrap R (S-Plus) functions. R package version, 1, 3-20

Goldschmidt, V.M., 1954. Geochemistry. LWW. 0038-075X

Gregory, B.R., Patterson, R.T., Reinhardt, E.G., Galloway, J.M., Roe, H.M., 2019. An evaluation of methodologies for calibrating Itrax X-ray fluorescence counts with ICP-MS concentration data for discrete sediment samples. Chem. Geol., 521, 12-27. https://doi.org/10.1016/j.chemgeo.2019.05.008

Oksanen, J., Blanchet, F.G., Kindt, R., Legendre, P., Minchin, P., O'hara, R., Simpson, G., Solymos, P., Stevens, M.H.H., Wagner, H., 2013. Community ecology package. R package version, 2, 321-326

Weltje, G.J., Bloemsma, M., Tjallingii, R., Heslop, D., Röhl, U., Croudace, I.W., 2015. Prediction of geochemical composition from XRF core scanner data: a new multivariate approach including automatic selection of calibration samples and quantification of uncertainties, Micro-XRF studies of sediment cores. Springer, pp. 507-534.

Appendix CB: Supplementary Materials

Table CB.1. Summary of the 37 lakes' sampling dates, locations and morphological information.

LakeID (*Lake Names*)	Sampling Date	Province	Latitude (DD)	Longitude (DD)	Maximum Depth (m)	Surface Area (km^2)	Watershed Area (km^2)	Altitude (m asl)
06-071 (*Lac Parentheses*)	8/13/2017	QC	50.379	-68.804	17.0	1.88	6.88	548
06-080 (*Lac Jerome*)	8/15/2017	QC	48.248	-69.638	11.0	0.16	26.48	106
06-103 (*Lac a la Croix*)	8/22/2017	QC	48.397	-71.780	34.0	0.72	10.02	156
06-126 (*Lac Paula*)	8/25/2017	QC	48.991	-74.028	17.0	0.55	3.38	445
06-133 (*Lac Duhamel*)	7/17/2017	QC	46.141	-74.635	26.0	0.54	3.19	244
06-137 (*Lac des Iles*)	8/29/2017	QC	46.459	-75.533	40.0	16.72	147.6	209
06-140 (*Lac Daine*)	8/22/2017	QC	49.874	-75.670	3.5	2.32	20.01	339
06-156 (*Wabun Lake*)	9/6/2017	QC	45.225	-76.834	26.0	0.46	2.28	215
06-178 (*Gull Lake*)	9/3/2017	QC	44.920	-79.359	6.7	1.39	11.62	249
06-199 (*Lillabelle Lake*)	8/15/2017	QC	49.112	-81.035	2.3	1.8	26.89	245
07-005 (*Long Lake*)	7/23/2017	NS	45.909	-64.145	1.6	1	21.92	9
07-006 (*Collins Lake*)	7/24/2017	NB	46.111	-64.151	4.6	0.65	2.4	13
07-008 (*Morice Pond*)	7/28/2017	NB	45.931	-64.368	3.0	1.48	50.95	9
07-013 (*Colwell Round Lake*)	8/14/2017	NS	44.846	-64.598	2.1	0.14	1.89	219
07-025 (*French Lake*)	8/21/2017	NS	43.650	-65.712	4.9	5.58	46.86	31
07-029 (*Ritchie Lake*)	8/5/2017	NB	45.415	-65.968	12.0	0.25	6.02	37

LakeID (*Lake Names*)	Sampling Date	Province	Latitude (DD)	Longitude (DD)	Maximum Depth (m)	Surface Area (km^2)	Watershed Area (km^2)	Altitude (m asl)
07-047 (*Magaguadavic Lake*)	8/29/2017	NB	45.710	-67.189	9.8	27	377.97	116
07-051 (*Blue Bell Lake*)	7/16/2017	NB	46.950	-67.538	0.9	0.1	4.31	226
08-120 (*Lac des Chicots*)	8/21/2017	QC	46.797	-72.523	21	0.71	16.64	148
08-135 (*Lac Georges*)	9/12/2017	ON	45.605	-74.981	10.2	0.61	33.7	39
08-160 (*Stoco Lake*)	7/25/2017	ON	44.472	-77.295	13.5	5.75	2225	139
08-179 (*Wilcox Lake*)	8/1/2017	ON	43.950	-79.433	17	0.58	7.56	295
08-191 (*Alder Lake*)	8/22/2017	ON	43.353	-80.537	1.5	0.16	73.17	318
08-192 (*Green Lake*)	8/8/2017	ON	43.840	-80.008	13	0.14	0.89	396
08-197 (*Copps Lake*)	7/25/2017	ON	44.260	-80.969	10.1	0.11	1.15	299
08-211 (*Sucker Lake*)	8/8/2017	ON	45.720	-81.869	3.2	2.28	5.56	246
17-027 (*Lac a l'Oie*)	7/25/2017	QC	48.213	-65.852	11	0.28	5.82	52
17-054 (*Eightmile Lake*)	7/31/2017	NB	47.694	-67.643	4.5	0.23	1.68	241
17-059 (*Lac de Saint-Damase*)	8/7/2017	QC	48.656	-67.808	3.4	0.66	16.23	187
17-060 (*Lac Michaud*)	8/1/2017	QC	48.601	-67.820	5.7	0.41	2.22	211
17-067 (*Grand lac Touradi*)	8/1/2017	QC	48.131	-68.667	17	7.7	118.08	216
17-075 (*Lac du Marin-à-Gouin*)	8/7/2017	QC	48.077	-69.104	9	0.15	7.84	170

LakeID (*Lake Names*)	Sampling Date	Province	Latitude (DD)	Longitude (DD)	Maximum Depth (m)	Surface Area (km^2)	Watershed Area (km^2)	Altitude (m asl)
17-081 (*Lac de l'Est*)	7/25/2017	QC	47.184	-69.564	26	7.53	181.87	321
17-090 (*Lac Volet*)	8/22/2017	QC	46.137	-70.810	6	0.27	27.97	266
17-105 (*Petit lac Saint-Francois*)	8/27/2017	QC	45.536	-72.035	2	0.83	20.37	207
17-112 (*Lac des Francais*)	8/31/2017	QC	45.439	-72.223	7	0.17	1.56	354
17-116 (*Lac Brais*)	7/15/2017	QC	45.457	-72.206	17	0.51	12.17	291

06-071
Max Core length: 34.3 cm

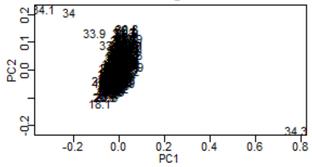

Outliers removed: 34, 34.1, 34.3

06-080
Max Core length: 31.6 cm

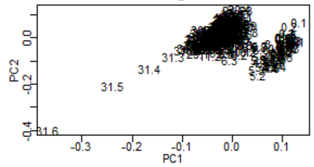

Outliers removed: 31.5, 31.6

06-103
Max Core length: 35.7 cm

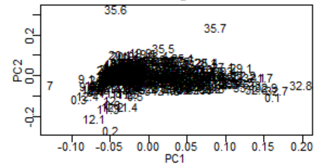

Outliers removed: 0.2, 35.6, 35.7

06-126
Max Core length: 39 cm

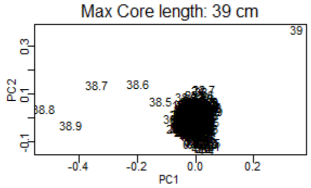

Outliers removed: 38.6, 38.7, 38.8, 38.9, 39

06-133
Max Core length: 29.5 cm

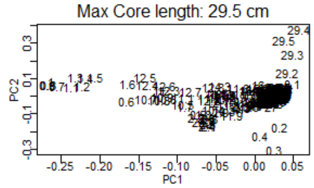

Outliers removed: 0.3, 0.7, 0.8, 0.9, 1, 1.3, 29.4, 29.5

06-137
Max Core length: 37.9 cm

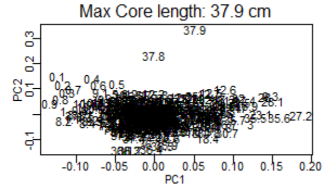

Outliers removed: 37.8, 37.9

06-140
Max Core length: 31.9 cm

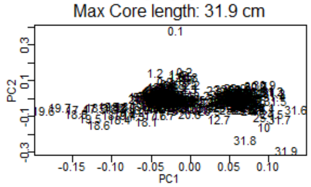

Outliers removed: 0.1, 31.8, 31.9

06-178
Max Core length: 30.2 cm

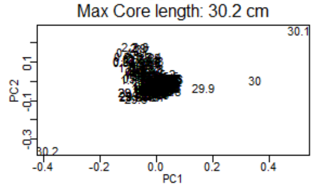

Outliers removed: 30, 30.1, 30.2

06-199
Max Core length: 34.4 cm

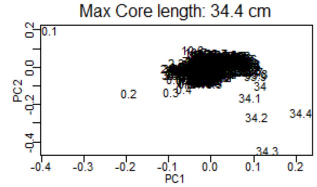

Outliers removed: 0.1, 0.2, 34.2, 34.3, 34.4

07-005
Max Core length: 31.9 cm

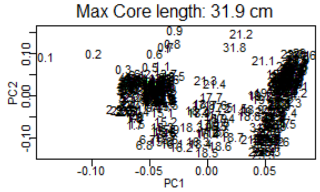

Outliers removed: None

07-006
Max Core length: 34.3 cm

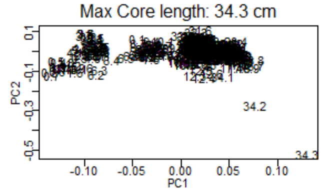

Outliers removed: 34.2, 34.3

07-008
Max Core length: 36.1 cm

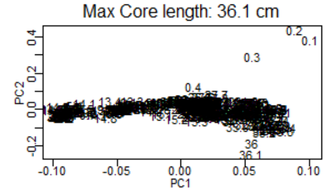

Outliers removed: 0.1, 0.2, 0.3, 36.1

07-013
Max Core length: 35.3 cm

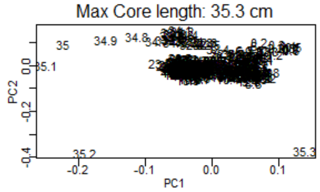

Outliers removed: 35, 35.1, 35.2, 35.3

07-025
Max Core length: 28.9 cm

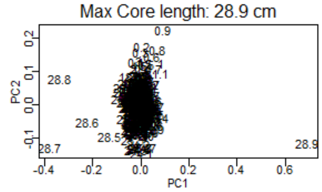

Outliers removed: 28.7, 28.8, 28.9

07-029
Max Core length: 34 cm

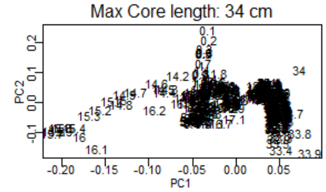

Outliers removed: 0.1, 15.7, 15.8

07-047
Max Core length: 31.1 cm

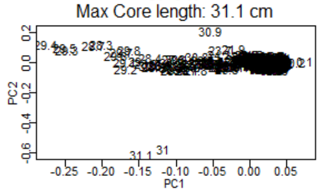

Outliers removed: 29.3, 29.4, 29.5, 31, 31.1

07-051
Max Core length: 33.8 cm

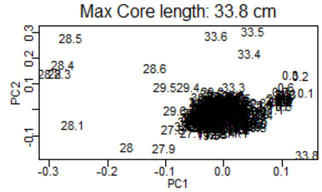

Outliers removed: 28.1, 28.2, 28.3, 28.4, 28.5, 33.5, 33.6

08-120
Max Core length: 36.5 cm

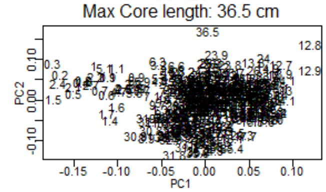

Outliers removed: None

08-135
Max Core length: 46.4 cm

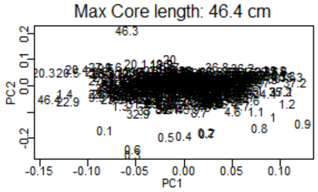

Outliers removed: 0.3, 0.6, 46.3

08-160
Max Core length: 28.6 cm

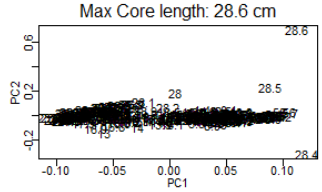

Outliers removed: 28.4, 28.6

08-179
Max Core length: 34.7 cm

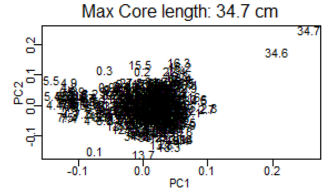

Outliers removed: 34.6, 34.7

08-192
Max Core length: 30.5 cm

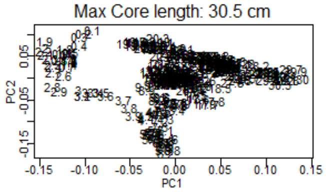

Outliers removed: None

08-197
Max Core length: 33 cm

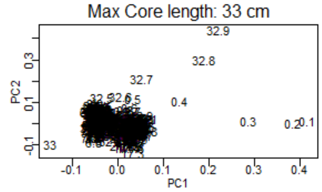

Outliers removed: 0.1, 0.2, 0.3, 32.8, 32.9

08-211
Max Core length: 32.7 cm

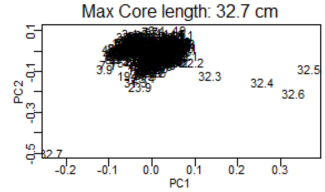

Outliers removed: 32.4, 32.5, 32.6, 32.7

17-027
Max Core length: 29.2 cm

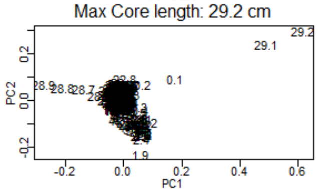

Outliers removed: 28.9, 29.1, 29.2

17-054
Max Core length: 32 cm

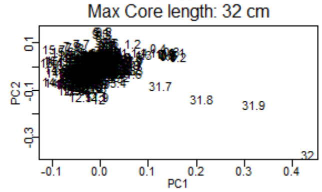

Outliers removed: 31.8, 31.9, 32

17-060
Max Core length: 41.9 cm

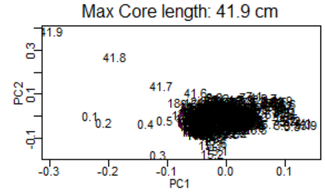

Outliers removed: 0.1, 0.2, 41.8, 41.9

17-067
Max Core length: 35 cm

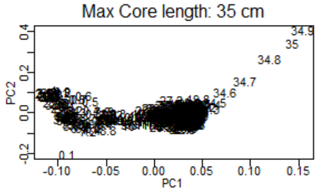

Outliers removed: 34.8, 34.9, 35

17-075
Max Core length: 36.2 cm

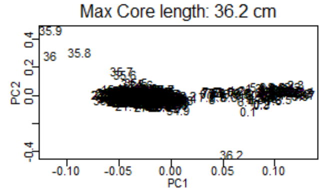

Outliers removed: 35.8, 35.9, 36, 36.2

17-081
Max Core length: 25.1 cm

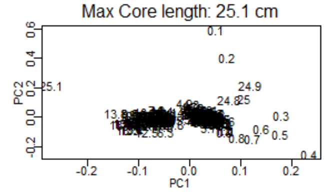

Outliers removed: 0.1, 0.2, 0.4, 25.1

17-090
Max Core length: 31.3 cm

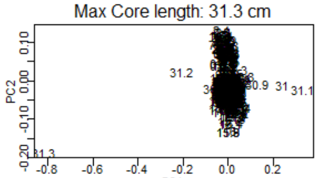

Outliers removed: 31, 31.1, 31.3

17-105
Max Core length: 22.7 cm

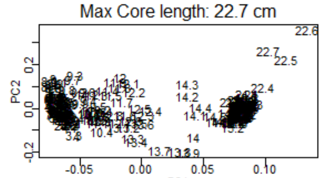

Outliers removed: 22.6, 22.7

17-112
Max Core length: 30.2 cm

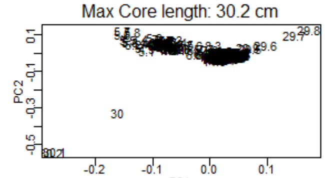

Outliers removed: 30, 30.1, 30.2

17-116
Max Core length: 41.2 cm

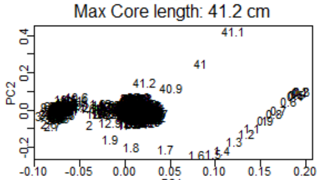

Outliers removed: 0.1, 0.2, 0.3, 1.4, 1.5, 1.6, 1.7, 41, 41.1

Figure CB.2. Ordination of each sediment core conducted to visualize the presence of non-sediment material added to stabilize the core top (sodium polyacrylate) or bottom (plug), that were deemed as outliers and thus excluded in downstream analyses. Non-sediment materials were identified using the Mahalanobis distance of each point from the lakes' centroid using the mahalanobisQC function in R (script provided below). Consecutive points from the start and end of the scans with a significance level p-value < 0.0001 were considered as outliers and removed from the dataset. In cases where not all consecutive outliers were not detected (e.g., 0.1 mm was not identified as an outlier but 0.2 was), these intervals were removed manually.

```
mahalanobisQC <- function(spca) {
 ss <- spca$CA$u[, 1:2]
 maha <- sapply(1:nrow(ss), function(i) {
   v <- matrix(1/apply(ss[-i,], 2, var), ncol=1)
   as.vector(ss[i,]^2 %*% v)
 })
 names(maha) <- rownames(spca$CA$u)
 pmaha <- 1-pchisq(maha, 2)
 data.frame(statistic=maha, p.value=pmaha)
}
```

```
#dx is defined as the union of all the measurements provided by the ITRAX output:

#Includes:

#"E.gain",    "E.offset",  "F.slope",   "F.offset",

#"cps",      "MSE",   "Dt", elemental intensities, elasticities and inelasticities parameters.
```

```
ItraxOutliers <- function(d) {

  d.pca <- rda(dx, scaling=1)

  maha <- mahalanobisQC(d.pca)

  maha$coreID <- d$CoreID

  outlier <- subset(maha,p.value < 0.0001)

  setDT(outlier, keep.rownames = TRUE)[]

  outlier$sign.level <- 0.0001

  dy <- d[ !(d$position %in% outlier$rn), ]

  return(dy)

}
```

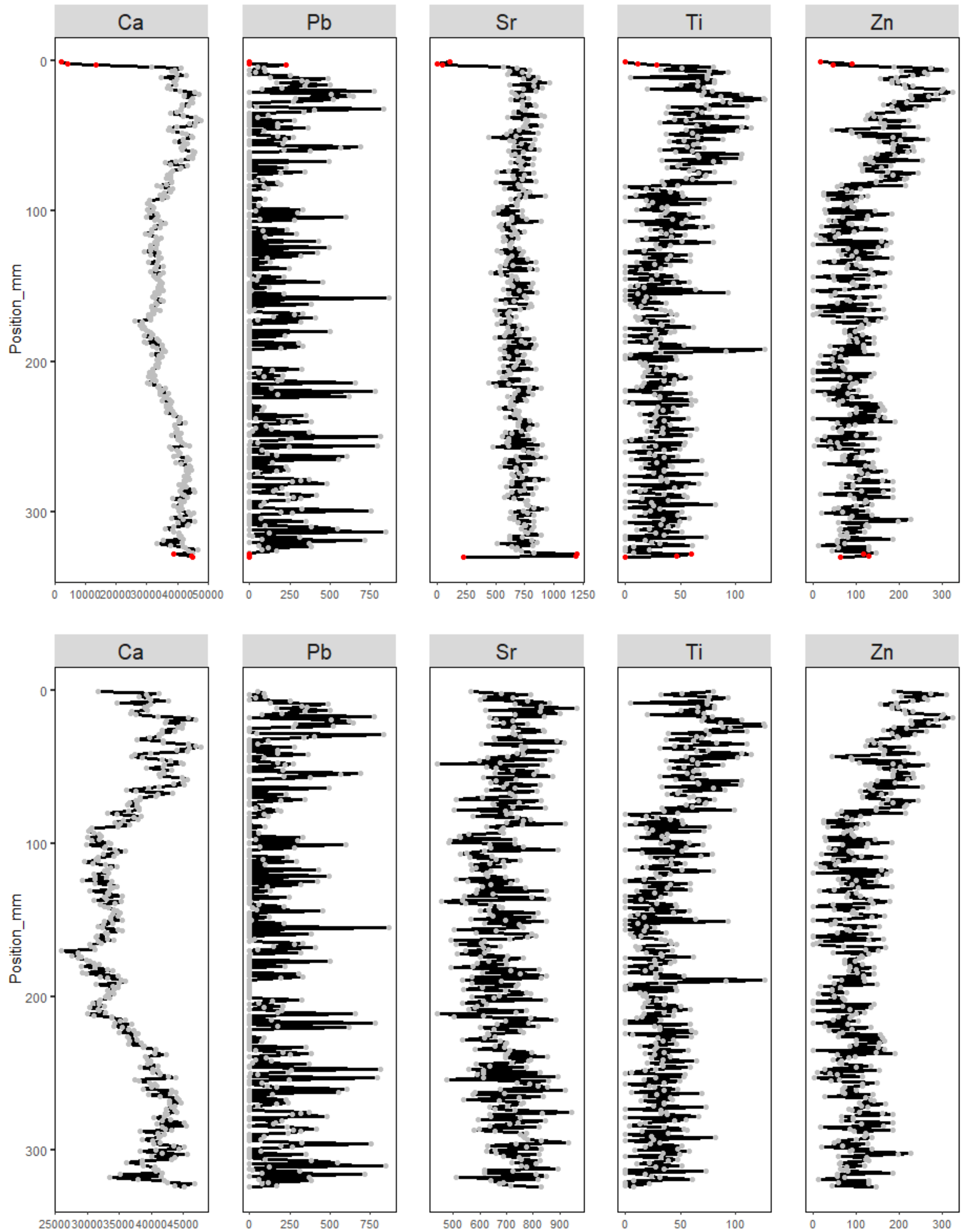

Figure CB.3. Comparative stratigraphies demonstrating the influence of outliers on the variation of elemental abundances. On the upper panel, the outliers are represented in the full

ITRAX scans as red points based on the Mahalanobis distance calculations. On the lower panel, the same elements for the same core are shown with the outliers removed.

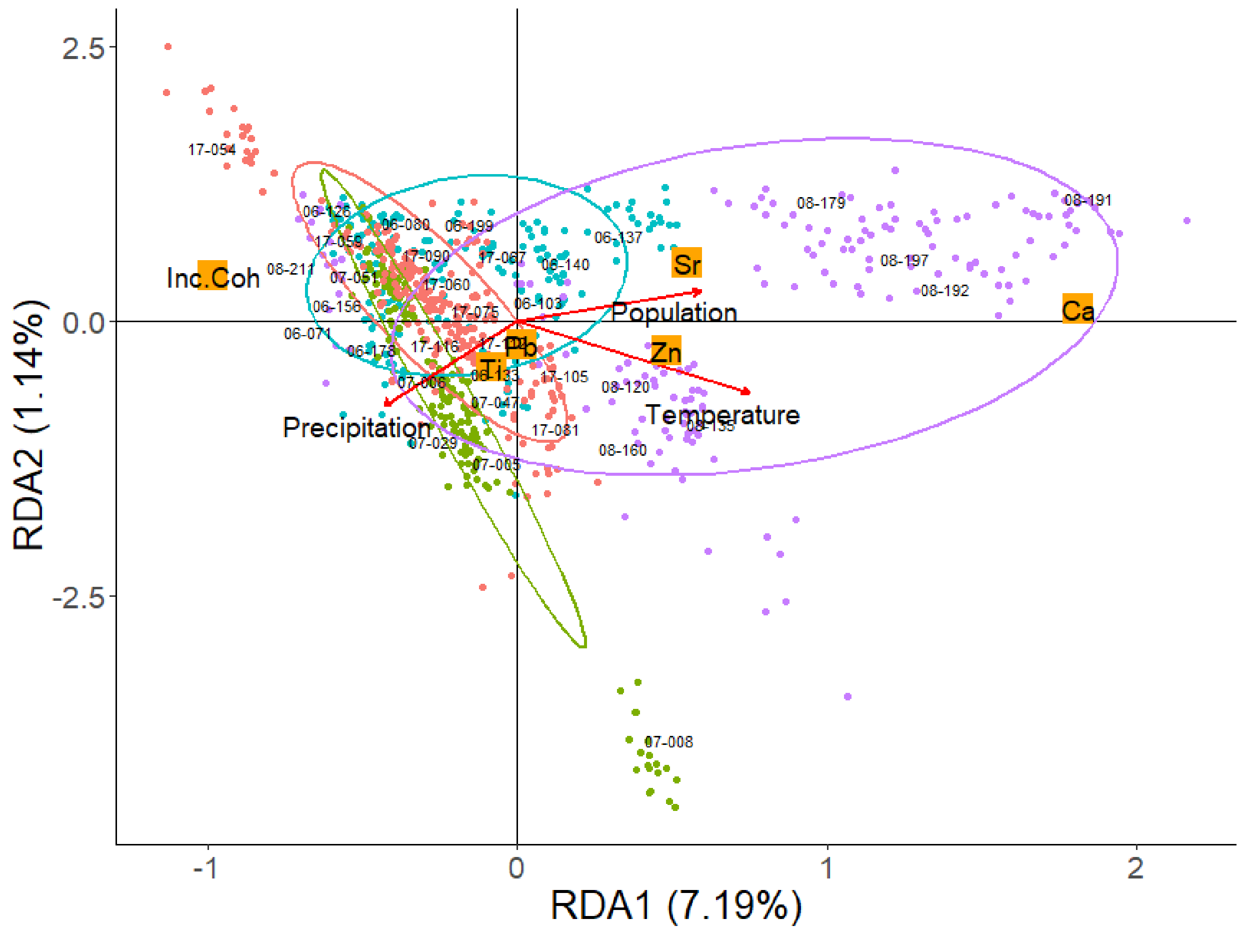

Figure CB.4. Redundancy analysis (RDA) investigating the relationship between the full temporal dataset of lake sediment geochemistry and temporal variation in climate (mean annual temperature and precipitation) and temporal population counts inferred from census.

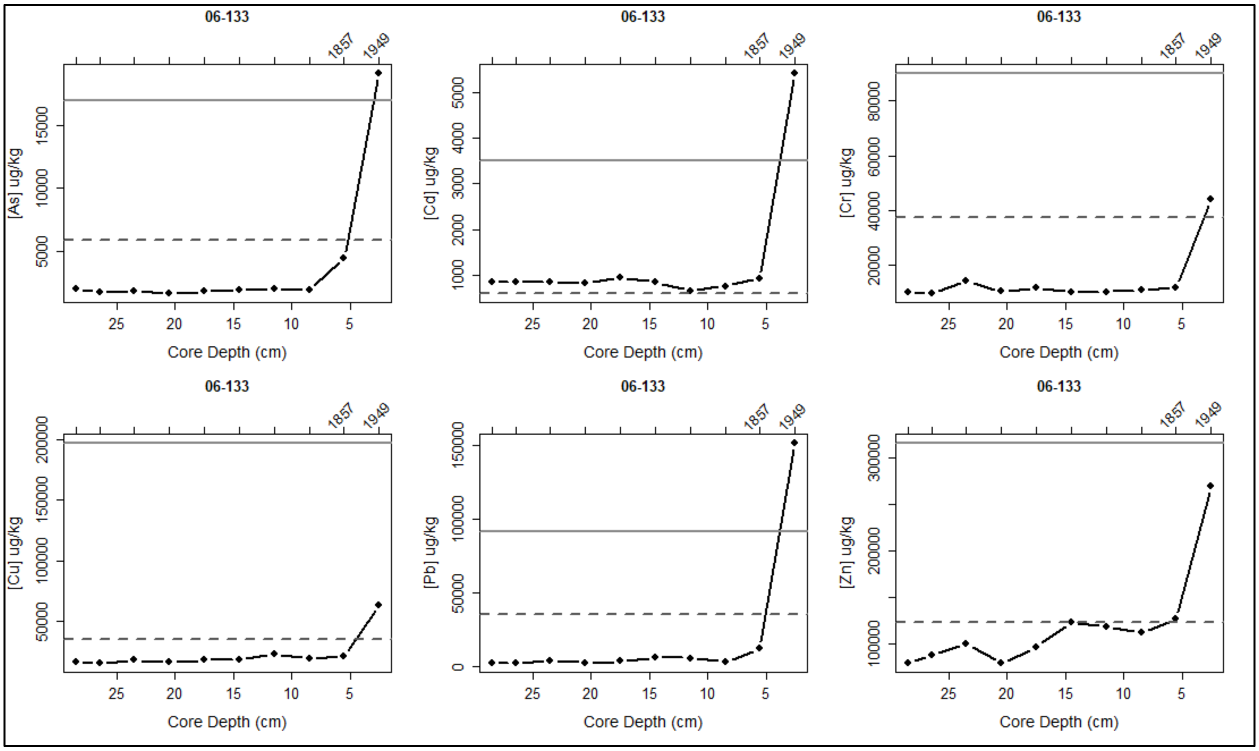
06-133
1857
1949
[As] ug/kg
[Cd] ug/kg
[Cr] ug/kg
[Cu] ug/kg
[Pb] ug/kg
[Zn] ug/kg
Core Depth (cm)

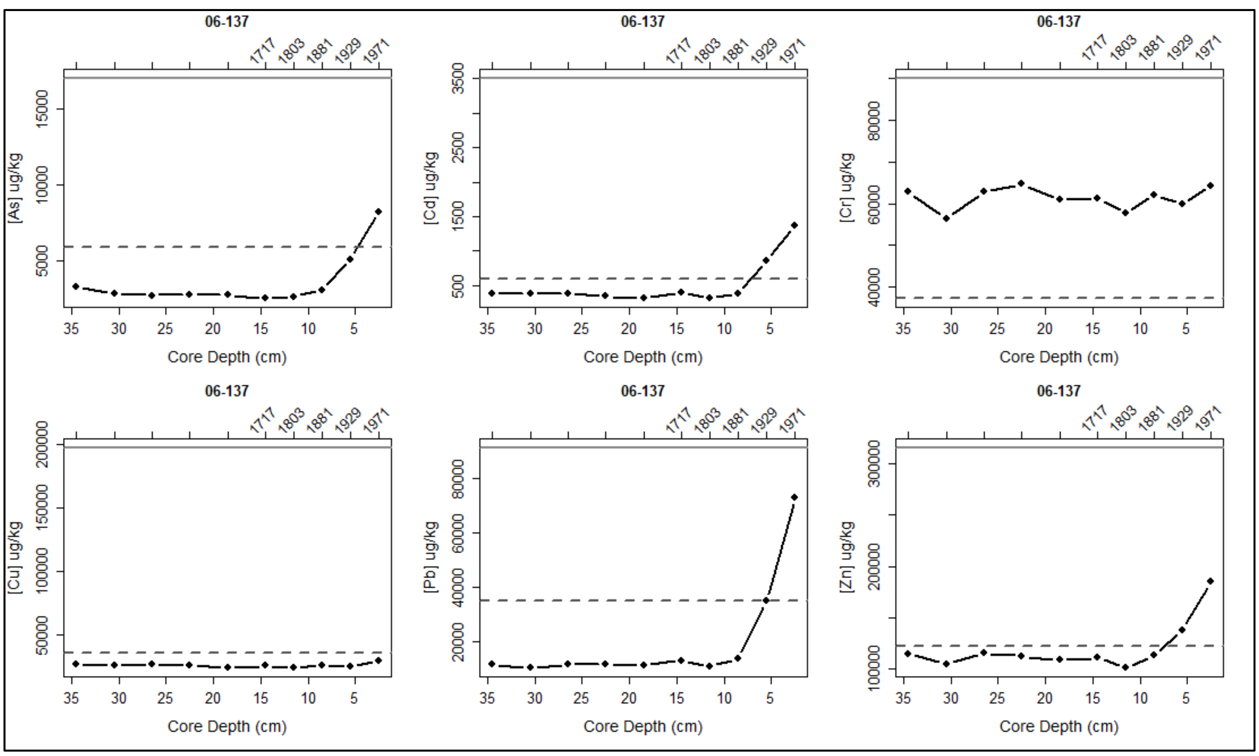
06-137
1717
1803
1881
1929
1971
[As] ug/kg
[Cd] ug/kg
[Cr] ug/kg
[Cu] ug/kg
[Pb] ug/kg
[Zn] ug/kg
Core Depth (cm)

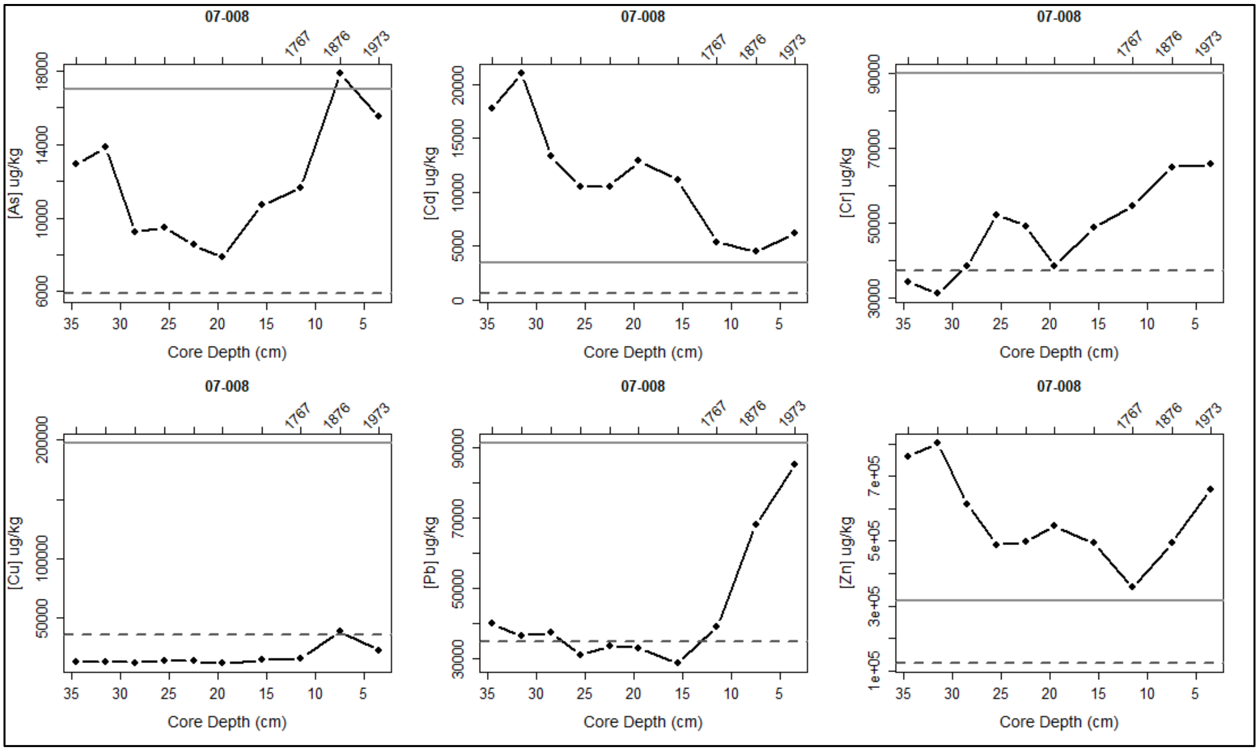
07-008
1767
1876
1973
[As] ug/kg
[Cd] ug/kg
[Cr] ug/kg
[Cu] ug/kg
[Pb] ug/kg
[Zn] ug/kg
Core Depth (cm)

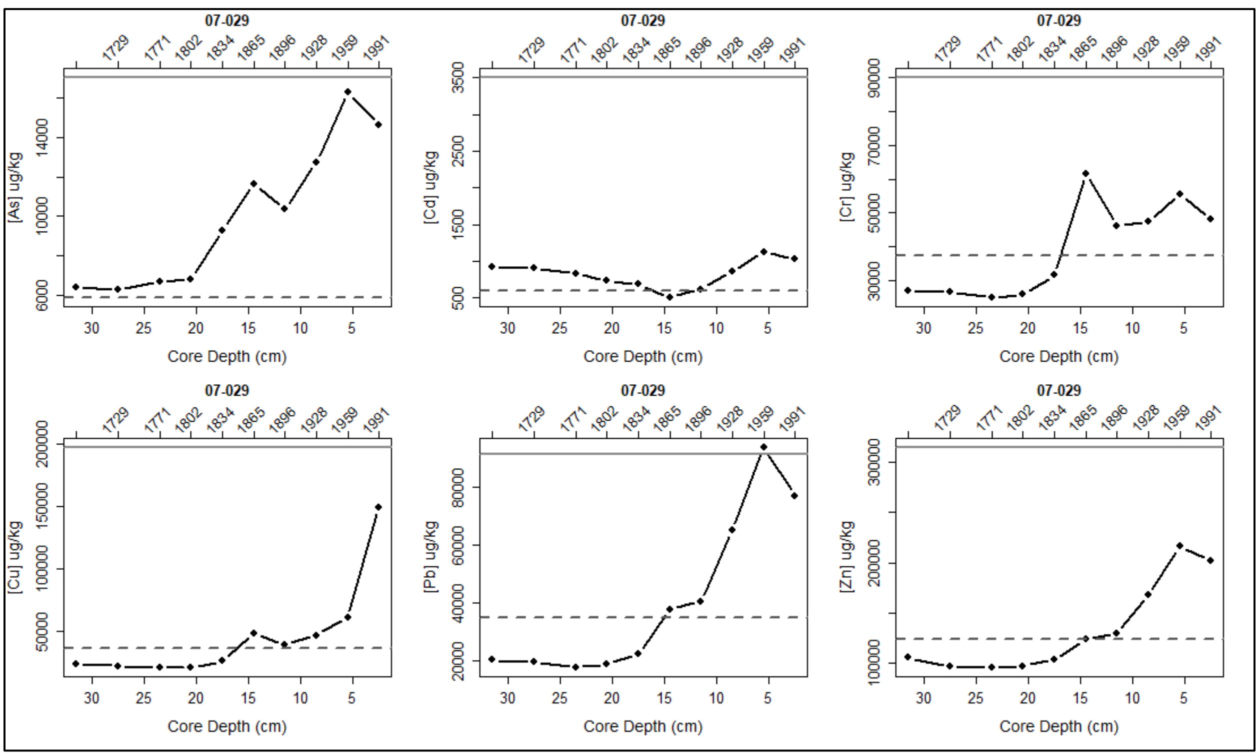
07-029
1729
1771
1802
1834
1865
1896
1928
1959
1991
[As] ug/kg
[Cd] ug/kg
[Cr] ug/kg
[Cu] ug/kg
[Pb] ug/kg
[Zn] ug/kg
Core Depth (cm)

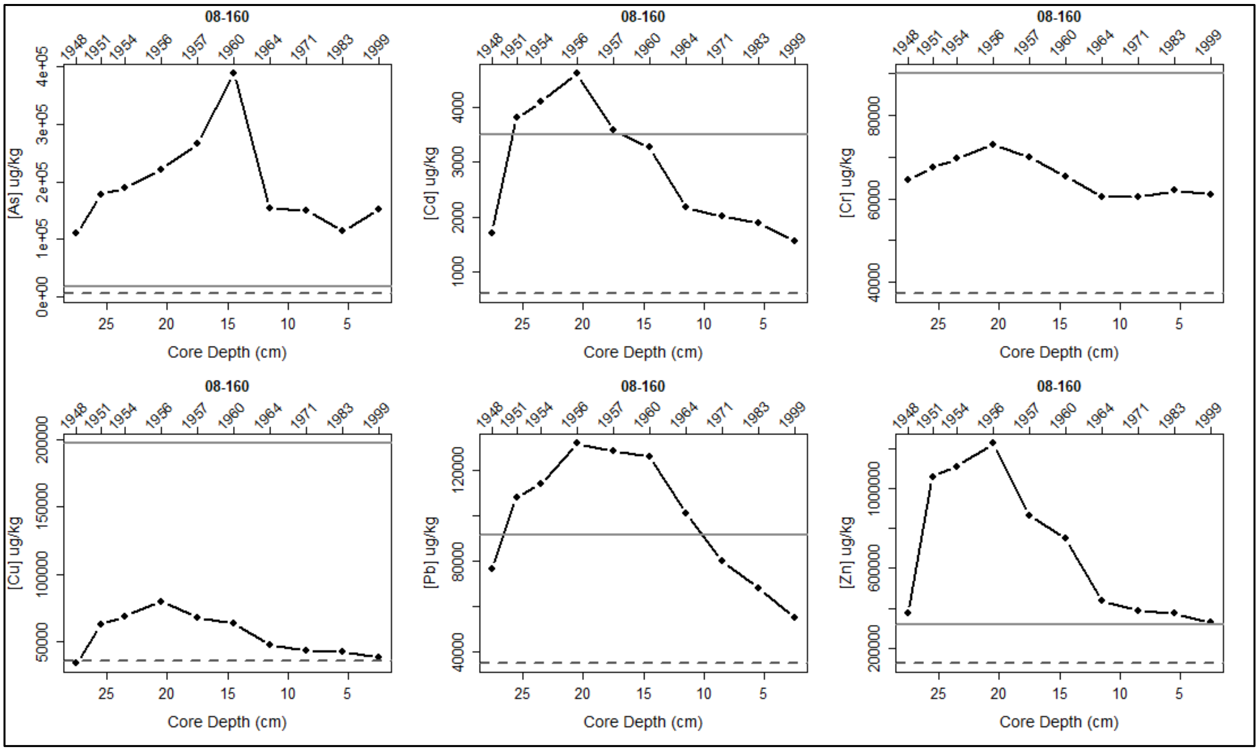
08-160
[As] ug/kg
[Cd] ug/kg
[Cr] ug/kg
[Cu] ug/kg
[Pb] ug/kg
[Zn] ug/kg
Core Depth (cm)
1948 1951 1954 1956 1957 1960 1964 1971 1983 1999

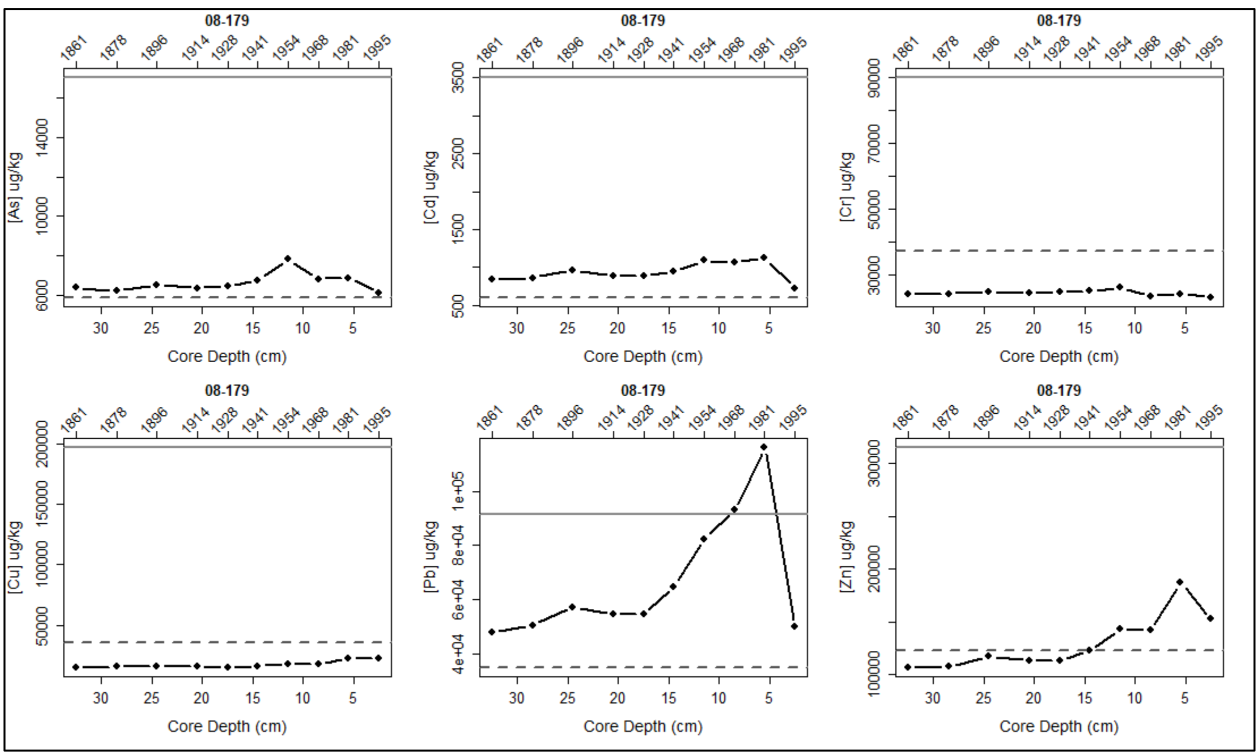
08-179
[As] ug/kg
[Cd] ug/kg
[Cr] ug/kg
[Cu] ug/kg
[Pb] ug/kg
[Zn] ug/kg
Core Depth (cm)
1861 1878 1896 1914 1928 1941 1954 1968 1981 1995

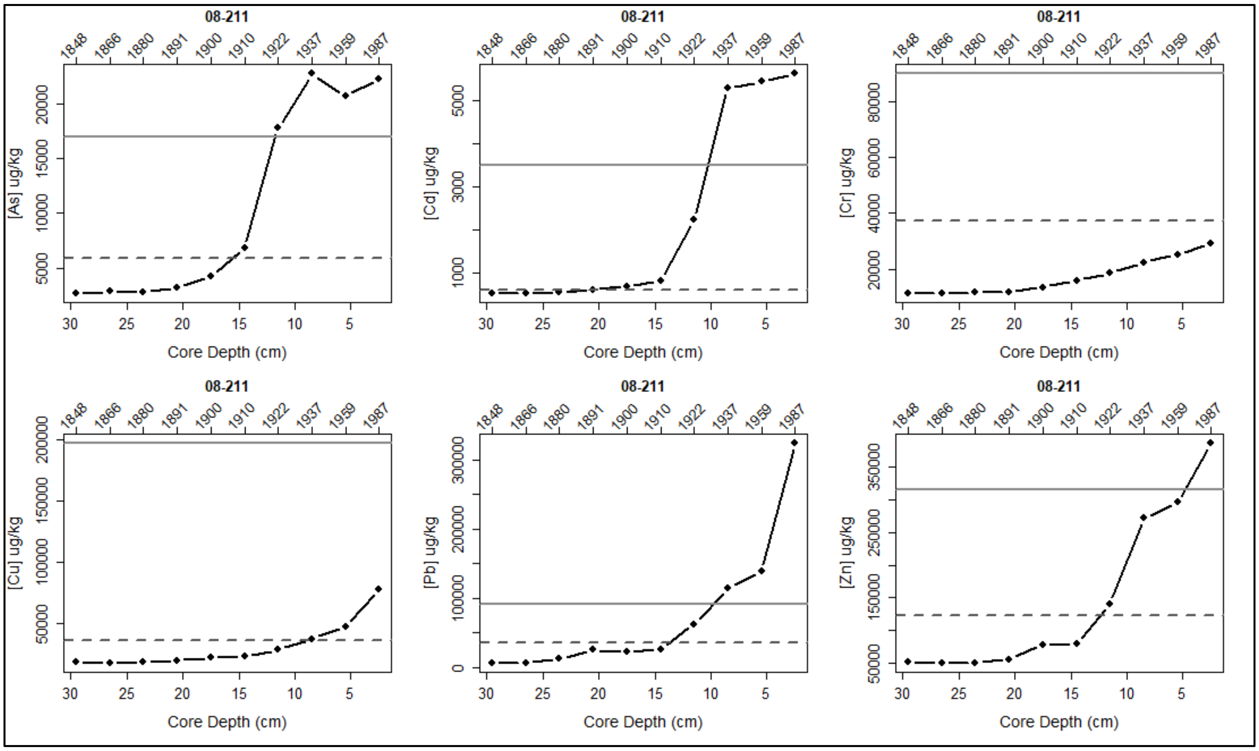

Figure CB.5. Temporal variation in the concentration (µg kg^{-1}) of elements with Sediment Quality Guidelines for the Protection of Aquatic Life available from the Canadian Council of Ministers of the Environment (CCME, 1999) (includes As, Cd, Cr, Cu, Pb and Zn) for the 7 lakes where ICP-MS concentrations were quantified. The dashed grey line represents the Interim Freshwater Sediment Quality Guidelines (ISQG, dry weight) and the solid grey line accounts for and Probable Effect Levels (PEL, dry weight). The secondary x-axis provides the estimated date based on ^{210}Pb analyses.

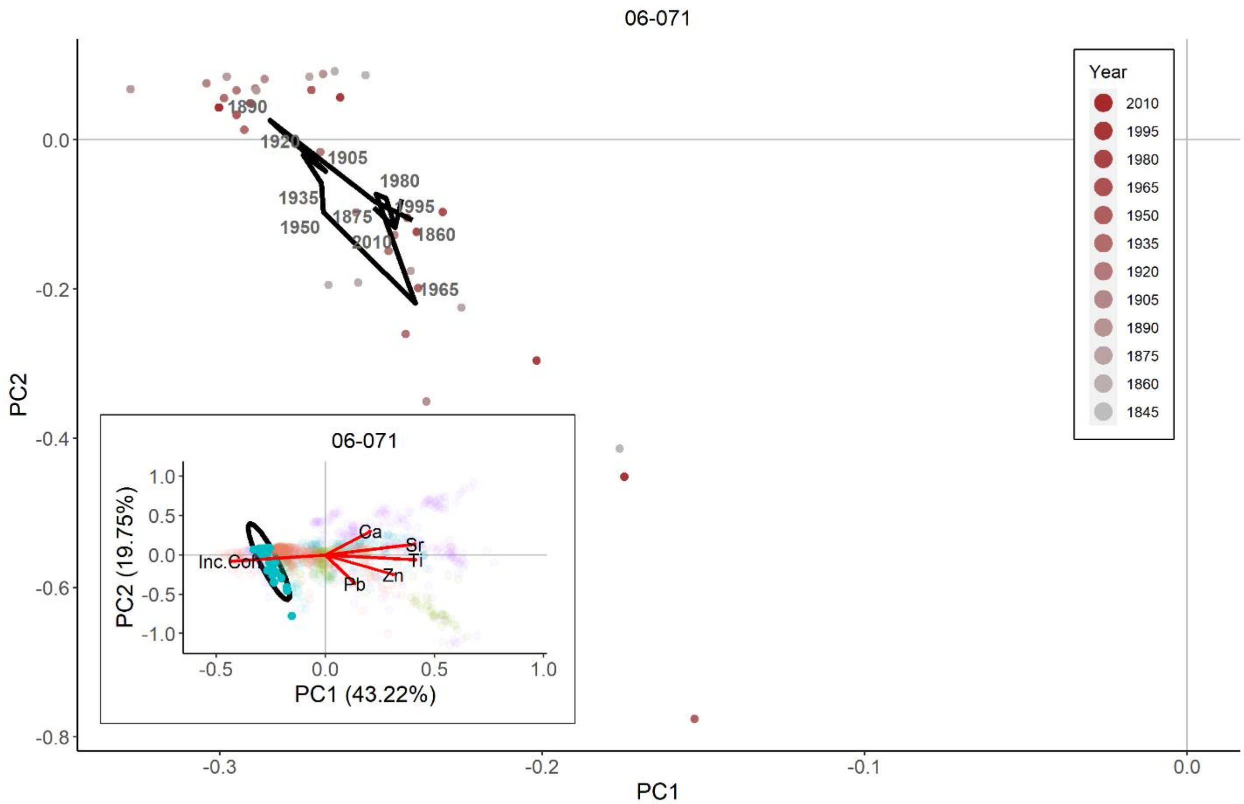
06-071
Year
2010
1995
1980
1965
1950
1935
1920
1905
1890
1875
1860
1845
PC2
PC1
PC2 (19.75%)
PC1 (43.22%)
Inc.Coh
Ca
Sr
Ti
Zn
Pb

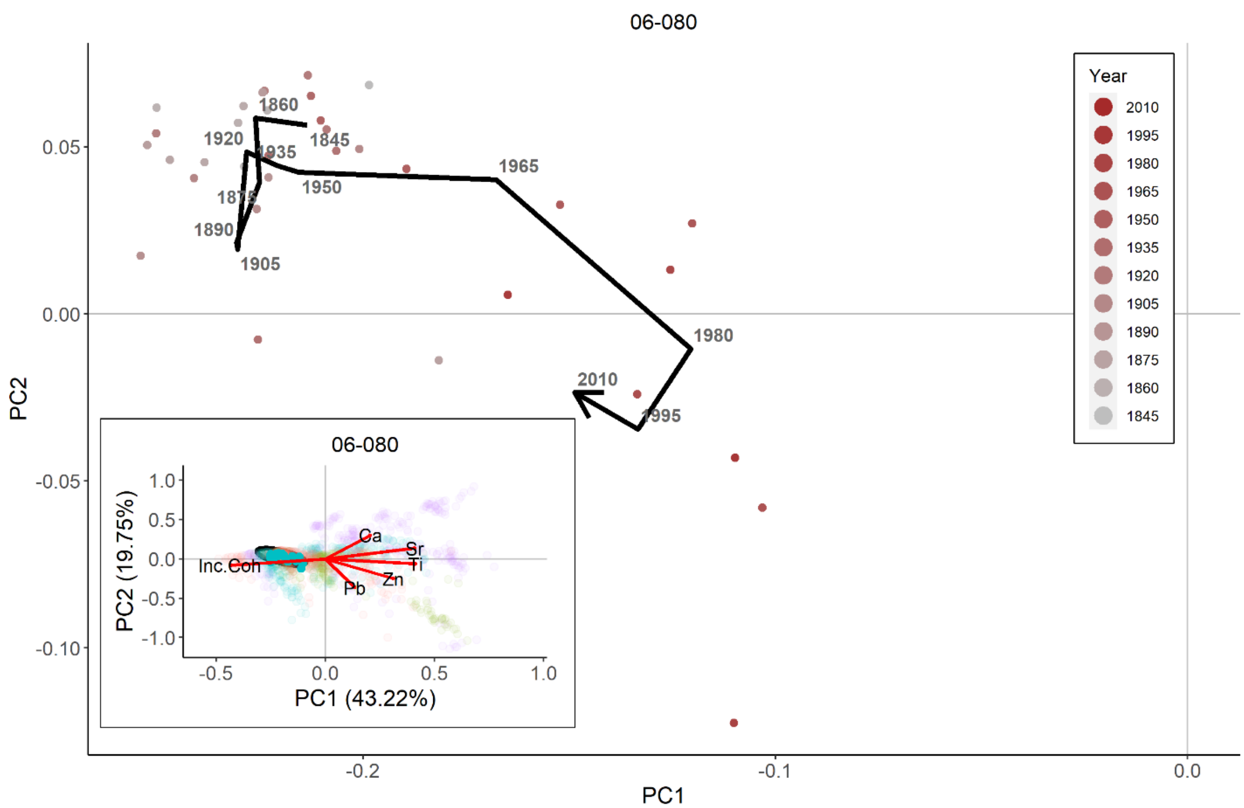
06-080
Year
2010
1995
1980
1965
1950
1935
1920
1905
1890
1875
1860
1845
PC2
PC1
PC2 (19.75%)
PC1 (43.22%)
Inc.Coh
Ca
Sr
Ti
Zn
Pb

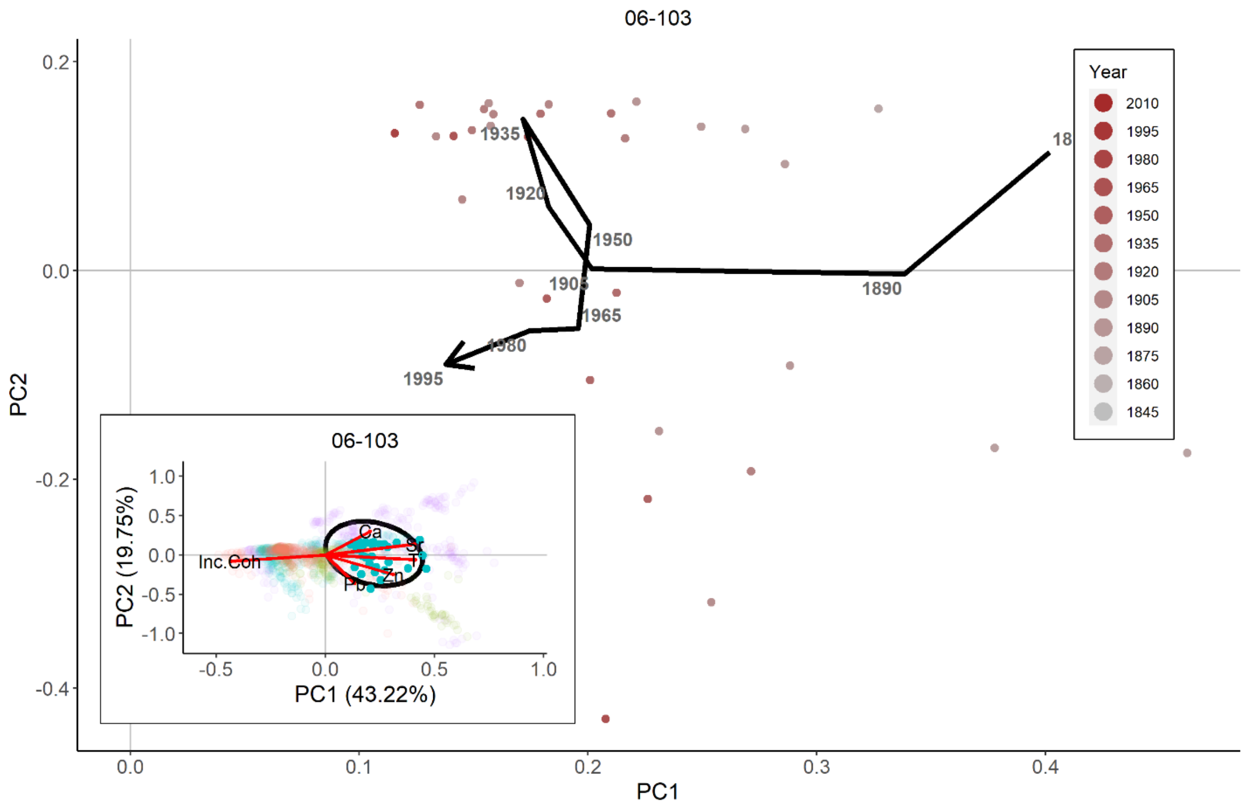
06-103
PC1
PC2
Year
2010
1995
1980
1965
1950
1935
1920
1905
1890
1875
1860
1845
06-103
PC1 (43.22%)
PC2 (19.75%)
Inc.Coh
Ca
Sr
Ti
Pb
Zn

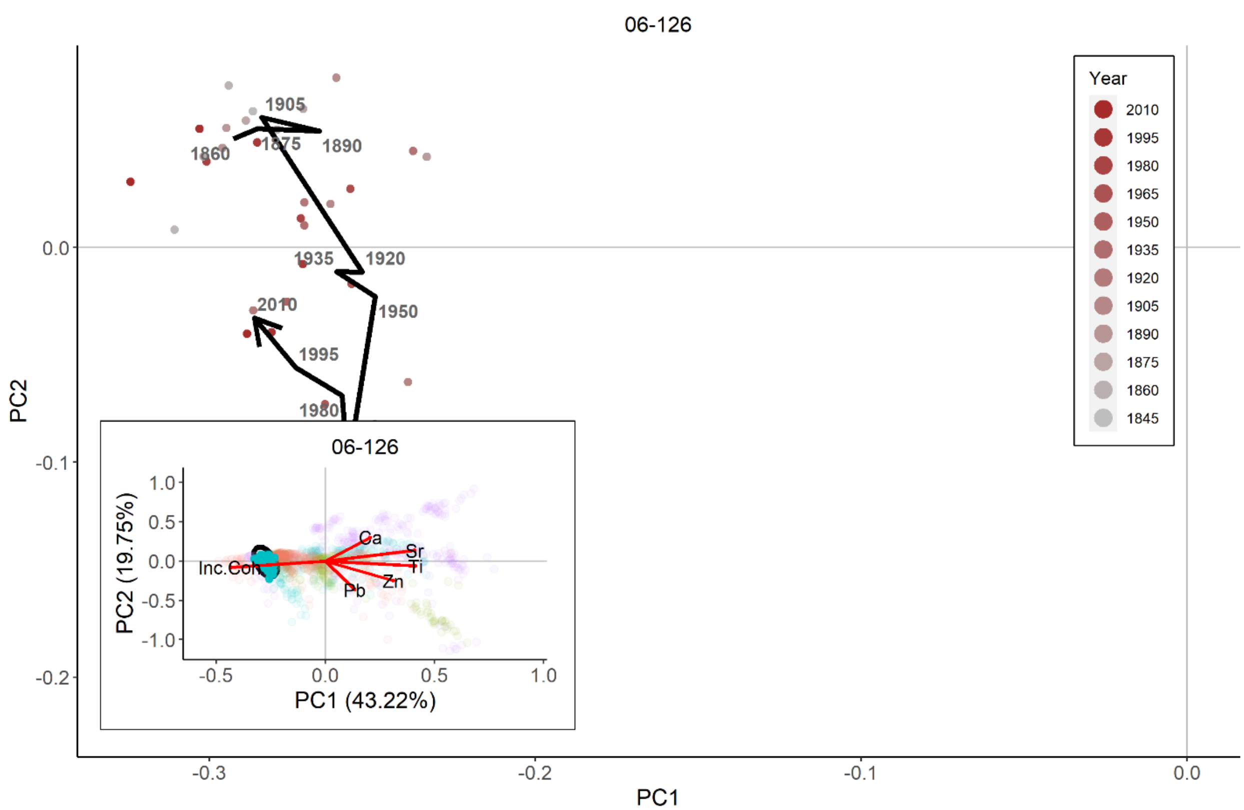
06-126
PC1
PC2
Year
2010
1995
1980
1965
1950
1935
1920
1905
1890
1875
1860
1845
06-126
PC1 (43.22%)
PC2 (19.75%)
Inc.Coh
Ca
Sr
Ti
Pb
Zn

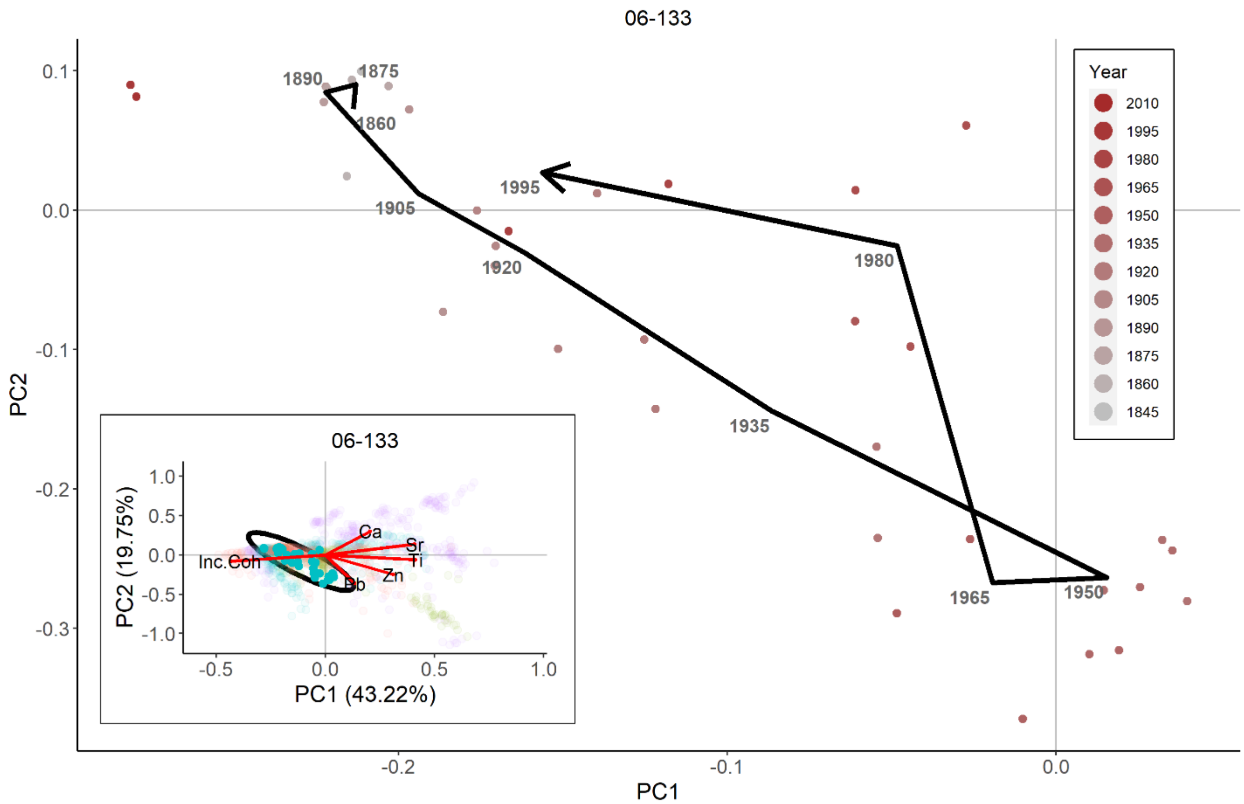
06-133
PC1
PC2
Year
2010
1995
1980
1965
1950
1935
1920
1905
1890
1875
1860
1845
PC1 (43.22%)
PC2 (19.75%)
Ca
Sr
Ti
Zn
Pb
Inc.Coh

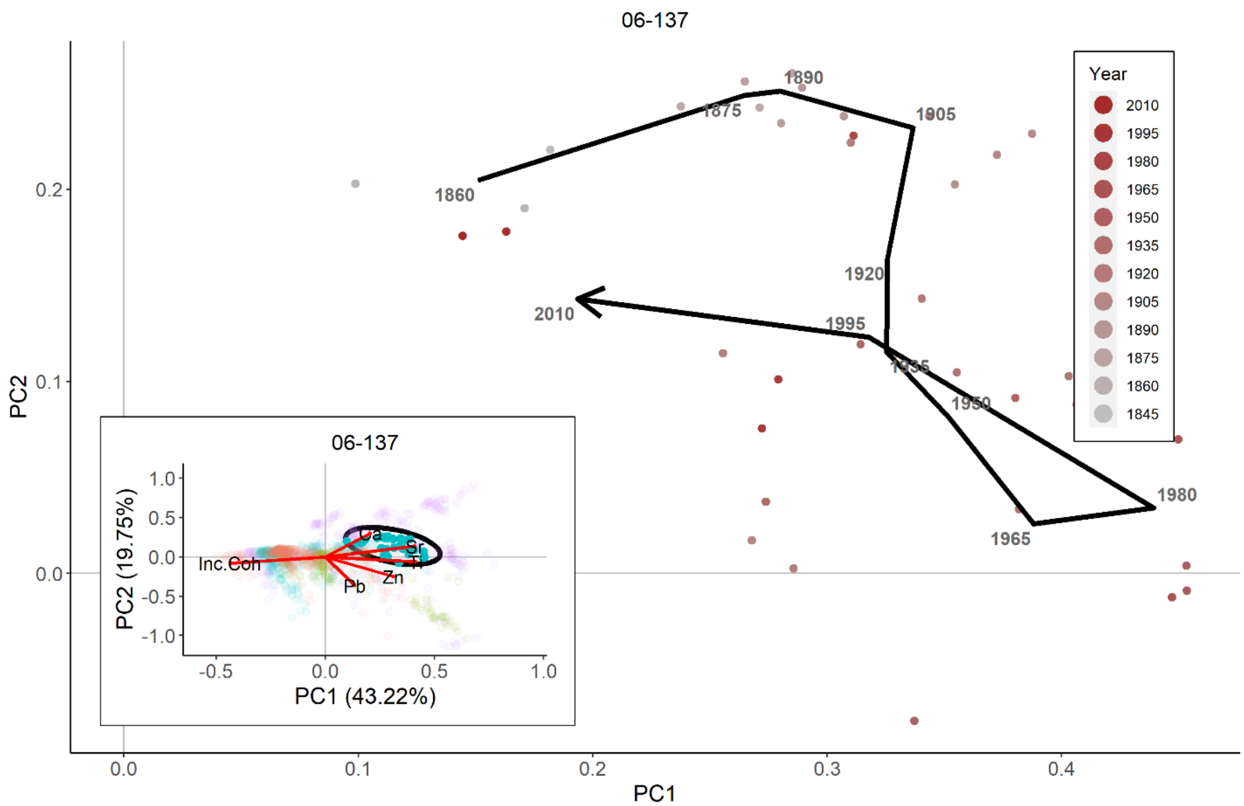
06-137
PC1
PC2
Year
2010
1995
1980
1965
1950
1935
1920
1905
1890
1875
1860
1845
PC1 (43.22%)
PC2 (19.75%)
Ca
Sr
Ti
Zn
Pb
Inc.Coh

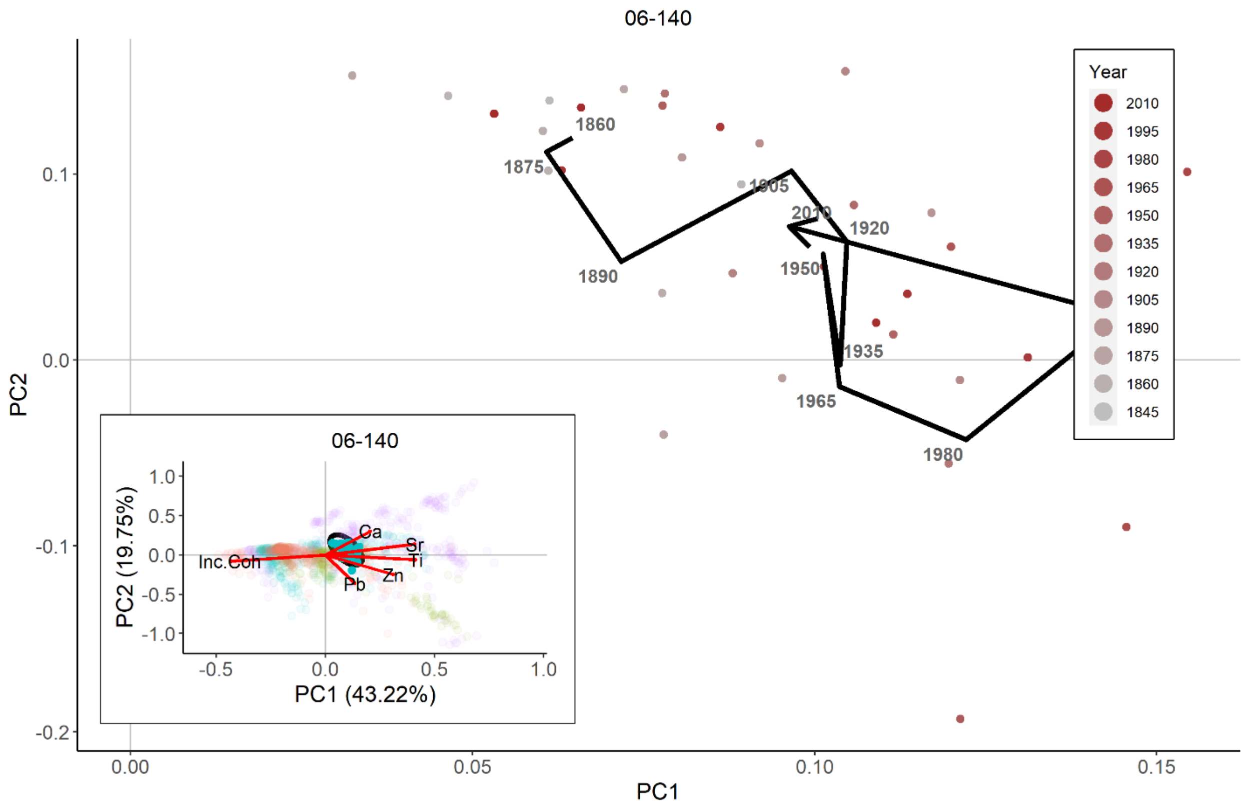

06-140
Year
2010
1995
1980
1965
1950
1935
1920
1905
1890
1875
1860
1845
1860
1875
1890
1905
2010
1920
1950
1935
1965
1980
PC2
PC1
0.1
0.0
-0.1
-0.2
0.00
0.05
0.10
0.15
06-140
Ca
Sr
Ti
Zn
Pb
Inc.Coh
PC2 (19.75%)
PC1 (43.22%)

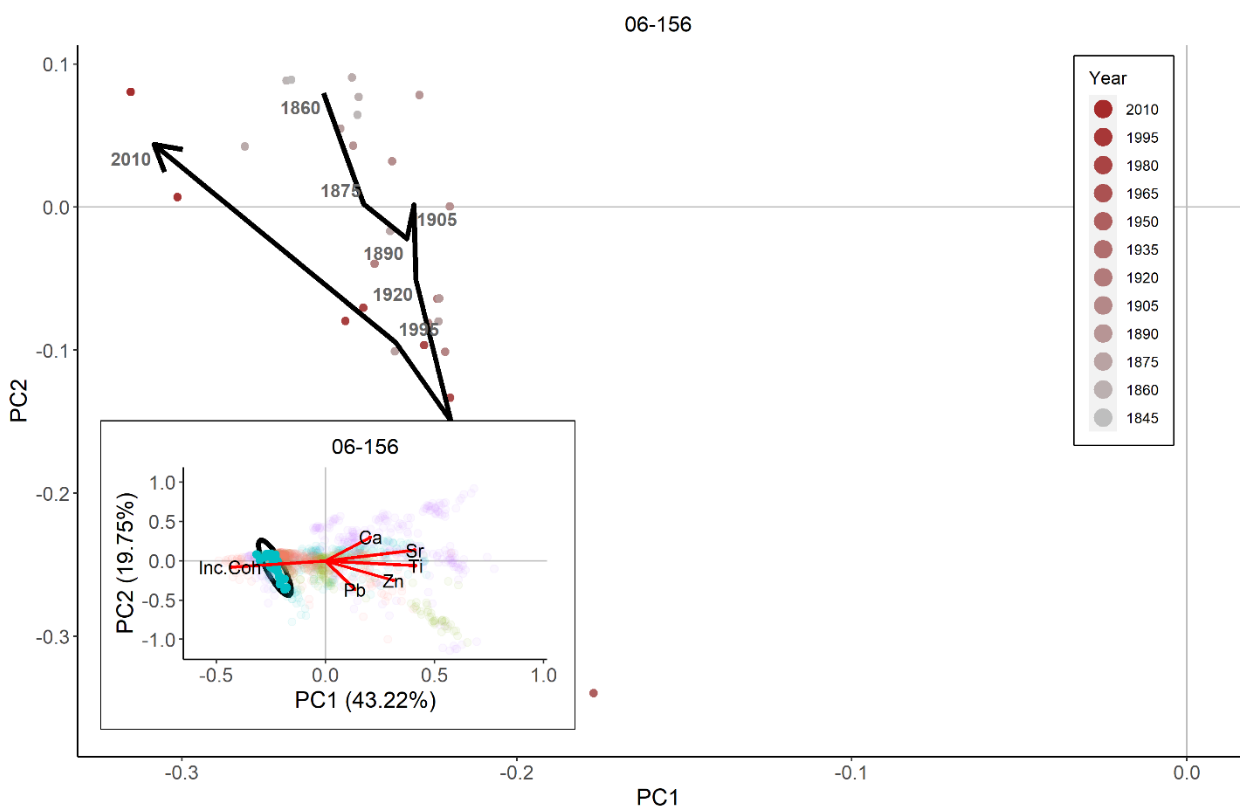

06-156
Year
2010
1995
1980
1965
1950
1935
1920
1905
1890
1875
1860
1845
1860
2010
1875
1905
1890
1920
1995
PC2
PC1
0.1
0.0
-0.1
-0.2
-0.3
-0.3
-0.2
-0.1
0.0
06-156
Ca
Sr
Ti
Zn
Pb
Inc.Coh
PC2 (19.75%)
PC1 (43.22%)

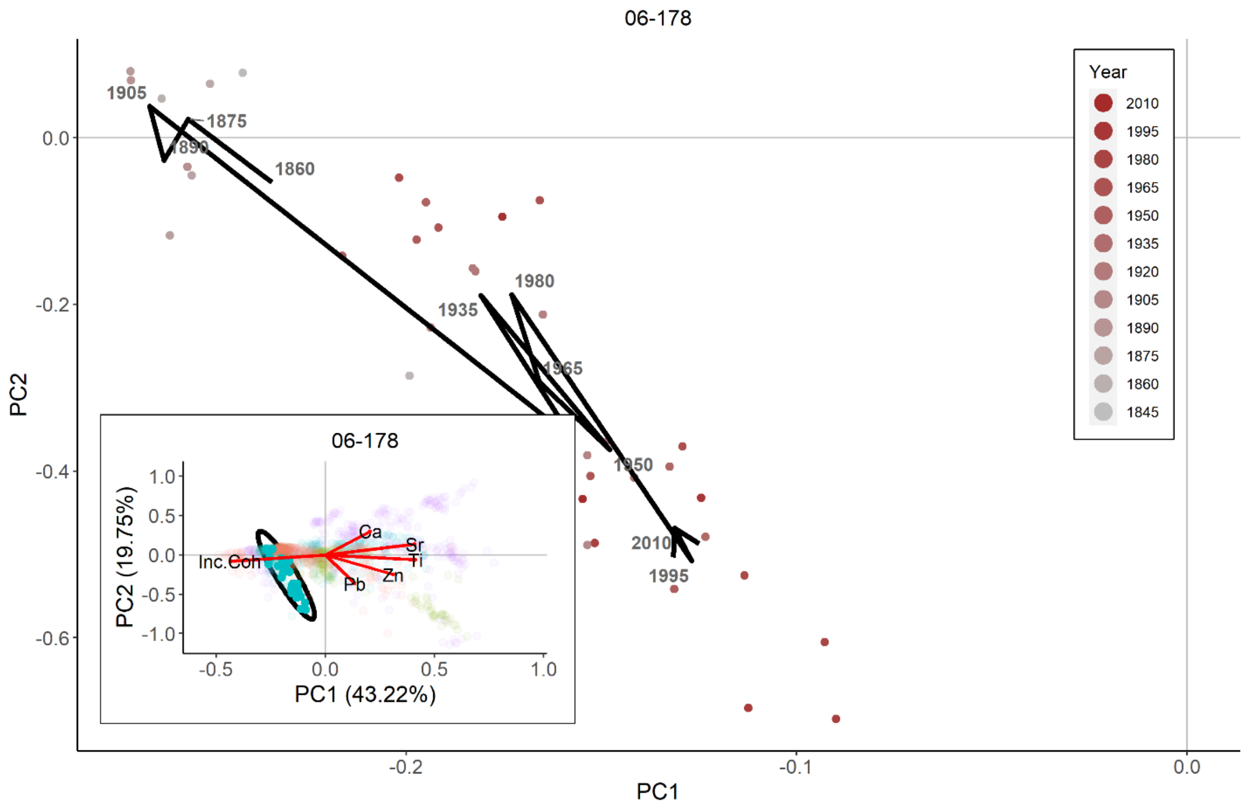

06-178
Year
2010
1995
1980
1965
1950
1935
1920
1905
1890
1875
1860
1845
PC2
PC1
1905
1875
1890
1860
1980
1935
1965
1950
2010
1995
PC2 (19.75%)
PC1 (43.22%)
Inc.Coh
Ca
Sr
Ti
Zn
Pb

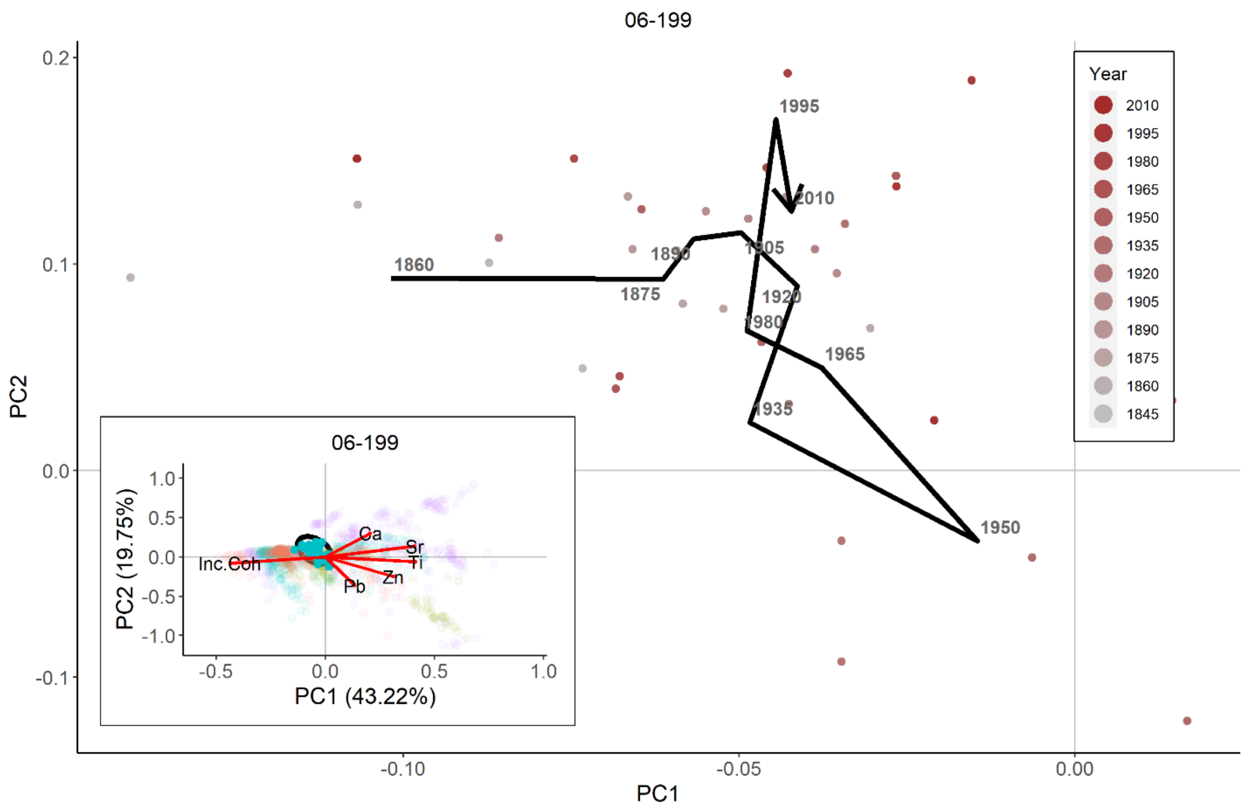

06-199
Year
2010
1995
1980
1965
1950
1935
1920
1905
1890
1875
1860
1845
PC2
PC1
1995
2010
1860
1890
1905
1875
1920
1980
1965
1935
1950
PC2 (19.75%)
PC1 (43.22%)
Inc.Coh
Ca
Sr
Ti
Zn
Pb

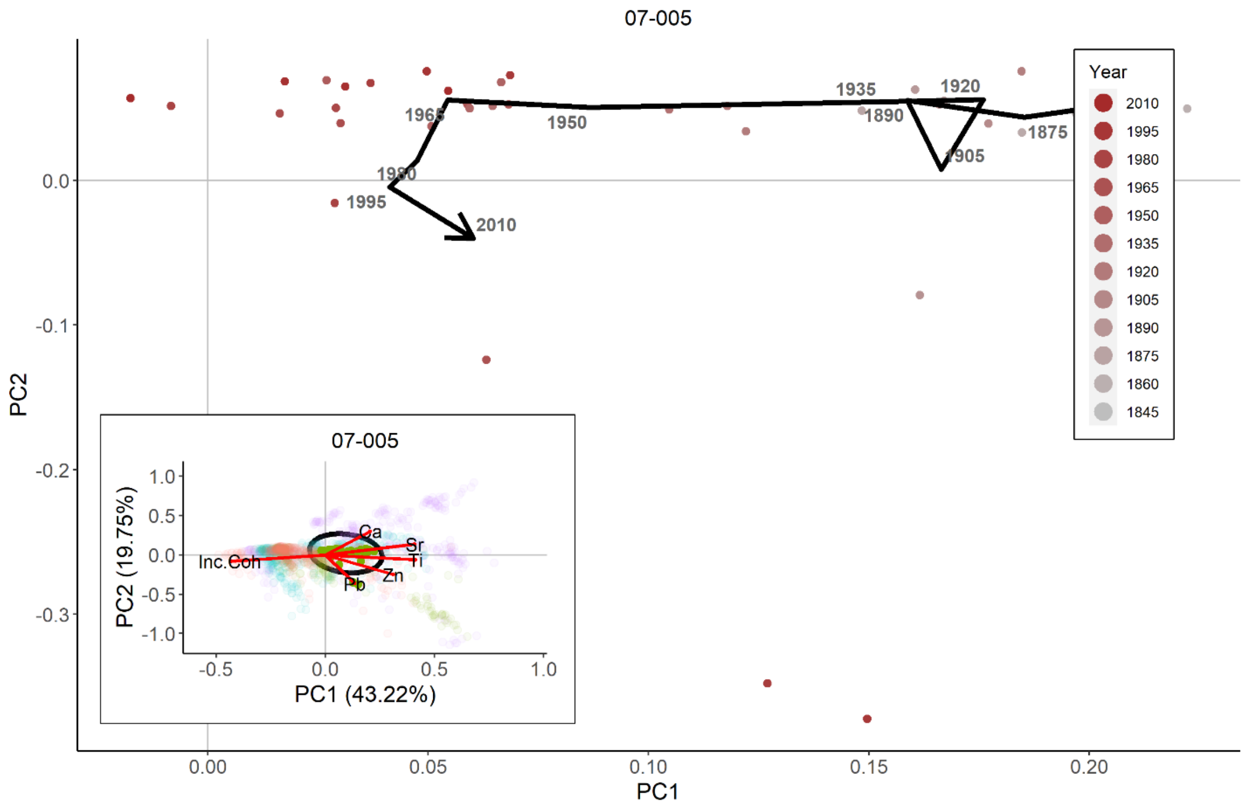
07-005
PC2
PC1
1965
1950
1935
1920
1890
1875
1905
1980
1995
2010
0.0
-0.1
-0.2
-0.3
0.00
0.05
0.10
0.15
0.20
Year
2010
1995
1980
1965
1950
1935
1920
1905
1890
1875
1860
1845
07-005
PC2 (19.75%)
PC1 (43.22%)
Inc.Coh
Ca
Sr
Ti
Zn
Pb

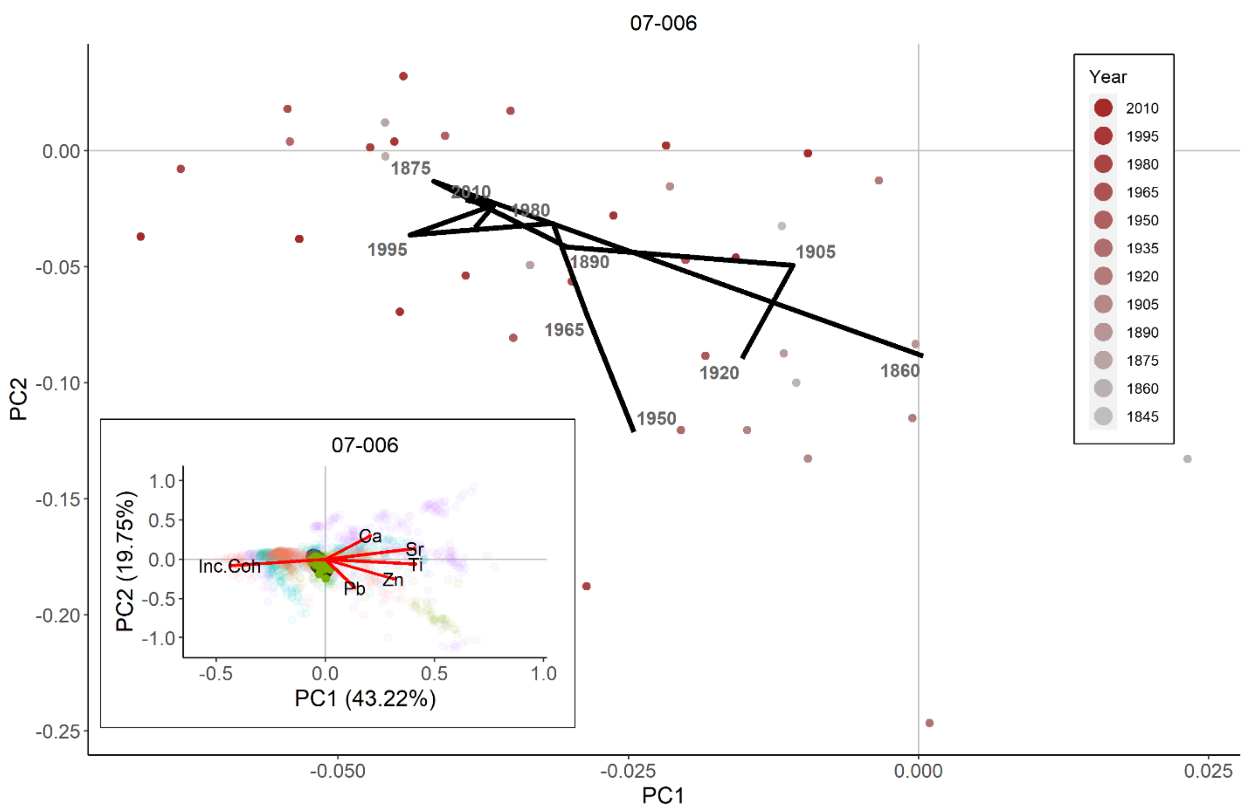
07-006
PC2
PC1
1875
2010
1980
1995
1890
1905
1965
1920
1860
1950
0.00
-0.05
-0.10
-0.15
-0.20
-0.25
-0.050
-0.025
0.000
0.025
Year
2010
1995
1980
1965
1950
1935
1920
1905
1890
1875
1860
1845
07-006
PC2 (19.75%)
PC1 (43.22%)
Inc.Coh
Ca
Sr
Ti
Zn
Pb

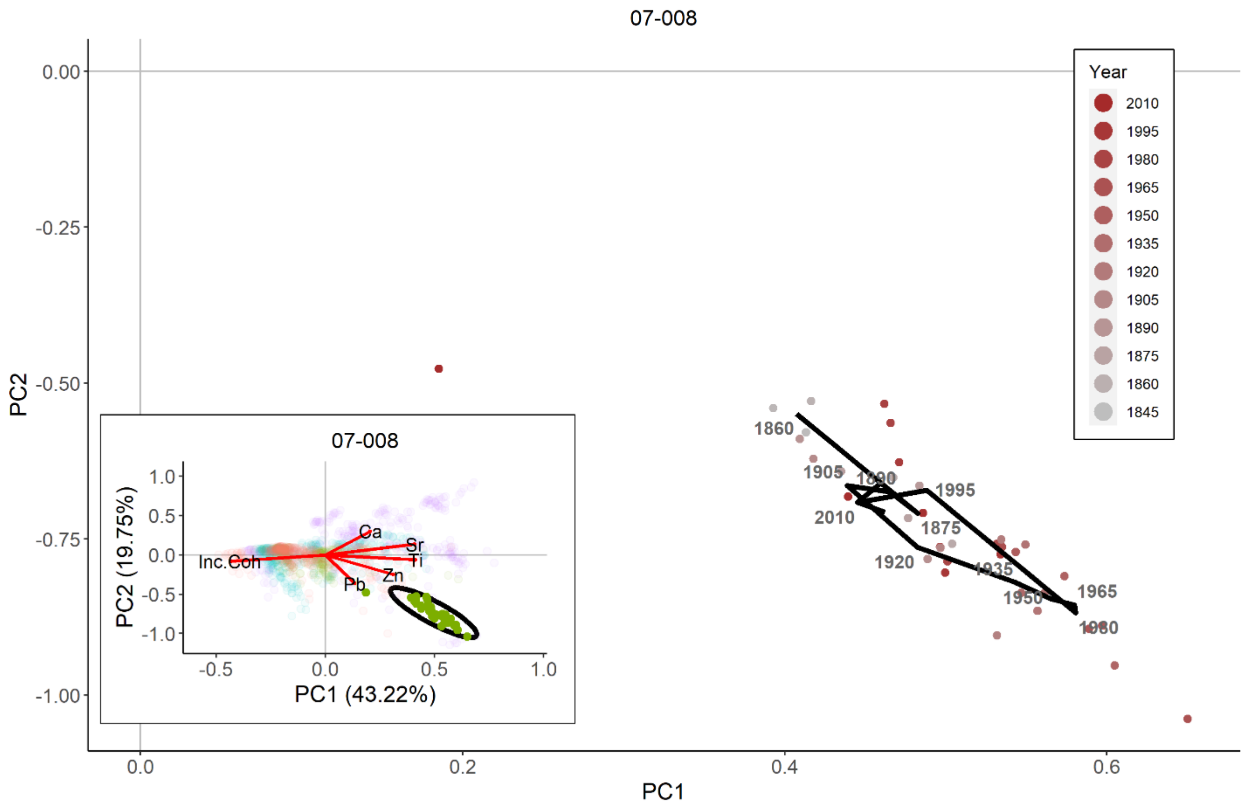
07-008
Year
2010
1995
1980
1965
1950
1935
1920
1905
1890
1875
1860
1845
PC2
PC1
07-008
PC2 (19.75%)
PC1 (43.22%)
Inc.Coh
Ca
Sr
Ti
Zn
Pb

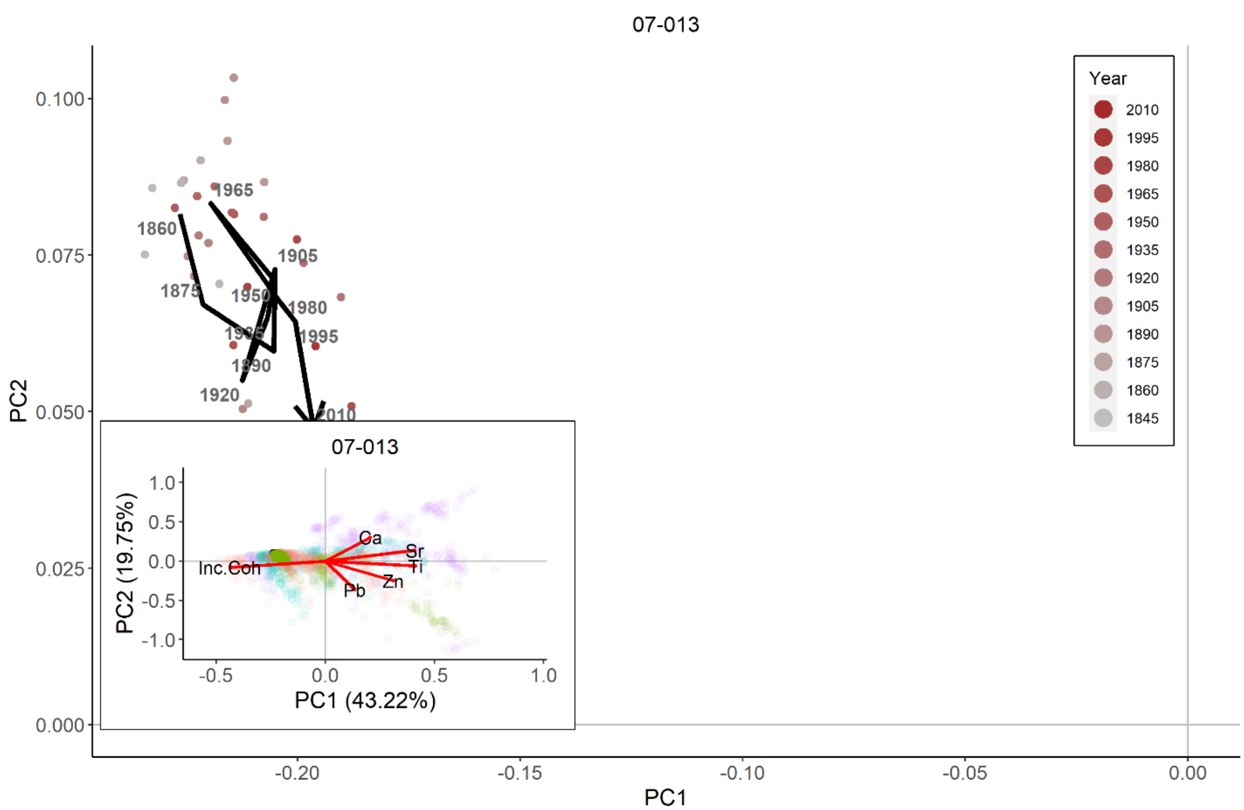
07-013
Year
2010
1995
1980
1965
1950
1935
1920
1905
1890
1875
1860
1845
PC2
PC1
07-013
PC2 (19.75%)
PC1 (43.22%)
Inc.Coh
Ca
Sr
Ti
Zn
Pb

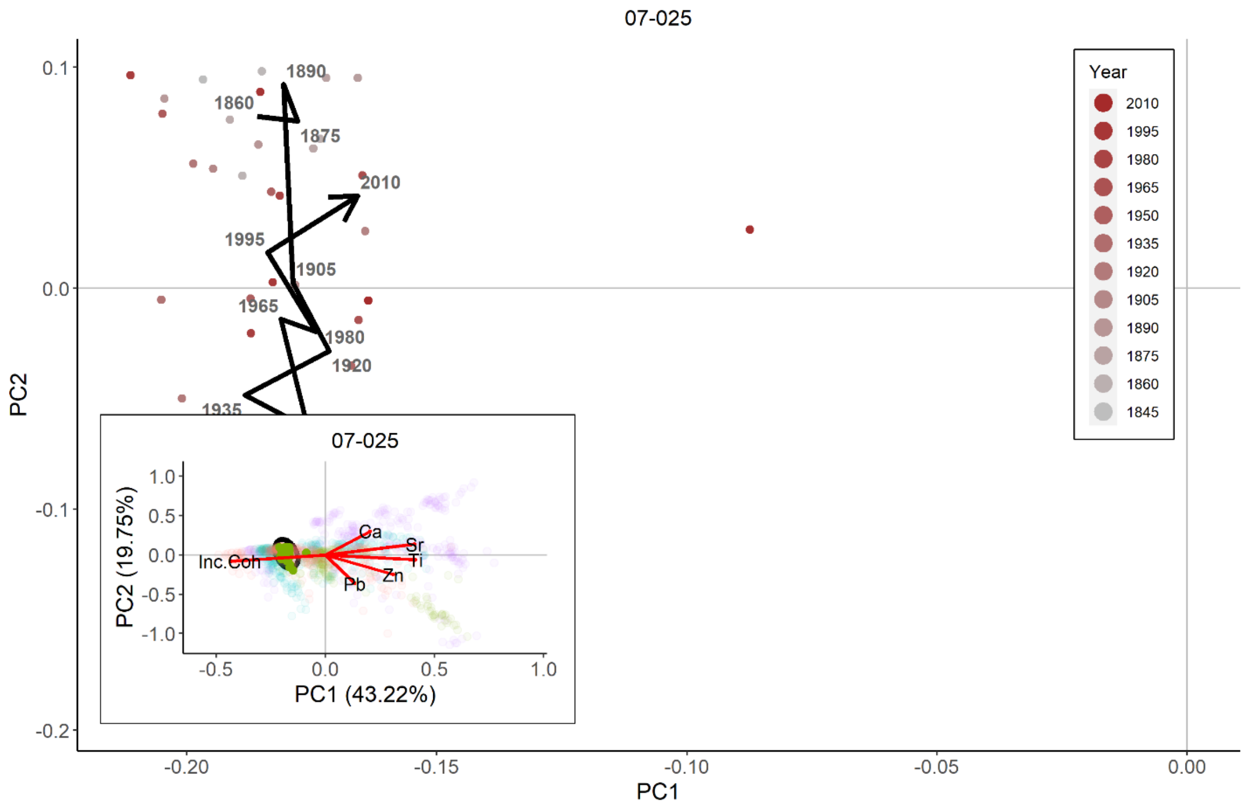
07-025
Year
2010
1995
1980
1965
1950
1935
1920
1905
1890
1875
1860
1845
PC1
PC2
PC1 (43.22%)
PC2 (19.75%)
Inc.Coh
Ca
Sr
Ti
Zn
Pb

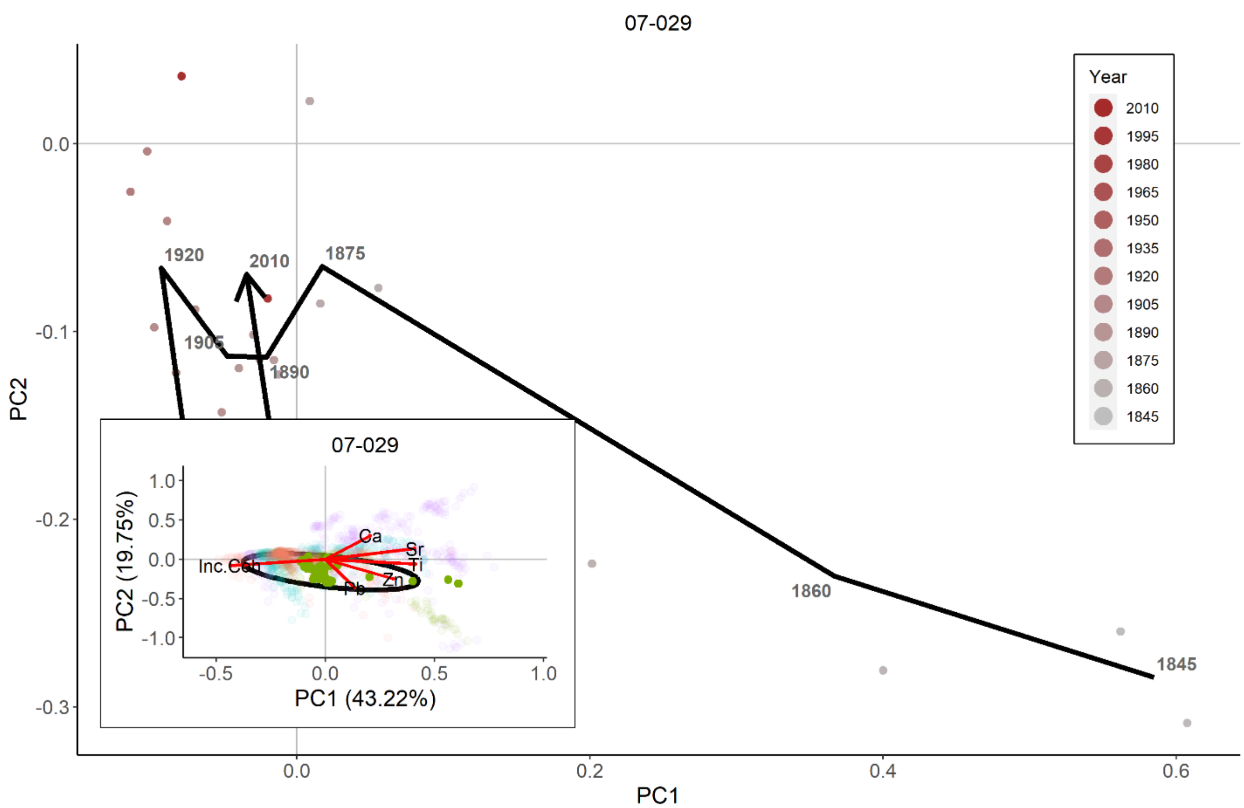
07-029
Year
2010
1995
1980
1965
1950
1935
1920
1905
1890
1875
1860
1845
PC1
PC2
PC1 (43.22%)
PC2 (19.75%)
Inc.Coh
Ca
Sr
Ti
Zn
Pb

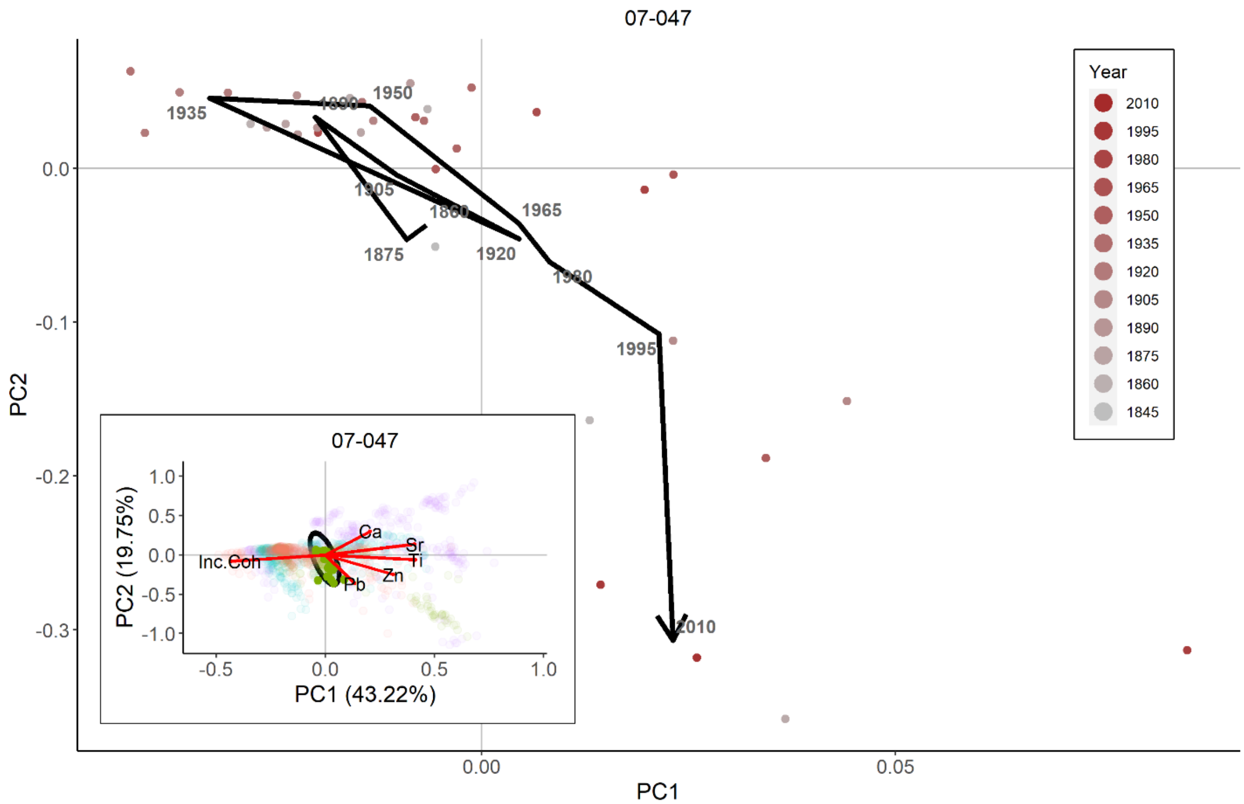
07-047
PC2
PC1
Year
2010
1995
1980
1965
1950
1935
1920
1905
1890
1875
1860
1845
1935
1950
1965
1980
1995
2010
1875
1920
Inc.Coh
Ca
Sr
Ti
Zn
Pb
PC2 (19.75%)
PC1 (43.22%)

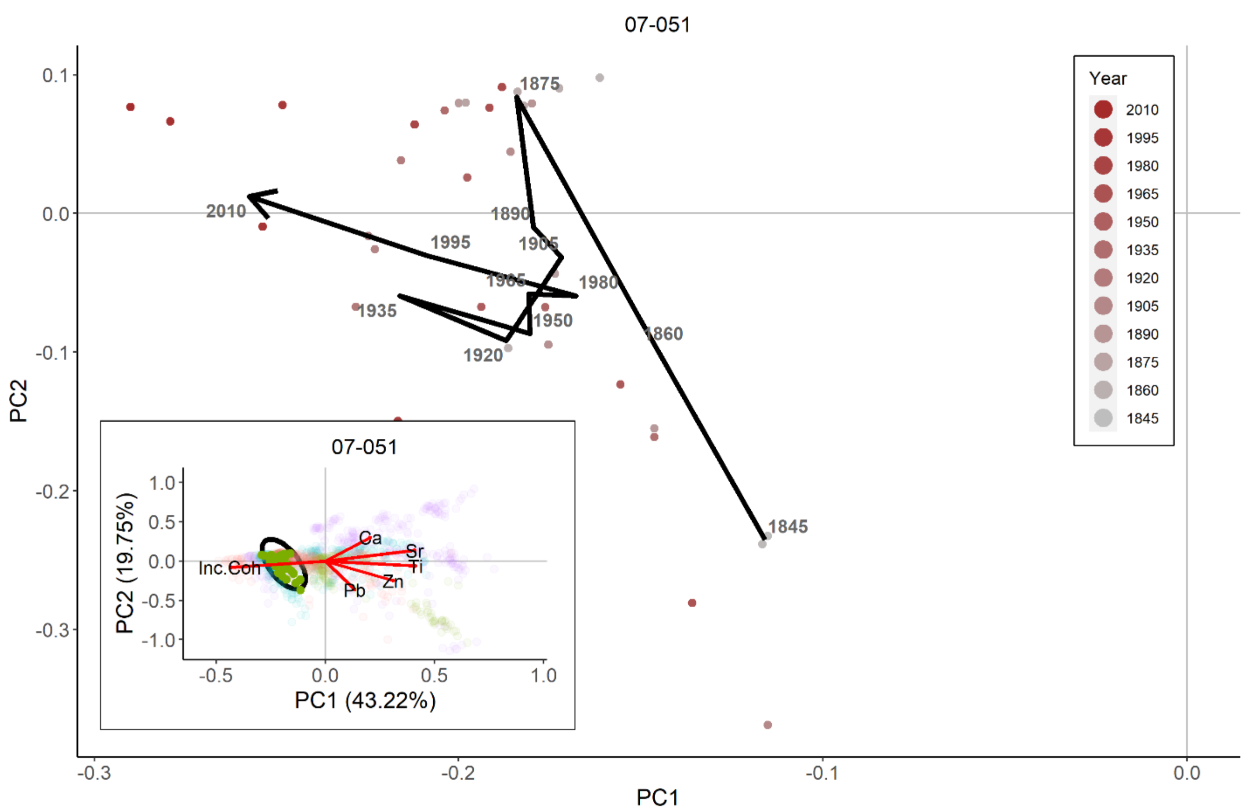
07-051
PC2
PC1
Year
2010
1995
1980
1965
1950
1935
1920
1905
1890
1875
1860
1845
1875
1890
2010
1995
1905
1965
1980
1935
1950
1920
1860
1845
Inc.Coh
Ca
Sr
Ti
Zn
Pb
PC2 (19.75%)
PC1 (43.22%)

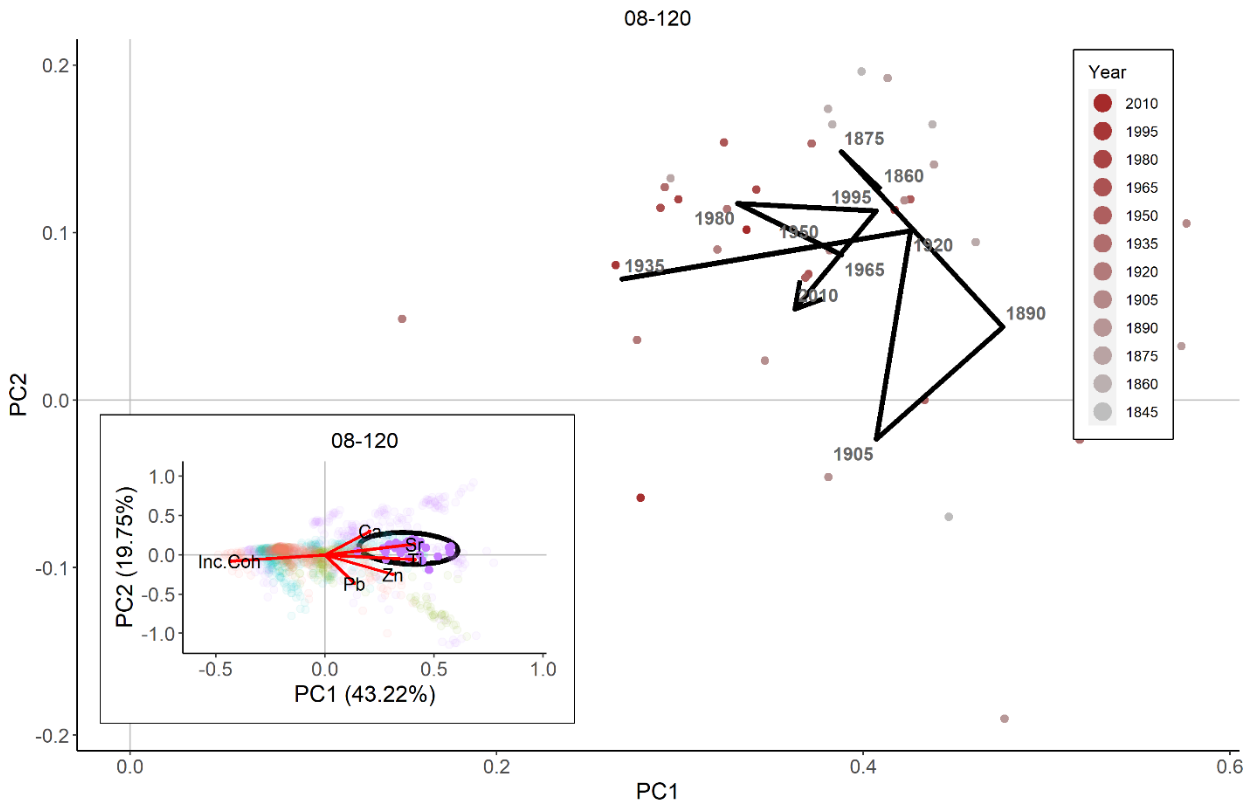
08-120
PC2
PC1
Year
2010
1995
1980
1965
1950
1935
1920
1905
1890
1875
1860
1845
1875
1860
1995
1980
1950
1935
1920
1965
2010
1890
1905
08-120
PC2 (19.75%)
PC1 (43.22%)
Inc.Coh
Ca
Sr
Ti
Zn
Pb

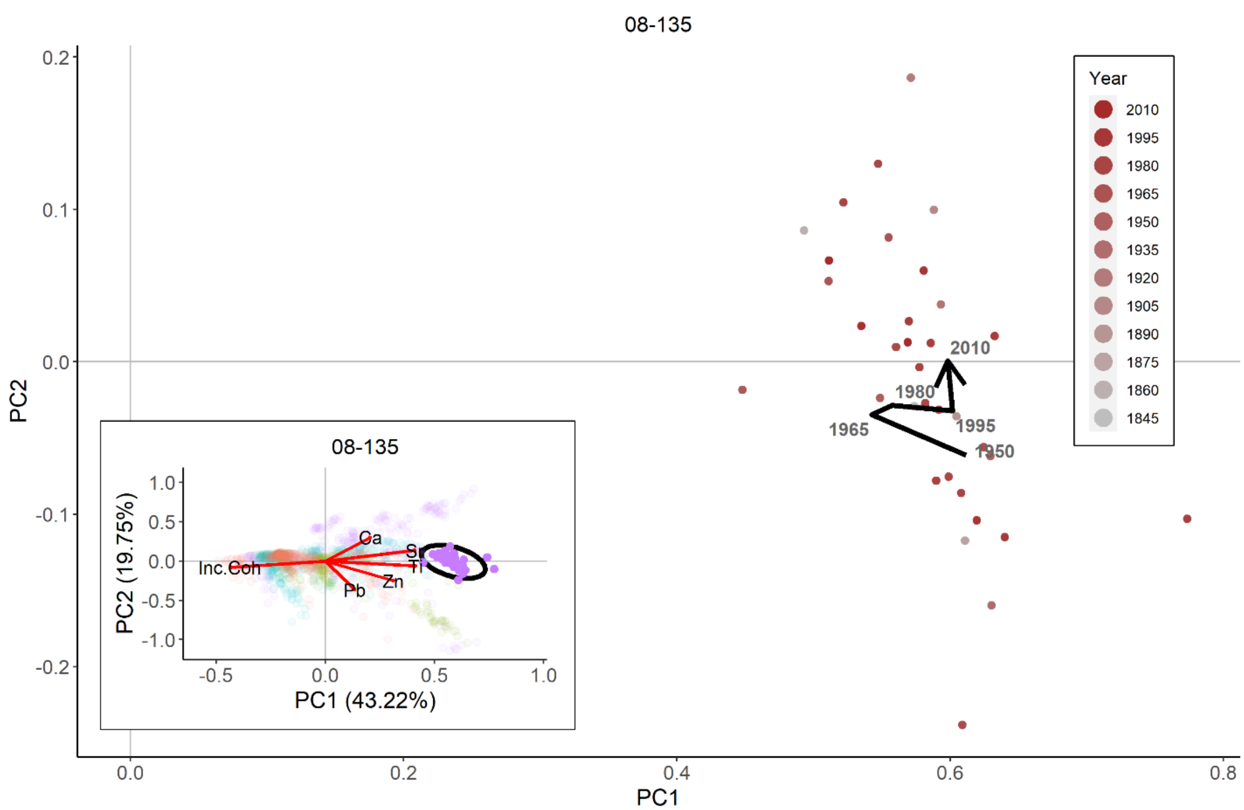
08-135
PC2
PC1
Year
2010
1995
1980
1965
1950
1935
1920
1905
1890
1875
1860
1845
2010
1980
1995
1965
1950
08-135
PC2 (19.75%)
PC1 (43.22%)
Inc.Coh
Ca
Sr
Ti
Zn
Pb

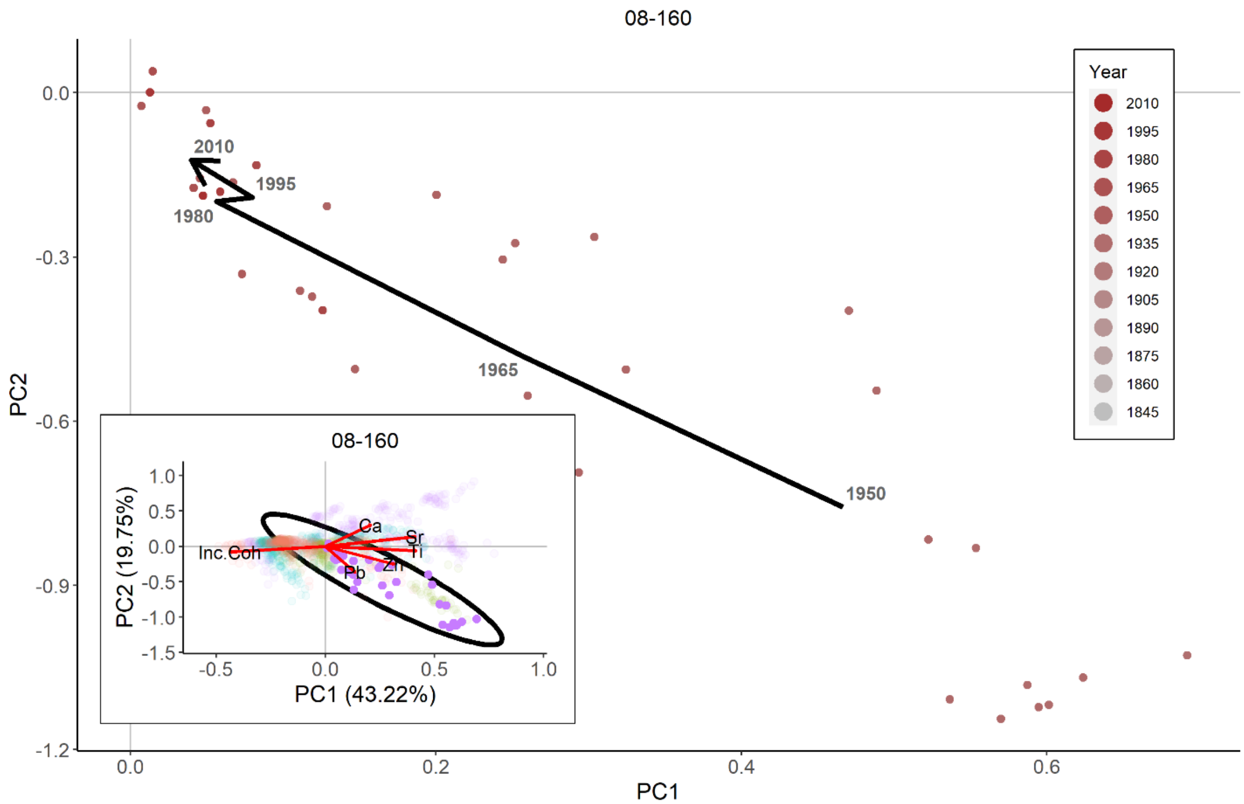
08-160
Year
2010
1995
1980
1965
1950
1935
1920
1905
1890
1875
1860
1845
PC1
PC2
PC1 (43.22%)
PC2 (19.75%)
Inc.Coh
Ca
Sr
Ti
Zn
Pb

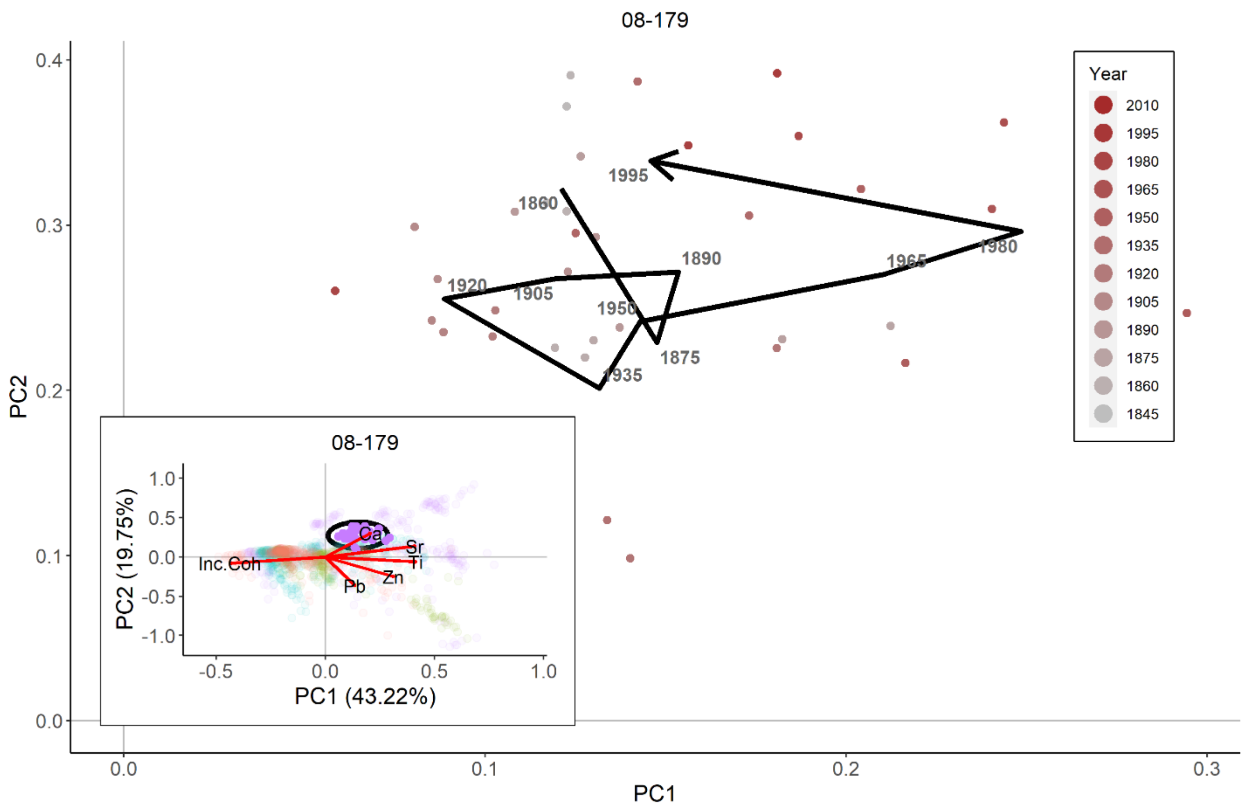
08-179
Year
2010
1995
1980
1965
1950
1935
1920
1905
1890
1875
1860
1845
PC1
PC2
PC1 (43.22%)
PC2 (19.75%)
Inc.Coh
Ca
Sr
Ti
Zn
Pb

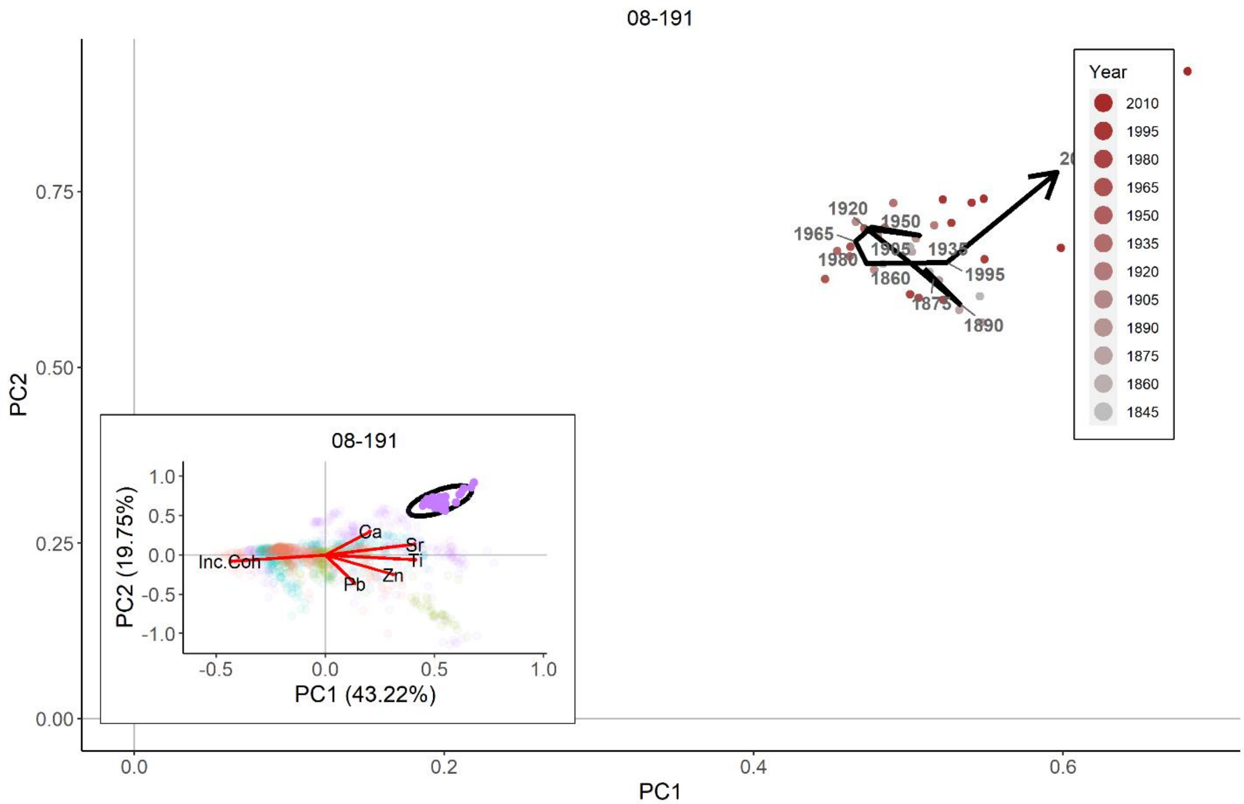

08-191
PC2
PC1
Year
2010
1995
1980
1965
1950
1935
1920
1905
1890
1875
1860
1845
08-191
PC2 (19.75%)
PC1 (43.22%)
Ca
Sr
Ti
Zn
Pb
Inc.Coh

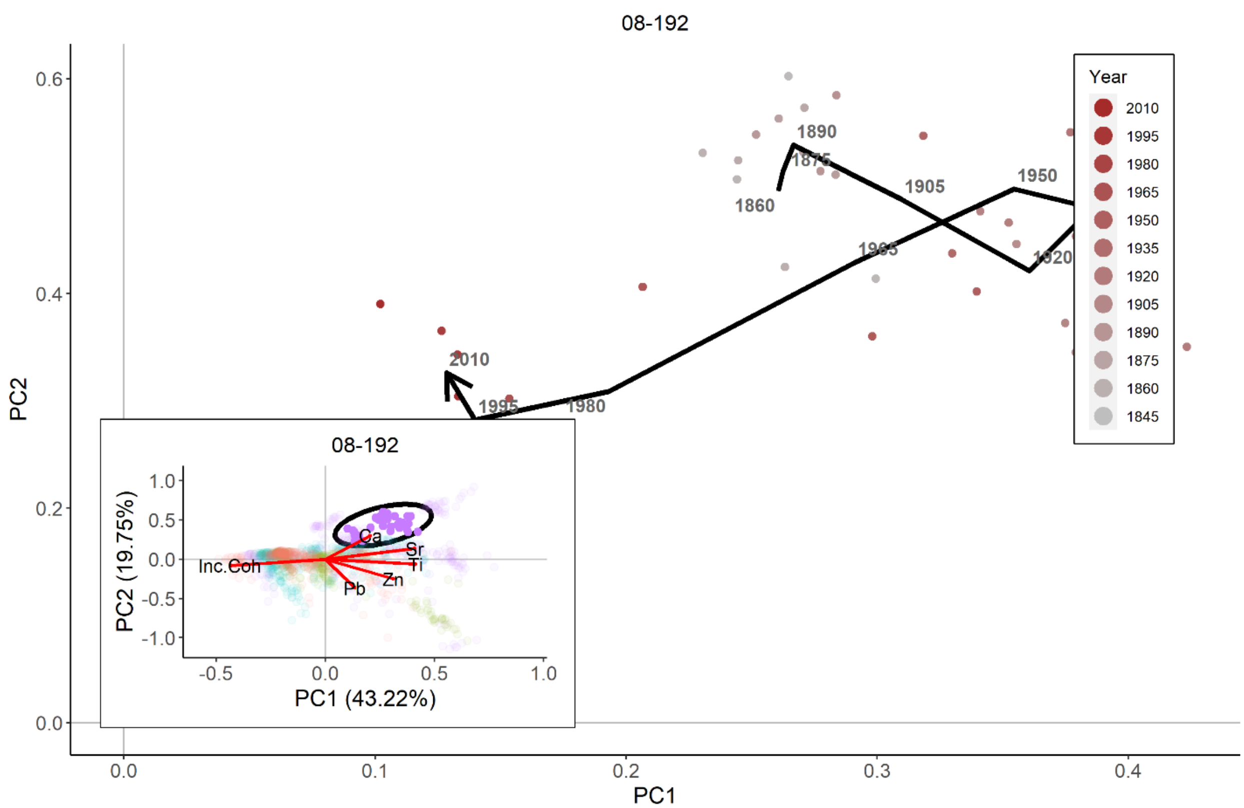

08-192
PC2
PC1
Year
2010
1995
1980
1965
1950
1935
1920
1905
1890
1875
1860
1845
08-192
PC2 (19.75%)
PC1 (43.22%)
Ca
Sr
Ti
Zn
Pb
Inc.Coh

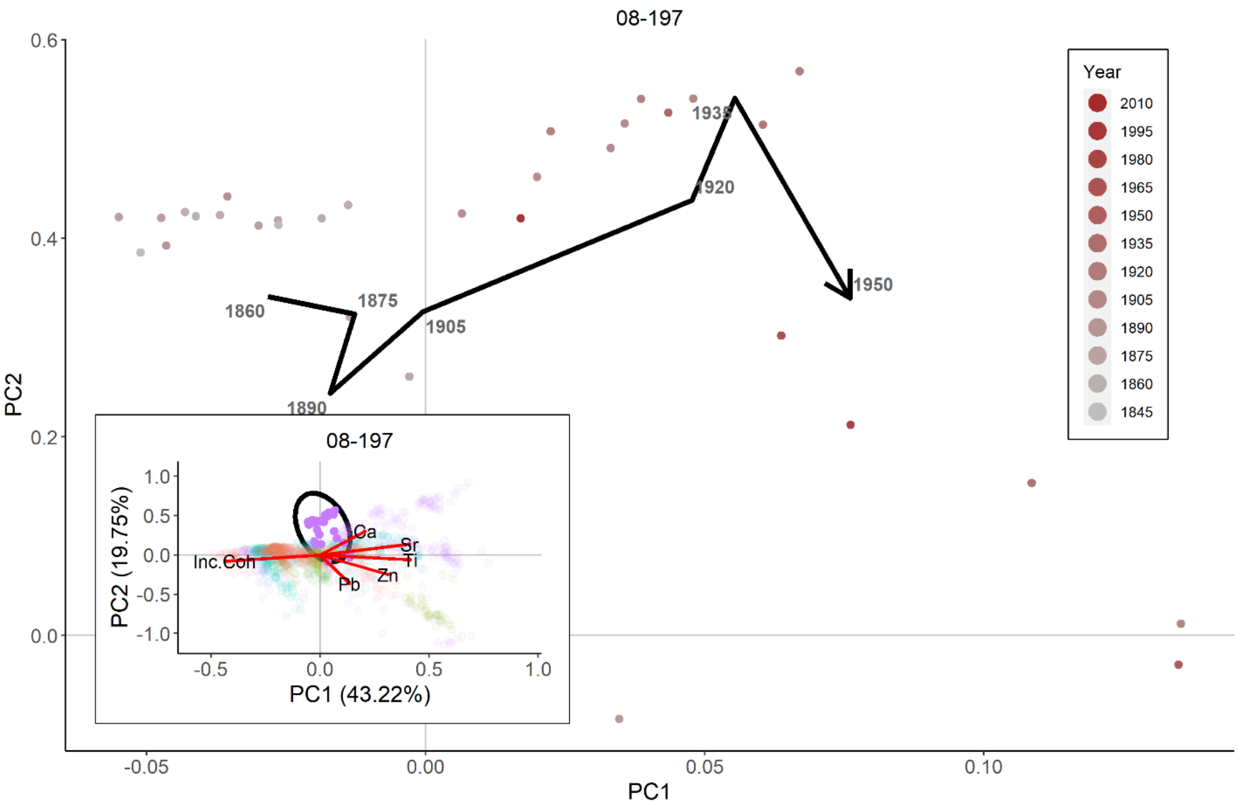
08-197
PC2
PC1
Year
2010
1995
1980
1965
1950
1935
1920
1905
1890
1875
1860
1845
1860
1875
1890
1905
1920
1935
1950
PC1 (43.22%)
PC2 (19.75%)
Inc.Coh
Ca
Sr
Ti
Zn
Pb

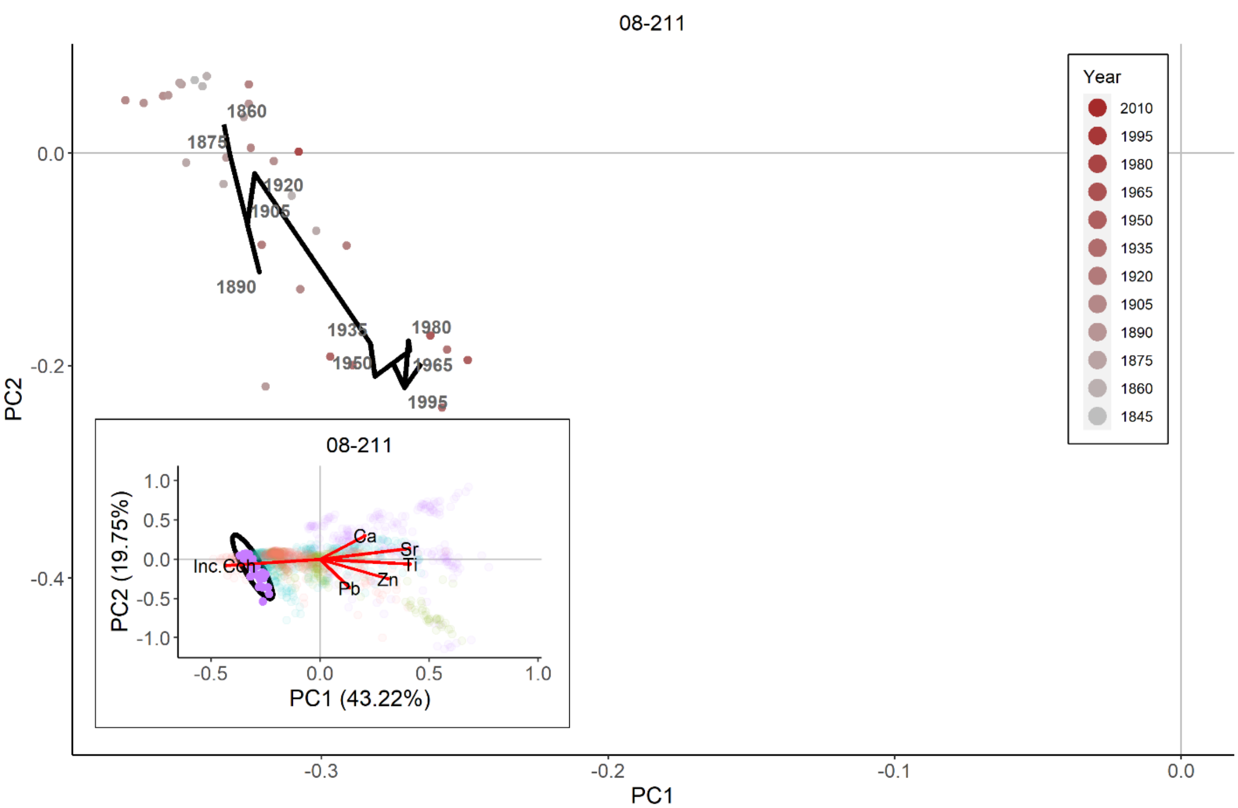
08-211
PC2
PC1
Year
2010
1995
1980
1965
1950
1935
1920
1905
1890
1875
1860
1845
1860
1875
1890
1905
1920
1935
1950
1965
1980
1995
PC1 (43.22%)
PC2 (19.75%)
Inc.Coh
Ca
Sr
Ti
Zn
Pb

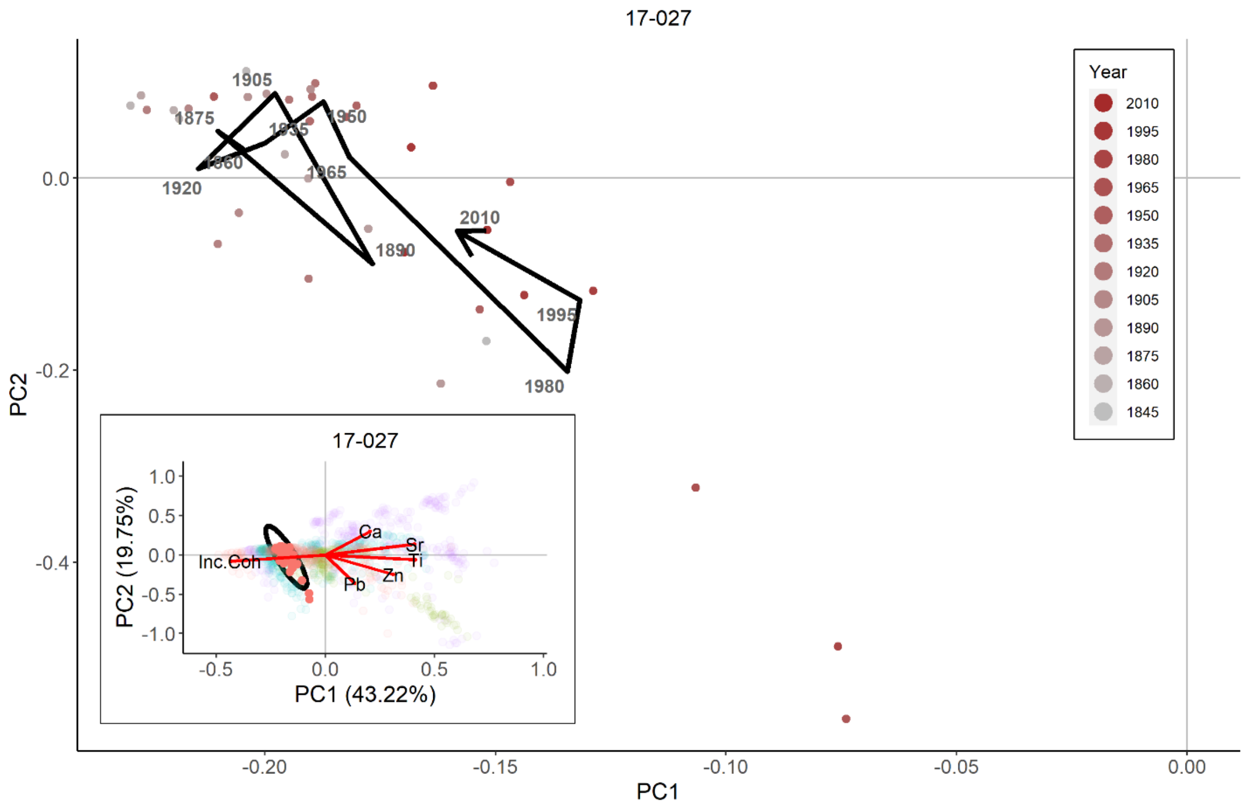
17-027
PC1
PC2
Year
2010
1995
1980
1965
1950
1935
1920
1905
1890
1875
1860
1845
PC1 (43.22%)
PC2 (19.75%)
Inc.Coh
Ca
Sr
Ti
Zn
Pb

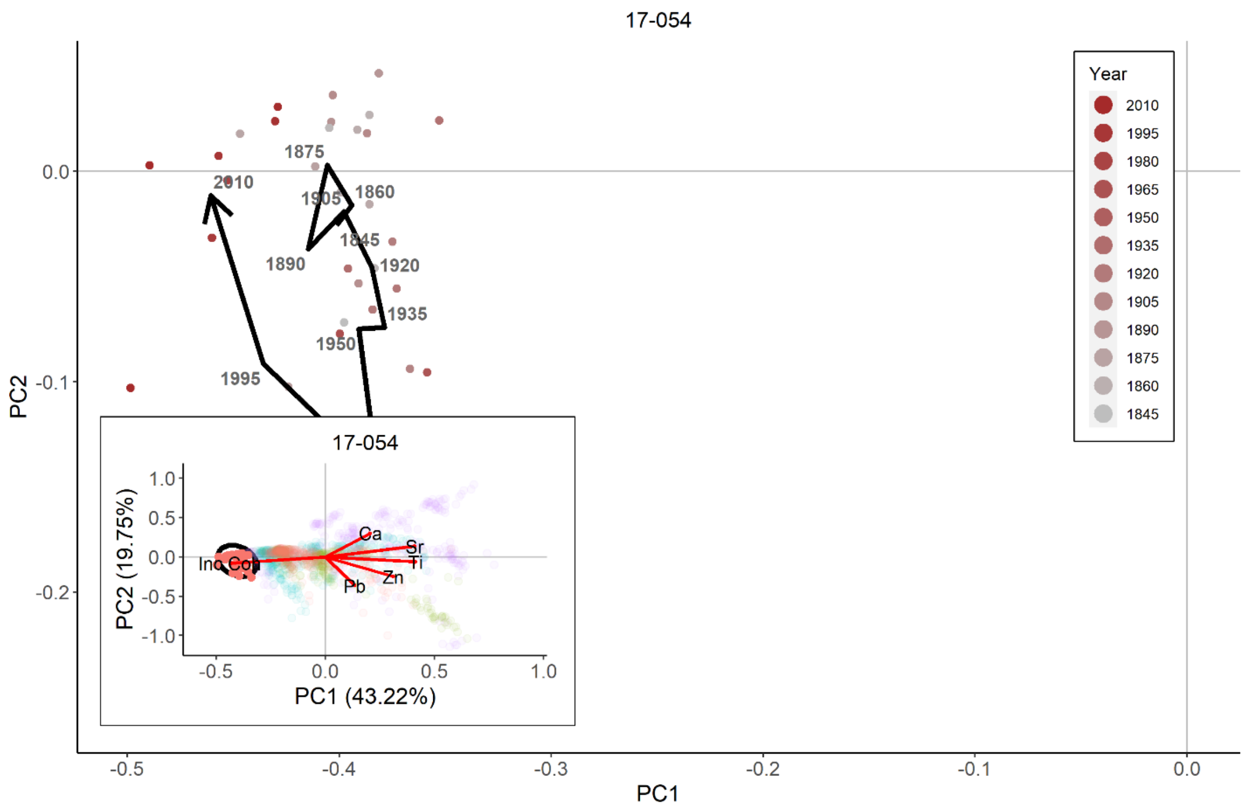
17-054
PC1
PC2
Year
2010
1995
1980
1965
1950
1935
1920
1905
1890
1875
1860
1845
PC1 (43.22%)
PC2 (19.75%)
Inc.Coh
Ca
Sr
Ti
Zn
Pb

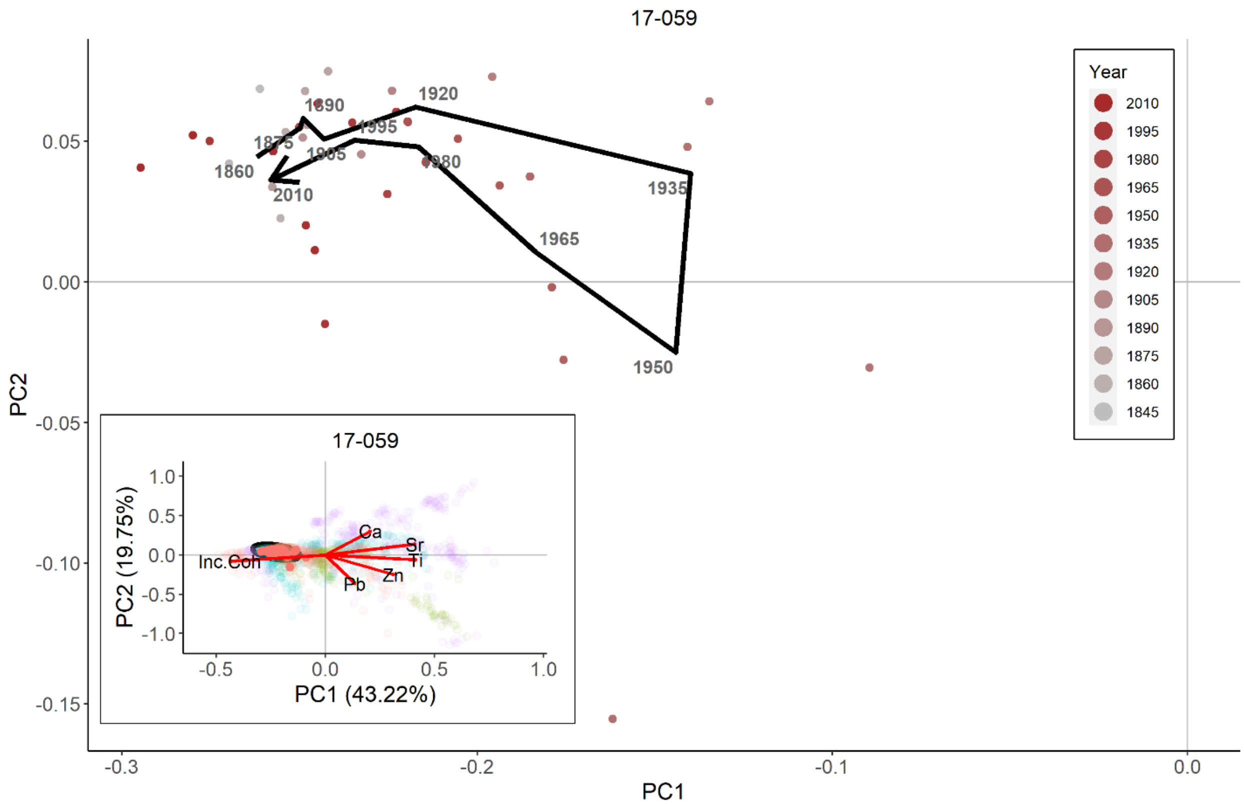
17-059
Year
2010
1995
1980
1965
1950
1935
1920
1905
1890
1875
1860
1845
PC2
PC1
PC2 (19.75%)
PC1 (43.22%)
Inc.Coh
Ca
Sr
Ti
Zn
Pb

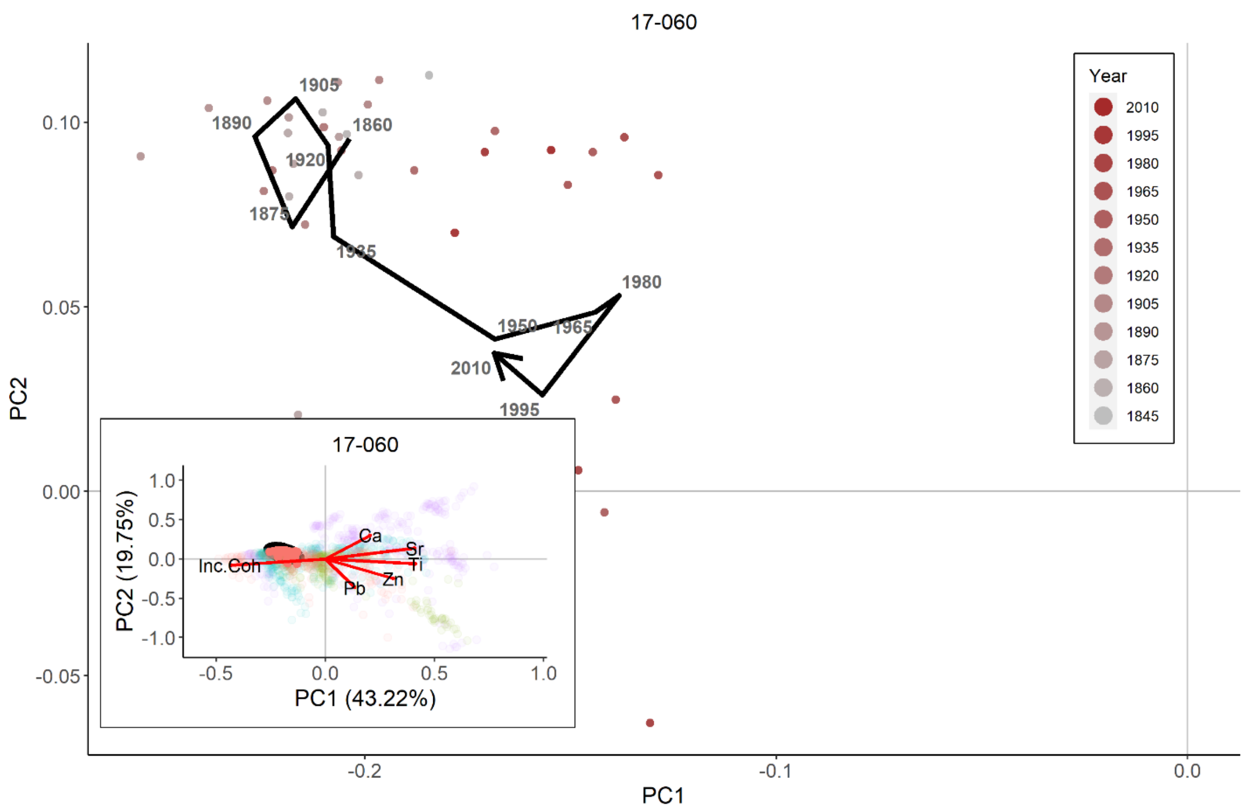
17-060
Year
2010
1995
1980
1965
1950
1935
1920
1905
1890
1875
1860
1845
PC2
PC1
PC2 (19.75%)
PC1 (43.22%)
Inc.Coh
Ca
Sr
Ti
Zn
Pb

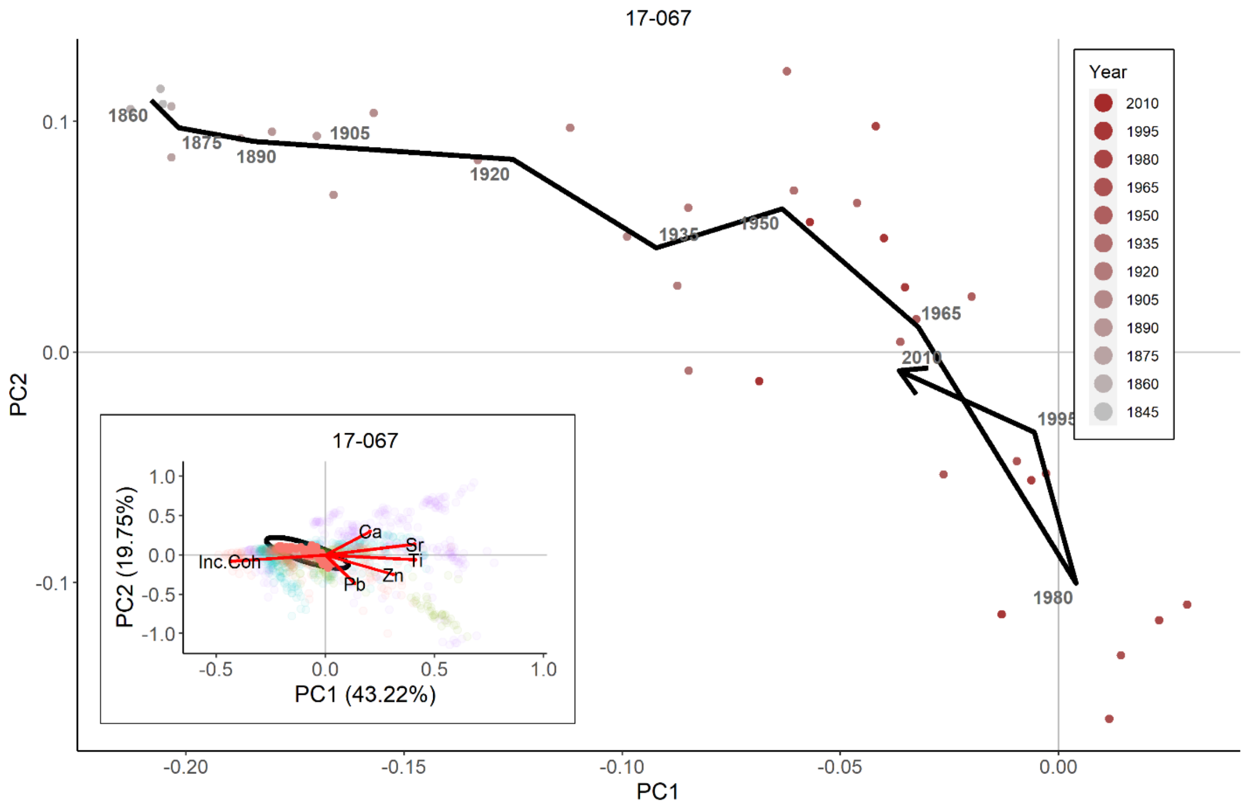
17-067
PC1
PC2
Year
2010
1995
1980
1965
1950
1935
1920
1905
1890
1875
1860
1845
PC1 (43.22%)
PC2 (19.75%)
Inc.Coh
Ca
Sr
Ti
Zn
Pb

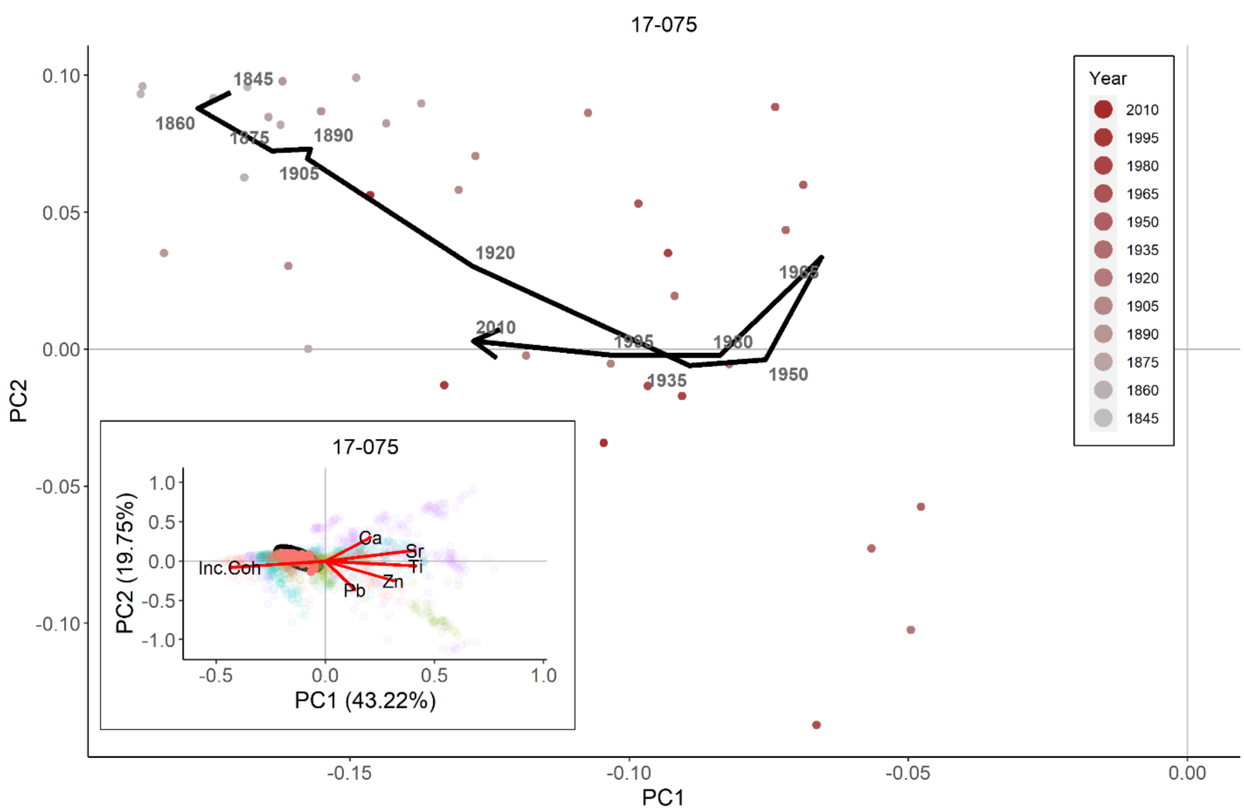
17-075
PC1
PC2
Year
2010
1995
1980
1965
1950
1935
1920
1905
1890
1875
1860
1845
PC1 (43.22%)
PC2 (19.75%)
Inc.Coh
Ca
Sr
Ti
Zn
Pb

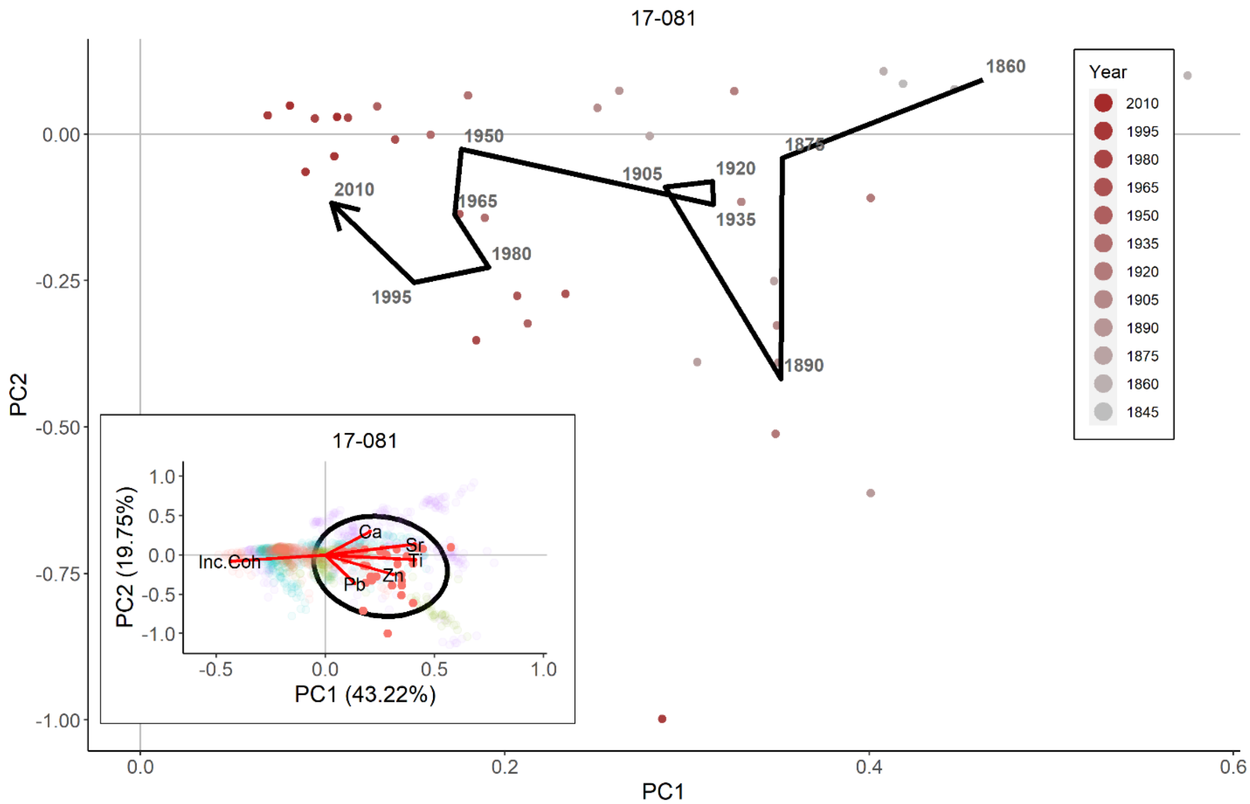
17-081
PC2
PC1
Year
2010
1995
1980
1965
1950
1935
1920
1905
1890
1875
1860
1845
PC2 (19.75%)
PC1 (43.22%)
Inc.Coh
Ca
Sr
Ti
Zn
Pb

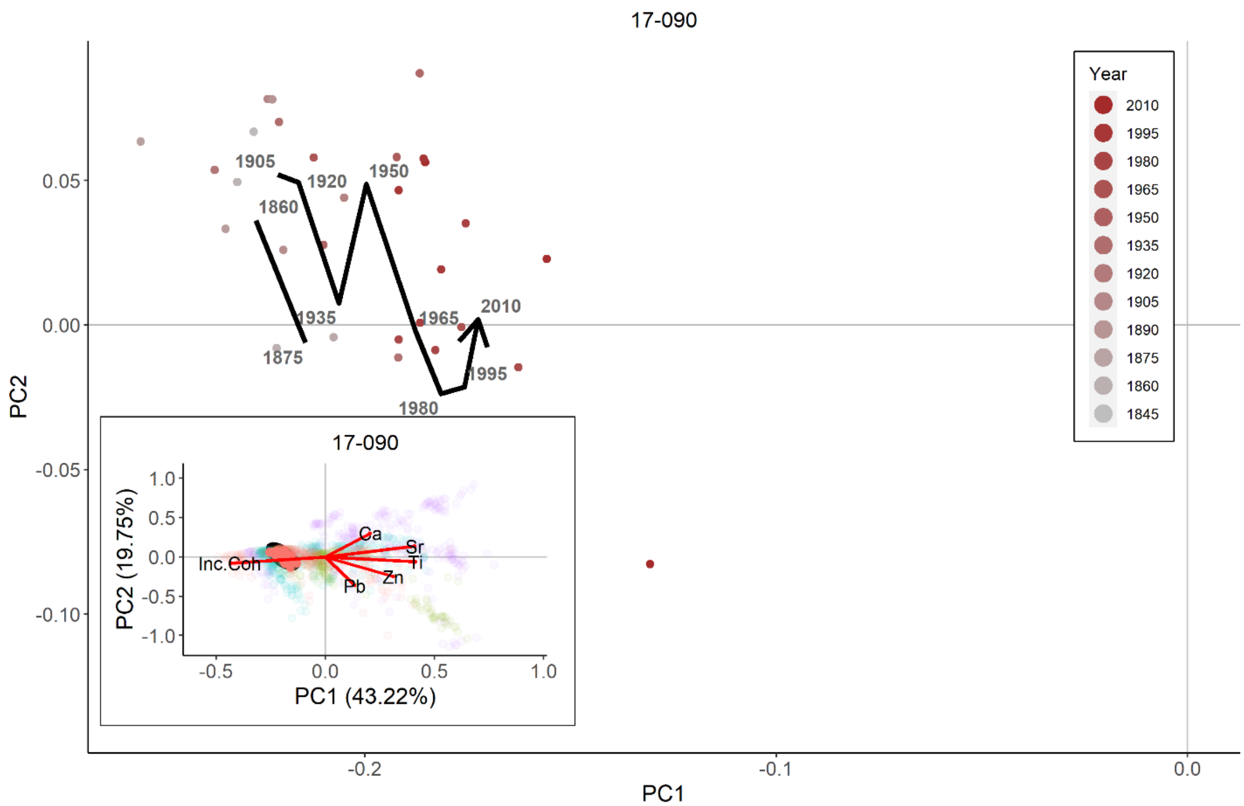
17-090
PC2
PC1
Year
2010
1995
1980
1965
1950
1935
1920
1905
1890
1875
1860
1845
PC2 (19.75%)
PC1 (43.22%)
Inc.Coh
Ca
Sr
Ti
Zn
Pb

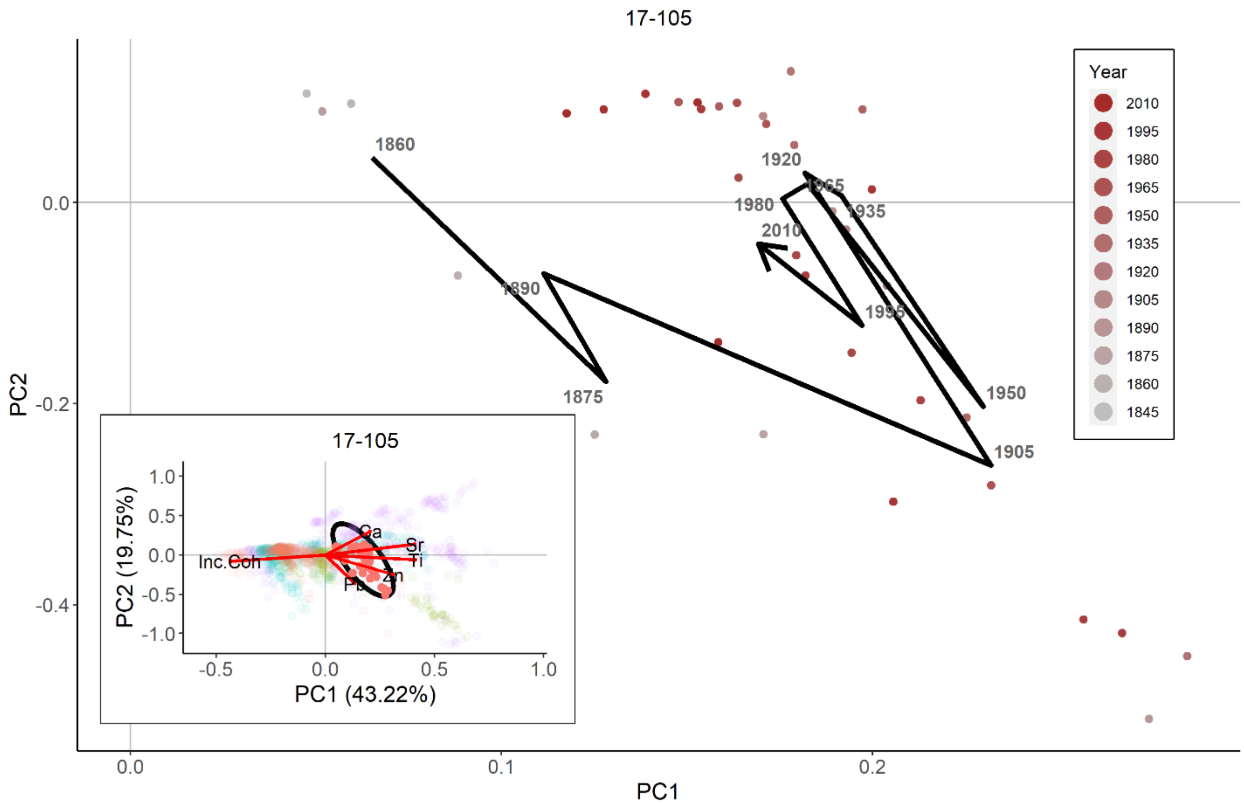
17-105
PC1
PC2
Year
2010
1995
1980
1965
1950
1935
1920
1905
1890
1875
1860
1845
1860
1920
1965
1980
1935
2010
1890
1995
1875
1950
1905
17-105
PC1 (43.22%)
PC2 (19.75%)
Inc.Coh
Ca
Sr
Ti
Pb
Zn

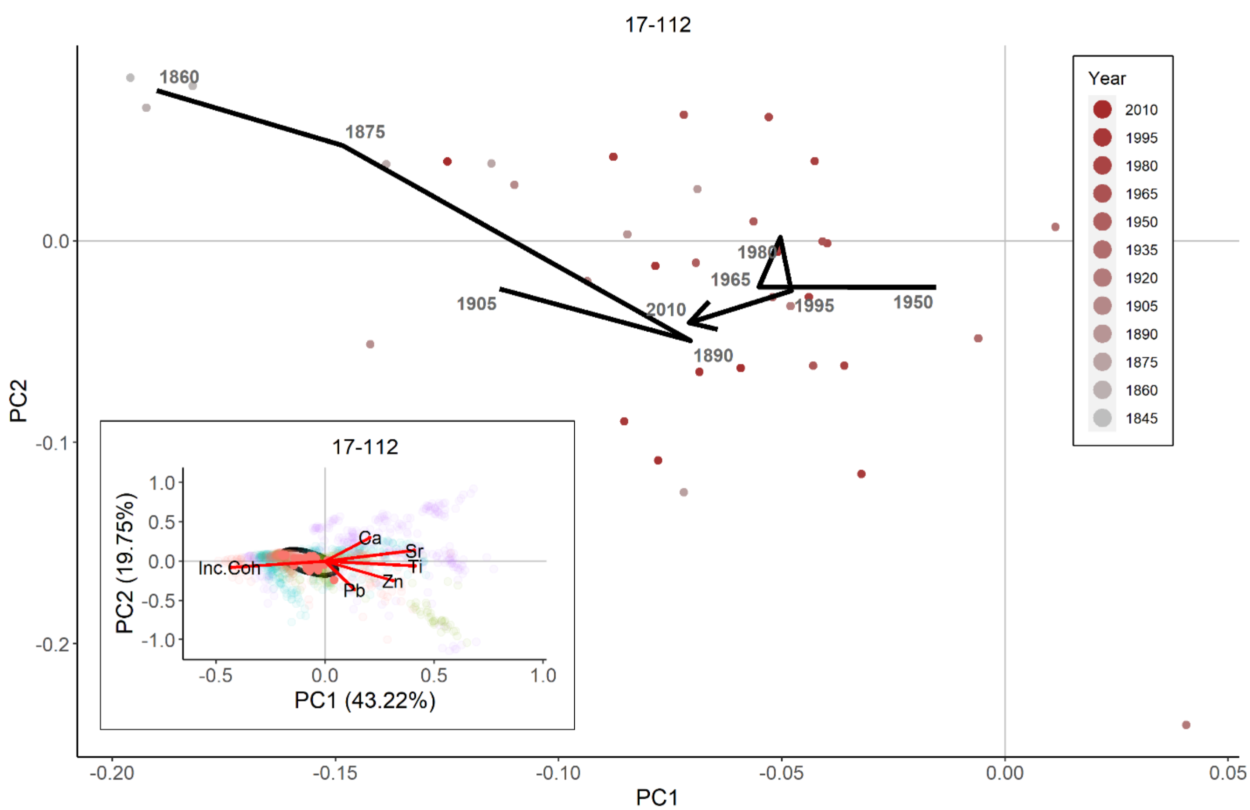
17-112
PC1
PC2
Year
2010
1995
1980
1965
1950
1935
1920
1905
1890
1875
1860
1845
1860
1875
1980
1965
1905
2010
1995
1950
1890
17-112
PC1 (43.22%)
PC2 (19.75%)
Inc.Coh
Ca
Sr
Ti
Pb
Zn

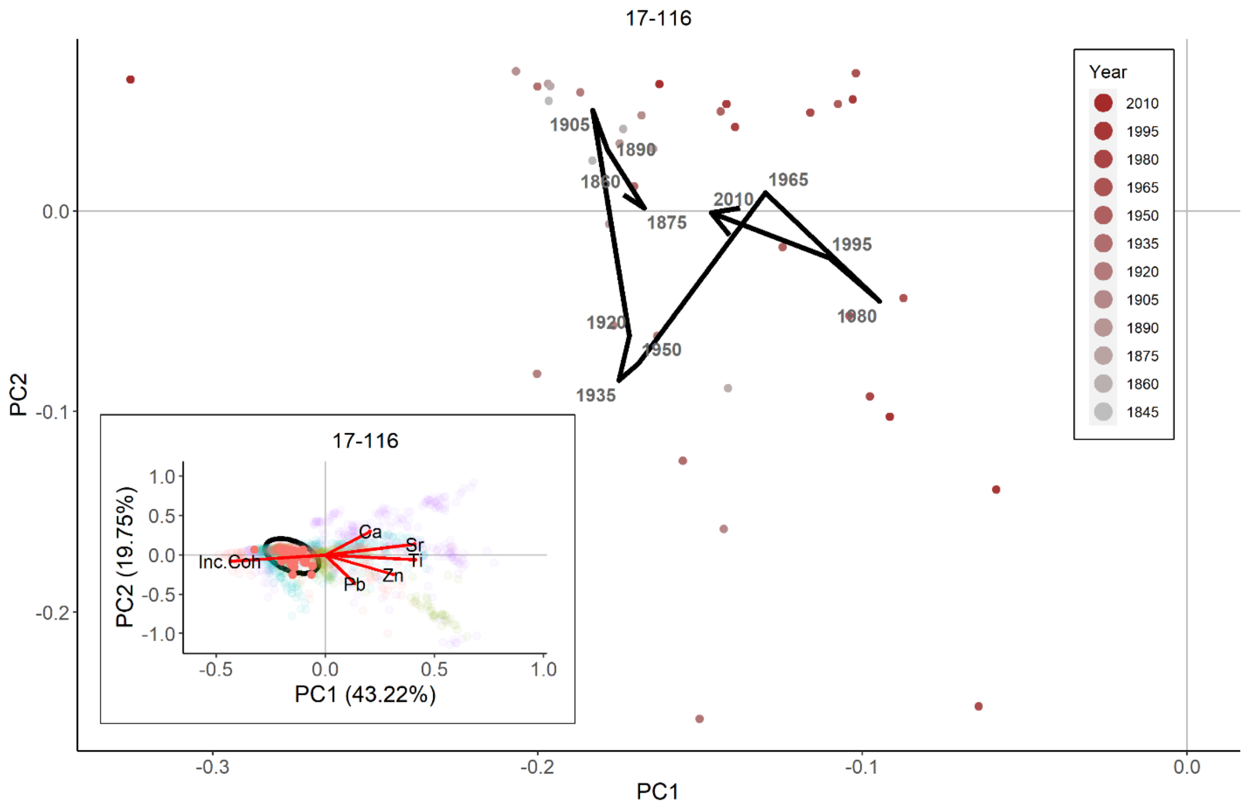

Figure CB.6. Principal component analysis (PCA) demonstrating individual lake trajectories of geochemical change, but where data from all lakes were used to construct the PCA. In the lower left panel is the original PCA where all 37 lakes were used to establish the loadings. The lake considered is represented by the color of its ecoregion and a single-lake 95% confidence interval ellipse. The lake-specific graph maximizes the extent of the single-lake trajectory of geochemical change (the ranges of the axes are modified to do so). Lake sediment intervals are color coded based on the time of deposition.

Connecting statement between Chapters III and IV

Results from Chapter III identified the widespread enrichment in heavy metals (Pb and Zn) in lake sediment cores starting during the early 20th century, before decreasing around the 1970s-1980s. This variation towards increased metal fraction was most strongly explained by the presence of human population in lake watersheds and has been recognized by others as the result of leaded gasoline combustion and overall increased smelter's emission before environmental regulations were put in place. While results of chapter III enabled the study of regional dynamics driving these varying levels of geochemical responses in lake sediments, consideration of how anthropogenic factors that alter a lake's chemistry can modify the geochemical record through changes in the speciation and burial of metals in lake sediments was not considered. Capitalizing on the generally well-recognized pattern of increased elemental Pb concentration in lake sediments mid to late 20th century in North America, we tested the potential influence of common lake stressors, such as lake eutrophication and lake acidification, in modulating metal accumulation in lake sediment. To do so, we considered an experimental setting where whole lake manipulations were conducted and water column monitoring data are available. We collected sediment cores from the International Institute for Sustainable Development - Experimental Lakes Area (IISD-ELA), a region donated to science for whole lake manipulations and monitoring since the late 1960s. For this chapter, we focused solely on elemental lead (Pb), a metal known to have been subjected to a ubiquitous accumulation in lake sediments worldwide and generally exhibiting a relatively small fraction of terrigenous input. We tested the hypothesis that greater accumulation of Pb would be observed in lakes having been subjected to lake eutrophication, while the reverse was expected for lakes subjected to lake acidification experiments. From this region, we collected two sediment cores from acidified lakes, three sediment cores from eutrophied lakes and two cores from reference lakes where no experimental had been carried out.

CHAPTER IV - THE IMPACTS OF WHOLE-LAKE ACIDIFICATION AND EUTROPHICATION ON THE ACCUMULATION OF LEAD IN SEDIMENTS FROM MANIPULATED LAKES IN THE EXPERIMENTAL LAKES AREA (IISD-ELA)

Alexandre Baud[1,2,*], John P. Smol[3], Carsten Meyer-Jacob[3], Michael Paterson[4], Pierre Francus[5,6], Irene Gregory-Eaves[1,2]

[1]Department of Biology, McGill University, Montréal, Québec, H3A 1B1, Canada

[2]Group for Interuniversity Research in Limnology and Aquatic Environments (GRIL)

[3] Paleoecological Environmental Assessment and Research Lab (PEARL), Department of Biology, Queen's University, Kingston, Ontario, K7L 3N6, Canada

[4]IISD-ELA International Institute for Sustainable Development Experimental Lakes Area, Kenora, Ontario, ON P0V 2V0, Canada

[5]Centre Eau Terre Environnement, Institut National de la Recherche Scientifique (INRS), Québec City, Québec, G1K 9A9, Canada

[6]GEOTOP, Geochemistry and Geodynamics Research Centre, Université du Québec à Montréal, Montréal, Québec H3C 3P8, Canada

Manuscript published in *Environmental Pollution* in December 2022

Abstract

Acidification and eutrophication are common limnological stressors impacting many water bodies across the globe. While the negative impacts of these stressors on limnetic communities are generally known, their influence on the accumulation of specific sediment constituents, such as metals, remains unclear. Benefitting from past research and long-term monitoring, lakes at the International Institute for Sustainable Development - Experimental Lakes Area (IISD-ELA) in northwestern Ontario, Canada are invaluable to understand the extent to which these two common lake stressors can influence the accumulation of metals in lacustrine sediment. To address these issues, sediment cores were retrieved from six lakes: four were subjected to past experimental acidification or eutrophication and two were reference lakes. Focusing on elemental lead (Pb), a metal known to have accumulated in lake sediments worldwide and generally exhibiting a relatively small fraction of terrigenous input, we assessed the hypothesis that greater accumulation of Pb would be observed in lakes subjected to eutrophication, while the reverse was expected for lakes subjected to acidification experiments. Our analyses support this hypothesis, whereby relatively low enrichment was recorded in sediments deposited in the acidified lake during the manipulation era. On the other hand, eutrophied lakes demonstrated a strong enrichment in Pb during experimental manipulation. When investigating the mechanisms behind these divergent responses, we found epilimnetic dissolved organic carbon (DOC) and conductivity were associated with a relative increase in Pb accumulation in sediments. Acidic pH is also expected to mediate these responses by decreasing epilimnetic DOC concentrations leading to reduced Pb accumulation in the sediment.

Introduction

Owing to their acute toxicity (Duruibe et al., 2007; Tchounwou et al., 2012), the accumulation of heavy metals in the environment has always been a topic of concern (Verta et al., 1989; Smol, 2009). Exacerbated by increasing human population growth and the onset of industrialization, the release of heavy metals to the environment intensified at the end of the 19th century (Likens et al., 1979; National Research Council, 1986). With a multitude of metals having the potential to make their way into the environment, accumulating in sediments and food webs (Mohod and Dhote, 2013; Chowdhury et al., 2016), heavy metal pollution has become one of the priorities for public health organizations. To this end, many environmental programs aimed at monitoring (Powell and Wharton, 1982; ECCC, 2021) and curbing heavy metal emissions (ECCC, 2022) have been put in place by governing bodies. Paleolimnological programs, capable of inferring past conditions, have been particularly useful in teasing apart natural variability from anthropogenic contributions and providing realistic guideline levels for a wide variety of pollutants (Smol, 1992). Lake sediments, because of their high trapping efficiency and adsorption potential (Jain and Ram, 1997), are particularly susceptible to metal accumulation and will typically harbor concentrations several orders of magnitude higher than those in overlying waters (Pulatsü and Topçu, 2015). This difference between water and sediment has long been recognized, with the existence of environmental guidelines for water and sediment quality (CCME, 2022).

Metal pollution seldom occurs independently of other anthropogenic impacts and can often be confounded by the presence of additional environmental stressors that have the potential to modulate the abundance of metals in the environment. One prominent example is the issue of environmental acidification (National Researh Council, 1986). Typically, ecosystem acidification is generated through the combustion of fossil fuels and emissions from smelters whereby sulfur and nitrogen compounds are emitted into the atmosphere, and subsequent acidic precipitation is deposited on the landscape (National Research Council, 1986). Lake eutrophication, on the other hand, which corresponds to an increase in limiting nutrient levels in lakes, is currently often linked to diffuse sources, such as agricultural run-off (Withers and Haygarth, 2007; Dupas et al., 2015), and has been particularly well documented to increase total organic carbon (TOC) and dissolved organic carbon (DOC) concentrations in lake water (Maranón et al., 2004). While insights into the deposition and accumulation of metals can be gained through a regional paleolimnological survey, the co-occurrence of anthropogenic land-use changes (i.e., urban, agriculture, industry) may hinder the mechanistic determination of the influence of lake acidification and eutrophication on the accumulation of metals in lake sediments. For example, despite metals generally exhibiting greater solubility in acidic pH (McBride, 1989; Chuan et al., 1996), trends in metal accumulation in regions of the world known to have experienced high rates of acid deposition may not reflect this increased within-lake solubility (Dixit et al., 1987), but rather reflect increased metal accumulation mediated by atmospheric deposition and catchment leaching. Conversely, in regions of important agricultural run-off, metal accumulation trends may overestimate the true atmospheric deposition patterns of metals and be biased by the greater proportion of organic compounds in lake water, whereby important complexation of metals with organic matter is expected (Weng et al., 2002; Likens, 2009). It would thus be important to investigate the influence of acidification and eutrophication in a more controlled experimental setting.

Located in north-western Ontario, the International Institute for Sustainable Development - Experimental Lakes Area (IISD-ELA) offers unique opportunities to assess the impacts of eutrophication and lake acidification in whole lake settings (Figure IV.1). Beginning in the late 1960s, whole lake manipulations have been carried out at the IISD-ELA to investigate the impacts and mechanisms of lake eutrophication and acidification (Schindler et al., 1971; Schindler et al., 1985; Schindler et al., 2008; Higgins et al., 2018). While these experiments were successful at highlighting the negative impacts of these stressors on the lakes' natural biotic and abiotic communities (Findlay and Kasian, 1986; Findlay and Kasian, 1987; Leavitt and Findlay, 1994) and their effects on the accumulation of radioisotopes and emerging contaminants (Anderson et al., 1987; Crusius and Anderson, 1995; Stephenson et al., 1995; Jeremiason et al., 1999; O'Connell et al., 2020; Huang et al., 2022), their influence on the accumulation of elemental lead during the 20-21st centuries remains unexamined. The legacy of these manipulations, however, is still present and remains accessible, captured within the sediment of these study lakes. Coincidentally, the timing at which these experiments took place was during a period of elevated elemental lead (Pb) deposition and accumulation in sediments (Dunnington et al., 2020b). Elemental Pb, through its relatively low abundance in Earth Crust (Fleischer, 1954) and its historical presence in gasoline (Nriagu, 1998), makes it a good candidate for evaluating the impacts of lake eutrophication and acidification on the accumulation of atmospherically deposited metals in sediments.

The objectives of this study are to assess the potential roles of lake acidification and lake eutrophication on the accumulation of metals, and specifically elemental Pb in lake sediments. With acidification, it is expected that, through the control of lakewater pH, increased solubility within the water column will favor a water-soluble phase of Pb and co-jointly reduce the presence of lake water DOC, thereby reducing the ability of Pb to bind to particulate matter, sink to the lake bottom and accumulate in sediment. Conversely, the effects of eutrophication are expected to fuel primary production and increase both algae (tracked by chlorophyll-a) and DOC concentrations in lake water with high trapping efficiency, favoring Pb accumulation in the sediment. The experiments at the IISD-ELA allow us to isolate the effects of *within* lake processes as chemicals were added directly to the lake-water, instead of the addition occurring in both the lake and its watershed, the latter of which typically occurs in ecosystems.

Methods

<u>IISD-ELA study sites and summary of experimental manipulations</u>

A total of six lakes, including two unmanipulated reference lakes, were selected to encompass the acidification and eutrophication experiments that had been carried out since the 1970s at the IISD-ELA (Figure IV.1 and Table IV.1). Considering lakes subjected to acidification experiments, we cored Lake 223 and Lake 302. For the eutrophication experiments, we collected sediment cores from Lake 227 and each basin of Lake 226 (North and South). Finally, two reference lakes, Lake 224 and Lake 373, were cored to capture the natural range of variability experienced in this region. Selection of these two reference lakes was based on an analysis of the lake morphology, catchment geology (Brunskill and Schindler, 1971; McCullough and Campbell, 1993) and direct communication with personnel from IISD-ELA. All six lakes were cored in August 2018.

A summary of the lakes sampled and associated chronologies for the main experiments considered, as well as morphometric variables, is available in Table IV.1. The seven sediment cores from the six IISD-ELA lakes were retrieved using a NLA gravity corer (Blomqvist, 1991) from the lakes' deepest points. After retrieval, we recorded the length of the sediment cores, and stabilized the sediment-water interface using sodium polyacrylate (Tomkins et al., 2008) by adding it in increments to limit porewater migration within the core following LakePulse field protocol (NSERC Canadian Lake Pulse Network, 2021).

Laboratory Analyses (^{210}Pb dating and elemental Pb measurements)

Approximately 15 discrete sediment intervals along the depth of the cores were prepared in tubes for dating via gamma spectrometry using an Ortec high-purity Germanium gamma spectrometer (Oak Ridge, TN, USA). Radionuclide profiles for lead-210 (^{210}Pb), lead-214 (^{214}Pb) and cesium-137 (^{137}Cs) were recorded, and sediment cores were dated using one of the following three dating models: Constant Flux Constant Sedimentation (C.F.C.S.), Constant Initial Concentration (C.I.C.) or Constant Rate of Supply (C.R.S.), as described in Baud et al. (2022). To accommodate the experimental addition of radiotracers (especially ^{226}Ra) to lakes 224, 226 and 227, a point-by-point subtraction of the supported activity from the total activity was performed. This method was chosen because we expect some of the daughter decay products (i.e., ^{214}Pb) to impact the supported activity in the deposited sediments (O'Connell et al., 2020) – (see supplementary material – Figure D.1).

Concentrations of elemental Pb were quantified using Inductively Coupled Plasma Atomic Emission Spectroscopy (ICP-AES). In preparation, 0.25 g of dry mass from selected subsamples underwent a total digestion method that consisted of heating under reflux at 100°C and treating samples with a sequence of concentrated 4 mL 15.9M nitric acid, 1.6 mL 10-11M perchloric acid, and 22 mL 8.9M hydrofluoric acid. These acids completely dissolved the organic matrix over a 72-hour period. Samples (covered) were left at room temperature over a 2-week period before analysis.

IISD-ELA Monitoring Data

To complement the time series data derived from the sediment cores, we analyzed data from IISD-ELA's water column monitoring program. Specifically, we used epilimnetic water chemistry data collected during the ice-free season (May-Oct.) from 1970 – 2020 CE and analyzed using methods from Staiton et al. (1977). Each of the relevant variables were sampled every two weeks and averaged by year and lake basins, by first calculating monthly averages, and then calculating the annual mean across the ice-free season. Variables with a large proportion of missing data (> 10%) were discarded. For all lakes, we also removed dissolved sodium and chloride lakewater concentrations from the dataset since these variables were highly dependent on the addition of nutrients, which took the form of Na_2HPO_4 and $NaNO_3$. The remaining monitoring water chemistry variables included: in-situ pH, conductivity, dissolved inorganic carbon, dissolved organic carbon, calcium, ammonium, nitrate, sulphate, soluble reactive silica, suspended carbon, suspended particulate carbon, suspended phosphorus, suspended nitrogen, total dissolved nitrogen, total dissolved phosphorus and chlorophyll-a.

Statistical Analyses

All statistical analyses were performed in R-studio v.4.0 (R Core Team, 2021). General additive mixed effect models (GAMMs) served to model the temporal variation in Pb concentrations (µg/g) and Pb accumulation rates (µg Pb/cm^2/year) in response to experimental manipulations. This statistical consideration objectively quantifies the inherent structure associated with the time series where multiple repeated measures are performed for the same sediment core (Simpson, 2018). Pb accumulation rates were calculated to consider the influence of changes in sediment mass accumulation rates and were corrected for sediment focusing. Mass accumulation rates were estimated following the C.R.S. methodology using the ratio of ^{210}Pb inventory over the unsupported ^{210}Pb activity for each dated core section, multiplied by the ^{210}Pb disintegration constant (Appleby, 2002; Sanchez-Cabeza and Ruiz-Fernández, 2012). Focusing factors were calculated for each lake, using the ratio between the atmospheric ^{210}Pb inventory and the core's ^{210}Pb inventory: (atmospheric ^{210}Pb flux/^{210}Pb decay constant) / core ^{210}Pb inventory. A value of 183 Bq/cm^2/year, corresponding to the average annual ^{210}Pb fallout value for the IISD-ELA region (Anderson et al., 1987; Crusius and Anderson, 1995), was used for calculating the atmospheric ^{210}Pb inventory.

To evaluate the statistical significance of the experimental manipulations, we used breakpoint analysis using the R-package segmented (Muggeo and Muggeo, 2017). This breakpoint analysis served two purposes; first, to detect for potential variation in the significant breakpoints associated with periods of increased Pb accumulation across lakes impacted by different experimental manipulations; second, it enabled the testing of potential significant differences in the slope of Pb accumulation across lakes. For all lakes, we tested the potential presence of up to two breakpoints, associated with the expected accelerated deposition in the early-mid 1900s and decreased rates in more recent decades (Dunnington et al., 2020b) for the temporal regression of Pb accumulation. The number of significant breakpoints was obtained via Bayesian information criterion (BIC), selecting for the lowest BIC comparing regressions with 0, 1 and 2 breakpoints. The significance of these breakpoints was computed using the hypothesis testing *davies.test* available within the segmented package. Using intervals delimited by significant breakpoints, we then tested for potential significance differences comparing the slope of Pb accumulation across lakes using Analysis of Variance (ANOVA) (Stepanova et al., 2015). To investigate the significance and the direction of the differences in slopes further, we used linear functions of least-squares means using the *lsmeans* R-package (Lenth, 2016).

To identify significant predictor variables associated with the temporal variation in elemental Pb accumulation during the period of accelerating Pb deposition (i.e., determined using breakpoints), we performed a backward stepwise linear mixed effect model using the *lme4* R-package (Bates, 2015) with Pb accumulation as the response variable and the selected IISD-ELA monitoring parameters as potential explanatory variables. Visual representations of the temporal variation of Pb and associated expected predictors were also generated.

Results

Sediment Chronology and Mass Accumulation Rate

The radioisotopic profiles recorded across the seven sediment cores demonstrated, for the most part, the expected exponential ^{210}Pb decay (Figure D.1). Using the methodological framework described in Baud et al. (2022), we found that all cores' radioisotopes were largely in accordance with assumptions of the C.R.S. model. All lakes demonstrated very strong correlations ($R^2 > 0.95$) between expected and observed ^{210}Pb, with the exception of Lake 302 where we observed a prolonged period (i.e., 10-20 centimeters) displaying relatively constant unsupported ^{210}Pb, likely indicating physical or biological mixing. As a result of this radioisotopic pattern, mass accumulation rates (MAR; expressed as: g/cm^2/year) in Lake 302 demonstrated elevated and likely erroneous MAR (0.0063 - 0.0570 g/cm^2/year). We therefore removed Lake 302 from the dataset and only considered Lake 223 as being impacted by experimental acidification. Similar dating issues have been reported by other studies trying to establish sediment chronologies for cores from Lake 302 (Anderson et al., 1987; M. Paterson, unpublished data).

We also observed the signature of radioisotopic addition in some of the lakes, especially in Lake 227 where short-lived ^{226}Ra addition was detected as a peak in ^{214}Pb occurring at around 5 cm sediment depth, corresponding to ~ 1975 CE, which matches the reported time of ^{226}Ra addition (Figure D.1). Lake sediment mass accumulation rates were found to be generally similar across the different lakes (0.004 - 0.022 g/cm^2/year) (Figure D.2). We observed that most lakes demonstrated an increase in MAR, with the exception of one of the Reference lakes, Lake 224, where MAR was recorded to have increased between ca. 1850 and 1925 CE and then decreased to present day. Another interesting feature in MAR spatio-temporal variation is the difference between the two basins of Lake 226. The north-basin, enriched with C, N and P, exhibited a strong temporal increase in MAR during experimental nutrient enrichment, which was less visible in the south basin (enriched only with C and N) during the same period. Lake

227, with continued eutrophication, showed a strong, almost linear, pattern of increasing MAR over time, which has also been reported in earlier publications (Wolfe et al., 1994; Jeremiason et al., 1999).

Temporal trends in elemental lead

The resulting trends from the GAMMs highlighted the hypothesized contrasting responses across the different experimental treatments for both Pb concentrations and Pb flux (Figure IV.2). All lakes exhibited similar Pb concentrations before the onset of experimental manipulation (ca. 1880 – 1950 CE) (38.8 ± 13.5 µg/g). When considering elemental Pb flux, we observed distinct levels of Pb accumulation across the different lakes prior to the experiments, with reference lakes accumulating more Pb compared to Lake 226N/S, Lake 223, and Lake 227. The cores from the north and south basins of Lake 226 tracked a strong temporal increase in Pb concentration, exceeding levels found in Reference lakes. Relatively small differences were found between the concentrations recorded in the north (C, N, and P addition) and south basins (only C and N added) of Lake 226. Pb flux in Lake 226 differed in magnitude between the two basins, with the north basin accumulating twice as much Pb than the south basin during the maximum accumulation period. Levels of Pb accumulation in Lake 226N exceeded Pb accumulation recorded in the Reference lakes, despite the initial opposite situation with higher Pb accumulation in the Reference lakes. In Lake 227, peak elemental Pb concentrations exceeded those found in Reference lakes. Even though there was a strong temporal increase in Pb accumulation, fluxes of Pb in Lake 227 equaled accumulation levels recorded in Reference lakes. Elemental Pb concentration in Lake 223, demonstrated little to no temporal increase during the expected period of rapid Pb emission, between 1950-1980 CE. When considering elemental Pb flux for this lake, we observed a slight temporal increase in Pb accumulation, but this increase was less striking than observed in other lakes.

The varying temporal patterns in Pb accumulation across different lakes are further highlighted by the GAMMs partial effects for each of the lake's level smooth terms (Table D.3). Lakes targeted by eutrophication were best modeled using non-linear trends with estimated degree of freedom (e.d.f.) for their partial effects being the greatest (e.d.f.$_{Lake226N}$ = 7.68; e.d.f.$_{Lake227}$ = 6.87) suggesting an important non-linear temporal increase in the accumulation of elemental Pb. The e.d.f. value for Lake 226S which was only partially fertilized (no P added) was smaller than for other eutrophied and reference lakes (e.d.f.$_{Lake226S}$ = 5.93; e.d.f.$_{References}$ = 6.47). On the other hand, e.d.f. in the acidified lake demonstrated the lowest e.d.f. value suggesting a more moderate accumulation of Pb compared to the other lakes (e.d.f.$_{Lake223}$ = 3.16).

For all lakes, the analysis of breakpoints identified two significant breakpoints when considering the temporal regression of Pb flux (Table D.4). Given the similar timing of experimental manipulations and the proximity of sites, similar breakpoints were expected across lakes. The initial breakpoint value associated with the onset of the acceleration in elemental Pb accumulation was moderately variable across lakes, with an average value of 1954 CE ± 12 years. Lake 223 was the lake returning the earliest breakpoint (~ 1938 CE) while Lake 226N the latest (~ 1967 CE). The date associated with the secondary breakpoint was highly consistent across lakes, with an average value of 1983 ± 4 years. Lake 227 was the lake yielding the earliest secondary breakpoint (~1978 CE), while Lake 223 returned the latest (1989 CE) (See Table D.4). When considering elemental Pb flux between the mean breakpoint dates across lakes (i.e., 1954 - 1983 CE), the ANOVA detected significant differences as a function of slopes (Sum Square = 0.094, Df = 1, F-value = 404.4, p-value = < 0.001), between LakeID (Sum Square = 0.120, Df = 5, F-value = 404.4, p-value = < 0.001) and their interaction (Sum Square = 0.040, Df = 5, F-value = 34.2, p-value = < 0.001). As indicated by the partial least-squares post-hoc test (Table IV.2), Lake 226N and Lake 227 demonstrated the strongest slope in Pb accumulation ($Slope_{L226N}$ = 0.016; $Slope_{L227}$ = 0.018). The slope associated with Lake 226S was lower than other eutrophied lake estimates but greater than for reference lakes ($Slope_{L226S}$ = 0.0090; $Slope_{References}$ = 0.0052) while Lake 223 returned the lowest slope between 1954 and 1983 ($Slope_{L223}$ = 0.044). No significant differences were found between L223, L226S and reference lakes while the slopes of Pb accumulation in L226N and L227 were significantly different from all other lakes.

Drivers of Pb Accumulation in lake sediments

Results from the backward stepwise linear mixed effects model highlighted the relative importance of water column DOC and conductivity recorded from in-lake measurements between 1971 – 1983 CE as predictors of elemental Pb flux in the sediment (Table IV.3). While additional monitoring variables were investigated, these variables did not account for a significant improvement of variance mean-square error in sedimentary Pb accumulation, after accounting for variance explained by lake-water DOC and conductivity. When considering trends in epilimnetic lake-water DOC, we observed an increase for lakes impacted by experimental eutrophication, especially in Lake 227 where this increase was the strongest. Following these increases, we observed a relative decrease of epilimnetic DOC during the 1980

- 1990 CE in all lakes. This reduction of lake-water DOC, however, was less striking in eutrophied and reference lakes than in the acidified lake (Figure IV.3).

Discussion

Temporal accumulation of Pb in Experimental Lakes

In support of our original hypotheses, we observed significant differences in the pattern of Pb accumulation in the sediment profiles of the experimentally manipulated lakes. Considering the temporal variation in Pb concentration and Pb flux, eutrophied and reference lakes displayed a "typical" pattern of Pb accumulation with relatively constant concentrations and accumulation between ca. 1880 – 1950 CE, before a period of increased accumulation between ca. 1954 – 1983 CE, followed by a decline back to original concentrations and fluxes. These trends echo observations from numerous lakes across central and eastern Canada (e.g., Dunnington et al., 2020b) and globally (e.g., Siver and Wizniak, 2001), where, through the combustion of coal, fossil fuels and leaded gasoline (Nriagu, 1998), a large quantity of Pb has been emitted and deposited across the landscape. While eutrophied and reference lakes displayed a similar pattern of Pb accumulation, the sediments of eutrophied lakes were found to exhibit a significantly greater rate of Pb accumulation during experimental manipulation as demonstrated from the results of the ANOVA and post-hoc tests comparing slopes in Pb accumulation during ca. 1954 – 1983 CE. In the context of the acidified lake, the GAMMs tracked only muted increases in Pb levels when considering Pb concentrations and Pb flux compared to other lakes (Figure IV.2). The results from the ANOVA and post-hoc tests corroborated these findings, indicating that, during the experimental period, the acidified lake had accumulated significantly lower Pb than eutrophied lakes, but these differences were not significant when compared to reference lakes.

As some authors have reported, using mass accumulation rates to calculate elemental flux has the potential to improve interpretability (Lamborg et al., 2002; Engstrom and Rose, 2013) but can also introduce uncertainties associated with sediment chronologies and its interpolation (Engstrom and Wright Jr, 1984; Dunnington et al., 2020a). In our case, the calculation of sediment-focused corrected elemental Pb flux yielded improved interpretability, especially when considering Pb accumulation in the basins of Lake 226. While the measured Pb concentrations in the two basins were similar, we observed significant differences in the Pb fluxes, with a greater rate and magnitude of accumulation in Lake 226N, reflective of the contrasting experimental fertilization history (only north basin received P addition). Another interesting observation is the difference between the Pb concentrations and fluxes in Lake 223. While there was a relatively small increase in Pb concentrations recorded from the core of Lake 223, the calculation of Pb fluxes yielded a notable increase in Pb accumulation. This increase in Pb flux was mediated via increased MARs, recorded to have increased 3 – 5 fold since the early 1900s, possibly due to decreased organic matter decomposition or following increased primary productivity, resulting from increased lake transparency. There were less marked differences when comparing Pb concentrations and fluxes across Reference lakes and Lake 227. Overall, we expect the calculation of elemental flux to be an important component in the calculation of elemental mass balances and to allow for a greater interpretability when comparing lakes from similar regions, where the delivery processes are similar but where sediment ontogeny and accumulation rates are expected to play an important contribution.

Limnological control on Pb mobilization and sediment accumulation

When considering potential variables associated with the varying responses of Pb accumulation in the sediment of these manipulated lakes, we observed a significant association with epilimnetic DOC and conductivity. An increased fraction of dissolved organic matter in eutrophied lakes as a result of the experimental fertilization likely contributed greater binding sites for Pb ions leading to its increased burial in the sediment. These results are in line with regional surveys and local case studies that have demonstrated the important association between organic matter and metal abundance in boreal lakes (Outridge et al., 2007; Muir et al., 2009; Ma et al., 2013). Regarding conductivity, it is possible that the observed relationship with Pb accumulation stems from the increased emission and deposition of metals and other elements during this period (Dixit et al., 1992), resulting in increased measured conductivity. Contrary to our original hypothesis, however, pH was not selected as a significant variable accounting for variation in elemental Pb accumulation. Given that important diel pH and other limnological fluctuations have been observed in Lake 227 during the experimental fertilization period (Schindler and Fee, 1973; unpublished data) and that pH readings can vary depending on the time-of-day measurements were made, this noise may have prevented a clear signal to be detected between epilimnetic pH and Pb accumulation in this lake. Furthermore, the removal of Lake 302 from our dataset due to chronological concerns also limited our ability to detect a statistical relationship with pH. Nonetheless, the visual representation of the various epilimnetic variables monitored from the IISD-ELA still enabled insights into the potential effects that lakewater pH could have in some lakes on the accumulation of Pb in the sediment. Specifically, in Lake 223 we observed an association between pH and epilimnetic DOC, whereby experimental acidification via addition of H_2SO_4 decreased the pH and led to a decrease in epilimnetic DOC. A similar reduction during this time period in epilimnetic DOC was also recorded for eutrophied and reference lakes, albeit more modest in magnitude. It is probable that DOC reduction in these lakes was mediated by both increased long-range atmospheric acid deposition and modification in the run-off from streamflow, associated with droughts, during the 1970-1980s (Schindler et al., 1990; Schindler et al., 1997; Hesslein et al., 2009; Meyer-Jacob et al. 2019; Imtiazy et al., 2020). As many authors have reported, the concentration of epilimnetic DOC in lakes of the IISD-ELA primarily results from allochthonous sources of DOC which is mainly fed to lakes via rivers and run off carrying soil organic matter (Solomon et al., 2015). Located approximately 1000 km North-West of Sudbury, a region renowned for its metallurgical industries that was particularly affected by acid deposition, the IISD-ELA is considered a region of relatively low acid deposition (Meyer-Jacob et al., 2019). It is still expected, however, that a fraction of elemental emissions, carried by wind and air currents, make their way to the lakes of the IISD-ELA (ECCC, 2019).

Mechanistic Pb accumulation in relation to experimental manipulations

One of the main differences when considering the “usual scenario” associated with environmental acidification and the experimental acidification carried out at the IISD-ELA is that typically acid deposition occurs simultaneously over lakes and their catchments. Wet and dry acid deposition of sulfur and nitrogen oxides (SO_x and NO_x) will increase chemical weathering via increased acidity. As described above, soil organic matter is expected to be altered under acid conditions, favoring the leaching of metals present in the soil and rocks of the catchment

(Bergkvist, 1987; Mannings et al., 1996). This phenomenon often results in an increased fraction of metals entering the lakes, which is often depicted as a relative increase of the metal fraction accumulating in lake sediments. These over-arching effects of acid deposition on the mobilization of metals from the catchment combined with the variability associated with metal emissions impede our understanding of the in-lake mechanisms associated with metal accumulation and acid deposition. Our approach, investigating the sediment record of lakes subjected to in-lake acidification with relatively low atmospheric deposition of SO_x and NO_x, has enabled the isolation of in-lake acid-mediated responses (with very modest catchment influences).

Mechanistically, we expected lakewater pH to exert an important control over Pb accumulation in lake sediment. This control of pH is expected to occur via multiple pathways (Figure IV.4), influencing both allochthonous and autochthonous sources of DOC. Reduction in epilimnetic DOC associated with acidification has been well documented (Davis et al., 1985) with multiple observations of increased lake's transparency in lakes of IISD-ELA (Schindler et al., 1980; Schindler et al., 1990) as well as other base-poor regions of the world (Jensen and Snekvik, 1972; Olsson and Pettersson, 1993; Fölster et al., 2014). The reduction in autochthonous DOC is mainly expected to occur through additional protonation (i.e., the addition of a hydrogen ion to an atom) found at acidic pH, exposing organic acids and phenols to protons, leading to the reduction of these molecules, which compose the greater bulk of DOC (Pettit, 2004; Koopal et al., 2005; Dryer et al., 2008; Pontoni et al., 2021). As such, individual organic acid molecules will not conglomerate, preventing the formation of larger DOC-metal complexes (Aiken et al., 2011; Dixon, 2013). Inputs of allochthonous sources of DOC are expected to decline with acidic pH via interactions with other ions in the soil organic matter under low pH conditions (Clark et al., 2006; Monteith et al., 2007). In turn, this reduction in epilimnetic DOC and particulate matter will have the consequence of providing fewer binding sites for free-flowing Pb ions present in the water, potentially leading to less Pb accumulation the sediment. Secondly, acidity has also been shown to impact the speciation of numerous metals favoring the ionic-soluble forms of metals (Stumm and Morgan, 2012), again potentially leading to less Pb accumulation in sediments under acidic conditions.

When considering eutrophied systems and the alkaline pH associated with experimental fertilization, higher pH is expected to favor the complexation of Pb ions with humic substances (Likens, 2009; Boguta and Sokołowska, 2016). In these systems, we also expect increased primary production fueled by nutrient addition to generate a greater fraction of autochthonous DOC and increased phytoplankton levels. In turn, increased concentrations of DOC and phytoplankton cells offer a greater abundance of effective binding sites for Pb, which will form particulate matter leading to Pb burial and accumulation in lake sediments. It is likely that additional mechanisms associated with eutrophication contribute to the mediation of Pb burial. For example, some authors have demonstrated the scavenging activity of algal taxa (Outridge et al., 2019) that has the potential to contribute to higher rates of Pb accumulation in the sediment.

Our investigation targeting the influence of experimental manipulations allowed us to isolate the influence of in-lake acidification and eutrophication on the accumulation of elemental Pb. While our approach does not simulate the expected pattern of atmospheric deposition and lateral transport, since catchment dynamics are minimal, our approach serves to improve our understanding of the dynamics and mechanisms that occur within the lakes' water columns and at the water-sediment interface. Our investigation aims to build upon field surveys where the effects of acidification on the accumulation of metals are often masked by the contribution of catchment dynamics. Our findings also highlight the observation that, while lake sediments are important archives of environmental change, sediment records are continuously shaped by surrounding environmental conditions. As such, a careful contextualization of the trends analyzed is required to properly address changes in sediment accumulation and composition over time. When considering regional surveys of lake sediment metal concentrations, it is possible the concentrations of metals measured in lake sediments from sites impacted by acid deposition are under-estimating the deposition and catchment-mediated leaching of metals into lake ecosystems. Conversely, eutrophic conditions in lakes have the potential to overestimate metal deposition. While regional and other large-scale field surveys cannot rely on yearly water column monitoring data to gain insights into such processes, other proxies, such as diatom reconstructions, quantification of sediment carbon-to-nitrogen ratio and the use of sedimentary flux, might be beneficial to contextualize some of the accumulation trends in metals.

Conclusion

Using dated sediment cores retrieved from experimentally manipulated and reference lakes, we highlighted the influential role of acidification and eutrophication on the accumulation of Pb in lake sediments. Our results suggest that experimental acidification, through the reduction of lakewater pH and its effects on DOC, may have reduced Pb accumulation rates. However, with only one lake targeted by experimental acidification, we failed to detect a significant difference when comparing slopes for Lake 223 and our reference lakes and thus recommend future investigations should be conducted on the potential for acidification to reduce sedimentary Pb accumulation. Meanwhile experimental eutrophication, through increases in epilimnetic water DOC and chlorophyll-*a*, led to a significantly greater abundance of Pb accumulating in sediment. Together, these results highlight the mechanistic relationships between DOC, which offers high binding capacity to form DOC-metal complexes, and acidity, which reduces DOC's binding capacity through increased protonation. Our results also have implications for regional field surveys, where it is likely that concentrations and the accumulation of Pb recorded in sediments are being modulated by the effects of lake acidification and eutrophication.

Acknowledgements

This research was supported by an FRQNT Team Research Grant awarded to IGE, PF and JPS. In addition, the collection of the sediment cores and associated environmental data was made possible through the NSERC Canadian Lake Pulse network, of which IGE and are co-PIs. We are also grateful to FRQNT for providing AB with a Doctoral scholarship and the Canada Research Chairs program for providing funding to IGE and PF. We would also like to acknowledge lab support by Michelle Gros and Chris Grooms, and the LakePulse field teams and director, Dr. Yannick Huot. Data on lake-water chemistry were provided by the IISD-ELA and analyses were completed by the IISD-ELA Chemical Laboratory under the direction of Sonya Havens. Feedback by members of the Gregory-Eaves' lab as well as by two anonymous reviewers also helped to improve the quality of this manuscript.

Data Availability Statement

Measured elemental Pb concentrations, radioisotopic activity profiles, calculated dates and mass accumulation rates were made available to the open science platform Zenodo accessible at https://zenodo.org/record/7429531.

References

Aiken, G.R., Hsu-Kim, H., Ryan, J.N., 2011. Influence of dissolved organic matter on the environmental fate of metals, nanoparticles, and colloids. ACS Publications

Anderson, R.F., Schiff, S.L., Hesslein, R.H., 1987. Determining sediment accumulation and mixing rates using 210Pb, 137Cs, and other tracers: problems due to postdepositional mobility or coring artifacts. Can. J. Fish. Aquat. Sci., 44, s231-s250.

Appleby, P.G., 2002. Chronostratigraphic Techniques in Recent Sediments. In: Last, W.M., Smol, J.P. (eds) Tracking Environmental Change Using Lake Sediments. Developments in Paleoenvironmental Research, vol 1. Springer, Dordrecht. https://doi.org/10.1007/0-306-47669-X_9.

Baud, A., Aulard, C., Ghanbari, H., Fradette, M., Antoniades, D., Del Giorgio, P., Huot, Y., Francus, P., Smol, J., Gregory-Eaves, I., 2022. A framework for ^{210}Pb model selection and its application to 37 cores from Eastern Canada to identify the dynamics and drivers of lake sedimentation rates. Earth Surf. Process Landf. https://doi.org/10.1002/esp.5391

Bergkvist, B., 1987. Soil solution chemistry and metal budgets of spruce forest ecosystems in S. Sweden. Water, Air, Soil Pollut., 33, 131-154.

Bird, G., Stephenson, M., Roshon, R., Schwartz, W., Motycka, M., 1995. Fate of ^{60}Co and ^{134}Cs added to the hypolimnion of a Canadian Shield lake. Can. J. Fish. Aquat. Sci., 52, 2276-2289.

Blomqvist, S., 1991. Quantitative sampling of soft-bottom sediments: problems and solutions. Mar. Ecol. Prog. Ser., 72, 295-304.

Boguta, P., Sokołowska, Z., 2016. Interactions of Zn (II) ions with humic acids isolated from various type of soils. Effect of pH, Zn concentrations and humic acids chemical properties. PLoS One, 11, e0153626.

Brunskill, G., Schindler, D., 1971. Geography and bathymetry of selected lake basins, Experimental Lakes Area, northwestern Ontario. Journal of the Fisheries Board of Canada, 28, 139-155.

CCME, 2022. Canadian Sediment Quality Guidelines for the Protection of Aquatic Life

Chowdhury, S., Mazumder, M.J., Al-Attas, O., Husain, T., 2016. Heavy metals in drinking water: occurrences, implications, and future needs in developing countries. Sci. Total Environ., 569, 476-488.

Chuan, M., Shu, G., Liu, J., 1996. Solubility of heavy metals in a contaminated soil: effects of redox potential and pH. Water, Air, Soil Pollut., 90, 543-556.

Clark, J.M., Chapman, P.J., Heathwaite, A.L., Adamson, J.K., 2006. Suppression of dissolved organic carbon by sulfate induced acidification during simulated droughts. Environ. Sci. Technol., 40, 1776-1783.

National Research Council, 1986. Acid deposition: Long-term trends. National Academies Press. 030903647X.

Crusius, J., Anderson, R.F., 1995. Sediment focusing in six small lakes inferred from radionuclide profiles. J. Paleolimnol., 13, 143-155.

D. Bates, M.M., B. Bolker and S. Walker, 2015. Fitting Linear Mixed-Effects Models Using {lme4}. J. Stat. Softw., 67, 1 - 48. https://doi.org/10.18637/jss.v067.i01

Davis, R.B., Anderson, D.S., Berge, F., 1985. Palaeolimnological evidence that lake acidification is accompanied by loss of organic matter. Nature, 316, 436-438.

Dixit, S.S., Dixit, A.S., Evans, R.D., 1987. Paleolimnological evidence of recent acidification in two Sudbury (Canada) lakes. Sci. Total Environ., 67, 53-67.

Dixit, S.S., Dixit, A.S., Smol, J.P., 1992. Assessment of changes in lake water chemistry in Sudbury area lakes since preindustrial times. Can. J. Fish. Aquat. Sci., 49, 8-16.

Dixon, J.C., 2013. 4.14 Chemical Weathering in cold climates. in: Shroder, J.F. (Ed.), Treatise on Geomorphology. Academic Press, San Diego, pp. 245-257.

Dryer, D.J., Korshin, G.V., Fabbricino, M., 2008. In situ examination of the protonation behavior of fulvic acids using differential absorbance spectroscopy. Environ. Sci. Technol., 42, 6644-6649.

Dunnington, D.W., Gregory, B.R., Spooner, I.S., White, C.E., Gagnon, G.A., 2020a. Evaluating the performance of calculated elemental measures in sediment archives. J. Paleolimnol., 64, 155-166.

Dunnington, D.W., Roberts, S., Norton, S.A., Spooner, I.S., Kurek, J., Kirk, J.L., Muir, D.C., White, C.E., Gagnon, G.A., 2020b. The distribution and transport of lead over two centuries as recorded by lake sediments from northeastern North America. Sci. Total Environ., 737, 140212. https://doi.org/10.1016/j.scitotenv.2020.140212

Dupas, R., Delmas, M., Dorioz, J.-M., Garnier, J., Moatar, F., Gascuel-Odoux, C., 2015. Assessing the impact of agricultural pressures on N and P loads and eutrophication risk. Ecol. Indicators, 48, 396-407.

Duruibe, J.O., Ogwuegbu, M., Egwurugwu, J., 2007. Heavy metal pollution and human biotoxic effects. International Journal of physical sciences, 2, 112-118.

ECCC, 2021. Canadian Air and Precipitation Monitoring Network (CAPMoN). in: Canada, E.a.C.C. (Ed.)

ECCC, 2022. Canada's air pollutant emissions inventory report.

ECCC, 2019. Atmospheric Precipitation Chemistry - Wet Deposition Maps

Elser, J.J., Sterner, R.W., Galford, A.E., Chrzanowski, T.H., Findlay, D.L., Mills, K.H., Paterson, M.J., Stainton, M.P., Schindler, D.W., 2000. Pelagic C: N: P stoichiometry in a eutrophied lake: responses to a whole-lake food-web manipulation. Ecosystems, 3, 293-307.

Emerson, S., Hesslein, R., 1973. Distribution and uptake of artificially introduced radium-226 in a small lake. Journal of the Fisheries Board of Canada, 30, 1485-1490.

Engstrom, D.R., Rose, N.L., 2013. A whole-basin, mass-balance approach to paleolimnology. J. Paleolimnol., 49, 333-347. https://doi.org/10.1007/s10933-012-9675-5

Engstrom, D.R., Wright Jr, H., 1984. Chemical stratigraphy of lake sediments as a record of environmental change. Lake sediments and environmental history: studies in palaeolimnology and palaeoecology in honour of Winifred Tutin/edited by EY Haworth and JWG Lund

Findlay, D., Kasian, S., 1986. Phytoplankton community responses to acidification of Lake 223, Experimental Lakes Area, northwestern Ontario. Water, Air, Soil Pollut., 30, 719-726.

Findlay, D., Kasian, S., 1987. Phytoplankton community responses to nutrient addition in Lake 226, Experimental Lakes Area, northwestern Ontario. Can. J. Fish. Aquat. Sci., 44, s35-s46.

Fleischer, M., 1954. The abundance and distribution of the chemical elements in the earth's crust. J. Chem. Educ., 31, 446.

Fölster, J., Johnson, R.K., Futter, M.N., Wilander, A., 2014. The Swedish monitoring of surface waters: 50 years of adaptive monitoring. Ambio, 43, 3-18.

Hesslein, R., Broecker, W., Schindler, D., 1980. Fates of metal radiotracers added to a whole lake: sediment–water interactions. Can. J. Fish. Aquat. Sci., 37, 378-386.

Hesslein, R.H., 1987. Whole-lake metal radiotracer movement in fertilized lake basins. Can. J. Fish. Aquat. Sci., 44, s74-s82.

Hesslein, R. H., Turner, M. A., Guss, D., Lyng, M., 2009. Separating the effects on water chemistry of climate variation and experimental manipulation in the long-term acidification and recovery of lakes. Can. J. Fish. Aquat. Sci., 66(11), 1864-1874.Higgins, S.N., Paterson, M.J., Hecky, R.E., Schindler, D.W., Venkiteswaran, J.J., Findlay, D.L., 2018. Biological nitrogen fixation prevents the response of a eutrophic lake to reduced loading of nitrogen: evidence from a 46-year whole-lake experiment. Ecosystems, 21, 1088-1100.

Huang, H., Mangal, V., Rennie, M.D., Tong, H., Simpson, M.J., Mitchell, C.P., 2022. Mercury methylation and methylmercury demethylation in boreal lake sediment with legacy sulphate pollution. Environ Sci Process Impacts

Imtiazy, M.N., Paterson, A.M., Higgins, S.N., Yao, H., Couture, S., Hudson, J.J., 2020. Dissolved organic carbon in eastern Canadian lakes: novel patterns and relationships with regional and global factors. Sci. Total Environ., 726, 138400.

Jain, C., Ram, D., 1997. Adsorption of metal ions on bed sediments. Hydrol. Sci. J., 42, 713-723.

Jensen, K., Snekvik, E., 1972. Low pH levels wipe out salmon and trout populations in southernmost Norway. Ambio;(Norway), 1

Jeremiason, J.D., Eisenreich, S.J., Paterson, M.J., 1999. Accumulation and recycling of PCBs and PAHs in artificially eutrophied Lake 227. Can. J. Fish. Aquat. Sci., 56, 650-660.

Koopal, L., Saito, T., Pinheiro, J., Van Riemsdijk, W., 2005. Ion binding to natural organic matter: General considerations and the NICA–Donnan model. Colloids Surf. Physicochem. Eng. Aspects, 265, 40-54.

Lamborg, C., Fitzgerald, W., Damman, A., Benoit, J., Balcom, P., Engstrom, D., 2002. Modern and historic atmospheric mercury fluxes in both hemispheres: global and regional mercury cycling implications. Global Biogeochem Cycles, 16, 51-1-51-11.

Leavitt, P., Findlay, D., 1994. Comparison of fossil pigments with 20 years of phytoplankton data from eutrophic Lake 227, Experimental Lakes Area, Ontario. Can. J. Fish. Aquat. Sci., 51, 2286-2299

Lenth, R.V., 2016. Least-Squares Means: The {R} Package {lsmeans}. J. Stat. Softw., 69, 1-33. doi:10.18637/jss.v069.i01

Likens, G.E., 2009. Encyclopedia of inland waters. Elsevier. 0123706262

Likens, G.E., Wright, R.F., Galloway, J.N., Butler, T.J., 1979. Acid rain. Scientific American, 241, 43-51

Ma, J., Hintelmann, H., Kirk, J.L., Muir, D.C., 2013. Mercury concentrations and mercury isotope composition in lake sediment cores from the vicinity of a metal smelting facility in Flin Flon, Manitoba. Chem. Geol., 336, 96-102

Mannings, S., Smith, S., Bell, J., 1996. Effect of acid deposition on soil acidification and metal mobilisation. Appl. Geochem., 11, 139-143

Maranón, E., Cermeno, P., Fernández, E., Rodríguez, J., Zabala, L., 2004. Significance and mechanisms of photosynthetic production of dissolved organic carbon in a coastal eutrophic ecosystem. Limnol. Oceanogr., 49, 1652-1666

McBride, M., 1989. Reactions controlling heavy metal solubility in soils, Adv. Soil Sci., Springer, pp. 1-56.

McCullough, G., Campbell, P., 1993. Lake variation and climate change study: ELA Lakes, 1968-1990. II. Watershed geography and lake morphometry. Canadian Technical Report of Fisheries and Aquatic Sciences. 1-32.

Meyer-Jacob, C., Michelutti, N., Paterson, A.M., Cumming, B.F., Keller, W.B., Smol, J.P., 2019. The browning and re-browning of lakes: Divergent lake-water organic carbon trends linked to acid deposition and climate change. Scientific reports, 9, (16676), 1-10

Mohod, C.V., Dhote, J., 2013. Review of heavy metals in drinking water and their effect on human health. International Journal of Innovative Research in Science, Engineering and Technology, 2, 2992-2996

Monteith, D.T., Stoddard, J.L., Evans, C.D., De Wit, H.A., Forsius, M., Høgåsen, T., Wilander, A., Skjelkvåle, B.L., Jeffries, D.S., Vuorenmaa, J., 2007. Dissolved organic carbon trends resulting from changes in atmospheric deposition chemistry. Nature, 450, 537-540

Muggeo, V.M., Muggeo, M.V.M., 2017. Package ‘segmented’. Biome, 58, 516

Muir, D., Wang, X., Yang, F., Nguyen, N., Jackson, T., Evans, M., Douglas, M., Kock, G., Lamoureux, S., Pienitz, R., 2009. Spatial trends and historical deposition of mercury in eastern and northern Canada inferred from lake sediment cores. Environ. Sci. Technol., 43, 4802-4809

NSERC Canadian Lake Pulse Network, N.C.L.P., 2021. NSERC Canadian Lake Pulse Network Field Manual 2017 – 2018 - 2019 surveys. (M-P. Varin, M. Beaulieu, & Y. Huot, Eds.). Univresité de Sherbrooke

Nriagu, J.O., 1998. Tales told in lead. Science, 281, 1622-1623

O'Connell, D., Ansems, N., Kukkadapu, R., Jaisi, D., Orihel, D., Cade-Menun, B., Hu, Y., Wiklund, J., Hall, R., Chessell, H., 2020. Changes in sedimentary phosphorus burial following artificial eutrophication of Lake 227, Experimental Lakes Area, Ontario, Canada. J Geophys Res Biogeosci, 125, e2020JG005713

Olsson, H., Pettersson, A., 1993. Oligotrophication of acidified lakes: a review of hypotheses. Ambio, 312-317

Outridge, P., Sanei, H., Stern, G., Hamilton, P., Goodarzi, F., 2007. Evidence for control of mercury accumulation rates in Canadian High Arctic lake sediments by variations of aquatic primary productivity. Environ. Sci. Technol., 41, 5259-5265

Outridge, P., Stern, G., Hamilton, P., Sanei, H., 2019. Algal scavenging of mercury in preindustrial Arctic lakes. Limnol. Oceanogr., 64, 1558-1571

Pettit, R.E., 2004. Organic matter, humus, humate, humic acid, fulvic acid and humin: their importance in soil fertility and plant health. CTI Research, 10, 1-7

Pontoni, L., La Vecchia, C., Boguta, P., Sirakov, M., D'Aniello, E., Fabbricino, M., Locascio, A., 2021. Natural organic matter controls metal speciation and toxicity for marine organisms: a review. Environ Chem Lett, 1-16

Powell, R., Wharton, L., 1982. Development of the Canadian Clean Air Act. J Air Pollut Control Assoc, 32, 62-65

Pulatsü, S., Topçu, A., 2015. Review of 15 years of research on sediment heavy metal contents and sediment nutrient release in inland aquatic ecosystems, Turkey. J. Water Resource Prot., 7, 85

Sanchez-Cabeza, J. A., & Ruiz-Fernández, A. C., 2012. ^{210}Pb sediment radiochronology: an integrated formulation and classification of dating models. Geochim. Cosmochim. Acta, 82, 183-200. https://doi.org/10.1016/j.gca.2010.12.024.

Schindler, D., Armstrong, F., Holmgren, S., Brunskill, G., 1971. Eutrophication of Lake 227, Experimental Lakes Area, northwestern Ontario, by addition of phosphate and nitrate. Journal of the Fisheries Board of Canada, 28, 1763-1782.

Schindler, D.W., Fee, E.J., 1973, Diurnal variation of dissolved inorganic carbon and its use in estimating primary production and CO2 invasion in Lake 227. Journal of the Fisheries Board of Canada, 30(10), 1501-1510.

Schindler, D., Frost, T., Mills, K., Chang, P., Davies, I., Findlay, L., Malley, D., Shearer, J., Turner, M., Garrison, P., 1990. Comparisons between experimentally-and atmospherically-acidified lakes during stress and recovery. Proceedings of the Royal Society of Edinburfgh, Section B: Biological Sciences, 97, 193-226.

Schindler, D. W., Curtis, P. J., Bayley, S. E., Parker, B. R., Beaty, K. G., & Stainton, M. P. (1997). Climate-induced changes in the dissolved organic carbon budgets of boreal lakes. Biochem., 36(1), 9-28.

Schindler, D., Hesslein, R., Wagemann, R., Broecker, W., 1980. Effects of acidification on mobilization of heavy metals and radionuclides from the sediments of a freshwater lake. Can. J. Fish. Aquat. Sci., 37, 373-377.

Schindler, D., Mills, K., Malley, D., Findlay, D., Shearer, J., Davies, I., Turner, M., Linsey, G., Cruikshank, D., 1985. Long-term ecosystem stress: the effects of years of experimental acidification on a small lake. Science, 228, 1395-1401.

Schindler, D.W., Hecky, R., Findlay, D., Stainton, M., Parker, B., Paterson, M., Beaty, K., Lyng, M., Kasian, S., 2008. Eutrophication of lakes cannot be controlled by reducing nitrogen input: results of a 37-year whole-ecosystem experiment. PNAS, 105, 11254-11258.

Simpson, G.L., 2018. Modelling palaeoecological time series using generalised additive models. Front. Ecol. Evol., 6, 149.

Siver, P.A., Wizniak, J.A., 2001. Lead analysis of sediment cores from seven Connecticut lakes. J. Paleolimnol., 26, 1-10.

Smol, J.P., 1992. Paleolimnology: an important tool for effective ecosystem management. J. Aquat. Ecosyst. Health, 1, 49-58.

Smol, J.P., 2009. Pollution of lakes and rivers: a paleoenvironmental perspective. 2nd edition. John Wiley & Sons. 1444307576.

Solomon, C.T., Jones, S.E., Weidel, B.C., Buffam, I., Fork, M.L., Karlsson, J., Larsen, S., Lennon, J.T., Read, J.S., Sadro, S., 2015. Ecosystem consequences of changing inputs of terrestrial dissolved organic matter to lakes: current knowledge and future challenges. Ecosystems, 18, 376-389.

Stainton, M.P, Capel, M. J., & Armstrong, F.A.J., 1977. The chemical analysis of Fresh Water. Can. Fish. Mar. Serv. Misc. Spec. Publ. 25.

Stepanova, O., Trunova, V., Sidorina, A., Zvereva, V., Melgunov, M., Petrovskii, S., Krapivina, S., Fedotov, A., Rakshun, Y.V., 2015. Investigating bottom sediments from proglacial Lake Ehoy (Eastern Sayan Ridge) by means of SR-XRF. Bulletin of the Russian Academy of Sciences: Physics, 79, 118-121.

Stephenson, M., Schwartz, W., Motycka, M., Rowan, D., Kelly, C., Roshon, R., 1995. Fate and distribution in sediments of carbon-14 added to Canadian Shield lakes of differing trophic state. Limnol. Oceanogr., 40, 779-790.

Stumm, W., Morgan, J.J., 2012. Aquatic chemistry: chemical equilibria and rates in natural waters. John Wiley & Sons. 1118591488.

Tchounwou, P.B., Yedjou, C.G., Patlolla, A.K., Sutton, D.J., 2012. Heavy metal toxicity and the environment. Molecular, Clinical and Environmental toxicology, 133-164.

Team, R.C., 2021. R: A language and environment for statistical computing. R Foundation for Statistical Computing. http://www.R-project.org/

Tomkins, J.D., Antoniades, D., Lamoureux, S.F., Vincent, W.F., 2008. A simple and effective method for preserving the sediment–water interface of sediment cores during transport. J. Paleolimnol., 40, 577-582. https://doi.org/10.1007/s10933-007-9175-1

Turner, M.A., Huebert, D.B., Findlay, D.L., Hendzel, L.L., Jansen, W.A., Bodaly, R., Armstrong, L.M., Kasian, S.E., 2005. Divergent impacts of experimental lake-level drawdown on planktonic and benthic plant communities in a boreal forest lake. Can. J. Fish. Aquat. Sci., 62, 991-1003.

Verta, M., Tolonen, K., Simola, H., 1989. History of heavy metal pollution in Finland as recorded by lake sediments. Sci. Total Environ., 87, 1-18.

Weng, L., Temminghoff, E.J., Lofts, S., Tipping, E., Van Riemsdijk, W.H., 2002. Complexation with dissolved organic matter and solubility control of heavy metals in a sandy soil. Environ. Sci. Technol., 36, 4804-4810.

Withers, P., Haygarth, P., 2007. Agriculture, phosphorus and eutrophication: a European perspective. Soil Use Manag., 23, 1-4.

Wolfe, B., Kling, H.J., Brunskill, G.J., Wilkinson, P., 1994. Multiple dating of a freeze core from Lake 227, an experimentally fertilized lake with varved sediments. Can. J. Fish. Aquat. Sci., 51, 2274-2285.

Tables Chapter IV

Table IV.1. Summary of the study lakes organized by experimental condition. Chronology of the relevant experimental manipulations in these lakes is also provided along with key lake morphological variables.

Lake (Latitude, Longitude)	Condition	Experimental Manipulation (Source)	Surface Area (ha)	Max Depth (m)	Volume (10^5 m^3)	Watershed area (ha)
L226 (49.6886, -93.7475)	Eutrophied	**1973:** W/E basins lake division **1973-1980**: Nutrient addition (Findlay and Kasian, 1987) **1977**: Epilimnion spiked with ^{75}Se, ^{203}Hg, ^{85}Sr, ^{134}Cs, ^{59}Fe, ^{60}Co (Hesslein, 1987) **1978**: ^{14}C, ^{226}Ra, and ^{3}H addition **1989**: Hypolimnion spiked with ^{60}Co, ^{134}Cs, ^{3}H (Bird et al., 1995) **1994-1997**: Drawdown experiment (Turner et al., 2005)	16.1	14.7	10.8	97
L227 (49.6879, -93.6889)	Eutrophied	**1969-1974**; 12:1 (N/P) addition (Schindler et al., 2008; Higgins et al., 2018) **1970**: ^{226}Ra addition (Hesslein et al., 1980) **1975**: ^{3}H addition **1975-1989**; 4:1 (N/P) addition **1993-1997**: Northern pike introduction (Elser et al., 2000) **1990-present**: Only P addition	5.0	10.0	2.21	34.4
L223 (49.6983, -93.7087)	Acidified	**1976-1993**: H_2SO_4 addition	27.3	14.4	19.5	259
L302 (49.6741, -93.7628)	Acidified	**1972-1976**: Nutrient addition (Schindler et al., 1980) **1981:** N/S basins lake division **1982-2000**: H_2SO_4 addition (Hesslein, 2009)	23.7	13.8	12.9	103
L224 (49.6903, -93.7173)	Reference	**1976**: ^{14}C and ^{226}Ra addition (Emerson and Hesslein, 1973; Hesslein et al., 1980) **1976**: Epilimnion spiked with ^{75}Se, ^{203}Hg, ^{137}Cs, ^{59}Fe, ^{65}Zn & ^{60}Co	26.1	27.3	30.6	98

		(Hesslein et al., 1980) **1976**: Tritiated Water (^3H) addition				
L373 (49.7438, -93.7999)	Reference	None	27.3	21.2	31.0	83

Table IV.2. Summary of the least-square mean contrasts in the slopes considering maximum elemental Pb loading as determined by breakpoint analysis.

Contrast	Estimated Diff.	Standard Error	Degree of Freedom	t-ratio	p-value (sign. level)
L226N - L226S	0.0074	0.0015	15	4.9	0.0015 (**)
L226N - References	0.0112	0.0014	15	8.0	< .0001 (***)
L226S – References	0.0004	0.0017	15	2.9	0.0680 (-)
L223 – References	-0.0009	0.0012	15	-0.7	0.952 (-)
L227 - References	0.0126	0.0015	15	8.4	< .0001 (***)

Table IV.3. Summary of the linear mixed effects model assessing the predictors associated with elemental Pb accumulation during period with available monitoring data (1971 – 1983 CE).

Effect	Estimate (Std. Error)	Degree of Freedom	t-value	p-value
(Marginal R^2 = 0.224, Conditional R^2 = 0.919)				
Intercept	0.12 (0.079)	22.4	1.53	
DOC Epilimnion	0.025 (0.010)	36.5	2.39	0.022
Conductivity Epilimnion	0.0069 (0.019)	37.2	3.68	< 0.001
DOC * Conductivity Epilimnion	-0.00049 (0.00025)	36.3	-1.98	0.056
Random effects (Proportion of variance explained by LakeID = 0.98)				
LakeID	0.0102 (0.101)			< .001
Residual	0.0012 (0.034)			

In a linear regression, an asterisk (*) denotes an *interaction* which allows for an independent variable (i.e., DOC) to have different effects on the outcome (i.e., Pb accumulation) depending on the values of another independent variable (i.e., conductivity).

Figures Chapter IV

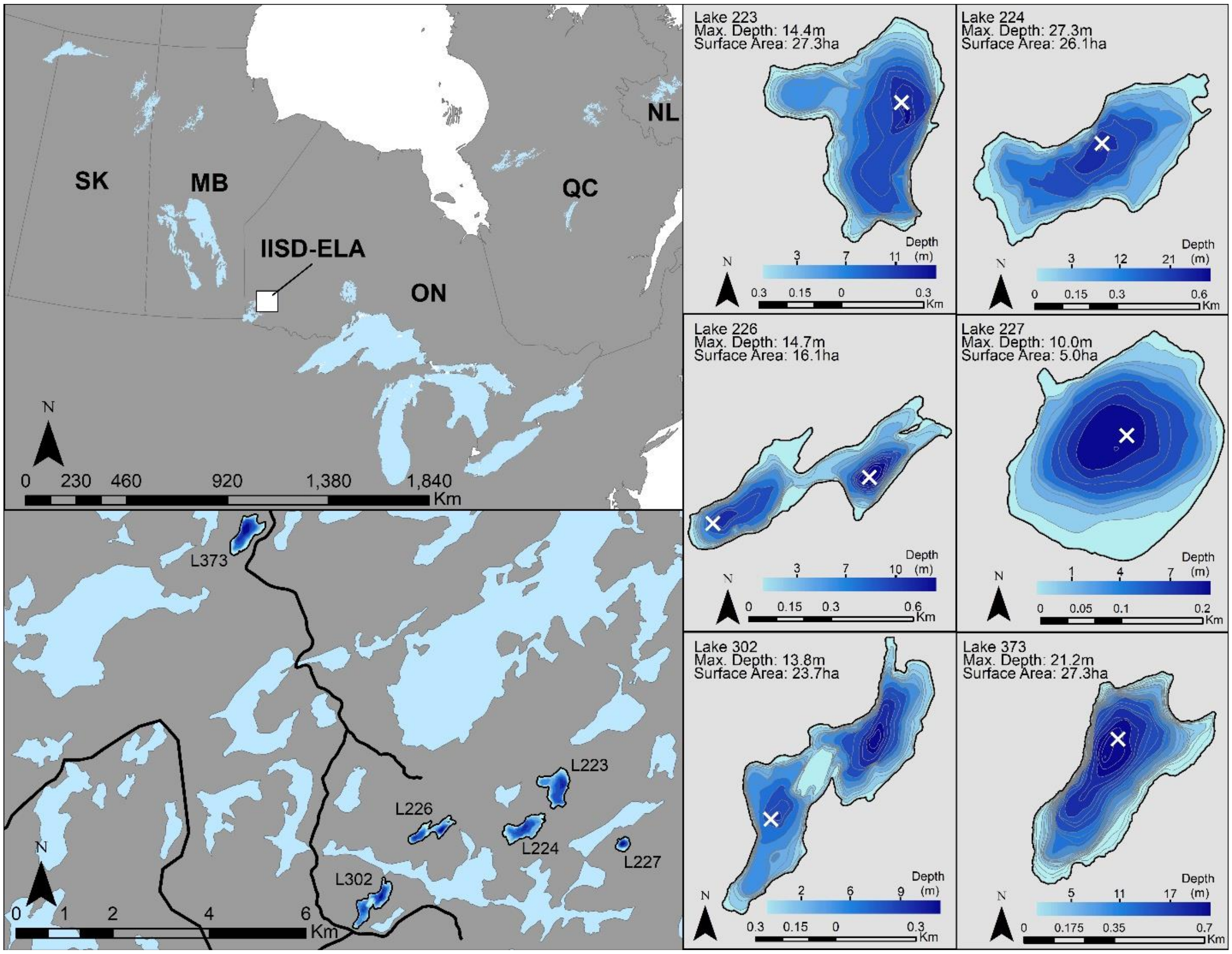

Figure IV.1. Map showing the regional and local geographical location of the six IISD-ELA lakes considered (left). Inset maps represent lake's bathymetry and coring location for each of the seven cores retrieved.

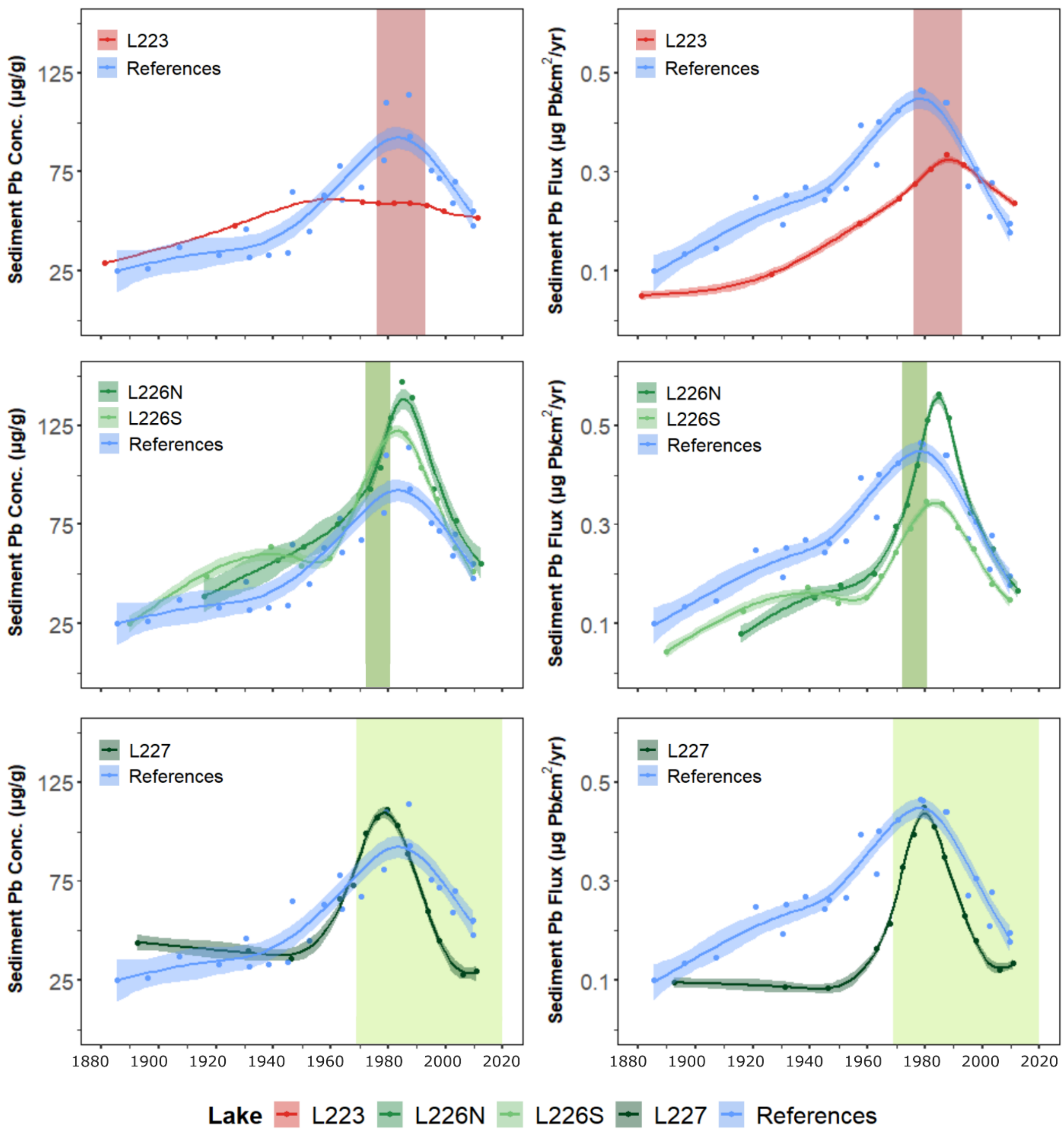

Figure IV.2. Temporal variation in elemental lead concentration (µg/g) (left) and elemental lead flux (µg Pb/cm^2/year) (right) modeled using General Additive Mixed Models (GAMMs) across the two experimental treatments and reference lakes. Acidified lakes are represented in red, eutrophied lakes in green, and reference lakes in blue. Main experimental manipulations are represented by colored rectangles. See Methods for full description of experimental manipulations.

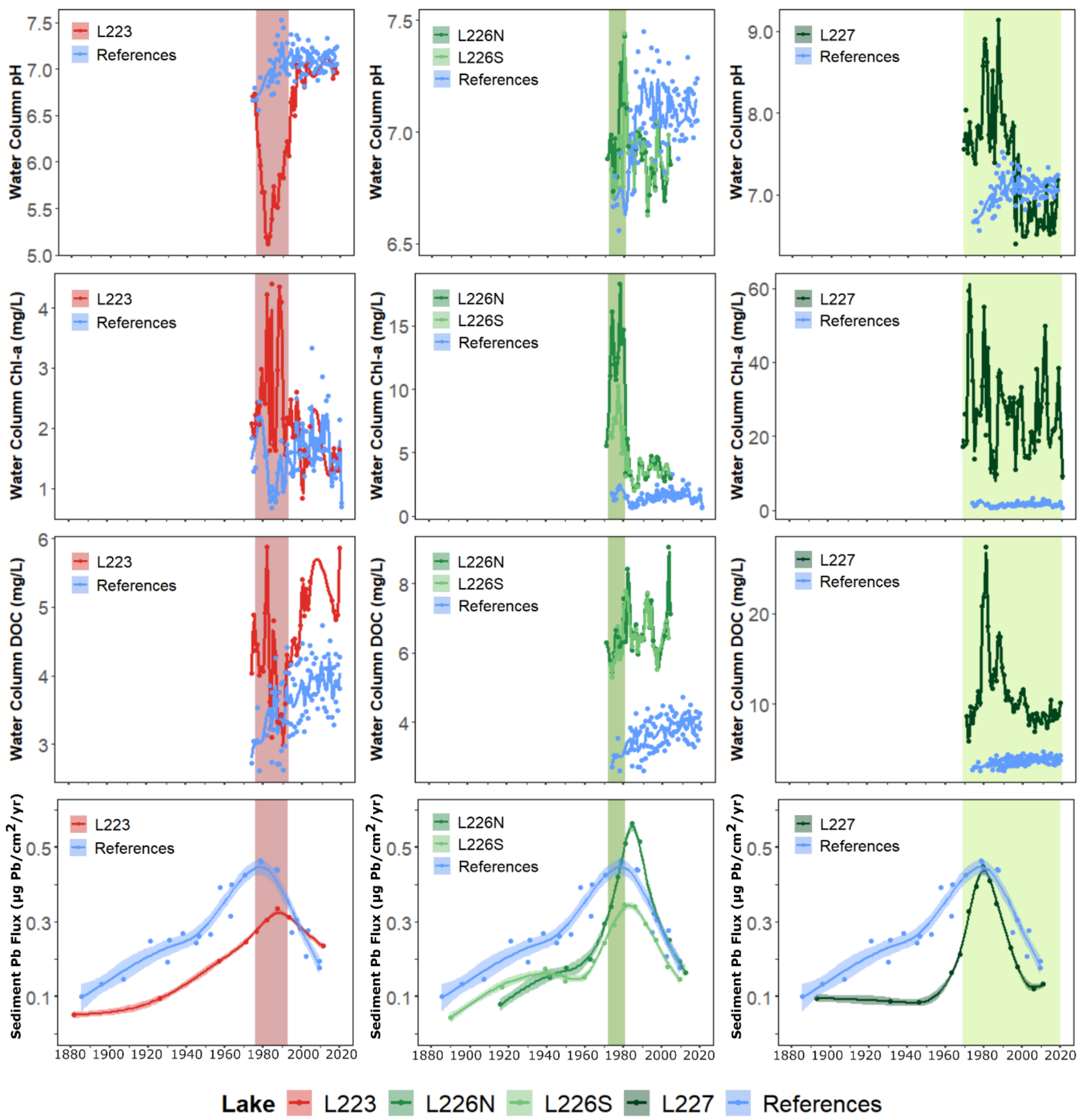

Figure IV.3. Temporal changes in measured limnological variables collected during 1970 – 2020 CE as part of the on-going IISD-ELA monitoring program. From left to right, the three experimental lakes presented: (left) Lake 223 (acidified) and references; (center) Lake 226

North & South (eutrophied) and references; and (right) Lake 227 (eutrophied) and references. *Top*: Water column pH; *Upper Middle*: Water column Chlorophyll-a (Chl-*a*; mg/L); *Lower Middle*: Water column Dissolved Organic Carbon (DOC; mg/L) and *Bottom*: Sediment Pb Flux (µg Pb/cm^2/year). Experimental treatments are color-coded with red representing acidified lakes, green the eutrophied lakes, and blue the reference lakes. Main experimental manipulations are represented by colored rectangles. See Methods for full description of experimental manipulations.

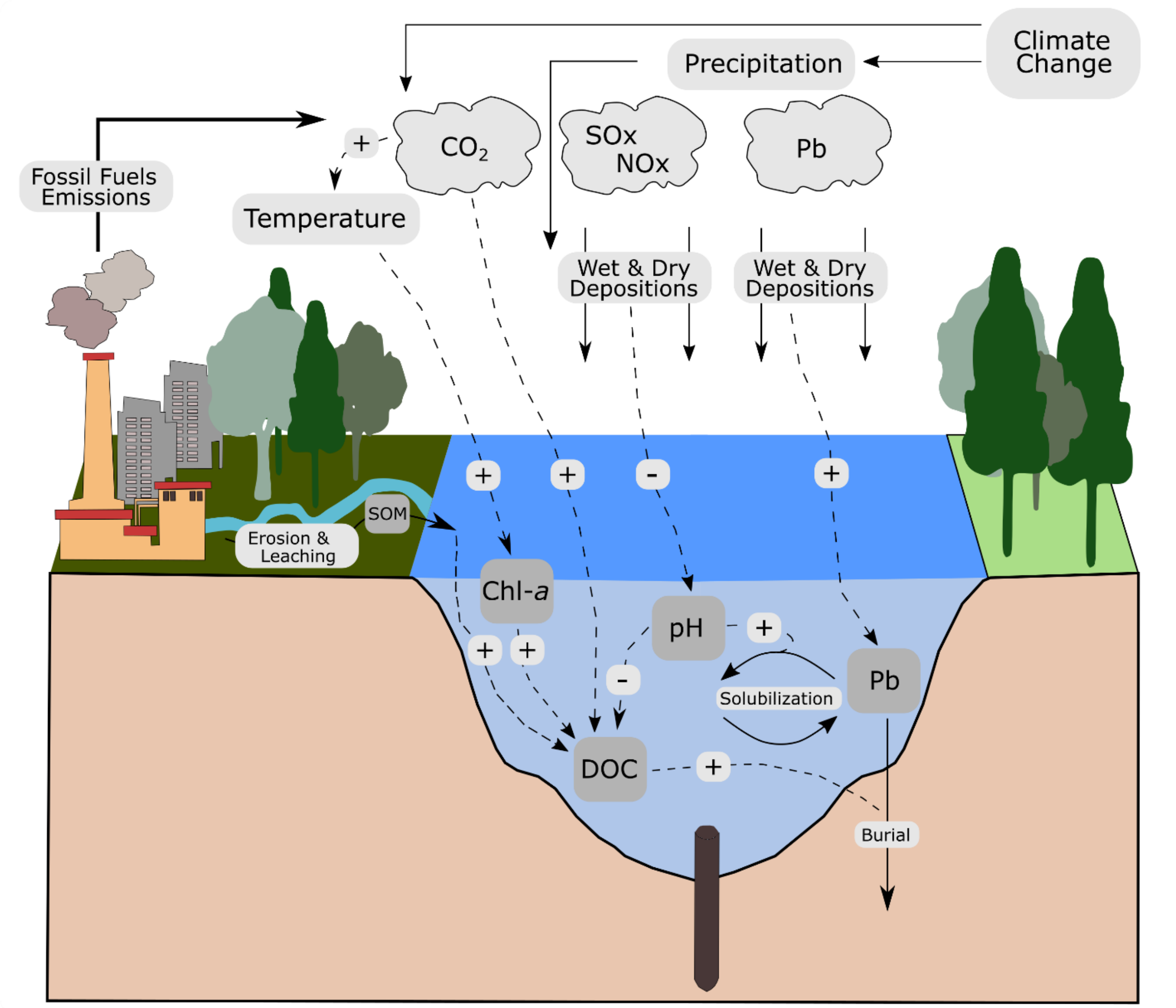

Figure IV.4. Mechanistic diagram summarizing the drivers implicated in the solubilization and burial of environmental lead in lake sediments.

Appendices Chapter IV

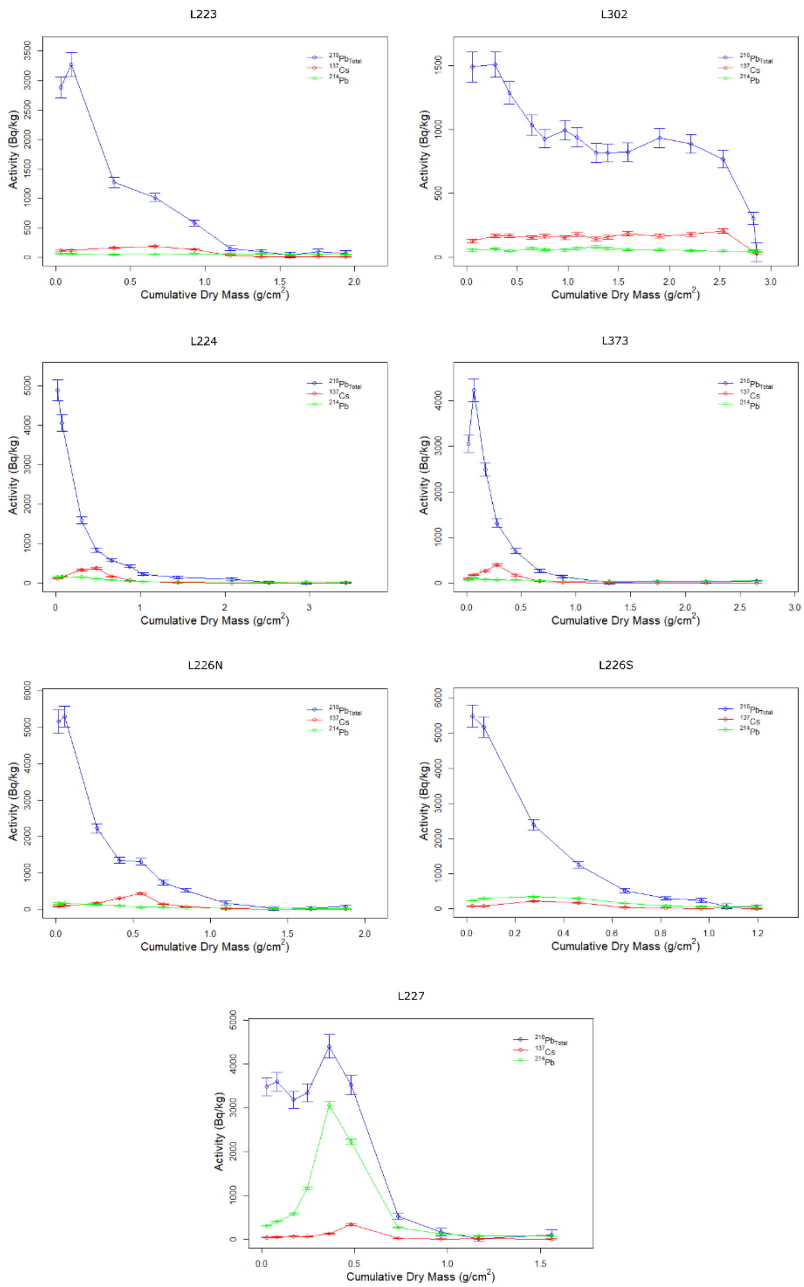

Figure D.1. Radioisotopic profiles for $^{210}Pb_{Total}$, ^{214}Pb and ^{137}Cs (Bq/kg) as a function of cumulative dry mass (g/cm^2) depth (cm) for the 7 lake sediment cores considered. The blue line is the $^{210}Pb_{Total}$, the green line is the ^{214}Pb, and the redline is that ^{137}Cs measurements.

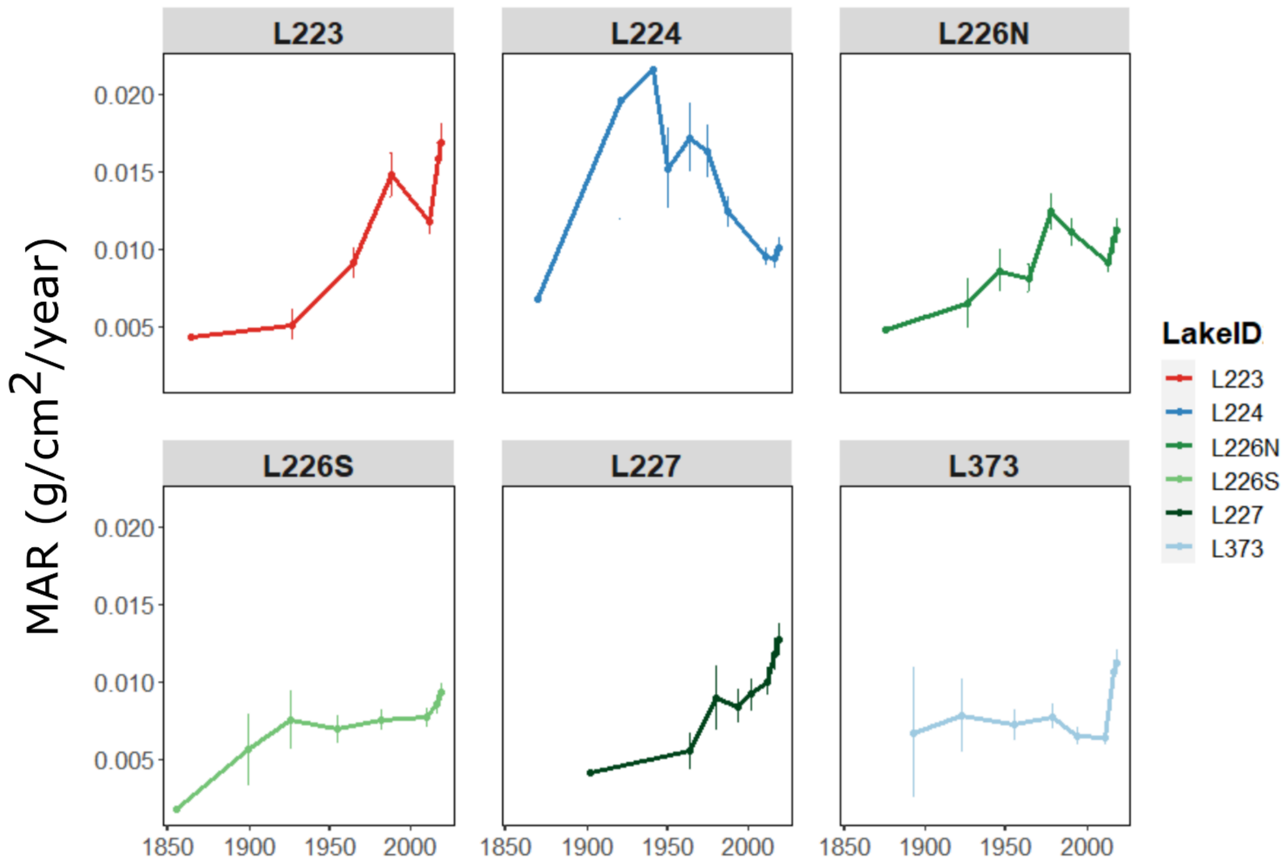

Figure D.2. Mass Accumulation Rate (MAR – g/cm^2/year) as a function of Year (CE) for the 6 lake sediment cores considered in this study. Experimental treatments are color-coded where red corresponds to acidified lakes, green to eutrophied lakes, and blue for reference lakes.

Table D.3. Summary of the parametric and smooth terms from the General Additive Mixed Effect Models (GAMMs) for each of the three experimental treatment levels across elemental Pb focus-corrected flux. For parametric coefficients, the intercept estimate, associated standard error, t-value and p-value with level of significance are reported. For smooth terms, the estimated degrees of freedom (edf), reference estimate degree of freedom (ref.edf), F-value and p-value of each lake partial effects are provided.

Parametric Coefficients	**Estimate**	**Standard Error**	**t-value**	**p-value**
Acidified	0.23	0.012	18.22	< 0.0001
Eutrophied	-0.0094	0.033	-0.69	0.497
Reference	0.095	0.040	6.90	< 0.0001
Smooth Terms	**edf**	**ref.edf**	**F-value**	**p-value**
s(Year):L226N	7.68	8.20	58.35	< 0.0001
s(Year):L226S	5.93	6.85	19.14	< 0.0001
s(Year):L223	3.16	3.77	15.19	< 0.0001
s(Year):L227	6.87	7.62	37.90	< 0.0001
s(Year):References	6.47	7.60	37.62	< 0.0001
s(LakeID)	0.00	4.00	0.00	0.3836

Table D.4. Summary table of the breakpoint analysis investigating the significance of 0, 1 and 2 breakpoints using Bayesian Information Criterion (BIC) in the temporal regression of elemental Pb accumulation, where bold font type corresponds to the selected number of breakpoints. The reported p-values are the overall p-values calculated using *davies.test* hypothesis testing for multiple breakpoints, comparing 0 vs 2 and 1 vs 2 breakpoints, with Bonferroni correction.

Lake	**1st Breakpoint**	**2nd Breakpoint**	**BIC (0 vs. 1 vs. 2 Breakpoints)**	**p-value**
L223	1938	1989	-28.13 vs. -35.98 vs. **-67.95**	0.0084
L226N	1967	1983	-10.65 vs. -20.33 vs. **-60.18**	0.0004
L226S	1963	1983	-28.71 vs. -41.93 vs. **-63.83**	0.0020
L227	1959	1978	-12.41 vs. -21.17 vs. **-46.83**	0.0012
References	1945	1981	-44.38 vs. -104.35 vs. **-157.06**	< 0.0001

Comprehensive Scholarly Discussion and Conclusions

The overarching motivation for this thesis was to investigate the physical and geochemical aspects of broad environmental change archived in lake sediments. To articulate my research projects, two main objectives were sought after: first, to identify the spatial and temporal patterns associated with variation in lake sedimentation rates; and second, to quantify the magnitude and direction of geochemical change experienced by lake sediments and the drivers associated to their distribution and abundance across the landscape. In the first two chapters (Chapter I and Chapter II), I addressed variation in lake sedimentation rates globally and across Eastern Canada and evaluated the influence of anthropogenic development. In the last two chapters (Chapter III and Chapter IV), I turned to the geochemical variation archived in lake sediment and identified the elements most responsible for the observed heterogeneity found in lake sediment elemental abundances. Each of my four chapters, generated insights into the influence of anthropogenic development of various aspects of lake sediments and their functioning. Together, the chapters of this thesis generate original scientific contributions advancing our current knowledge of the magnitude of global environmental change and the state of our environment.

Summary of Findings and Original Contributions

In Chapter I, I evaluated the variation in global lake sedimentation rates across both space and time. Our temporal analysis indicated a general increase in lake sedimentation rate, recording a strong acceleration around 1950 CE. These findings extend on our current knowledge of the temporal variation in lake sedimentation rates and their relationship to land use, building on earlier work evaluating trends across the Holocene (Jenny et al., 2019). Our findings demonstrated that since the Holocene, lake sedimentation rates have increased on average by 3 – 4 folds. We also observed that the more densely populated terrestrial ecozones displayed an earlier acceleration when compared to less densely populated ecozones. Furthermore, densely populated regions of the world also demonstrated the greatest rate of sediment accumulation (for both MAR & SAR). Our analysis was also successful at highlighting the correlation between anthropogenic activities as predicted, where sites/timepoints with a greater proportion of cropland cover or urban density in lake watershed had greater sedimentation rates. Collectively, the findings from the spatial and temporal analysis of lake sedimentation rate presented in Chapter I demonstrated the growing influence of anthropogenic development on the inland aquatic realm. Along with having created and made accessible this large database of nearly 500 records, we improved on the current methodology by clearly articulating some of the confounding factors that can be associated with the study of lake sedimentation. For example, we accounted for the coring apparatus used to retrieve the cores which was shown to influence the degree of compaction associated with some measure of lake sedimentation rate, namely sediment accumulation rate (SAR). While this metric of sedimentation rate tends to be more readily available, it is inherently affected by sediment dewatering processes, inflating SAR rates towards the top of the core. Our analysis presented as Chapter I clearly identified this issue and provided an equation that could be used to estimate MAR from the associated SAR.

In Chapter II, I focused on a specific region of Canada, Eastern Canada, where I established sediment chronologies based on a novel and replicable framework for 37 sediment cores that were retrieved across a range of human impact and lake sizes. The necessity of this framework was made clear by recent research by Barsanti et al. (2020) where the authors reported on the lack of a common approach when establishing ^{210}Pb chronologies to lake sediment. The formulation of my framework can be considered an original contribution to knowledge as future researcher can use the methodologies developed to assess on the applicability of the different age models. Furthermore, I also used Chapter II, as an opportunity to build on the findings from Chapter I and tested whether similar conclusions would be drawn from the modelled temporal and spatial variation in lake sedimentation rates across Eastern Canada. Our findings presented in Chapter II demonstrated that lakes across Eastern Canada experienced a similar onset time (1956 CE ± 8 years) for the recorded acceleration in lake sedimentation rates. My findings for Chapter II also corroborated the ones reported in Chapter I whereby the most densely populated ecoregion of Canada, the Mixedwood Plains, yielded the greatest increase lake sediment mass accumulation rates. Using high resolution spatial and temporal datasets such as historical Canadian meteorological station data and historical census reconstructions, I was able to apply a similar methodology as I had developed for my first chapter and quantified the association between metrics of anthropogenic development and lake sedimentation rates. As it was observed in Chapter I, human population counts within lake's watershed was found to be significantly correlated with increase in lake sedimentation rates. Finally, the main finding of this chapter shed light on the growing evidence of the influence of human population of the environment, constituting another example of environmental consequences associated with global human activities.

In chapter III, I turned from the physical to the geochemical variation archived in lake sediments. Using the lake sediment cores mentioned in my second chapter, I used novel technologies to generate a spatio-temporal portrait of elemental composition in lakes sediments across the Eastern Canadian landscape. In this exploratory analysis, we shed light on the heterogenous nature of lake sediments and identified regional patterns. In particular, I found that lake cores from the Mixedwood Plains (M.W.P.) ecoregion were most distinct from those of the three other ecoregions of Eastern Canada. The composition of lake cores collected from the Atlantic Highlands, Atlantic Maritime and Boreal Shield were generally richer in organic matter while lake cores collected from the M.W.P. had greater relative abundance of inorganic elements such as titanium, strontium and calcium, which may be due to sediments deposited on the landscape as part of the Champlain Sea. However, a commonality across most lakes was the observed increase in heavy metals (lead and zinc), showing peak values in the 1970s and ‘80s. Finally, our findings also demonstrated the combined influence of the geological watershed composition and the current watershed land-use where metal elements such as zinc and lead were positively associated with human population estimates. This chapter addressed new questions and served to demonstrate some of the novel applicability when considering emerging technologies. Our findings are also complemented by methodological improvements considering the influence of multiple published processing steps to move towards quantitative analyses of data from XRF-scanners.

In Chapter IV, I evaluated the potential for common lake stressors, known to impact lakes globally, to influence the accumulation of elemental lead in lake sediments. For this chapter, I turn to lakes of IISD-ELA, a region where whole-lake manipulations had been carried out starting in the 1970s. Having the opportunity to investigate these phenomena in an experimental setting is very beneficial because it isolates some of the catchment dynamics related to these stressors and instead focuses on within lake functioning. My findings demonstrated the influence of both lake acidification and lake eutrophication on the accumulation of Pb in lake sediments. In the lake subject to experimental lake acidification, we observed a lesser increase in concentration and accumulation of Pb relative to reference lakes, while eutrophied lakes demonstrated an increase in the concentration and accumulation of Pb in their sediment records during the manipulation window. This chapter also provided insights into the mechanistic processes associated with the burial of Pb in lake sediments. My results highlighted the important influence of epilimnetic DOC in mediating the accumulation of Pb in lake sediments. The influence of DOC was demonstrated through both fertilization and acidification experiments. With lake eutrophication, DOC concentrations increased following addition of nitrogen and phosphorus, and with acidification experiment, DOC concentrations decreased following acid addition. The influence of pH on DOC is expected to occur through the increased protonation and subsequent reduction of organic acids functional groups such as phenols, carboxylic and fulvic acids that are responsible for composing over 90% of DOC molecules (Thurman, 1985). The association between acidic pH and reduction of epilimnetic DOC has been described before, where increased lake transparency was observed following reduction in epilimnetic DOC concentrations following acidification (Schindler et al., 1980; Olsson and Pettersson, 1993). In systems where allochthonous contributions represent an important fraction of the material deposited, such as lakes at the IISD-ELA, acidic pH is also expected to reduce the fraction of organic matter from terrestrial inputs via interactions with other ions in the soil organic matter under low pH conditions (Clark et al., 2006; Monteith et al., 2007). One example is Aluminum, which has been shown to bind organic matter effectively (Tipping and Woof, 1991), and is expected to compete with Pb-binding with DOC thereby further reducing its burial in lake sediments. The findings reported in Chapter IV constitute an original contribution to knowledge as it demonstrates the influence of environmental conditions in shaping the magnitude and the nature of the constituents accumulating in lake sediments. These results also hold strong implications for regional surveys attempting to reconstruct portrait of elemental deposition, where concentrations are routinely being measured and compared across systems. In future, investigators should consider elemental accumulation rates and the potential for lake trophic state or other environmental conditions to influence the mechanisms associated with elemental burial in lake sediment.

During my PhD thesis, I was also able to contribute to original knowledge by being involved in multiple collaborations, some of which are still on-going. My earliest collaboration, which has been personally highly influential, was the study of Holocene sedimentary flux published by Jenny et al. (2019). Not only did it immerse me in the world of paleolimnology and global environmental change, it also sparked my curiosity to learn more about the impact of anthropogenic development on the environment. I also had the opportunity to contribute to additional collaborations, some involving the influence of climate change and nutrient enrichment on diatom assemblages (Cheng et al., 2022); the biological responses experienced across multiple taxa over the past ~150 years (Griffiths et al., 2021); the influence of hydrology and industry on lake's biological communities (Simmatis et al., 2020) and the development of new methodologies, such as environmental DNA, to reconstruct biological species variation (Mejbel et al., 2021).

The growing influence of anthropogenic development on the environment

Since the origin of humankind, *Homo sapiens* has been modifying their environment (Fisher et al., 2003; Zhao et al., 2007). Only recently, however, with the development of new technologies and the exponential growth in human populations have we collectively been jeopardizing the sustainability of the environment (Dodds, 2008). It is often difficult to fully appreciate this loss of sustainability. One attempt has been to frame the environmental issue through a financial lens, in what is known as ecosystem services (Daily, 2003; Daily and Matson, 2008). While considering the environment in terms of the financial repercussions can be insightful for policy makers, generating a comprehensive portrait of the financial ramifications for conservation has proven very challenging (Bennett et al., 2009). Nonetheless, it should be recognized that important improvements towards the protection of the environment have been made since the 1950s both in terms of the public awareness for the environmental cause (Dunlap and Scarce, 1991) and the political steps taken to reduce impact of industries on the environment (Faure, 2004; Salomons and Stigliani, 2012). The introduction of numerous environmental regulations and monitoring programs aimed at improving the conditions of the environment are some examples. However, it can also be argued that the same environmental consciousness and regulatory framework are not shared by all countries equally, which continues to add on the global environmental burden as contaminants and greenhouse gases move across national borders (Zhao et al., 2012).

Integrating materials from all realms of the environment, lake sediments provide important insights into the functioning of multiple aspects of the environment. Understanding modifications brought to our environment is perhaps the most valuable and insightful research opportunity that lake sediments offer. Across all chapters of this thesis, my findings demonstrated the growing influence of anthropogenic development on the environment. In Chapter I and II, increasing lake sedimentation rates were observed to be highly correlated to the proportion of anthropogenic land-use in lake's watershed. While urban and cropland land-cover are expected to increase the surface soil erosion during the conversion stage from natural to anthropogenic land-cover (Miller et al., 1997; Schiefer et al., 2013), these anthropogenic developments are expected to continue contributing sediment delivery to aquatic inland ecosystems after forest clearance (Bonk et al., 2016). Increased sedimentation rates are expected to be mediated via the removal of vegetative cover and the subsequent soil exposure to precipitation and surface runoff (Kerr, 2007). In addition to these physical modifications, agriculture, through the application of fertilizer, is also expected to fuel primary productivity in lakes (Koroluk and De Boer, 2007; Keatley et al., 2011; Anderson et al., 2020) which will further increase sedimentation rates in lakes (Acton and Gregorich, 1995; Bunting et al., 2016). When considering the influence of urban development, it is expected that dust, soil, and other detrital matter associated with urban development will contribute to increased sedimentary material via the street runoff and storm sewers (Kerr, 2007). In turn, increases in the rate of lake sedimentation can precipitate important modifications in the natural communities present these ecosystems (Richard Albert et al., 2010). These deleterious impacts can be mediated via increases in the lake water turbidity, which attenuates light penetration (Brown, 1984;

Koenings and Edmundson, 1991) and impacts the photosynthetic capacity of algae and macrophyte (Hanson and Butler, 1994). Increased turbidity via increased input of suspended solids has also been documented to negatively impact planktivorous species (Horppila et al., 2004). Increased fraction of suspended solids in the water can also reduce water quality for human consumption and use (Tan et al., 2017). Sedimentation rates which are often mediated through increased suspended solids also have the potential to adsorb and concentrate potentially harmful contaminants, increasing their bioavailability to aquatic life (Sansalone et al., 1995; Song et al., 2010; Arnnok et al., 2017).

Lake sedimentation rates also hold a profound impact on global geochemical fluxes and the importance of the freshwater realm in the sequestration of carbon (von Wachenfeldt et al., 2008; Anderson et al., 2014). Freshwater environments are generally considered to be responsible for a significant fraction of the total carbon sequestration (anywhere between 12% - 34%) (Drake et al., 2018) with sediments and wetlands accounting for the greatest sequestration. While these estimates provide insight into the functioning of carbon sequestration, a lot of uncertainties associated with these estimates currently remain (Regnier et al., 2013; Wehrli, 2013). Despite these uncertainties, when considering lakes by their surface area, these ecosystems hold a disproportionate effect on the global carbon cycle (Anderson et al., 2020). In addition to offering carbon sequestration by burying organic carbon in their sediments, lakes also mediate and participate in carbon transformation across the atmosphere and the terrestrial realms (Dean, 1999; Cardille et al., 2007). With increased sedimentation rates, lakes are also expected to contribute to a greater extent to global carbon sequestration. As demonstrated by Anderson et al. (2020), carbon sequestration in lakes has been reported to be increasing, nearly tripling since 1900 CE. These results are in line with our findings presented in Chapter I and II, where a similar increase in lake sedimentation rate has been reported. It would thus be interesting to evaluate the contribution of changes in carbon concentration in the sediment and tease apart the contribution of changes in sediment mass accumulation rates. Another interesting account of global environmental change has been reported as the increase of global nitrogen and phosphorus. These nutrients have been reported to have increased by nearly 20-fold (Anderson et al., 2020). As mentioned in the discussion of Chapter I, it is possible that an important fraction of these nutrients are being stored on the landscape, in soil or in plants. Heterogeneity across sites, in terms of hydrology, topology and geography may also contribute to the disconnect between trends in sediment mass accumulation rates and in nutrient export rates.

Heterogeneity across the landscape remains one of the largest challenges when considering environmental change. These challenges have been embodied throughout multiple aspects of Chapter I, II and III. One example when considering Chapter II, is the fact that some of the remote lakes still demonstrated important rates of sedimentation. These findings suggest that a large contribution in lake sedimentation rates can be expected from the hydrological conditions of the lakes' watershed, lake's morphometry and nutrient status, all influential in autochthonous production (Håkanson, 2005; Staehr et al., 2012). Often a careful inspection of multiple proxies (i.e., radioisotopic profiles, core photographs, water content measures) are required to contextualize more profoundly the observed heterogeneity within and across sites. The impact of landscape heterogeneity when considering environmental change was also demonstrated in Chapter III where I considered the geochemical change archived in lake sediments. One example of this phenomenon was observed when considering a lake located in Tweed (Ontario). This lake clearly demonstrated impacts of metal pollution with Arsenic concentration exceeding the probable effect levels (PELs) by 22-fold despite the absence of mining and industries directly within its watershed. The source of this pollution was in fact attributed to the presence of the Deloro mines located 35 km upstream contributing polluted effluents through the Moira River which feeds in Stoco Lake (Simmatis et al., 2020). This example also serves to illustrate how even though lake watersheds are powerful to carry spatial investigations of the potential variables associated with a specific behavior recorded in lakes, contribution originating from outside the lake watershed can also be influential.

Current limitations and future considerations

While all of the chapters of this thesis attempt to make use of the best practices, there were inherent limitations associated with each of these chapters. One of the most important limiting factors towards our greater understanding of sedimentary delivery to lake, and its numerous ramifications evaluated across the four chapters of this thesis (e.g., lake sedimentation rates – Chapter I, radio-isotope deposition – Chapter II, metal deposition and accumulation - Chapter III and IV) is the lack of a readily available spatially resolved particle transport models. These models typically focus on either sediment transport, such as Revised Soil Loss Equation (RUSLE) (Renard, 1997) or atmospheric transport models, such as AEROMOD or CALPUFF (Levy et al., 2002; Stock et al., 2002; Holnicki et al., 2016). RUSLE is a soil erosion model which relies on the application of five watershed factors including rainfall, soil erodibility, watershed slope and vegetation. In practice, these factors take the form of geospatial raster layers which when multiplied yield a metric relatable to the potential rates of soil erosion. While application of the RUSLE models exists for Canada (Wall et al., 2002) and the United States (Lab, 2015), the available resolution of the data covering these broad geographical regions do not align with the size of the lakes considered in this thesis. Moreover, while contemporary rates of soil erosion have the potential to yield insights into the likelihood of a lake watershed to be more prone to soil erosion, to be fully applicable to paleolimnological investigations, temporally-resolved RUSLE factors would have to be scaled to the longer time scales captured in sediment accumulation rates. AEROMOD and CALPUFF on the other hand focus on the atmosphere driven pattern of emission and deposition. Both models have been recognized by the Environmental Protection Agency (EPA) in the study of long-range transport of pollutants (EPA, 2017). The main difference between the two models is the fact that AEROMOD relies on a plume dispersion model (e.g., steady-state dilution as a function of distance from emission) and CALPUFF relies on a puff dispersion model (e.g., non-steady state dilution following air current) (Dresser and Huizer, 2011). While there has been considerable effort made by governing bodies to monitor and launch sampling program to inventory metal emissions, these data are generally not accessible to the public and such models require an intensive training to implement (Scire et al., 2000). When corroborated with historical archives about the development of industries (such as the data archived in Canadian census surveys (CCRI, 2016) and abandoned mines (NOAMI, 2004)), these transport models have the potential to yield strong and novel insights into the accumulation of various sediment constituents. These models are specifically expected to contribute significant knowledge when considering the sources of environmental pollution such as the ones investigated in Chapter III.

It would also be interesting to bridge knowledge between riverine sediment loads and lake sediment accumulation rates. Integrating the modeling of river sediments, that carry a non-negligible extent of the total suspended load entering lakes, with lake models could more precisely link sediment delivery to its accumulation in lake sediment. One of the current limitations towards this implementation is the disconnect in the temporal resolution considered among study types. In river studies, sediment load is measured over very short time periods and considers the whole watershed (*metric tons*$\cdot$*km*$^{-2}$$\cdot$*year*$^{-1}$) while in paleolimnology these measurements can span decades and are typically estimated from a lake sediment core (in *g*$\cdot$*cm*$^{-2}$$\cdot$*year*$^{-1}$).

When considering specifically my first chapter, where I investigated the global variation in lake sedimentation rates, one limitation is the use of a single scientific journal. While the *Journal of Paleolimnology* arguably features most of the published lake sediment chronologies relative to other journals, it is possible that some regions of the world might have been underrepresented. Restricting our analysis to a single journal was mainly motivated by time constraints and reproducibility considerations. Ultimately, it was satisfactory in drawing a global picture of lake sedimentation rates as we focused on a peer reviewed publication that arguably publishes the greatest number of lake sediment records spanning the last ~150 years. However, like other investigations focusing on the global extent (Messager et al., 2016), our global analysis has limited applicability when considering a specific regional location. To this end, if the aim is to estimate a specific behavior over a defined geographical extent, it is recommended to instead maximize the number of publications covering this specific geographical extent, independent of the scientific journal that published the chronologies. This approach has proven particularly effective when performing a nationwide investigation of sedimentation rate for the LakePulse field campaign; (Huot et al., 2019) an exercise that I led. Indeed, this large-scale sampling exercise required the *a priori* knowledge of the estimated sedimentary background depth across the different regions of Canada, to ensure similar contextualization could be made across top-bottom samples (a technique where only the first and the last centimeters of a sediment core are considered) retrieved across different Canadian ecoregions. In addition of providing a clear target length of a sediment core to be retrieved for the field sampling teams, this Canadian-wide analysis of sedimentation rates provided for a unique dataset, yielding significant insights into the similarity in lake sedimentation rate within ecozones (Figure E2 - unpublished). My work on this aspect provided additional context for the study of environmental change to lakes of Eastern Canada featured in Chapter II and III, where we observed the important patterns among ecoregions on the distribution of geochemical elements and rates of sediment mass accumulation.

Being aware of the issue of varying sedimentation within and across lake sediment cores was critical as it was shown to influence several subsequent analyses. Since sediment cores are typically subsampled vertically into intervals of set height, for example 1 cm, the process of subsampling sediment cores can result in a wide difference in the number of years being encapsulated within each 1 cm intervals (2 – 50 years). The discrepancy associated with sediment subsampling was most relevant when considering the establishment of sediment chronologies covered in Chapter II. Lakes with low sedimentation rates will have intervals encapsulating more years. It is thus expected that the measured ^{210}Pb activity will reflect increased decay as a function of core depth. To take this into account, a more probabilistic approach when determining sediment chronologies from measured ^{210}Pb may provide significant improvements over the basis of the three current classical dating models.

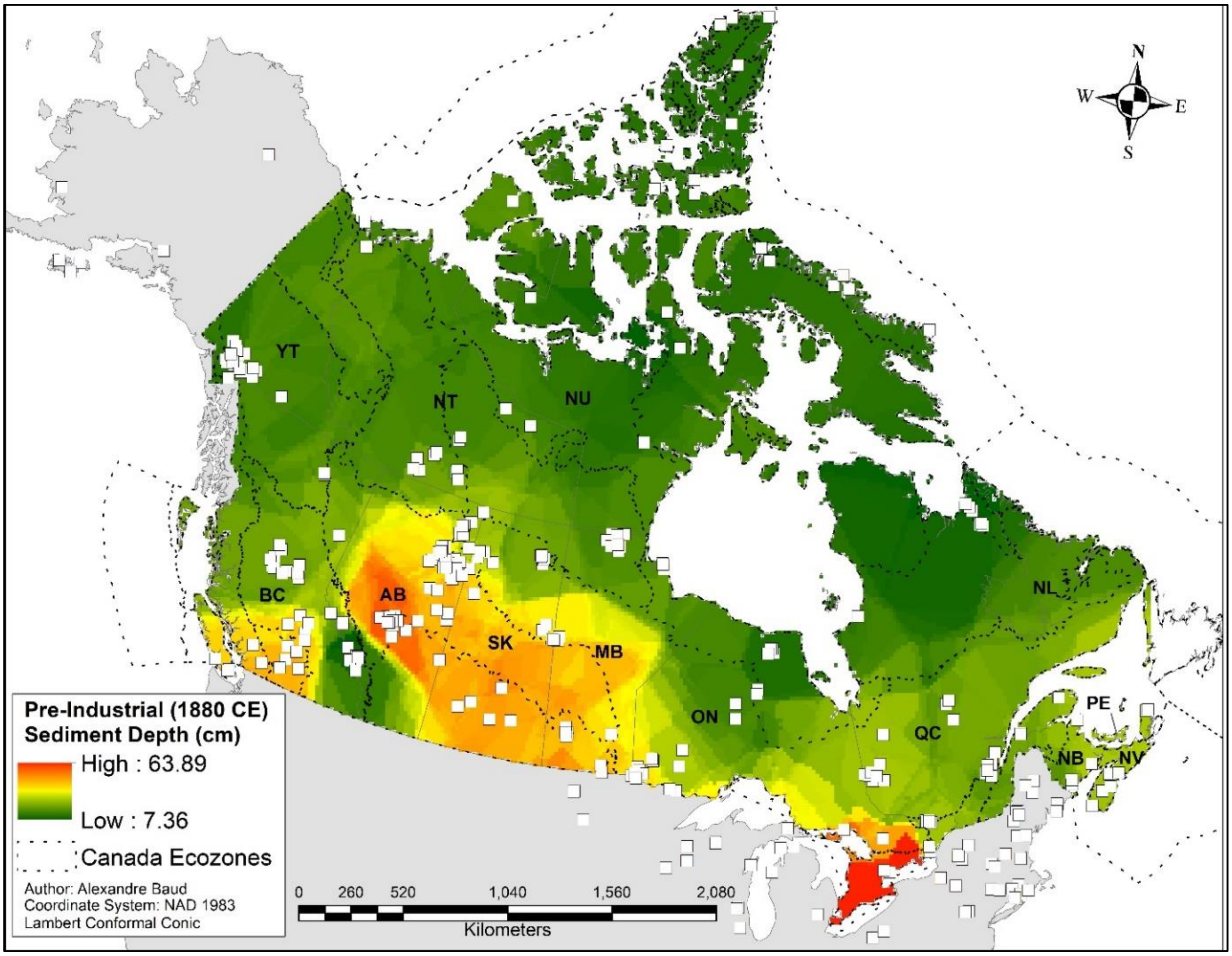

Figure E2. Interpolated spatial distribution of pre-industrial (1880 CE) sediment depth using kriging methods based on empirical survey collected from the literature.

Using the datasets collected as part of Chapter I and II, I am currently leading an effort to refine Bayesian modeling approaches for sediment chronologies to assess the applicability and harness prior information more fully. Examples of such approaches include *BACON*, developed for the estimation of radiocarbon ages (Blaauw and Christen, 2011) and Plum, developed for the calibration of recent chronologies with radiocarbon ages (Aquino-López et al., 2020). Plum uses three prior distributions, evaluating variation in the supported ^{210}Pb activity, ^{210}Pb supply rate and overall sedimentation rate (Aquino-López et al., 2020). While Plum holds a great potential to improve the establishment of ^{210}Pb-based lake sediment chronologies, one of the current limitations to Plum's applicability to the establishment of lake sediment chronologies is the fact that these three priors rely on distributions observed from marshes and wetlands (Aquino-López et al., 2020). Investigating the applicability of these prior distributions using a dataset like the one generated across Chapter II holds strong potential on the improvement the applicability of the Plum's model for lake sediments. While the findings of this thesis participate in advancing our current knowledge of global environmental change and its archival in lake sediments, additional efforts and research considerations will be required to expand on the current limitations towards our understanding of global environmental change so we can be better equipped to monitor and reduce the influence of humankind on its environment.

References

Acton, D.F., Gregorich, L., 1995. The health of our soils: toward sustainable agriculture in Canada.

Anderson, N.J., Bennion, H., Lotter, A.F., 2014. Lake eutrophication and its implications for organic carbon sequestration in Europe. Global Change Biol., 20, 2741-2751

Anderson, N.J., Heathcote, A., Engstrom, D., contributors, G.d., 2020. Anthropogenic alteration of nutrient supply increases the global freshwater carbon sink. Science advances, 6, eaaw2145

Aquino-López, M.A., Ruiz-Fernández, A.C., Blaauw, M., Sanchez-Cabeza, J.-A., 2020. Comparing classical and Bayesian 210Pb dating models in human-impacted aquatic environments. Quaternary Geochronology, 60, 101106

Arnnok, P., Singh, R.R., Burakham, R., Pérez-Fuentetaja, A., Aga, D.S., 2017. Selective uptake and bioaccumulation of antidepressants in fish from effluent-impacted Niagara River. Environ. Sci. Technol., 51, 10652-10662

Barsanti, M., Garcia-Tenorio, R., Schirone, A., Rozmaric, M., Ruiz-Fernández, A.C., Sanchez-Cabeza, J.-A., Delbono, I., Conte, F., Godoy, J.D.O., Heijnis, H., 2020. Challenges and limitations of the 210Pb sediment dating method: Results from an IAEA modelling interlaboratory comparison exercise. Quaternary Geochronology, 59, 101093

Bennett, E.M., Peterson, G.D., Gordon, L.J., 2009. Understanding relationships among multiple ecosystem services. Ecol. Lett., 12, 1394-1404

Blaauw, M., Christen, J.A., 2011. Flexible paleoclimate age-depth models using an autoregressive gamma process. Bayesian analysis, 6, 457-474

Bonk, A., Kinder, M., Enters, D., Grosjean, M., Meyer-Jacob, C., Tylmann, W., 2016. Sedimentological and geochemical responses of Lake Żabińskie (north-eastern Poland) to erosion changes during the last millennium. J. Paleolimnol., 56, 239-252

Brown, R., 1984. Relationships between suspended solids, turbidity, light attenuation, and algal productivity. Lake Reserv. Manage., 1, 198-205

Bunting, L., Leavitt, P., Simpson, G., Wissel, B., Laird, K., Cumming, B., St. Amand, A., Engstrom, D., 2016. Increased variability and sudden ecosystem state change in Lake Winnipeg, Canada, caused by 20th century agriculture. Limnol. Oceanogr., 61, 2090-2107

Cardille, J.A., Carpenter, S.R., Coe, M.T., Foley, J.A., Hanson, P.C., Turner, M.G., Vano, J.A., 2007. Carbon and water cycling in lake-rich landscapes: Landscape connections, lake hydrology, and biogeochemistry. Journal of Geophysical Research: Biogeosciences, 112

CCRI, 2016. Census of Population: Selected Tables for Census Subdivisions and Census Divisions. in: (CCRI), C.C.R.I. (Ed.). University of Alberta

Cheng, Y., Baud, A., Gregory-Eaves, I., Simmatis, B., Smol, J.P., Griffiths, K., 2022. Climate change and nutrient enrichment altering sedimentary diatom assemblages since pre-industrial time: evidence from Canada's most populated ecozone.

Clark, J.M., Chapman, P.J., Heathwaite, A.L., Adamson, J.K., 2006. Suppression of dissolved organic carbon by sulfate induced acidification during simulated droughts. Environ. Sci. Technol., 40, 1776-1783

Daily, G., 2003. What are ecosystem services. Global environmental challenges for the twenty-first century: Resources, consumption and sustainable solutions, 227-231

Daily, G.C., Matson, P.A., 2008. Ecosystem services: From theory to implementation. PNAS, 105, 9455-9456

Dean, W.E., 1999. The carbon cycle and biogeochemical dynamics in lake sediments. J. Paleolimnol., 21, 375-393

Dodds, W.K., 2008. Humanity's footprint: momentum, impact, and our global environment. Columbia University Press. 0231139667

Drake, T.W., Raymond, P.A., Spencer, R.G., 2018. Terrestrial carbon inputs to inland waters: A current synthesis of estimates and uncertainty. Limnology and Oceanography Letters, 3, 132-142

Dresser, A.L., Huizer, R.D., 2011. CALPUFF and AERMOD model validation study in the near field: Martins Creek revisited. J. Air Waste Manage. Assoc., 61, 647-659

Dunlap, R.E., Scarce, R., 1991. Poll trends: Environmental problems and protection. The public opinion quarterly, 55, 651-672

EPA, 2017. Revisions to the Guideline on Air Quality Models: Enhancements to the AERMOD Dispersion Modeling System

and Incorporation of Approaches To Address Ozone and Fine Particulate Matter. in: AGENCY, E.P. (Ed.), Federal Register

Faure, N.J.V.M.G., 2004. Green giants?: environmental policies of the United States and the European Union. MIT press. 0262720442

Fisher, C.T., Pollard, H.P., Israde-Alcántara, I., Garduño-Monroy, V.H., Banerjee, S.K., 2003. A reexamination of human-induced environmental change within the Lake Patzcuaro Basin, Michoacan, Mexico. PNAS, 100, 4957-4962

Griffiths, K., Jeziorski, A., Paquette, C., Taranu, Z.E., Baud, A., Antoniades, D., Beisner, B., Hamilton, P.B., Smol, J.P., Gregory-Eaves, I., 2021. Multi-trophic level responses to environmental stressors over the past~ 150 years: Insights from a lake-rich region of the world. Ecol. Indicators, 127, 107700

Håkanson, L., 2005. The importance of lake morphometry and catchment characteristics in limnology–ranking based on statistical analyses. Hydrobiologia, 541, 117-137

Hanson, M.A., Butler, M.G., 1994. Responses of plankton, turbidity, and macrophytes to biomanipulation in a shallow prairie lake. Can. J. Fish. Aquat. Sci., 51, 1180-1188

Holnicki, P., Kałuszko, A., Trapp, W., 2016. An urban scale application and validation of the CALPUFF model. Atmospheric Pollution Research, 7, 393-402

Horppila, J., Liljendahl-Nurminen, A., Malinen, T., 2004. Effects of clay turbidity and light on the predator prey interaction between smelts and chaoborids. Can. J. Fish. Aquat. Sci., 61, 1862-1870

Huot, Y. et al., 2019. The NSERC Canadian Lake Pulse Network: A national assessment of lake health providing science for water management in a changing climate. Sci Total Environ, 695, 133668. 10.1016/j.scitotenv.2019.133668

Jenny, J.P. et al., 2019. Human and climate global-scale imprint on sediment transfer during the Holocene. Proc Natl Acad Sci U S A, 116, 22972-22976. 10.1073/pnas.1908179116

Keatley, B.E., Bennett, E.M., MacDonald, G.K., Taranu, Z.E., Gregory-Eaves, I., 2011. Land-use legacies are important determinants of lake eutrophication in the anthropocene. PloS one, 6, e15913

Kerr, R.A., 2007. Global warming is changing the world. Science, 316, 188-190

Koenings, J., Edmundson, J., 1991. Secchi disk and photometer estimates of light regimes in Alaskan lakes: Effects of yellow color and turbidity. Limnol. Oceanogr., 36, 91-105

Koroluk, S., De Boer, D., 2007. Land use change and erosional history in a lake catchment system on the Canadian prairies. Catena, 70, 155-168

Lab, U.N.S.E.R., 2015. Revised Universal Soil Loss Equation, Version 2 (RUSLE2). in: Lab, U.N.S.E.R. (Ed.)

Landers, D.H., Simonich, S., Jaffe, D., Geiser, L., Campbell, D.H., Schwindt, A., Schreck, C., Kent, M., Hafner, W., Taylor, H.E., 2008. The fate, transport, and ecological impacts of airborne contaminants in western national parks (USA). Western Airborne Contaminants Assessment Project Final Report. Corvallis

Levy, J.I., Spengler, J.D., Hlinka, D., Sullivan, D., Moon, D., 2002. Using CALPUFF to evaluate the impacts of power plant emissions in Illinois: model sensitivity and implications. Atmospheric Environment, 36, 1063-1075

Mejbel, H.S., Dodsworth, W., Baud, A., Gregory-Eaves, I., Pick, F.R., 2021. Comparing quantitative methods for analyzing sediment DNA records of cyanobacteria in experimental and reference lakes. Frontiers in microbiology, 12, 1532

Messager, M.L., Lehner, B., Grill, G., Nedeva, I., Schmitt, O., 2016. Estimating the volume and age of water stored in global lakes using a geo-statistical approach. Nature communications, 7, 1-11

Miller, L., McQueen, D., Chapman, L., 1997. Impacts of forest harvesting on lake ecosystems: a preliminary literature review. British Columbia Ministry of Environment, Lands and Parks, Wildlife Branch. 0772630119

Monteith, D.T., Stoddard, J.L., Evans, C.D., De Wit, H.A., Forsius, M., Høgåsen, T., Wilander, A., Skjelkvåle, B.L., Jeffries, D.S., Vuorenmaa, J., 2007. Dissolved organic carbon trends resulting from changes in atmospheric deposition chemistry. Nature, 450, 537-540

NOAMI, 2004. National Orphaned/Abandoned Mines Initiative Inventory. in: (NOAMI), N.O.A.M.I. (Ed.)

Olsson, H., Pettersson, A., 1993. Oligotrophication of acidified lakes: a review of hypotheses. Ambio, 312-317

Regnier, P., Friedlingstein, P., Ciais, P., Mackenzie, F.T., Gruber, N., Janssens, I.A., Laruelle, G.G., Lauerwald, R., Luyssaert, S., Andersson, A.J., 2013. Anthropogenic perturbation of the carbon fluxes from land to ocean. Nat Geosci, 6, 597-607

Renard, K.G., 1997. Predicting soil erosion by water: a guide to conservation planning with the Revised Universal Soil Loss Equation (RUSLE). United States Government Printing. 0160489385

Richard Albert, M., Chen, G., MacDonald, G.K., Vermaire, J.C., Bennett, E.M., Gregory-Eaves, I., 2010. Phosphorus and land-use changes are significant drivers of cladoceran community composition and diversity: an analysis over spatial and temporal scales. Can. J. Fish. Aquat. Sci., 67, 1262-1273

Salomons, W., Stigliani, W.M., 2012. Biogeodynamics of pollutants in soils and sediments: risk assessment of delayed and non-linear responses. Springer Science & Business Media. 3642794181

Sansalone, J.J., Buchberger, S.G., Koechling, M.T., 1995. Correlations between heavy metals and suspended solids in highway runoff: implications for control strategies. Transportation research record

Schiefer, E., Petticrew, E.L., Immell, R., Hassan, M.A., Sonderegger, D.L., 2013. Land use and climate change impacts on lake sedimentation rates in western Canada. Anthropocene, 3, 61-71

Schindler, D., Hesslein, R., Wagemann, R., Broecker, W., 1980. Effects of acidification on mobilization of heavy metals and radionuclides from the sediments of a freshwater lake. Can. J. Fish. Aquat. Sci., 37, 373-377

Scire, J.S., Strimaitis, D.G., Yamartino, R.J., 2000. A user's guide for the CALPUFF dispersion model. Earth Tech, Inc, 521, 1-521

Simmatis, B., Baud, A., Gregory-Eaves, I., Francus, P., Smol, J.P., 2020. Subfossil Simuliidae track past river flow into an industrially contaminated lake. J. Paleolimnol., 64, 179-192. https://doi.org/10.1007/s10933-020-00130-4

Song, Y., Ji, J., Mao, C., Yang, Z., Yuan, X., Ayoko, G.A., Frost, R.L., 2010. Heavy metal contamination in suspended solids of Changjiang River—environmental implications. Geoderma, 159, 286-295

Staehr, P.A., Baastrup-Spohr, L., Sand-Jensen, K., Stedmon, C., 2012. Lake metabolism scales with lake morphometry and catchment conditions. Aquat. Sci., 74, 155-169

Stock, D.E., Lamb, B., Hoffman, M., 2002. Predictions of the Transport and Dispersion of a Power Plant Plume for Hilly Terrain Computed With AEROMOD and Measured in a Wind Tunnel, ASME International Mechanical Engineering Congress and Exposition, pp. 139-147

Tan, C., Thishalini, A., Goh, E., Edlic, S., 2017. Studies on turbidity in relation to suspended solid, velocity, temperature, pH, conductivity, colour and time. ARPN Journal of Engineering and Applied Sciences, 12, 5626-5635

Thurman, E., 1985. Functional Groups of Dissolved Organic Carbon, Organic Geochemistry of Natural Waters. Springer, pp. 87-101.

Tipping, E., Woof, C., 1991. The distribution of humic substances between the solid and aqueous phases of acid organic soils; a description based on humic heterogeneity and charge-dependent sorption equilibria. J. Soil Sci., 42, 437-448

von Wachenfeldt, E., Sobek, S., Bastviken, D., Tranvik, L.J., 2008. Linking allochthonous dissolved organic matter and boreal lake sediment carbon sequestration: The role of light-mediated flocculation. Limnol. Oceanogr., 53, 2416-2426

Wall, G., Coote, D., Pringle, E., Shelton, I., 2002. RUSLEFAC—Revised universal soil loss equation for application in Canada: A handbook for estimating soil loss from water erosion in Canada. Research Branch, Agriculture and Agri-Food Canada. Ottawa. Contribution No. AAFC/AAC2244E, 117

Wehrli, B., 2013. Conduits of the carbon cycle. Nature, 503, 346-347

Zhao, Y., Hölzer, A., Yu, Z., 2007. Late Holocene natural and human-induced environmental change reconstructed from peat records in eastern central China. Radiocarbon, 49, 789-798

Zhao, Y., Zhang, J., Nielsen, C., 2012. The effects of recent control policies on trends in emissions of anthropogenic atmospheric pollutants and CO2 in China. Atmos. Chem. Phys. Discuss, 12, 24985-25036